

Distribution Agreement

In presenting this thesis or dissertation as a partial fulfillment of the requirements for an advanced degree from Emory University, I hereby grant to Emory University and its agents the non-exclusive license to archive, make accessible, and display my thesis or dissertation in whole or in part in all forms of media, now or hereafter known, including display on the world wide web. I understand that I may select some access restrictions as part of the online submission of this thesis or dissertation. I retain all ownership rights to the copyright of the thesis or dissertation. I also retain the right to use in future works (such as articles or books) all or part of this thesis or dissertation.

Signature:

Ching-Chieh Chou

Date

**Identification of molecular mechanisms and suppressors of
TDP-43 pathology**

By

Ching-Chieh Chou
Doctor of Philosophy

Graduate Division of Biological and Biomedical Science
Neuroscience

Wilfried Rossoll, Ph.D.
Advisor

Gary J. Bassell, Ph.D.
Advisor

Thomas Kukar, Ph.D.
Committee Member

Xiao-Jiang Li, M.D., Ph.D.
Committee Member

Nicholas T. Seyfried, Ph.D.
Committee Member

Accepted:

Lisa A. Tedesco, Ph.D.
Dean of the James T. Laney School of Graduate Studies

Date

**Identification of molecular mechanisms and suppressors of
TDP-43 pathology**

By

Ching-Chieh Chou
B.S., Chang Gung University, 2007
M.S., National Yang-Ming University, 2009

Advisor: Wilfried Rossoll, Ph.D.
Advisor: Gary J. Bassell, Ph.D.

An abstract of
A dissertation submitted to the Faculty of the
James T. Laney School of Graduate Studies of Emory University
in partial fulfillment of the requirements for the degree of
Doctor of Philosophy

in Graduate Division of Biological and Biomedical Science
Neuroscience
2017

Abstract

Identification of molecular mechanisms and suppressors of TDP-43 pathology

By Ching-Chieh Chou

Amyotrophic lateral sclerosis (ALS) and frontotemporal dementia (FTD) are fatal neurodegenerative disorders with overlapping clinical, pathologic and genetic features. Cytoplasmic inclusions that contain the TAR DNA-binding protein 43 (TDP-43) are found as a common pathological hallmark in the brain and spinal cord of individuals with ALS and FTD. TDP-43 is an RNA-binding protein that predominantly resides in the nucleus. TDP-43 pathology is characterized by loss of this protein from the nucleus and the accumulation of insoluble TDP-43 aggregates in the cytoplasm. The reported global impairments in RNA and protein homeostasis may be caused by the sequestration of its interacting proteins into the TDP-43-positive inclusions. The exact cellular mechanisms for TDP-43 pathology remain unclear, which is also due to the limited understanding of the components of TDP-43 aggregates. Here, I demonstrate that proximity-dependent biotin identification (BioID) allows for successful interactome mapping of insoluble TDP-43 aggregates. I have identified proteins involved in nucleocytoplasmic transport, such as nucleoporins and transport factors, as its major components. Aggregated and mutant form of TDP-43 triggered the cytoplasmic aggregation of several nucleoporins and transport factors, disrupted nuclear pore complex and nuclear membrane structure, and disturbed nuclear transport of protein and RNA. I also found Nup205-positive inclusions as well as a widespread loss of Nup205 immunoreactivity in the motor and frontal cortex of sporadic ALS cases and those with genetic mutations in *TARDBP* and *C9orf72*. Furthermore, I report poly(A)-binding protein nuclear 1 (PABPN1) as a novel TDP-43 interaction partner that acts as a potent suppressor of TDP-43 toxicity. Overexpression of PABPN1 significantly reduced TDP-43-mediated neurotoxicity and protein aggregates in an ubiquitin proteasome-dependent manner. PABPN1 also restored the nuclear localization of TDP-43 and proper stress responses that were compromised by TDP-43 pathology. Taken together, these findings advance our understanding of the nucleocytoplasmic transport defects as a common disease mechanism in ALS/FTD and PABPN1 as a novel target to halt or even reverse the progression of TDP-43 pathology.

**Identification of molecular mechanisms and suppressors of
TDP-43 pathology**

By

Ching-Chieh Chou
B.S., Chang Gung University, 2007
M.S., National Yang-Ming University, 2009

Advisor: Wilfried Rossoll, Ph.D.
Advisor: Gary J. Bassell, Ph.D.

A dissertation submitted to the Faculty of the
James T. Laney School of Graduate Studies of Emory University
in partial fulfillment of the requirements for the degree of
Doctor of Philosophy

in Graduate Division of Biological and Biomedical Science
Neuroscience
2017

Acknowledgements

I am grateful to my advisors, Drs. Wilfried Rossoll and Gary Bassell, for their guidance, patience and coffee over the years. They have given me intellectual freedom in my work, inspired me with new thought, engaged me in many collaborative opportunities and supported my attendance at various conferences. I have learned from them their genuine passion for science, positive attitude to achieve success and tenacity to overcome frustrations. Those are invaluable and irreplaceable assets for my future career. I am deeply grateful for all their contributions of time and efforts to make my Ph.D. experience productive and enjoyable. Many past and present lab members have made great contributions to my training. I specifically want to thank Kathryn Moss, Paul Donlin-Asp, Marius Ifrim, Megan Merritt and Claudia Fallini for experimental support and Tawana Randall for administrative support. I am greatly appreciative of my committee members, Drs. Nicholas Seyfried, Thomas Kukar and Xiao-Jiang Li, for their knowledge and resources. They always had great suggestions and ideas. I also appreciate the collaboration with Dr. Daniela Zarnescu, Dr. Maureen Powers, Dr. Jonathan Glass and Mfon Umoh. I would like to thank my friends, both at Emory and beyond. Of course, I want to thank my parents and younger brother for their support and encouragement. They are always available for talk when I need them even though we are thousands miles away. Of all the people, I am deeply grateful to my wife, Hui-Ju Chang, and son, Edward Y. Chou, for their unconditional love and support. They have always been there for me and given me confidence when I encounter frustration. Their belief in me becomes my strength and allows me to accomplish greater things than I ever thought possible. Thank you. I would not be here today without you.

Table of Contents

Abbreviations	1
Chapter 1	4
General Introduction	4
1.1 Overview of neurodegenerative diseases with TDP-43 pathology	5
1.1.1 Amyotrophic lateral sclerosis (ALS)	6
1.1.2 Frontotemporal dementia (FTD).....	12
1.1.3 Other TDP-43 proteinopathy: Alzheimer’s disease (AD)	15
1.2 TAR DNA-binding protein 43 (TDP-43)	17
1.2.1 Structure	17
1.2.2 Normal TDP-43 function	19
1.2.3 TDP-43 mislocalization and aggregation.....	20
1.3 Models of TDP-43 aggregation	24
1.3.1 Aberrant stress granule (SG) formation	24
1.3.2 Inhibiting nucleocytoplasmic transport.....	27
1.4 Hypothesis and Objective	33
1.5 Figures	35
1.6 Table	42
Chapter 2	44
Materials and Methods	44
2.1 Yeast two hybrid assay	45
2.2 Yeast spotting assays	45
2.3 Constructs	46
2.4 <i>Drosophila</i> genetics	48
2.5 Adult Eye Imaging	48
2.6 Larval Turning Assays	48
2.7 Primary neuron and mammalian cell culture and transfection	49
2.8 Immunofluorescence and image acquisition and analysis	50
2.9 Fluorescence <i>in situ</i> hybridization (FISH) and immunofluorescence	52
2.10 Metabolic labeling of newly synthesized proteins	53
2.11 Electron microscopy of nuclear envelope	53
2.12 Immunohistochemistry	54
2.13 Cell death assay	55
2.14 Co-immunoprecipitation of FLAG-tagged constructs from mammalian cells	55
2.15 Co-immunoprecipitation of endogenous protein from mouse brain tissue	56
2.16 Histidine pulldown assay	56
2.17 Affinity pulldown of biotinylated proteins and immunoblotting	57
2.18 Sample digestion for mass spectrometry analysis	58
2.19 LC-MS/MS analysis	58
2.20 Database search	59
2.21 Identification of the TDP-43 and TDP-CTF interactome	59
2.22 Bioinformatics analysis	60
2.23 Protein extract, subcellular fractionation and western blots	61
2.24 Cycloheximide chase assay	62
2.25 Time-lapse live-cell imaging	63
2.26 Stress granule formation assay	64

2.27 Statistical analyses.....	64
Chapter 3.....	65
TDP-43 pathology disrupts nuclear pore complexes and nucleocytoplasmic transport in ALS/FTD.....	65
3.1 Abstract.....	66
3.2 Introduction.....	66
3.3 Results.....	68
3.3.1 Cytoplasmic TDP-43 aggregates are enriched for components of nucleocytoplasmic transport pathway.....	68
3.3.2 TDP-43 pathology causes the cytoplasmic aggregation and mislocalization of nucleoporins (Nups) and transport factors (TFs).....	70
3.3.3 FG-Nups contain prion-like domains (PrLDs) that mediate cytoplasmic co-aggregation with TDP-CTF.....	71
3.3.4 TDP-43 pathology disrupts the morphology of the nuclear membrane (NM) and nuclear pore complexes (NPCs).....	72
3.3.5 TDP-43 pathology disrupts nuclear import of proteins and export of mRNA.....	74
3.3.6 PABPN1, a suppressor of TDP-43 toxicity, rescues nucleocytoplasmic transport defects.....	75
3.3.7 Nucleoporin genes act as modifiers of TDP-43 pathology in <i>Drosophila</i> models for ALS.....	76
3.3.8 Nuclear pore pathology is common in brain tissue of ALS cases with TDP-43 inclusions.....	77
3.4 Discussion.....	77
3.5 Figures.....	82
3.6 Supplementary Figures.....	94
3.7 Supplementary Tables.....	113
Chapter 4.....	118
PABPN1 suppresses TDP-43 toxicity in ALS disease models.....	118
4.1 Abstract.....	119
4.2 Introduction.....	119
4.3 Results.....	123
4.3.1 TDP-43 is a novel interaction partner of PABPN1.....	123
4.3.2 PABPN1 modulates TDP-43 toxicity in yeast and primary neuron models.....	124
4.3.3 PABPN1 loss of function enhances TDP-43 toxicity in <i>Drosophila</i> models.....	127
4.3.4 PABPN1 specifically reduces protein levels of pathological TDP-43.....	128
4.3.5 PABPN1 facilitates the clearance of pre-formed pathological TDP-43 aggregates...	130
4.3.6 PABPN1 facilitates the clearance of pathological TDP-43 via the ubiquitin-proteasome mechanism.....	131
4.3.7 PABPN1 levels regulates nuclear localization of endogenous TDP-43.....	132
4.3.8 PABPN1 overexpression rescues defects in SGs caused by TDP-43 pathology.....	134
4.4 Discussion.....	136
4.5 Figures.....	146
4.6 Supplementary Figures.....	165
4.7 Table.....	169
4.8 Supplementary Table.....	170
Chapter 5.....	171
Conclusions and Future Directions.....	171

5.1 Summary	172
5.2 Remaining Questions and Future Directions.....	176
5.2.1 Mapping PABPN1 protein functional domains	176
5.2.2 PABPN1 rescues TDP-43 toxicity mediated by gain-of-function but not loss-of- function	177
5.2.3 Effects of PABPN1 truncation mutants on TDP-CTF levels.....	178
5.2.4 Effects of PABPN1 on the degradation of aggregate-prone proteins	179
5.2.5 Effects of PABPN1 on ubiquitin-proteasomal degradation.....	180
5.2.6 Effects of PABPN1 on proteasome activity.....	183
5.2.7 Future directions	184
5.3 Conclusions	185
5.4 Figures	187
References	197

List of Figures and Tables

Chapter 1

Figure 1-1 TDP-43 pathology in the FTD-ALS disease spectrum.....	35
Figure 1-2 Overview of the clinical, genetic and pathological classification of FTD.....	37
Figure 1-3 Schematic of functional domains and disease-causing mutations in TDP-43.	39
Figure 1-4 Essential functions of TDP-43 in the nucleus and cytoplasm.....	40
Table 1-1. The genetics of the ALS/FTD disease continuum	42

Chapter 3

Figure 3-1 A modified BioID method identifies the composition of pathological detergent-insoluble TDP-43 aggregates.	82
Figure 3-2 Pathological TDP-43 aggregates contain components of the nucleocytoplasmic transport machinery.	83
Figure 3-3 Electron microscopy (EM) analysis reveals abnormal nuclear membrane (NM) morphology in N2a cells.	85
Figure 3-4 TDP-43 pathology disrupts NPC and nuclear lamina structures and nucleocytoplasmic transport.	87
Figure 3-5 Identification of genetic suppression of TDP-43 toxicity in <i>Drosophila</i> disease models of ALS.	90
Figure 3-6 Nuclear pore pathology in ALS patient brain tissue with TDP-43 inclusions.	91
Figure 3-7 A model for TDP-43 pathology-mediated nucleocytoplasmic transport defects.....	92
Supplementary Figure 3-1 BirA*-tagged TDP-CTF catalyzes the biotinylation of proximate proteins in cytoplasmic aggregates.	94
Supplementary Figure 3-2 Gene ontology (GO) analysis of the TDP-43 and TDP-CTF interactomes.....	96
Supplementary Figure 3-3 GO analysis of differential protein interactions with TDP-43 and TDP-CTF.	97
Supplementary Figure 3-4 TDP-CTF expression alters the cellular localization of nucleoporins (Nups) and lamins in N2a cells.....	99
Supplementary Figure 3-5 TDP-CTF expression alters the cellular localization of nucleocytoplasmic transport factors (TFs) in N2a cells.	100
Supplementary Figure 3-6 ALS-causing TDP-43 mutation enhances mislocalization and cytoplasmic aggregation of Nups and TFs as compared to wild-type TDP-43 in N2a cells.....	102
Supplementary Figure 3-7 Prediction of prion-like domains (PrLDs) and intrinsically disordered regions in human Nups and TFs.	103

Supplementary Figure 3-8 PrLDs of FG-Nups mediate the co-aggregation with TDP-CTF.	105
Supplementary Figure 3-9 Mutant and aggregated forms of TDP-43 cause disruption of the nuclear lamina and nucleocytoplasmic transport defects.	106
Supplementary Figure 3-10 PABPN1 promotes the clearance of TDP-CTF and ameliorates nucleocytoplasmic transport defects.	108
Supplementary Figure 3-11 Immunohistochemical staining of pTDP-43 in the motor cortices of <i>TARDBP</i> , <i>C9orf72</i> , and sporadic ALS cases. Scale bar: 100 μ m.	110
Supplementary Figure 3-12 Immunohistochemical staining of Nup205 in the frontal cortices of <i>TARDBP</i> , <i>C9orf72</i> , and sporadic ALS cases. Scale bar: 100 μ m.	111
Supplementary Figure 3-13 Immunohistochemical staining of Rangap1 in the motor cortices of <i>TARDBP</i> , <i>C9orf72</i> , and sporadic ALS cases. Scale bar: 100 μ m.	112
Supplementary Table 3-1. Summary of human cases	113
Supplementary Table 3-2. Summary of reagents and sources	114

Chapter 4

Figure 4-1 TDP-43 and PABPN1 associate by protein-protein interaction in mammalian cells and tissue.	146
Figure 4-2 PABPN1 modulates TDP-43 toxicity in several <i>in vitro</i> and <i>in vivo</i> models of TDP-43 proteinopathy.	149
Figure 4-3 PABPN1 overexpression reduces pathological TDP-43 protein levels.	152
Figure 4-4 Induction of PABPN1 expression promotes the clearance of pre-formed pathological TDP-43 aggregates.	154
Figure 4-5 PABPN1 promotes TDP-CTF turnover through proteasomal degradation.	156
Figure 4-6 PABPN1 promotes mutant and wild-type TDP-43 turnover through proteasomal degradation.	158
Figure 4-7 PABPN1 expression restores the nuclear localization of endogenous TDP-43.	160
Figure 4-8 PABPN1 expression rescues SG formation defects caused by TDP-43 pathology.	162
Figure 4-9 Model of PABPN1's effects on TDP-43 proteinopathy phenotypes.	164
Supplementary Figure 4-1 TDP-CTF interacts with PABPN1.	165
Supplementary Figure 4-2 Expression of GFP-TDP-CTF induces the formation of cytoplasmic aggregates with the hallmarks of pathogenic TDP-43 inclusions in motor neurons.	166
Supplementary Figure 4-3 PABPN1 but not hnRNPA3 specifically reduces pathological TDP-CTF and does not affect aggregation of poly-glutamine repeat containing huntingtin.	167
Supplementary Figure 4-4 PABPN1 restores localization of endogenous TDP-43 in primary motor neurons.	168
Table 4-1. TDP-43 and PABPN1 interact in yeast two-hybrid assays.	169

Supplementary Table 4-1. List of primary antibodies used in the present study. 170

Chapter 5

Figure 5-1 | PABPN1 associates with TDP-43 via last C-terminal 50 aa. 187
Figure 5-2 | PABPN1 modulates TDP-43 toxic gain-of-function. 189
Figure 5-3 | PABPN1 truncation mutants affect TDP-CTF levels. 190
Figure 5-4 | PABPN1 changes the levels of TDP-CTF and other aggregation-prone
proteins. 191
Figure 5-5 | PABPN1 modulates ubiquitin homeostasis. 193
Figure 5-6 | PABPN1 promotes protein degradation via enhancing proteasome activity.
..... 194
Figure 5-7 | Future directions. 196

Abbreviations

AD	Alzheimer's disease
ADLD	Adult-onset autosomal dominant leukodystrophy
AHA	Azidohomoalanine
ALS	Amyotrophic lateral sclerosis
APP	Amyloid precursor protein
BioID	Proximity-dependent biotin identification
BirA*	Promiscuous mutant of <i>E. coli</i> biotin ligase
bvFTD	Behavioral-variant FTD
C9-ALS	ALS with genetic mutations in <i>C9orf72</i>
CBS	Corticobasal syndrome
CLM	Calicheamicin γ 1
CNS	Central nervous system
DAVID	Database for Annotation, Visualization, and Integrated Discovery
DN	Dystrophic neuritis
Dox	Doxycycline
DPRs	Dipeptide repeat proteins
EM	Electron microscopy
EthD-I	Ethidium homodimer-1
fALS	Familial ALS
FG	Phenylalanine-glycine
FISH	Fluorescence <i>in situ</i> hybridization
FL	Full-length
FTD	Frontotemporal dementia
FTLD	Frontotemporal lobar degeneration
G ₄ C ₂	GGGGCC
GA	Glycine-alanine
GO	Gene ontology
GP	Glycine-proline
GR	Glycine-arginine
GWAS	Genome-wide association studies
HD	Huntington's disease
hnRNP	Heterogenous nuclear ribonucleoprotein
HRE	Hexanucleotide repeat expansion
Htt	Huntingtin
IBMPFD	Inclusion body myopathy with Paget's disease of bone and frontotemporal dementia

IPZ	Importazole
LAAHD	Lethal arthrogryposis with anterior horn cell disease
LCCS1	Lethal congenital contracture syndrome 1
LCD	Low-complexity domain
LINC	LIInkers of Nucleoskeleton and Cytoskeleton
MND	Motor neuron disease
MSP	Multisystem proteinopathy
mtNLS	Mutant nuclear localization signal
N-to-C	Nuclear-to-cytoplasmic
N2a	Neuro-2a neuroblastoma cell
NCI	Neuronal cytoplasmic inclusions
NE	Nuclear envelope
NES	Nuclear localization signal
NFTs	Neurofibrillary tangles
NII	Neuronal intra-nuclear inclusions
NLS	Nuclear localization signal
NM	Nuclear membrane
NPC	Nuclear pore complex
Nups	Nucleoporins
OPMD	Oculopharyngeal muscular dystrophy
PA	Proline-alanine
PABPN1	Poly(A)-binding protein nuclear 1
PBP	Progressive bulbar palsy
PD	Parkinson's disease
PDB	Paget's disease of the bone
PLS	Primary lateral sclerosis
PMA	Progressive muscular atrophy
PNFA	Progressive nonfluent aphasia
PPA	Primary progressive aphasia
PR	Proline-arginine
PrLD	Prion-like domain
PSM	Peptide spectrum matches
PSP	Progressive supranuclear palsy
RAN	Repeat-associated non-ATG-dependent
RBP	RNA-binding protein
RRM	RNA-recognition motif
sALS	Sporadic ALS
SCA2	Spinocerebellar ataxia type 2

SD	Semantic dementia
SG	Stress granule
STS	Staurosporine
$t_{1/2}$	Half-life
TDP-43	TAR DNA-binding protein 43
TDP-ALS	ALS with genetic mutations in <i>TARDBP</i>
TDP-CTF	TDP-43 C-terminal fragment
TF	Transport factor
UPS	Ubiquitin proteasome system
UTR	Untranslated region
WT	Wild-type
Δ NLS18	Deletion of C-terminal 18aa
Δ NLS50	Deletion of C-terminal 50aa

Chapter 1

General Introduction

1.1 Overview of neurodegenerative diseases with TDP-43 pathology

Our understanding of mechanisms in motor neuron diseases underlying the progression of amyotrophic lateral sclerosis (ALS) begins with the identification of mutations in *SOD1* gene¹. Neuropathological evidence reveals the cytoplasmic inclusions containing mutant SOD1 in the affected motor neurons as with in the case that inclusion pathology has also been found in many different neurodegenerative disorders, such as Alzheimer's disease (AD), Parkinson's disease (PD), and Huntington's disease (HD). Evolving knowledge of genetic etiology provides insights into disease biology and suggests possible directions to unravel cellular pathways by establishing cell and animal models or develop therapeutic strategies by investigating genetic and chemical modifiers. The discovery of ALS-associated causal genes and variants relies on the advance in sequencing technologies from Sanger sequencing, genome-wide association studies (GWAS), whole-genome sequencing to whole-exome sequencing²⁻⁸. Genetic research has shown that ALS is not just a single clinical entity among motor neuron diseases, but rather a heterogeneous group of neurodegenerative disorders after the discovery of causative mutations in *TARDBP* gene in ALS and frontotemporal dementia (FTD) cases⁷⁻¹². The identification of the *TARDBP* encoded protein, TDP-43, as the major component of ubiquitin-positive and SOD1-negative inclusions in the central nervous system (CNS) of ca. 97% of ALS and 50% of FTD cases^{13,14} raised an interesting question: how does TDP-43 connect the pathogenesis of two seemingly unrelated diseases? To date, the overlap between ALS and FTD is widely supported by clinical, genetic and pathologic evidence^{15,16}. These findings may change the existing viewpoint that we should not see ALS and FTD as two different diseases, but rather an ALS/FTD disease continuum. In

addition to ALS/FTD, a high incidence of TDP-43 pathology has also been reported in many other neurodegenerative disorders, including AD and PD. Presently, the significance of the observed TDP-43 pathology for their disease process is unclear.

1.1.1 Amyotrophic lateral sclerosis (ALS)

ALS is a motor neuron disease that is characterized by the progressive degeneration of motor neurons in the brain and spinal cord. The name reflects the degeneration of upper motor neurons in the brain (a.k.a. corticospinal motor neuron) and the descending lateral corticospinal tracts (“lateral sclerosis”, scar formation of the spinal cord), and demise of lower motor neurons (a.k.a. spinal motor neuron), which leads to muscle denervation followed by muscle wasting (“amyotrophy”). Clinical manifestations of ALS include lower motor neuron signs (i.e. muscle atrophy in limb, trunk or bulbar region, areflexia and paralysis) and upper motor neuron signs (i.e. hyperreflexia and spasticity). Patients gradually lose their arm and hand function and walking ability, and develop slurred speech and swallowing difficulties. The characteristic onset is from unilateral symptoms and progresses to contiguous regions. Fatal respiratory failures often associate with aspiration pneumonia and occur within 3–5 years after disease onset¹⁷. So far, there is no cure or effective treatment for ALS. Riluzole, the only FDA-approved treatment for ALS, extends ALS patients by only 3–4 months¹⁸.

ALS is a heterogeneous disease. The phenotypic variability and genetic heterogeneity greatly contribute to the complexity of the disease. Clinical subtypes of ALS are described on the basis of the pathological locations in the CNS that influence the symptom onset in different regions of the body (i.e. bulbar onset: 25%, limb onset: 70%,

trunk or respiratory system onset: 5%)¹⁹. There are four main subtypes: **(1) ALS**: the most common form presenting with mixed upper and lower motor neuron signs with median survival time of 3 years; **(2) Progressive muscular atrophy (PMA)**: the disease is characterized by the presence of pure lower motor neuron signs with asymmetrical onset of symptoms. Disease onset of PMA is a little earlier than ALS. Individuals with PMA have median survival time of 3 years, but may slowly progress to ALS when they survive more than 4 years. **(3) Primary lateral sclerosis (PLS)**: the disease is defined by the presence of pure upper motor neuron signs with a symmetrical onset of symptoms. Individuals with PLS usually have a longer life expectancy of more than 10 years after disease onset but may also progress to ALS after 3 years. **(4) Progressive bulbar palsy (PBP)**: the disease may have only upper or lower motor neuron signs or mixed signs with slow progression. PBP reflects the involvement of motor neurons in the lower brainstem as well as corticobulbar tract, and causes the clinical symptoms, such as slurred speech and swallowing difficulties. If the symptoms are restricted into either upper or lower motor neuron signs, it is usually resistant to progress to ALS. Other less common subtypes include Flail arm and Flail leg syndrome²⁰.

Epidemiological studies have reported that the incidence of ALS is 2–3 per year per 100,000 population over the age of 18 years in most countries²¹. The prevalence of ALS is about 5 per 100,000 population, indicating the rapid progression and lethality of the disease. The lifetime risk for men developing sporadic ALS (sALS) is 1.6 times higher than women, while the incidence of developing familial ALS (fALS), which means a patient inheriting the genetic mutation from the family, is similar between men and women. Both age and genetic mutation are considered risk factors for ALS. sALS

has an average onset-age of 58–63 years, whereas fALS has an average onset-age of 47–52 years, suggesting that genetic causes indeed accelerates the disease onset. A large-scale epidemiological study from the National ALS Registry reported that the peak risk of ALS was at 70–79 years of age but the risk declined after the age of 80 years old in the United State²². This may be due to diagnostic uncertainty. Medical problems occurring at that ages are more likely referred to as a normal consequence of aging or other most common neurodegenerative diseases, such as AD and PD, rather than ALS.

About 90% of ALS cases are sporadic but ~10% are considered to be fALS¹⁵. Mutations in more than 30 causal or susceptibility genes have been found associated with ALS²³ (**Table 1-1**). Notably, genetic mutations passed within the families from generation to generation usually belong to the autosomal dominant inheritance with high penetrance. Of the known genes, mutations in *SOD1*, *TARDBP*, *FUS* and *C9orf72* account for ~60% of fALS^{2,24}. Dominant missense mutations in *SOD1* gene were the first identified genetic cause of ALS¹. Although more than 100 mutations have been found in *SOD1*, which are responsible for 12–20% of fALS and 1–3% of sALS, mutations in the same gene can generate a wide range of phenotypes. The A4V mutation causes a very aggressive form of ALS and leads to death within a year after disease onset, whereas the D90A mutation leads to a slow disease progression and patients with this mutation may survive more than 10 years²⁵. The primary function of SOD1 (superoxide dismutase 1) acts as a cytosolic and mitochondrial antioxidant enzyme to catalyze the reduction of the superoxide anion to O₂ and H₂O₂. Mutations in SOD1 may lead to the loss of normal function, which was considered to cause sensitivity to oxidative stress as the mechanism leading to the death of motor neurons. However, as compared to the wild-type protein,

SOD1 mutant protein forms misfolded oligomers and ultimately aggregates. Aggregation of mutant SOD1 and neuronal degeneration were observed in cultured cells and an SOD1^{G93A} transgenic mouse model²⁶, suggesting that protein aggregation may also contribute to neurotoxicity. The detection of mutant SOD1 in cytoplasmic ubiquitin-positive inclusions in the affected motor neurons of fALS cases would further support the role of pathological protein aggregation underlying the disease mechanism of fALS²⁷. Although the pathogenicity of SOD1 mutants is not fully understood, its toxic gain-of-function has been widely accepted as the major cause of SOD1 ALS²⁸.

Mutations in *TARDBP* gene account for ~4% of fALS. More than 70 missense mutations or variants have been identified across exons, introns, 5'- and 3'-untranslated region (UTR) region of *TARDBP*²⁹. The majority of mutations are clustered in *TARDBP* exon 6, which encodes the C-terminal glycine-rich domain of the TDP-43. Several causative missense mutations in this domain have been identified, such as G294A, Q331K and M337V. TDP-43 mutants cause neural apoptosis and developmental delay in the chick embryos expressing TDP-43^{Q331K} and TDP-43^{M337V} as compared to wild-type TDP-43⁷. TDP-43 and other ALS-associated RNA-binding proteins (RBPs), FUS and hnRNPA1, are the members of heterogeneous nuclear ribonucleoprotein (hnRNP) family that play role in various aspects of transcriptional and post-transcriptional regulation. TDP-43 and FUS exhibit a similar function in RNA binding and splicing, whereas TDP-43 and hnRNPA1 share structural similarity in the glycine-rich domains. Some missense mutations in TDP-43 and hnRNPA1 take place in the evolutionarily conserved positions in this domain²⁹. The glycine-rich domains of TDP-43, hnRNPA1 as well as hnRNPA2/B1 participate in RNA-protein or protein-protein interactions. Once the

function to the glycine-rich domain is compromised, it could cause neuronal dysfunction and degeneration in ALS from a common pathological mechanism. Notably, although genetic mutations in *TARDBP* are relatively rare in ALS, cytoplasmic inclusions of TDP-43 were discovered in the CNS tissue of ~97% ALS^{13,14}. This initial finding has been confirmed in numerous independent studies³⁰⁻³⁵ (**Fig. 1-1**). The exceptions are the SOD1 and FUS-related proteinopathies, accounting for the remaining 3% of TDP-43 inclusion-negative ALS cases. TDP-43 proteinopathy stands out as the most common pathological signature in ALS. The histopathology reflects the loss of nuclear TDP-43 immunoreactivity and the formation of aberrant inclusions in the cytoplasm containing TDP-43 with typical disease features of hyper-phosphorylation, ubiquitination and cleavage into C-terminal fragments. Strikingly, TDP-43 proteinopathy is also found in ~50% of FTD cases, and ~45% of AD and PD cases, suggesting its broad impact on other neurodegenerative disorders^{15,36}.

Hexanucleotide repeat expansion (HRE) of a GGGGCC (G_4C_2) sequence in the first intron of the chromosome 9 open reading frame 72 (*C9orf72*) gene accounts for 25–40% of fALS and 7–10% of sALS cases, representing the most common genetic cause of ALS^{2,5,6}. G_4C_2 repeats less than 30 in length are commonly seen in healthy individuals, whereas typically hundreds or even thousands of repeats are present in ALS cases. Interestingly, the repeat expansion mutations in *C9orf72* are also detected in 40% of FTD cases. The length of the G_4C_2 repeats is not correlated with the disease severity and onset, unlike the characteristic correlation of clinical phenotypes with the increasing repeat sizes of CGG sequence in fragile X-associated tremor/ataxia syndrome³⁷ or CTG sequence in myotonic dystrophy type 1³⁸. The biological function of *C9orf72* protein is

poorly understood, but from the aspect of protein structure, it may associate with the function of GDP-GTP nucleotide exchange factor³⁹. However, the knockout of *C9orf72* did not cause noticeable neuronal phenotypes and motor dysfunction in the mouse model, but the mice developed neuroinflammation, splenomegaly and lymphadenopathy^{40,41}. Although, these studies implicated the non-cell autonomous toxicity underlying the mechanism of *C9orf72* ALS, how the pathological repeat expansion in *C9orf72* links to motor neuron disease remains unclear. Several mechanisms have been proposed. G₄C₂-repeat RNA can undergo a non-canonical translation in the absence of a start codon, called repeat-associated non-ATG-dependent (RAN) translation, and generate dipeptide repeat proteins (DPRs). The sense and antisense *C9orf72* RNA potentially encodes a total of five different DPRs, including glycine-proline (GP), glycine-alanine (GA) and glycine-arginine (GR), proline-arginine (PR) and proline-alanine (PA)^{42,43}. These DPRs have been detected in the frontal cortex, motor cortex, hippocampus and spinal cord of individuals with disease-associated expansions in *C9orf72*⁴². Among these DPRs, poly-GA carries misfolding and aggregation properties and is highly susceptible to form cytoplasmic inclusions. Poly-GP and poly-GR, to lesser extent, can also form protein aggregates⁴⁴. Notably, these aggregation-prone DPRs form p62-positive but TDP-43-negative inclusions in the brain⁴⁴, but are only occasionally observed in the affected motor neurons of spinal cord where p62- and ubiquitin-positive TDP-43 aggregates are commonly seen⁴⁵. Therefore, whether DPRs associated toxic gain-of-function contributes to motor neuron degeneration in ALS remains controversial. Other possible mechanisms include a toxic gain-of-function from G₄C₂-repeat RNA or a loss-of-function due to haploinsufficiency of *C9orf72* protein^{24,46}. As no consensus has been reached on the

molecular mechanism, it is imperative to gain a better understanding of the role of *C9orf72*-mediated pathology in ALS.

1.1.2 Frontotemporal dementia (FTD)

FTD is the second common form of early-onset dementia in the age group of 45–64 years. The disease is associated with the selective neuronal loss in the frontal lobe, anterior temporal lobe, anterior cingulate cortex and insular cortex, and frequently referred to an anatomopathological term frontotemporal lobar degeneration (FTLD)⁴⁷.

FTD is a typical presenile degenerative dementia as the presence of initial clinical symptoms before age of 65 years accounts for ~80% of FTD cases. The incidence of FTD is 2.7–4.1 per year per 100,000 population and the prevalence of the disease is 10–30 per 100,000 population between age of 45–65 years⁴⁷⁻⁴⁹. The average survival time after symptom onset is ~8 years and death is often caused by respiratory failures (i.e. pneumonia). FTD can manifest as three clinical subtypes on the basis of the initial symptoms: alteration of social behavioral and personality or deficits in language production and comprehension. (1) The most common subtype of FTD is behavioral-variant FTD (bvFTD), which accounts for more than 50% of FTD cases. The clinical symptoms include behavioral disinhibition, personality changes, apathy, loss of empathy and stereotypical or compulsive behaviors. Individuals with bvFTD often exhibit impaired executive skills, while their visuospatial skills and memory are relatively preserved during the early stages. Some cases meet the criteria for bvFTD but show very slow disease progression. This is called bvFTD phenocopy syndrome which often has primary psychiatric disorders such as bipolar disorder⁵⁰. (2) Individuals with primary

progressive aphasia (PPA) have progressive and prominent language deficits including the difficulties in language production, object naming, syntax or word comprehension. The visuospatial skills and episodic and visual memory is usually spare in the early stages, while if the patients have visuospatial impairment or episodic and visual memory impairment, they are frequently referred to AD. PPA can be sub-classified into semantic dementia (SD) and progressive nonfluent aphasia (PNFA). Individuals with SD constitute 20–25% of FTD case. These patients exhibit anomia for people, places and objects, and impaired word comprehension and object knowledge, but retain correct grammar and fluent speech in the early stages⁵¹. SD is usually caused by the asymmetrical degeneration of anterior temporal lobes and amygdala⁵². Individuals with PNFA compose of 25% of FTD cases. The patients present hesitant and effortful speech with misuse of grammar and impaired sentence comprehension while single-word comprehension and object knowledge are relatively preserved^{51,53}. Despite the establishment of diagnostic criteria for different subtypes of FTD, the clinical symptoms are often mixed and patients may develop global cognitive impairments and motor dysfunction as the disease spreads from focal to diffuse degeneration in the frontal and temporal lobes. In the past decade, researchers have gained greater insights into the co-occurrence of cognitive impairments and motor neurons disease^{54,55}. Clinical analysis of FTD cases with motor neuron disease revealed that 27–36% of FTD cases exhibited minor motor system dysfunction and 12–15% of FTD cases had definite motor neuron disease⁵⁵⁻⁵⁷. On the other hand, studies have also reported that 22–51% of ALS cases presented mild cognitive impairments and 15–22% had severe cognitive impairments with clinical diagnosis of FTD^{55,58,59}.

Genetic and pathological evidence also supports that ALS and FTD could be a disease continuum. Approximate 60% of FTD cases are considered to be sporadic, whereas the remaining 40% show a family history with an autosomal dominant pattern of inheritance. Mutations in *MAPT*⁶⁰, *GRN*^{61,62} and *C9orf72*⁵ genes accounts for 40–50% of familial FTD cases⁶³. Mutations in several other FTD-associated genes, such as *CHMP2B* and *VCP* gene as well as ALS-associated *TARDBP* and *FUS* gene are relatively rare (< 1%). Genetic analysis showed the first conclusive linkage to chromosome 17 associated with autosomal dominant FTD, termed FTDP-17⁶⁴. Affected families members exhibited a common clinical symptoms including dementia, parkinsonism and disinhibition. *MAPT* (encoding microtubule-associated protein tau) and *GRN* (encoding progranulin) are the most prevalent FTD genes located on chromosome 17. Mutations in *MAPT* gene account for 10–41% of familial FTD cases and the majority of FTDP-17 cases, and more than 50 mutations have already been reported^{65,66}. The most common mutations, N279K and P301L, and intronic mutations near *MAPT* exon 10 both affect the alternative splicing of this exon and pathologically increase the expression of tau with four microtubule-binding repeats than three repeats isoform. Other mutations within exon 10 can disturb the binding properties of tau to microtubules and generate a large number of unbound tau species. Either the defects in alternative splicing or the increased abundance of free tau proteins enhances the aggregation propensity and trigger the intracellular accumulation of tau⁶⁷. Mutations in *GRN* account for 5–20% of FTD cases and show age-dependent penetrance⁶⁸. Progranulin, a secreted glycoprotein growth factor, is a *GRN* encoded protein widely expressed in many cell types. It is composed of seven smaller proteins called granulins, which can be individually liberated by proteolytic cleavage. More than

60 mutations have been found in *GRN* and primarily cause a loss-of-function, resulting in progranulin haploinsufficiency. Although the role of progranulin in the CNS is not clear, their neurotrophic function may regulate neuronal survival and neurite outgrowth^{69,70}. The reduction of progranulin is associated with the progression of neurodegeneration^{71,72}. Additionally, mutations in *C9orf72* account for 11–25% of familial FTD and 17% of ALS-FTD cases^{5,73}.

Pathological subtypes of FTLN can be characterized by the types and patterns of protein inclusion from the neuropathological evidence. Tau-positive aggregates are the first identified pathology in ca 50% of FTLN, while the other half of patients show tau-negative but ubiquitin-positive inclusions. Around 80–95% of the ubiquitin-positive inclusions are positive for TDP-43 and FUS, whereas the nature of the remaining inclusions is still unknown. Based on these major inclusion components, FTLN subtypes are classified into FTLN-Tau and FTLN-U, which can be further classified into FTLN-TDP, FTLN-FUS and FTLN-UPS⁴⁹ (**Fig. 1-2**). FTLN-Tau accounts for 36–45% of FTLN cases, whereas more than 45–50% of FTLN cases are characterized as FTLN-TDP^{32,74} (**Fig. 1-1**). FTLN-TDP can be sub-classified into four types on the basis of TDP-43 aggregation patterns and cortical neuronal pathology. Notably, the identification of TDP-43 proteinopathy and mutations in *C9orf72* and *VCP* gene strongly suggests a common pathogenetic defect in the ALS/FTD disease spectrum.

1.1.3 Other TDP-43 proteinopathy: Alzheimer's disease (AD)

AD is the most common form of dementia and accounts for over 50% of all dementia cases. Age is the most largest risk factor. The incidence of AD is 6.25 per year per 1000

population but the incidence significantly increases with age from 2.8 per year per 1000 population at the age of 65–69 years to 56.1 over age the of 90 years. It has been predicted from longitudinal and population-based studies that 3% of people at the age of 65–74 years but 32% of people over the age of 85 years have AD^{75,76}. The lifespan for AD cases is 3–10 years⁷⁷. The development of AD starts from **(1) Preclinical stage**: patients have normal cognitive function, **(2) Predementia AD or mild cognitive impairment stage**: patients have mild impairment in memory but preserve functional activities to **(3) Dementia**: patients present severe loss of memory and daily function⁷⁸.

AD is probably caused by an interplay of complex genetic, molecular and environmental factors. Several genetic mutations have been found highly associated the pathogenesis of AD, including the mutations in *APP*, *APOE*, *PS-1* and *PS-2* genes⁷⁹. While the molecular mechanism for AD is still unclear, it is generally accepted that AD is a poly-proteinopathy, resulting from the inter- and intra-cellular deposition of multiple proteins, including amyloid plaques composed of A β peptides, the metabolites derived from amyloid precursor protein (APP), and neurofibrillary tangles (NFTs) made up of aggregated tau with abnormal phosphorylation and acetylation⁷⁹. Recently, TDP-43 pathology was found in 23–50% of AD and 71 % of hippocampal sclerosis cases as a potential co-factor^{80,81}. Full-length or C-terminally truncated TDP-43 is present in both granular NII and NCI in either soma or neurites, whereas TDP-43 immunoreactivity can also be detected in a few of A β ₁₋₄₂ and NFTs^{80,82}. It is hypothesized that the deposition of TDP-43 can act as a secondary pathology dependent on tau or A β pathogenic pathways³⁶. In addition, the topographical analysis of TDP-43 proteins in AD brains showed the spreading patterns of pathological TDP-43 from amygdala (stage I), entorhinal cortex and

subiculum (stage II), dentate gyrus and occipitotemporal cortex (stage III), inferior temporal cortex (stage IV) to frontal cortex and basal ganglia (stage V)⁸¹. Therefore, understanding of the role of TDP-43 in neurodegeneration will help to shed light on the molecular pathways of AD.

1.2 TAR DNA-binding protein 43 (TDP-43)

1.2.1 Structure

TDP-43 is a 414 amino acid protein encoded by the *TARDBP* gene and is highly conserved across multiple species from mammals, *Drosophila* to *C. elegans* (**Fig. 1-3**). TDP-43 is an RBP and belongs to the hnRNP family, a group of proteins with diverse roles in RNA metabolism⁸³. It contains two well-conserved RNA-recognition motifs (RRM1 and RRM2) at the N-terminus. The RRM domains of human TDP-43 share ~70% evolutionary conservation with those of mouse and *Drosophila* but less with *C. elegans*. However, beyond RRM domains, the similarity drops to 30%⁸⁴. RRM1 has higher nucleotide-binding activity than RRM2, and plays a dominant role in RNA binding, splicing and auto-regulation. TDP-43 preferentially binds to RNA UG-rich RNA sequences, which are found abundantly in long introns and 3'-UTR, for the regulation of RNA processing, but it may also bind to non-UG rich sequences for polyadenylation site selection^{85, 86, 87}. Six tandem UG repeats have significantly higher binding activity to TDP-43 RRMs⁸⁵. High-throughput sequencing for RNA targets of TDP-43 in human brain using individual-nucleotide resolution crosslinking immunoprecipitation (iCLIP) identified introns, 3'-UTRs and long non-coding RNAs as the preferential binding sites of TDP-43^{86, 87}, and found more than 6000 binding targets, such as *CNTFR*, *MEF2D* and

BIM mRNA, and *NEAT1* and *MALAT1* (also known as *NEAT2*) long noncoding RNAs. Structural analysis revealed that TDP-43 RRM1, especially RRM1, were also responsible for homodimerization^{88,89}.

TDP-43 has a bipartite nuclear localization signal (NLS) at amino acids 82-98 and a nuclear export signal (NES) at amino acids 239-250. Although TDP-43 predominantly resides in the nucleus, these sequences allow the protein to shuttle between the nucleus and cytoplasm to participate in various biological functions within these two compartments. The nucleocytoplasmic shuttling property adds to the complexity of TDP-43 function. The disturbance of the protein localization in disease may interfere with multiple cellular functions and may be a crucial aspect for disease pathogenesis. Mutations of the NLS induced the cytoplasmic mislocalization of TDP-43, whereas mutation of the NES triggered the formation of intranuclear inclusions^{90,91}.

The C-terminal glycine-rich domain of TDP-43 is a low-complexity domain with prion-related Q/N sequence^{92,93}. The glycine-rich domain only exists in the mammalian and *Drosophila* but not the *C. elegans* ortholog, suggesting the divergence of TDP-43 function in different organisms. The prion-like domain of TDP-43 is not structurally similar to mammalian prion protein, but rather to yeast prion, which may form reversible and functional aggregation without infectivity. However, the identification of the prion-like domain in TDP-43 may implicate the potential cellular propagation, similar to tau and α -synuclein^{94,95}, and the aggregation properties, which has been shown in several *in vitro* assays^{96,97}. The C-terminus of TDP-43 participates in transcriptional suppression, alternative splicing and protein-protein interaction with other hnRNP family members⁹⁸⁻¹⁰⁰. The deletion of the C-terminus resulted in the loss of exon-skipping of exon 9 in

cystic fibrosis transmembrane regulator (*CFTR*) transcript⁸⁴. Notably, the glycine-rich domain harbors most of the missense mutations identified in ALS patients^{7,8,29}. Disease-causing mutations in this region have been shown to remodel the protein dynamics and energy landscape of TDP-43 to favor the formation of amyloid fibrils or irreversible aggregation. These mutations also promoted the cytoplasmic TDP-43 mislocalization and pathological aggregation in cultured cells and animal models of TDP-43 proteinopathy¹⁰¹⁻

103

1.2.2 Normal TDP-43 function

A thorough understanding of protein structure provides a fundamental basis for determining protein function. Biochemical and molecular analysis reveal essential and multiple functions of TDP-43 in the transcription regulation, RNA metabolism, miRNA biogenesis, RNA transport and local translation¹⁰⁴ (**Fig. 1-4**). TDP-43 was originally identified as a transcriptional suppressor of TAR DNA of the human immunodeficiency virus type 1 (HIV-1) and *SP-10* gene^{100,105}. TDP-43 plays an important role in the regulation of alternative splicing by binding to intronic UG-repeats and its overexpression causes exon skipping in transcripts, such as *CFTR*, *ApoA2* and *SMN*¹⁰⁶⁻¹⁰⁸. Importantly, the nuclear and cytoplasmic levels of TDP-43 are tightly regulated¹⁰⁹. TDP-43 auto-regulates its mRNA level to control the expression by binding to the 3'-UTR of its transcript and interplaying between alternative splicing, nonsense-mediated decay and alternative polyadenylation site selection through a negative feedback loop¹¹⁰. TDP-43 may be involved in miRNA biogenesis via interaction with argonaute 2 and DDX17¹¹¹. The knockdown of TDP-43 altered the miRNA levels of let-7b, miR-663 and miR-132¹¹². TDP-43 is actively transported in axons of motor neurons and regulates axon

outgrowth¹¹³. It has been reported to play a direct role in the axonal transport of *NFL* mRNA to the injured site for local translation following axotomy^{114,115}. Under stressful conditions, the incorporation of TDP-43 into stress granules (SGs) is mediated by the interaction with SG-associated proteins TIA-1 and G3BP. Knockdown of TDP-43 did not cause the disappearance but slowed the assembly of SGs, suggesting it may play an indirect role in the regulation of SG dynamics¹¹⁶.

1.2.3 TDP-43 mislocalization and aggregation

The histopathology of ALS/FTD is characterized by the presence of abundant TDP-43 inclusions mainly in the cytoplasm but occasionally in the nucleus of the affected neurons in brain and spinal cord. As a consequence of this mislocalization, TDP-43 is depleted from the nucleus. Other pathological changes include aberrant post-translational modifications, such as hyper-phosphorylation at serine residues 379, 403/404 and 409/410, ubiquitination at multiple sites, acetylation at two lysine residues 145 and 192, and C-terminal cleavage. Aside from age and genetic mutation, prolonged stress and nucleocytoplasmic transport defects have been reported as potential contributing factors for TDP-43 pathology¹¹⁷⁻¹²¹. To date, two non-exclusive disease mechanisms have been proposed with respect to TDP-43 pathology, loss-of-function due to the depletion of normal nuclear TDP-43 or toxic gain-of-function via protein sequestration into pathological cytoplasmic TDP-43 aggregates (**Fig. 1-4**). Therefore, the specific molecular mechanisms for TDP-43 pathology still need to be determined.

The increased cytoplasmic mislocalization of TDP-43 in the CNS tissue of patients has been proposed to be the first step of TDP-43 proteinopathy. In various

cellular and animal models the expression of either wild-type or ALS-linked mutant TDP-43 consistently triggered the cytoplasmic mislocalization of TDP-43 and induced apoptosis and neurotoxicity^{35,122-124}. Although overexpression of wild-type TDP-43 increased cytoplasmic TDP-43 levels, mutant TDP-43 indeed increased a greater proportion of cytoplasmic mislocalization than wild-type TDP-43 did^{124,125}, suggesting the localization of TDP-43 is crucial to neuronal survival. However, the nuclear depletion of TDP-43 also may be a consequence of the cytoplasmic mislocalization. In TDP-43-knockout *Drosophila* and zebrafish models, the animal exhibited a severe loss of neuromuscular junctions and motor dysfunction^{126,127}. What triggers the relocation of nuclear TDP-43 into the cytoplasm is still unclear. As TDP-43 plays a cytoplasmic role in the regulation of SG dynamics, it has been hypothesized that chronic stress may trigger the increased cytoplasmic localization of TDP-43¹¹⁷. Fluorescent staining in cultured cells and human post-mortem tissue revealed the co-localization of TDP-43 with the SG marker TIA-1 in the cytoplasm³⁵. The evidence provides the first evidence for a connection between SG formation and TDP-43 pathology in age-dependent neurodegenerative diseases.

Following initial cytoplasmic mislocalization, the formation of granular aggregates, designated ‘pre-inclusions’, is considered the next event in TDP-43 pathology. The round or skein-like inclusions in the cytoplasm of affected cortical and spinal motor neurons are the disease hallmark of TDP-43 pathology in ALS, whereas a wider variety of TDP-43 aggregate patterns, cortical neuropathology and affected regions have been systemically described in FTLTDP (Fig.1.1). Double-label immunofluorescence indicates that TDP-43 aggregates are hyper-phosphorylated and

ubiquitinated, and co-localized with p62/SQSTM1 (sequestosome-1), an autophagy adaptor. Notably, aggregated C-terminal cleavage products (20–25 kDa) are only observed in the brain tissue of ALS and FTLD-TDP cases, whereas full-length TDP-43 aggregates are both detected in the brain and spinal cord^{13,30}. Biochemical studies demonstrate that purified TDP-43 is intrinsically aggregation-prone and rapidly forms oligomeric complexes and aggregates after agitation⁹⁷. TDP-43 protein extracted from the CNS tissue of ALS or FTD cases exhibited seeded polymerization and toxic effects in cells¹²⁸. The aggregated proteins are sarkosyl-insoluble and contain hyper-phosphorylated 45-kDa species and ubiquitinated high-molecular oligomeric and truncated 20–25-kDa C-terminal species^{13,30,129}. Similar TDP-43 oligomers were also detected in the brain of FTD cases¹³⁰, suggesting that toxic TDP-43 oligomers may be associated with the pathogenesis. The C-terminal truncation may be generated by proteolytic cleavage of full-length TDP-43. Apoptotic effector caspase-3 and calpain, Ca²⁺-dependent cysteine protease, have been identified as the major proteases involved in the generation of 25–35 kDa C-terminal products. TDP-43 contains three different caspase-3 cleavage sites. The activation of apoptosis by staurosporine induction increased the production of C-terminal fragments. Furthermore, the C-terminal glycine-rich domain of TDP-43 has a propensity for aggregation. This prion-like domain drives TDP-43 misfolding, while the deletion of the prion-like domain prevents TDP-43 aggregation¹³¹. The expression of C-terminal fragments recapitulates cytoplasmic TDP-43 aggregation and disease-related post-translational modifications *in vivo* and *in vitro*^{34,113,125,132,133}, suggesting that the protease-mediated TDP-43 cleavage may be a factor that triggers the cytoplasmic aggregation of TDP-43. However, other TDP-43 transgenic mice also exhibit similar neuropathological

phenotypes without the expression of C-terminal fragments^{91,123}. The C-terminal fragments can enhance cellular toxicity and apoptosis in neurons^{125,133}. As the C-terminal domain of TDP-43 is responsible for protein-protein interaction, whether the sequestration of TDP-43 binding protein including itself causes a toxic gain-of-function or a dominant-negative mechanism leads to a loss-of-function requires further investigation.

Causative mutations in TDP-43 have been characterized in a small subset of ALS cases^{7,8}. Among those mutations, functional study for Q331K and M337V mutation revealed increased apoptosis and delayed development of limbs and tail in the chicken embryos expressing TDP-43 mutants but not wild-type TDP-43⁷. The prion-like domain is intrinsically disordered and allows for the formation of dynamic and reversible oligomers. Several missense mutations in the domain increase the tendency of TDP-43 to form aggregates. Purified TDP-43 protein with A315E and M337V mutations but not wild-type TDP-43 accelerated self-assembly with increased protein concentrations and formed amyloid structure¹⁰². Furthermore, in a cell culture system, inhibiting proteasomal degradation via the proteasomal inhibitor MG-132, consistently induced the accumulation of detergent-insoluble protein products of ~25–35 kDa in lymphoblastoid cell lines derived from ALS cases with M337V, N345K, G348C, R361S, I383V or N390D mutations but not from control individuals^{8,11}. The A315T mutant enhanced neurotoxicity, accumulation of high-molecular-weight (60–75 kDa) and protease-resistant TDP-43 species, and protein aggregation and fibrillation in cultured cells and *Drosophila* models¹⁰¹. These studies explored the biochemical properties of wild-type, C-terminal truncated and mutant TDP-43 *in vivo* and *in vitro*, and suggested that the

misfolding and aggregation properties may explain the widespread TDP-43 inclusions in ALS/FTD cases.

1.3 Models of TDP-43 aggregation

1.3.1 Aberrant stress granule (SG) formation

SGs as one type of membraneless and phase-dense organelles present in the cytoplasm under stress conditions (e.g. heat shock, viral infection, oxidative conditions, ultraviolet irradiation, hypoxia)¹³⁴. The core constituents of SGs include translation-initiation factors and polyA-binding proteins (e.g. eIF4E, eIF4G, eIF3, PABP1/PABPC1), non-translating mRNAs, and RBPs (e.g. TIA-1/ TIAR, G3BP, HuR, FXR1, CPEB)¹³⁴. SG formation is initiated by the phosphorylation of eIF2 α , which prevents the assembly of the 48S pre-initiation complex and stalls translation. Non-translating mRNAs and their RBPs form the aggregate-like structures¹³⁵. In eukaryotic cells, SG formation has been considered a protective mechanism when a cell is exposed to stress. SGs silence global translation to conserve energy but selectively upregulate expression of heat shock proteins to prevent protein misfolding. Interestingly, many SG-associated RBPs contain aggregation-prone yeast prion-like domains, which are important for RNA-protein and protein-protein interactions¹¹⁷. The presence of prion-like domains allows proteins to rapidly assemble and nucleate RNP granules, and reversibly disassemble when stress is removed. Importantly, recent studies showed that several ALS-associated RBPs (e.g. TDP-43, FUS, TAF15, hnRNPA1, hnRNPA2/B1, ataxin-2) were also detected in the SGs¹³⁶. Considering the high percentage of proteins carrying prion-like sequences among SG components, it has been hypothesized that the persistent

or aberrant SG formation may act as a cause of the cytoplasmic aggregation of TDP-43¹³⁶.

Studies have consistently shown that TDP-43 has a role in SG regulation. TDP-43 is recruited into SGs under various stress conditions and co-localizes with well-known SGs markers TIA-1, TIAR or G3BP in cultured cells and postmortem tissue from ALS cases^{35,137}. Similarly, other ALS-associated proteins with prion-like domains, FUS and hnRNPA1, are also found in SGs^{138,139}. However, TDP-43 is not an essential component of SGs. It regulates the transcript levels of SG-associated proteins but not the integrity of SG formation, although TDP-43 knockdown also affected SG size¹¹⁶. Additionally, mutations in TDP-43 as well as other SG-associated proteins caused delayed disassembly of SGs and enhanced the liquid-to-solid phase transition and aggregated state^{140,141}. Moreover, TDP-43 might receive multiple post-translational modifications in the SGs, such as phosphorylation, ubiquitination and cleavage¹⁴². These modifications increased TDP-43 stability and prevented the protein from returning into the soluble phase, which may accelerate TDP-43 aggregation. As TDP-43 is sensitive to proteases, the protein may be exposed to proteolytic processing in the SGs and generate small C-terminal cleavage products. The sequestration of TIA-1, G3BP and eIF3 into cytoplasmic TDP-43 aggregates was found in cultured cells and postmortem tissue from ALS and FTD cases³⁵. This abnormal accumulation of RBPs and translation initiators may subsequently interfere with SG formation and disturb RNA and protein homeostasis by interfering with transcriptional and translational regulation. However, pathological aggregation is thought to be a long-term process *in vivo*. It has been speculated that the persistent SG formation caused by chronic stress may nucleate aggregation-prone proteins for oligomeric seeding.

The self-assembly properties of TDP-43 as well as other ALS-associated proteins may be responsible for the increased protein stability and aggregation formation in disease¹³⁶.

These common features strongly suggest the role of aberrant SG formation underlying the mechanism of neurodegenerative diseases.

An unbiased genetic screen in yeast identified the loss of *Pbp1*, the yeast homolog of human *ATXN2*, as an exclusive and potent suppressor of TDP-43 toxicity but not of other neurodegenerative disorder-associated proteins (e.g. α -synuclein, mutant huntingtin)¹⁴³. Notably, an expanded CAG trinucleotide repeats encoding poly-glutamine (polyQ) within the open reading frame of the *ATXN2* gene causes spinocerebellar ataxia type 2 (SCA2), one type of autosomal dominant cerebellar ataxias. Interestingly, motor neuron degeneration is also observed in SCA2. A polyQ expansion with more than 34 repeats is typically associated with SCA2, whereas a large-scale analysis of ALS populations revealed that the intermediate-length polyQ expansion of 27–33 repeats increased the risk of ALS^{143,144}. Ataxin-2 protein interacts with TDP-43 in an RNA-dependent manner through its PAM2 motif, which mediates interaction with PABP¹⁴⁵. The overexpression of *ATXN2* and *PABP* (human homolog of yeast *Pab1*) in *Drosophila* retinal neurons enhanced TDP-43 toxicity, resulting in severe age-dependent retinal degeneration and accumulation of insoluble TDP-43. Ataxin-2 with intermediate-length polyQ expansion has stronger binding activity for TDP-43 than wild-type ataxin-2, and may cause the redistribution of TDP-43 into SGs and the generation of phosphorylated TDP-43 C-terminal fragments^{143,146}. Given that ataxin-2 and PABP exhibited important roles in SG regulation¹⁴⁷, the

intermediate-length polyQ expansion and aberrant stress response may be a shared mechanism underlying pathological TDP-43 aggregation. The frequency of the presence of cytoplasmic mislocalized ataxin-2 and PABP and punctate-like aggregates in the spinal motor neurons of ALS were moderate.

Other SG-related gene *YGR054W* (homolog of human translation initiation factor, eIF2 α) was also a genetic modifier of TDP-43 toxicity¹⁴⁵. The study showed an increase in eIF2 α phosphorylation in fly's brain after long-term expression of TDP-43, which indicated a prolonged repression of translation. The knockdown of PEK (*Drosophila* homolog of mammalian PERK), a kinase responsible for eIF2 α phosphorylation, inhibited SG formation and suppressed TDP-43-mediated motor deficits, suggesting the suppression of vibrant SG activity via the inhibition of eIF2 α phosphorylation may mitigate TDP-43 toxicity. For potential disease treatment, the authors tested a pharmacological rescue strategy by targeting eIF2 α phosphorylation. The inhibition of PEK activity via a small-molecule, GSK2606414, significantly reduced eIF2 α phosphorylation and mitigated the TDP-43-mediated cell death and motor dysfunction in mammalian neurons and flies. These data suggest that the changes in signaling pathways due to prolonged stress is highly associated with TDP-43 toxicity, and that reduction of aberrant stress response may be a novel therapeutic strategy for TDP-43 pathology.

1.3.2 Inhibiting nucleocytoplasmic transport

The nuclear envelope (NE) is made up of phospholipid bilayers and associated proteins and separates the genome and nuclear contents from the cytosol. The physical barrier

provides the eukaryotic cell with exclusive environments for transcription and translation. Therefore, the cell requires an elaborate transport system to communicate between these two compartments by exporting RNAs to cytoplasm and importing proteins into the nucleus, to support a variety of biological functions. The nucleocytoplasmic transport of molecules, such as proteins and mRNA packaged in ribonucleoprotein complexes, is accomplished at a cylindrical structure called nuclear pore complex (NPC). The NPC allows passive diffusion of small molecules (< 40 kDa), whereas larger macromolecules require the assistance of nuclear transport factors (TFs) binding to transport signals for their active transport. Most pathways involve an active role of the karyopherin family of transport factors, which can be categorized into the import factors (importins), export factors (exportins) and those that participate in both nuclear import and export. The classic nuclear import pathway requires the recognition of cargos by specific import factors orchestrated by the nucleotide state of Ran and the interaction between cargo:carrier complexes and nuclear pore components termed nucleoporins (Nups). A specific subset of Nups contains phenylalanine-glycine (FG) repeats and is crucial to mediate the translocation of cargo:carrier complexes through NPCs¹⁴⁸. Once Nups age and accumulate oxidative damage, these proteins need to be replaced as the cell requires continuous nucleocytoplasmic shuttling of molecules to sustain proper functions for survival. In dividing cells, NPCs disassemble during mitosis and newly generated NPCs assemble and integrate into NE during interphase¹⁴⁹. Since neurons are post-mitotic cells and exhibit a high degree of morphological polarization due to the outgrowth of long processes (dendrites and axon), they may be especially vulnerable to nucleocytoplasmic transport defects. Recent evidence showed that several Nups were very long-lived

proteins in post-mitotic cells, such as neurons, and the damaged Nups were poorly replaced by protein turnover¹⁵⁰. These Nups were susceptible to oxidative insults during aging, which led to age-related deterioration of NPC integrity^{150,151}. The imbalance of orchestrated nuclear and cytoplasmic RNA and protein levels can lead to irreversible neuronal dysfunction and death. To understand how the impairments of NPC structure and nucleocytoplasmic transport function associate with age-related neurodegenerative diseases will be helpful to unravel the pathogenesis of ALS and FTD.

Nucleocytoplasmic transport dysfunction and the associated pathogenic mechanisms have been widely investigated in various disorders, such as immune diseases, viral infections and cancers¹⁵²; however, little is known about its role in neurodegeneration. Cytoplasmic accumulation of nuclear transport factor 2 (NTF2) in the hippocampal neurons of AD cases has been reported previously¹⁵³. Intriguingly, Kinoshita et al. (2009) examined the integrity of nuclear membrane (NM) in the spinal motor neurons of sALS cases, and found a loss of karyopherin- β 1 immunoreactivity as well as an irregular and ruffled morphology of NMs stained with anti-Nup62 and Nup153. The NM morphological defects were independent of apoptosis and could be observed even in the earlier pre-symptomatic stage. A fragmented contour of NM was seen when the disease progressed¹⁵⁴. The neuropathology may result from the loss or mislocalization of Nups on the NM. The dysfunction of nucleocytoplasmic transport impairs the signal transduction to the nucleus and protein synthesis in the cytoplasm for the replenishment of the loss or damaged proteins, which may subsequently cause neuronal degeneration and death.

On the other hand, defects in the nuclear import of proteins may also result in the nuclear depletion and cytoplasmic mislocalization of normally predominantly nuclear proteins. Loss-of-function and toxic gain-of-function may be non-exclusive mechanisms underlying age-dependent neurodegenerative diseases. An unbiased genetic screen in yeast found that exportin-5 was an enhancer of TDP-43 toxicity when overexpressed¹⁴⁵. Nishimura and Župunski et al. (2010) discovered that knockdown of Nup54, Nup58/45, Nup62, CAS or karyopherin- β 1 consistently caused the cytoplasmic accumulation of TDP-43 in SHSY-5Y cells. Reduction of CAS, karyopherin- α 1 and karyopherin- α 2 protein levels was found in the brain lysates from FTLD-TDP cases, but an increase of karyopherin- α 2 protein level in the spinal cord of ALS cases with TDP-43 inclusions may result from its cytoplasmic increase¹⁵⁵. Mutations in *Gle1* gene (encoding the Gle1 RNA export factor) were recently found in sALS and fALS, including three rare variations: two deletion mutations and one missense mutation. The expression of Gle1 mutants in the Gle1 knockdown zebrafish failed to rescue motor neuron symptoms, suggesting that the affected gene led to a loss-of-function. Interestingly, Gle1 also plays an essential role in translation initiation¹⁵⁶ and SG regulation¹⁵⁷. The expression of ALS-link IVS14-2A>C mutation in Gle1 not only induced larger SG formation but also triggered its cytoplasmic aggregation and co-localization with TDP-43 and Hsp90¹⁵⁸.

The P56S mutation in the ALS-associated VAPB protein caused a dominant-negative effect on the function of endogenous VAPB, and triggered aberrant vacuole-like structures in the NE and cytoplasmic accumulation of Nup214 and Gp210 and inner NM protein, emerin, without affecting the localization of lamin A/C. The knockdown of endogenous VAPB also caused similar deficits¹⁵⁹. Interestingly, the P56S mutant but not

wild-type VAPB induced TDP-43-mediated toxicity and cytoplasmic TDP-43 mislocalization and aggregation without inducing proteolytic cleavage^{160,161}. Those data suggest that inhibition of the nuclear transport of Nups by ALS-linked P56S mutation in VAPB may be the mechanism behind TDP-43 pathology. The novel R86S mutation in *NEMF* (encoding nuclear export mediator factor NEMF) also caused nucleocytoplasmic transport defects and ALS-like phenotypes in the transgenic mouse model¹⁶². Furthermore, neuropathological evidence revealed that pathological TDP-43 aggregates were exclusively found in the affected motor neurons of sALS cases with lower levels of adenosine deaminase acting on RNA 2 (ADAR2), an enzyme for proper RNA editing of AMPA receptor GluA2¹⁶³. The loss of ADAR2 function enhances the influx of Ca²⁺ via the compromised AMPA receptors and activates calpain, a protease that has been previously shown to trigger the cleavage of TDP-43 into C-terminal fragments^{163,164}. Calpain may also increase NPC permeability¹⁶⁵. A recent study showed that calpain induced the cleavage and degradation of Nup62, Nup88 and Nup153 in the ADAR2 conditional knockout mouse model. Co-localization of Nup62 and karyopherin- β 1 with cytoplasmic TDP-43 aggregates and the loss of lamin B immunoreactivity were both observed in the ADAR2-devoid motor neurons of mice and sALS cases¹⁶⁶. These data provide the evidence to support the connection between the deficits in nucleocytoplasmic transport as well as RNA metabolism and the occurrence of TDP-43 inclusions in ALS/FTD cases.

The mechanistic pathway for TDP-43 aggregation in the affected motor neurons of individuals with C9orf72 ALS is still unclear. Three recent studies published in the same year provided mutually supportive evidence that G₄C₂ HRE-mediated neuronal

toxicity may be caused by nucleocytoplasmic transport defects¹¹⁹⁻¹²¹. The first study used a candidate-based genetic screen in a *Drosophila* model that expressed 30x G₄C₂ repeats in the fly eyes, and identified overexpression of RanGAP as a potent suppressor of (G₄C₂)₃₀-mediated toxicity. The sequestration of RanGAP protein by (G₄C₂)₃₀ RNA may disturb the nuclear levels of Ran and impair the nuclear import-export function, which was consistently correlated with the depletion of nuclear TDP-43^{119,167}. As an inter-dependent feedback loop, Ran is the major regulator for the nuclear import of TDP-43, whereas TDP-43 also regulates the transcript levels of Ran through the binding to its 3'UTR¹⁶⁷. These data imply that the compromised nucleocytoplasmic transport may lead to the cytoplasmic accumulation of TDP-43, providing a potential mechanism that may explain the presence of TDP-43 pathology in *C9orf72*-linked ALS. The second study used an unbiased genetic screen in *Drosophila* expressing 58x G₄C₂ repeats in combination with RNAi knockdown of certain gene in the fly eyes, and identified the loss-of-function in 18 genes involving nucleocytoplasmic transport as either genetic enhancers or suppressors of (G₄C₂)₅₈-mediated toxicity¹²⁰. Of these candidates, mutations in genes encoding Nup98, Nup107, Nup160 and Alyref acted as suppressors, whereas mutations in genes encoding Nup50, Nup153, Gle1 and exportin-1 acted as enhancers. Interestingly, Alyref and RanBP1 were also found as components of cytoplasmic TDP-43 aggregates¹⁶⁸. *Nup50* has also been identified as a genetic interactor and modifier of TDP-43 in the *Drosophila* model of TDP-43 pathology. Partial loss-of-function of *Nup50* rescued the survival of TDP-43 flies, which was independence of the change in TDP-43 expression level and localization¹⁶⁹. The third study used unbiased screen in yeast for identifying genetic modifiers of poly-PR toxicity. When overexpressed, several

karyopherin proteins, such as exportin-5, transportin-1 and karyopherin- α 3, acted as potent suppressors, implicating nucleocytoplasmic transport dysfunction as a potential molecular mechanism that underlies DPR pathology¹²¹. The establishment of a poly-GA mouse model shed light on the mechanism of aggregated poly-GA-mediated toxicity and demonstrated that aggregated poly-GA sequestered Pom121, RanGAP1 and HR23 protein whose function involves protein degradation and nucleocytoplasmic transport¹⁷⁰. Taken together, these studies support the idea that the disruption of NPC morphology and nucleocytoplasmic transport processes may be a common pathogenesis of *C9orf72*-linked ALS, and that blocking nuclear transport may be one of the mechanisms leading to TDP-43 proteinopathy. However, TDP-43 proteinopathy occurs in the vast majority of ALS and FTD cases without obvious genetic cause. The nucleocytoplasmic transport dysfunction mediated by ALS-linked genetic mutations may only explain a small subset of ALS/FTD cases. How to mechanistically connect nucleocytoplasmic transport defects to the cytoplasmic TDP-43 accumulation for the majority of ALS/FTD cases has not yet been explained.

1.4 Hypothesis and Objective

To fully understand ALS, it is imperative to unravel how TDP-43 pathology interferes with neuronal function and induces neurotoxicity. Previous studies have shown that cytoplasmic TDP-43 aggregates can sequester a variety of proteins and cause global impairments in RNA and protein homeostasis, which has been proposed as a key mechanism for TDP-43-mediated toxicity within the ALS/FTD continuum. Given neither the composition of TDP-43 aggregates nor the relevant disease mechanisms are well

characterized, we hypothesize that pathologic TDP-43 aggregates sequester essential proteins required for neuronal cell homeostasis and survival. We expect that these findings will be relevant for the pathogenesis of the vast majority of ALS and FTD cases and improve our understanding of cellular and molecular mechanisms of TDP-43 pathology. However, due to the technical limitation, a major challenge in proteomics is to analyze the protein interaction within insoluble TDP-43 aggregates. Therefore, the objective of this project was to develop a new method for characterizing the interactome of aggregated TDP-43 and investigating the molecular pathways underlying TDP-43 pathology, and to identify candidates for modulating TDP-43 toxicity and aggregation. In Chapter 2, I will characterize the methods and materials used in the dissertation project. Chapter 3 is focused on the identification of nucleocytoplasmic transport defects in TDP-43 pathology using proximity-dependent biotin identification (BioID) method. Chapter 4 addresses the identification of poly(A)-binding protein nuclear 1 (PABPN1) as a potent suppressor of TDP-43 toxicity. In Chapter 5, I will discuss the remaining questions and future directions including addressing the protein-protein interaction between TDP-43 and PABPN1 and a novel role of PABPN1 in the regulation of ubiquitin proteasomal degradation.

1.5 Figures

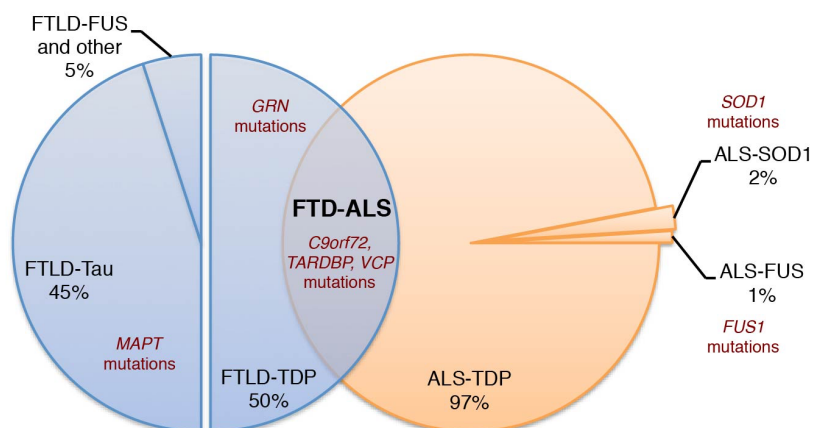


Figure 1-1 | TDP-43 pathology in the FTD-ALS disease spectrum.

ALS with TDP-43 pathology accounts for 97% of ALS cases, and SOD1 and FUS pathology account for the remaining 3%. About 50% of FTD cases belong to FTLD-TDP with TDP-43 pathology and carries pathogenic mutations in *GRN*, *C9orf72*, *TARDBP* and *VCP* and other genes. FTLD-Tau represents cases with mutations in *MAPT* and tau pathology in ~45% of FTD cases. The remaining cases are characterized by FUS-positive inclusions and other unknown pathology. FTD-ALS shows the clinicopathological and genetic overlap of FTLD-TDP and ALS. Although TDP-43 pathology and mutations in *TARDBP*, *C9orf72* and *VCP* genes are found in both ALS and FTD, *TARDBP* mutations are more commonly associated with clinical manifestation as ALS. Abbreviations: ALS, amyotrophic lateral sclerosis; ALS-TDP, ALS with TDP-43-positive inclusions; ALS-SOD1, ALS with SOD1-positive inclusions; ALS-FUS, ALS with FUS-positive inclusions; FTD, frontotemporal dementia; FTLD, frontotemporal lobar degeneration;

FTLD-Tau, FTLD with tau-positive inclusions; FTLD-TDP, FTLD with TDP-43-positive inclusions; FTLD-FUS, FTLD with FUS-positive inclusions.

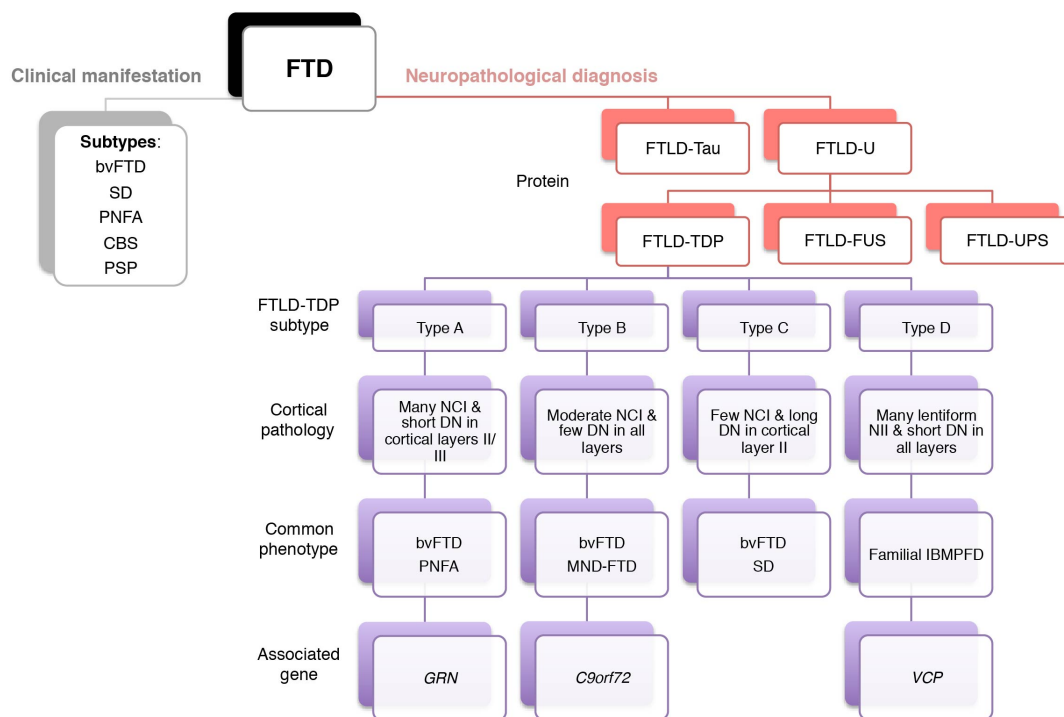


Figure 1-2 | Overview of the clinical, genetic and pathological classification of FTD.

FTD can be classified on the basis of clinical manifestation or neuropathological diagnosis. Clinical subtypes of FTD mainly include: bvFTD, SD, CBS and PSP.

Neuropathological subtypes are characterized by the deposited proteins including FTLD-Tau and FTLD-U, which can be further categorized by the types of ubiquitinated aggregates (i.e. FTLD-TDP, FTLD-FUS and FTLD-UPS). Four subtypes of FTLD-TDP are defined by the morphology of TDP-43-positive aggregates and their distribution in cortical layers, their common phenotypes, and the associated genes. Abbreviations: FTD, frontotemporal dementia; FTLD, frontotemporal lobar degeneration; bvFTD, behavioral variant of FTLD; SD, semantic dementia; progressive non-fluent aphasia; CBS, corticobasal syndrome; PSP, progressive supranuclear palsy; FTLD-Tau, FTLD with tau-positive inclusions; FTLD-U, FTLD with ubiquitin-positive inclusions; FTLD-TDP,

FTLD with TDP-43-positive inclusions; FTLD-FUS, FTLD with FUS-positive inclusions. FTLD-UPS, FTLD with p62-positive and other unknown protein inclusions. NCI, neuronal cytoplasmic inclusions; NII, neuronal intra-nuclear inclusions; DN, dystrophic neuritis; IBMPFD, inclusion body myopathy with Paget's disease of bone and frontotemporal dementia; MND, motor neuron disease; *GRN*, progranulin gene; *C9orf72*, *C9orf72* gene; *VCP*, valosin-containing protein gene.

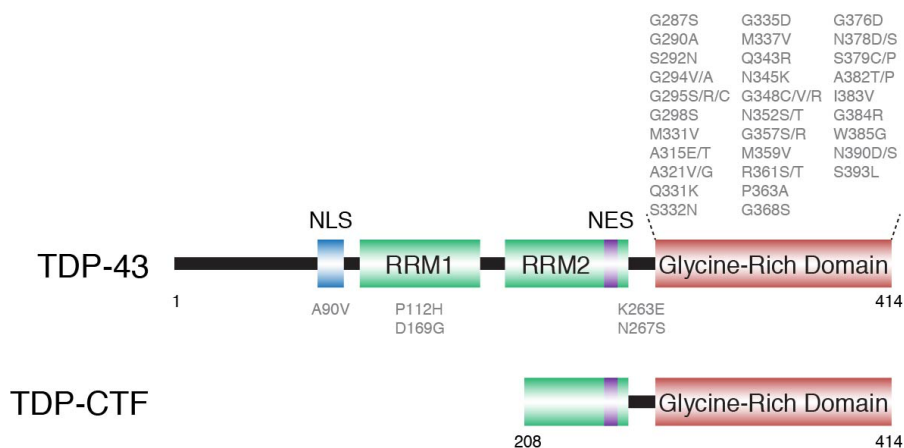


Figure 1-3 | Schematic of functional domains and disease-causing mutations in TDP-43.

TDP-43 shares structural similarities with other RBPs as a member of the hnRNP protein family. **(Top)** Human TDP-43 protein contains a nuclear localization sequence (NLS, aa 82-98), two RNA-recognition motifs (RRMs), a nuclear export signal (NES, aa 239-250), and a glycine-rich C-terminal domain, where the majority of ALS-associated mutations are located. About 50 disease-causing missense mutations are known and indicated. Two mutations, G295S and K263E, are associated with FTD. **(Bottom)** C-terminal fragment from aa 208-414 (TDP-CTF) is a common cleavage product in the brain tissue of ALS and FTLTDP cases.

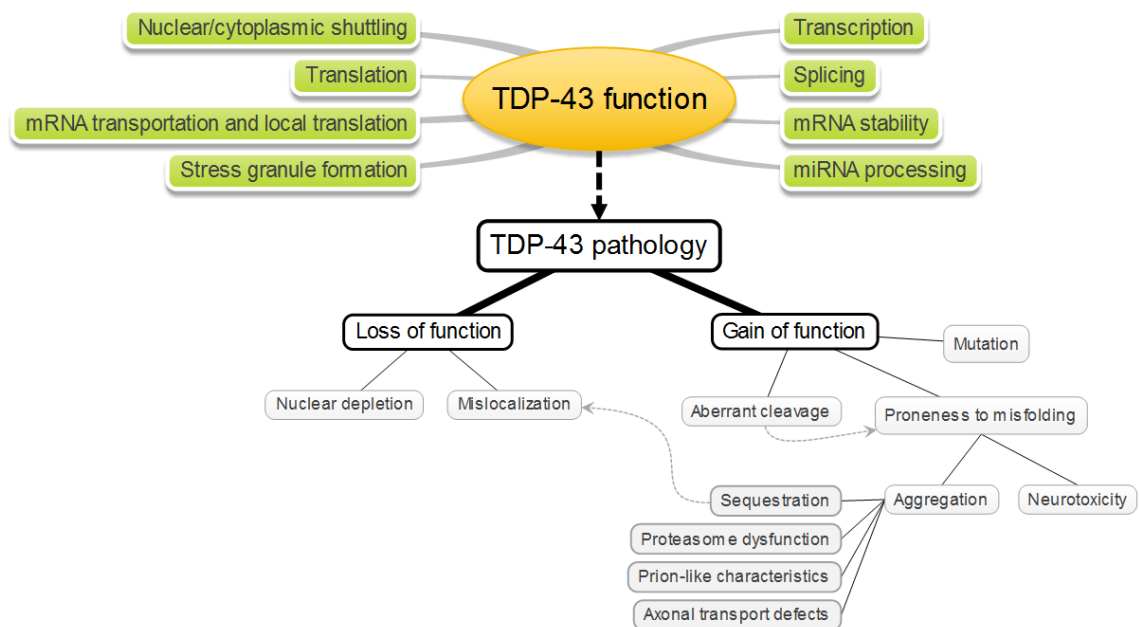


Figure 1-4 | Essential functions of TDP-43 in the nucleus and cytoplasm.

TDP-43 is ubiquitously expressed and exhibits multiple biological functions in transcription, RNA metabolism and transport, miRNA processing, SG regulation and local translation. TDP-43 pathology can be caused by two nonmutually exclusive mechanisms: loss of TDP-43 function or toxic gain of function. The exposure of neurons to stress triggers the relocation of nuclear TDP-43 to SGs in the cytoplasm. It has been hypothesized that prolonged stress would ultimately cause the nuclear depletion of TDP-43. However, genetic mutations in *TARDBP* can cause the accumulation of misfolded and toxic TDP-43 species in detergent-insoluble cytoplasmic aggregates. Additionally, the persistent and aberrant SG formation may also increase protein misfolding, stability and oligomer formation. TDP-43 undergoes abnormal post-translational modifications including C-terminal cleavage. The C-terminal fragments are highly misfolded, aggregation-prone and toxic. Aggregated TDP-43 seeds may sequester its interacting proteins, impair ubiquitin proteasome degradation, trigger prion-like propagation and

disrupt axonal transport. By trapping additional TDP-43 protein, the number and size of TDP-43 aggregates would grow, which may ultimately result in neuronal degeneration and death.

1.6 Table

Table 1-1. The genetics of the ALS/FTD disease continuum

Locus	Gene	Protein	Inheritance	Proportion of fALS	Clinical syndromes	Putative protein function
Causal genes						
21q22.1	<i>SOD1</i>	Cu-Zn superoxide dismutase	AD & AR	12-20%	ALS	Superoxide dismutase
1p36.2	<i>TARDBP</i>	TDP-43	AD	4%	ALS, ALS/FTD	RNA metabolism
16p11.2	<i>FUS</i>	FUS	AD & AR	4%	ALS, ALS/FTD	RNA metabolism
5q31.2	<i>MATR3</i>	Matrin-3	AD	<1%	ALS, ALS/FTD	RNA metabolism
12q13.1	<i>hnRNPA1</i>	hnRNP A1	AD	<1%	ALS, ALS/FTD, FTD, MSP	RNA metabolism
9p21.2	<i>C9orf72</i>	C9orf72	AD	25-40%	ALS, ALS/FTD, FTD	Possible guanine nucleotide exchange factor
Xp11.21	<i>UBQLN2</i>	Ubiquilin-2	XL	<1%	ALS, ALS/FTD	Ubiquitin proteasome degradation
5q35.3	<i>SQSTM1</i>	p62/Sequestosome-1	AD	1%	ALS, ALS/FTD, PDB	Autophagy adaptor
9p13.3	<i>VCP</i>	Valosin-containing protein	AD	1%	ALS, ALS/FTD, FTD, IBMPFD	Ubiquitin segregase
10p15-p14	<i>OPTN</i>	Optineurin	AD & AR	<1%	ALS, ALS/FTD	Autophagy
12q14.2	<i>TBK1</i>	TANK-binding kinase	AD	1%	ALS	Autophagy
20q13.33	<i>VAPB</i>	Vesicle-associated membrane protein-associated protein B/C	AD	<1%	ALS, SMA	Vesicle trafficking
22q11.23	<i>CHCHD10</i>	Coiled-coil-helix-coiled-coil-helix domain-containing protein 10	AD & AR	<1%	ALS, ALS/FTD, FTD	Oxidative phosphorylation
17p13.2	<i>PFN1</i>	Profilin-1	AD	<1%	ALS, ALS/FTD	Cytoskeleton

2q36.1	<i>TUBA4A</i>	Tubulin α -4A chain	AD	1%	ALS	Cytoskeleton
2p13.1	<i>DCTN1</i>	Dynactin subunit 1	AD	<1%	ALS, ALS/FTD, PMA	Axonal transport
17q21.31	<i>GRN</i>	Progranulin	AD	<1%	ALS/FTD, FTD	Growth factor
17q21	<i>MAPT</i>	Microtubule-associated protein tau	AD	N/A	FTD	Cytoskeleton
3p11.2	<i>CHMP2B</i>	Charged multivesicular body protein 2b	AD	<1%	ALS/FTD, FTD	Endosomal trafficking

Risk or susceptibility genes

12q24	<i>ATXN2</i>	Ataxin-2	AD	<1%	ALS, SCA2	RNA metabolism, endocytosis
19p13.11	<i>UNC13A</i>	Unc-13 homolog A	N/A	N/A	ALS, ALS/FTD	Neurotransmitter release
8p21.1	<i>ELP3</i>	Elongator complex protein 3	N/A	<1%	ALS, ALS/FTD	Neurotransmitter release
5q23.2	<i>LMNB1</i>	Lamin B1	N/A	N/A	ALS, ADLD	Nuclear scaffold
9q34.11	<i>GLE1</i>	Nucleoporin GLE1	N/A	<1%	ALS, LCCS1, LAAHD	RNA export mediator
7p21.3	<i>TMEM106B</i>	Transmembrane protein 106B	N/A	N/A	FTD	Endolysosomal pathway

Abbreviations: **AD**: autosomal dominant; **AR**: autosomal recessive; **XL**: X-linked dominant; **ADLD**: adult-onset autosomal dominant leukodystrophy; **IBMPFD**: inclusion body myopathy with Paget disease of bone and frontotemporal dementia; **LAAHD**: lethal arthrogyryposis with anterior horn cell disease; **LCCS1**: lethal congenital contracture syndrome 1; **MSP**: multisystem proteinopathy; **PDB**: Paget's disease of the bone; **PMA**: progressive muscular atrophy; **SCA2**: spinocerebellar ataxia type 2; **SMA**: spinal muscular atrophy.

Chapter 2

Materials and Methods

Portions of this chapter were adapted from the following manuscripts:

Ching-Chieh Chou, Olga M. Alexeeva, Shizuka Yamada, Amy Pribadi, Yi Zhang, Bi Mo, Kathryn R. Williams, Daniela C. Zarnescu, and Wilfried Rossoll. PABPN1 suppresses TDP-43 toxicity in ALS disease models. *Hum Mol Genet.* 2015.

Ching-Chieh Chou*, Yi Zhang*, Mfon E. Umoh, Spencer W. Vaughan, Paul G. Donlin-Asp, Yu Han Chen, Duc M. Duong, Nicholas T. Seyfried, Maureen A. Powers, Thomas Kukar, Kevin B. Boylan, Dennis W. Dickson, Rosa Rademakers, Daniela C. Zarnescu, Jonathan D. Glass & Wilfried Rossoll. Proximity-dependent biotin identification of protein interactome links nucleocytoplasmic transport defects to TDP-43 pathology. (*co-first author) (Under review at Nature Neuroscience)

2.1 Yeast two hybrid assay

Full-length murine TDP-43 (mTDP-43) was cloned as fusion with the GAL4 DNA-binding domain (pGBKT7, Clontech), transformed into the yeast strain AH109 (Mat a) and used as a bait in a yeast-two-hybrid screen with the pretransformed 17 day murine embryo cDNA library (Clontech) in strain Y187 (MAT α). A total of 2.91×10^7 diploid yeast cells containing both bait and prey plasmids were screened according to the Matchmaker 3 protocol (Clontech) and a C-terminal fragment of PABPN1 was identified as a potential new interaction partner and further analyzed. To confirm the interaction of full-length proteins, full-length human TDP-43 (hTDP-43) and PABPN1 (hPABPN1) cDNA were cloned as fusions with the GAL4 DNA-binding domain (pGBKT7, Clontech) and the GAL4 activation domain (pGADT7, Clontech). Plasmids were transformed into the *S. cerevisiae* GAL4 reporter strain AH109 (Clontech) using the PEG/lithium acetate method according to the Matchmaker protocol (Clontech). Transformants were streaked out onto selective plates (SD/-Ade/-His/-Leu/-Trp; + 20 μ g/mL X- α -Gal) to assess growth and to visualize blue colonies positive for yeast-two-hybrid interaction.

2.2 Yeast spotting assays

Expression cassettes for hTDP-43-YFP (Addgene plasmid 27447) and hPABPN1 fused to monomeric Cerulean fluorescent protein (Addgene plasmid 14417) under control of the galactose-inducible GAL1 promoter, were cloned into 2 μ high-copy plasmids pRS425 (LEU2) and pRS426 (URA3). As control plasmids, pRS425-YFP and pRS426-mCerulean were used. Yeast cells were co-transformed with plasmids using the

PEG/lithium acetate method and plated onto synthetic drop out media (SD/-Leu/-Ura; +2% glucose). For spotting assay, cells were grown overnight at 30°C. The cell numbers were determined by OD₆₀₀, serially diluted by a factor of 10 (1, 0.1, 0.01 and 0.001), and spotted onto solid synthetic drop out media (SD/-Leu/-Ura; + 2% glucose or + 2% galactose). Cells were grown at 30°C for 2-3 days.

2.3 Constructs

The expression plasmids encoding Nup and nucleocytoplasmic TF fusion proteins were obtained from multiple sources (**Supplementary Table 3-2**). PCR-amplified human TDP-43 and TDP-CTF were cloned into the pcDNA3.1 myc-BioID vector (Addgene)¹⁷¹ as XhoI/KpnI fragments, and cloned from GFP expression plasmids into the Kpn2I/MluI sites of the APEX2-Actin plasmid (Addgene)¹⁷². TDP-CTF (aa 208-414) were generated by PCR, and Q331K, M337V, A382T and NLS (KRK...KVKR > AAA...AVAA)⁹⁰ mutations were generated by site-directed mutagenesis (QuikChange II, Agilent), and cloned into pEGFP-C1 (Clontech), mCherry or enhanced blue fluorescent protein 2 (BFP) vector. HA-tagged Htt Exon1-150Q was a generous gift from Dr. Xiao-Jiang Li. GFP-PABPN1 was a generous gift by the Rouleau lab. BFP, GFP or mCherry fluorescent proteins were also fused to human full-length PABPN1 and truncation mutations of PABPN1 (PABPN1^{ΔNLS18} and PABPN1^{ΔNLS50}). GFP and GFP-PABPN1 were cloned behind the doxycycline-inducible Tet-On promoter in the expression vector pTRIPZ (Open Biosystems). A flexible linker [(SGGG)3] was inserted between all the fusion partners to facilitate correct protein folding. PCR primers used to generate PrLD and non-PrLD fragments of Nup98: 5'-

CAGATCTCCGGAGGCGGCTCCATGGAGATGTTTAACAAATCATTTGG-3'; 5'-
ACAATTGCATCAACCTCCAGGCTGTGAGGCTTG-3'; 5'-

CAGATCTCGATGCTTTTTGGGACAGCTACAAACACC-3'; 5'-

ACAATTGATTCACTGTCCTTTTTTCTCTACCTGAGG-3'. PCR products were
cloned into the BglII/MfeI sites of pEGFP-Nup98. PCR primers used to generate PrLD
and non-PrLD fragments of Nup153: 5'-

CGCTAGCTCTAGACTAGGGGACACCATGG-3'; 5'-

GACCGGTGGTACAAAGGAGGATCCTGCAGAGCTAG-3'; 5'-

CGCTAGCTCTAGACTAGGGGACACCATGTTTGGAACTGGACCCTCAGCACC-
3'; 5'-GACCGGTGGTTTCCTGCGTCTAACAGC-3'. PCR products were cloned into

the NheI/AgeI sites of pNup153-EGFP. PCR primers used to generate PrLD and non-
PrLD of Nup214: 5'-

CAGATCTCCGGAGGCGGCGCGATGGGAGACGAGATGGATG-3'; 5'-

ACAATTGCATCAGGCAGCTGCTGTGCTGGCTGTG-3'; 5'-

CAGATCTCCGGAGGCGGCGCGATGACACCACAGGTCAGCAGCTCAGG-3'; 5'-

ACAATTGCCTCAGCTTCGCCAGCCACCAAAACCCTGG-3'. PCR products were
cloned into pEGFP-Nup214 as BglII/MfeI fragments. GIPZ TDP-43 shRNA constructs

(shTDP-43 #2, V3LHS_636490; shTDP-43 #3, V3LHS_636491), GIPZ PABPN1

shRNA constructs (shPABPN1#1, V3LHS_646409; shPABPN1#2, V3LHS_644004) and

a non-silencing control (shCtrl, RHS4346) were obtained from Open Biosystems.

2.4 *Drosophila* genetics

All *Drosophila* stocks and crosses were maintained on standard yeast/cornmeal/molasses food at 22°C. GAL4 drivers (GMR GAL4 for retinal expression and D42 GAL4 for motor neuron expression) were used to express human TDP-43 (hwt), D169G (hD169G), A315T (hA315T), ΔRRM and G298S (hG298S) with C-terminal YFP tag as previously described¹⁷³. For controls, *w*¹¹¹⁸ flies were crossed with the appropriate GAL4 driver. For genetic interactions, in PABPN1 experiments, stock FBst0038390 with a loss of function allele of Pabp2 was used (Pabp2 [55]/CyO, P(w[+mC]=ActGFP)cJMR1). In nucleocytoplasmic transport experiments, *Drosophila* lines harboring mutations in nuclear pore components were obtained from the Bloomington *Drosophila* Stock Center and have the following genotypes: y[1]; P{y[+mDint2] w[BR.E.BR]=SUPor-P}Nup50[KG09557]; ry[506], w[*] P{w[+mC]=EP}Nup93-1[G9996], Nup98-96[339]/TM3, Sb[1] and y[1] w[67c23]; P{y[+t7.7] w[+mC]=wHy}Nup107[DG40512]/SM6a.

2.5 Adult Eye Imaging

Adult fly eyes were imaged with a Leica MZ6 microscope equipped with an Olympus DP73 camera and controlled by Olympus DP Controller and Olympus DP Manager software. Individual images were processed using Adobe Photoshop CS6 (Adobe).

2.6 Larval Turning Assays

Crosses were carried out at 22°C and wandering third instar larvae were placed on a grape juice plate. After a short acclimation period, larvae were gently turned ventral side

up. They were observed until they turned over (dorsal side up) and began making a forward motion.

2.7 Primary neuron and mammalian cell culture and transfection

All procedures for animal experiments were approved by the Emory University Institutional Animal Care and Use Committee. Primary cortical neurons were isolated from cerebral cortices of mixed male and female C57BL/6J mouse embryos at day 16.5 (E16.5) and cultured as previously described¹⁷⁴. Briefly, cells were plated on coverslips coated with 0.5 mg/ml poly-L-ornithine (Sigma-Aldrich) for 2 hrs in MEM (Life Technologies) containing 10% FBS (Hyclone). After switching to complete neural cell culture medium (Neurobasal medium (Life Technologies), 1% Glutamax (Life Technologies) and 2% B-27 supplements (Life Technologies)), cells were cultured for 5 days. Neurons were transected via magnetofection with 0.5 µg plasmid DNA and 1.75 µL NeuroMag (Oz Biosciences) as described¹⁷⁵. Cells were cultured for 24 hrs and processed for immunofluorescence. Transfection efficiency was in the range of 20-30%. For TDP-43 knockdown, cells were transfected with expression plasmids for shTDP-43 #2, shTDP-43 #3 or shCtrl and cultured for another 5 days to efficiently reduce TDP-43 protein levels¹¹³.

Mouse Neuro-2a (N2a) neuroblastoma cells were plated in 6-well plates for immunoblotting or on coverslips in 12-well plates for immunofluorescence, and cultured in DMEM medium (Life Technologies) containing 10% FBS and 1% PenStrep (Sigma-Aldrich). Cells were transfected with either Lipofectamine 3000 (Life Technologies) or PolyMag Neo (Oz Biosciences) according to the manufacturer's protocol and the medium

was changed the next day. Cells were fixed 48 hrs after transfection. Transfection efficiency was in a range of 70-80%. N2a cells were obtained from ATCC (CCL-131) and tested for mycoplasma contamination.

2.8 Immunofluorescence and image acquisition and analysis

For the overexpression experiments, primary neurons were fixed one day and N2a cells were fixed two days after transfection. For shRNA-mediated knockdown experiment, cells were fixed four days after transfection. Transfected cells expressing shRNA constructs, identified by GFP expression. To validate the interaction of Nups and TFs with TDP-CTF, N2a cells were co-transfected with expression plasmids for GFP or epitope-tagged Nups or TFs (Supplementary Table 2) and mCherry or mCherry-tagged TDP-CTF. Cells were fixed with 4% paraformaldehyde (PFA) in 1×PBS 48 hrs after transfection for 15 mins at room temperature (RT), permeabilized with 0.2% Triton X-100 in 1×PBS for 5 mins, and blocked with 5% bovine serum albumin (BSA) for 45 mins. Cells were incubated with primary antibodies overnight at 4°C, followed by incubation with fluorophore-conjugated secondary antibodies and streptavidin for 1 hr at RT. F-actin was labeled with Rhodamine-conjugated phalloidin (1:1000) for 1 hr at RT.

To examine DNA damage following TDP-43-mediated lamin defects, cortical neurons were transfected with expression plasmids for GFP or GFP-tagged TDP-CTF, TDP-43^{WT} or TDP-43^{Q331K}. γ H2AX has been identified as a marker of DNA double-strand breaks¹⁷⁶. The mean pixel intensity of stained γ H2AX in the nucleus was analyzed by ImageJ software (National Institutes of Health). DNA damage inducing calicheamicin γ 1 (CLM) was added at 5 nM for 2 hrs as a positive control.

For 3D reconstructions of whole nuclei, lamin B staining was used to outline the nuclear region of cortical neurons. On average 45 to 50 Z-stack sections at 0.3 μm steps were required to reconstruct the whole nucleus using Imaris software (Bitplane). A surface was created to mask the nucleus with a smooth factor of 0.3 μm . The optical sections at XY, XZ and YZ plane were generated.

To investigate the nucleocytoplasmic transport of proteins, cortical neurons were co-transfected with expression plasmids for GFP or GFP-tagged TDP-CTF, TDP-43^{WT}, TDP-43^{Q331K}, TDP-43^{M337V} or TDP-43^{mtNLS} and NES-tdTomato-NLS (a gift from Martin Hetzer), a protein transport reporter. The mean pixel intensity of NES-tdTomato-NLS and GFP-TDP-43 in the nucleus and cytoplasm were measured for calculating the nuclear-to-cytoplasmic (N-to-C) ratio. To examine whether induction of apoptosis causes a similar defect in the nucleocytoplasmic transport of proteins, the GFP transfected cells were incubated with staurosporine (STS) at 50 nM or 250 nM for 12 hrs to induce caspase-3/9-dependent apoptosis¹⁷⁷. The inhibition of nuclear protein import was induced by importazole (IPZ)¹⁷⁸ at 5 μM or 10 μM for 12 hrs. DMSO was added as the vehicle control.

For high resolution imaging, Z-series (15-50 sections, 0.15-0.3 μm steps) were acquired according to the different experimental designs with an epifluorescence microscope (Ti, Nikon) equipped with a cooled CCD camera (HQ2, Photometrics). Within each experiment, all groups were imaged with the same acquisition settings. Image stacks were deconvolved using a 3D blind constrained iterative algorithm (AutoQuant, Media Cybernetics).

For visualization of NPCs, 3D structured illumination microscopy (SIM) was performed on a Nikon SIM microscope using a 100x (1.49 NA) object. 10-30 Z-stacks were acquired per image to capture the entire nuclear volume and SIM reconstructions were performed in NIS elements (Nikon). Fourier transformations were applied to assess reconstruction quality. 3D SIM images were analyzed in Fiji/ImageJ. For GFP and GFP-tagged TDP-CTF, series of widefield images were acquired and merged with the super-resolution image of the mAb414 staining.

2.9 Fluorescence *in situ* hybridization (FISH) and immunofluorescence

Cortical neurons were washed with 1×PBS and fixed with 4% PFA in 1×PBS for 10 mins. FISH was performed with some modifications of previously described method¹⁷⁹. Briefly, fixed cells were permeabilized with 50%, 70% and 100% ethanol in subsequent steps and stored at -20°C for overnight and rehydrated the next day with 1×SSC for 10 mins. Cells were washed with 10% formamide (Sigma-Aldrich) for 5 mins and incubated in hybridization buffer (20% dextran sulfate, 4×SSC, 4 mg/mL BSA, 20 mM ribonucleoside vanadyl complex, and 10 mM sodium phosphate buffer, pH 7.0) at 37°C for 1.5 hrs. To detect poly(A) RNAs, 1 μL biotinylated oligo-(dT) probes (Biosearch Technologies) were resuspended with 10 μg each of *E. coli* tRNA and salmon sperm DNA in 50 μL of hybridization buffer and incubated with the coverslips at 37°C overnight. Oligo-(dA) probes were used as a negative control. Cells were washed by 1×PBS for 10 mins to remove formamide, blocked with 5% BSA for 45 mins, and incubated with Cy3-conjugated streptavidin for 1 hr at RT to detect the biotinylated oligo-(dT) probes. Mean pixel intensities for poly(A) RNA in the nucleus and cytoplasm

of cells expressing GFP or GFP-tagged TDP-CTF, TDP-43^{WT}, TDP-43^{Q331K}, TDP-43^{M337V} or TDP-43^{mtNLS} were determined with ImageJ software.

2.10 Metabolic labeling of newly synthesized proteins

Cortical neurons were transfected with expression vectors for GFP or GFP-tagged TDP-43^{WT} or TDP-CTF. After 24 hrs, cells were incubated in methionine-free DMEM (Thermo Fisher Scientific) with or without 40 μ M anisomycin (Sigma-Aldrich) for 1 hr at 37°, followed by incubation with 5 mg/mL L-azidohomoalanine (AHA) (Thermo Fisher Scientific) for 5 mins. Cells were washed with 1 \times PBS and fixed by 4% PFA, permeabilized with 0.2% Triton X-100 for 5 mins and blocked with 3% BSA in 1 \times PBS for 30 mins. Click-iT reaction cocktail (50 μ L per sample) was prepared right before the end of blocking using Click-iT assay kits and Alexa Fluor 647-conjugated alkyne (Thermo Fisher Scientific). Samples were incubated for 30 mins at RT and washed with 3% BSA in 1 \times PBS before mounting. The mean pixel intensity of AHA in the cell body was quantified with ImageJ software.

2.11 Electron microscopy of nuclear envelope

To visualize nuclear envelope morphology in transfected N2a cells by electron microscopy (EM), we used fusion constructs of the engineered APEX2 peroxidase with FLAG-tagged TDP-43 and TDP-CTF¹⁷². N2a cells were transfected with expression plasmids for FLAG-APEX2-TDP-43, FLAG-APEX2-TDP-CTF or GFP-TDP-CTF. Cells were fixed with PFA and 2.5% glutaraldehyde in 0.1 M phosphate buffer. APEX2

catalyzes the deposition of 3,3'-diaminobenzoic acid (DAB), which allowed us to identify APEX2-TDP-43 and APEX2-TDP-CTF expressing cells under EM (JEOL JEM-1400).

2.12 Immunohistochemistry

All procedures for collection of human brain tissue were approved by the Emory University Institutional Review Board. Informed consent was obtained from all patients or their authorized legal representatives. Paraffin embedded sections from post-mortem human motor and frontal cortices of 8 μm thickness were deparaffinized by incubation in a 60°C oven for 30 mins and rehydrated by immersion in Histo-Clear and 100% ethanol and 95% ethanol solutions. Antigen retrieval was then performed as sections were microwaved in 10mM citrate buffer pH 6.0 for a total of 5 mins and allowed to cool to RT for 30 mins. Peroxidase quenching was performed as sections were incubated in a 3% hydrogen peroxide solution in methanol for 5 mins at 40°C and then rinsed in Tris-Brij buffer (1M Tris-Cl pH 7.5, 100mM NaCl, 5mM MgCl₂, 0.125% Brij 35). For blocking, sections were incubated in normal goat serum (Elite Vectastain ABC kit) for 15 mins at 40°C. Sections were then incubated with Nup205, Lamin B1 or Rangap1 at a concentration of 1:50 or 1:300 (diluted in 1% BSA in tris-brij 7.5) overnight at 4°C. The following day sections were incubated in biotinylated secondary antibody at 5 $\mu\text{L}/\text{mL}$ (Elite IgG Vectastain ABC kit) for 30 mins at 37°C and then incubated with the avidin-biotin enzyme complex (Vector Laboratories) for 30 mins. Stains were visualized by incubation of DAB Chromogen (Sigma-Aldrich) for 5 mins at RT. Slides were then dehydrated in an ethanol series and mounted with cover slips.

2.13 Cell death assay

Cell death of primary cortical neurons was assessed by the uptake of membrane-impermeant ethidium homodimer-1 (EthD-1, Biotium). EthD-1 labels nucleic acids of membrane-compromised dying/dead cells and reveals strong red fluorescence in nucleus (excitation/emission maxima ~528/617nm). After transfection, 2 μ M EthD-1 was added to culture medium for 1 hr at 37°C. Cell death was determined by visually counting under an epifluorescent microscope. Rate of cell death in % = number of transfected cells with red fluorescence in nucleus / number of transfected cells * 100%.

2.14 Co-immunoprecipitation of FLAG-tagged constructs from mammalian cells

N2a cells were co-transfected with FLAG-TDP-43, and GFP or GFP-tagged PABPN1, PABPN1 ^{Δ NLS18} or PABPN1 ^{Δ NLS50} using Turbofect reagent (Fermentas). Two days after transfection, cells were resuspended in lysis buffer (50mM Tris-HCl [pH 7.5], 150mM NaCl, 1mM EDTA, 1% Triton X-100, Roche complete protease inhibitor cocktail) and centrifuged for 20 minutes at 20,000 g. RNaseA was added at 37°C for 30 minutes. A small aliquot of the supernatant was collected as input extract, and the rest was used for co-immunoprecipitation. The supernatant was incubated with anti-FLAG (Sigma-Aldrich) agarose beads for 2 hrs at 4°C with rotation. Beads were washed 5 times with lysis buffer. Input extract and anti-FLAG immunoprecipitates were boiled with Laemmli buffer and used for western blot analysis. Primary antibodies were used according to the supplementary table.

2.15 Co-immunoprecipitation of endogenous protein from mouse brain tissue

Brains from E-13.5 mouse embryos were flash frozen in liquid nitrogen immediately following dissection and kept at -80° until needed. Brains were homogenized with a dounce homogenizer on ice in 1 mL of lysis buffer, then sonicated and spun down at 20,000g for 15 minutes. A small aliquot of input from the supernatant was set aside, and the rest was used for co-immunoprecipitation. Immunoprecipitation of PABNP1 was performed with rabbit monoclonal anti-PABNP1 (Epitomics) and Protein A-agarose beads (Calbiochem) according to manufacturer's instructions. Normal rabbit serum (Millipore) was used as a control. Beads were washed 5 times with lysis buffer and boiled in Laemmli sample buffer. Samples were separated on a 10% SDS-PAGE gel, blotted onto nitrocellulose membranes and blocked with Odyssey blocking buffer (LiCor). Primary antibodies were used according to the supplementary table.

2.16 Histidine pulldown assay

N2a cells were co-transfected with histidine-tagged mCherry-TDP-CTF, and GFP or GFP-tagged PABNP1. Cells were resuspended in lysis buffer (50mM Tris-HCl, 150mM NaCl, 1mM EGTA, 1% NP-40, 0.25% sodium deoxycholate, 1mM Na_3VO_4 and Roche complete protease inhibitor cocktail) and centrifuged for 20 minutes at 20,000g. The supernatant was incubated with Nickel-resin (His60 Ni Superflow Resin, Clontech) for 2 hrs at 4°C with rotation. The mixture was washed with lysis buffer and boiled with Laemmli buffer to elute bound proteins for western blot analysis.

2.17 Affinity pulldown of biotinylated proteins and immunoblotting

N2a cells were transfected with expression plasmids for GFP, myc-BirA*-TDP-43 or myc-BirA*-TDP-CTF using Lipofectamine 3000. The culture medium was changed after 4 hrs and, the next day, biotin was added to the medium at 50 μ M. After 24 hrs, cells were harvested and washed with cold 1 \times PBS three times before cell lysis in urea buffer (8M urea, 50 mM Tris-HCl pH 7.5) supplemented with 1 \times protease inhibitor (Roche) and phosphatase inhibitor (Roche) for 20 mins at RT with occasional vortexing. Cells were sonicated three times in two-second pulses and centrifugated at 20,000 g at RT for 15 mins. A small aliquot from the supernatant (input sample) was mixed with Laemmli buffer and boiled for 5 mins. For the pulldown of biotinylated proteins, neutravidin beads (ThermoFisher Scientific) were pre-washed with lysis buffer and incubated with the remaining lysate sample with constant rotation overnight at RT. Beads were collected by centrifugation and washed five times with lysis buffer. Twenty percent of the sample was reserved for immunoblotting and 80% were used for mass spectrometry analysis.

Immunoblotting was performed according to standard protocols. Samples mixed with Laemmli buffer were heated for 5 minutes at 98°C and spun-down before running on a 10% SDS-PAGE gel and electro-transfer to a nitrocellulose membrane. The membrane was blocked with Odyssey blocking buffer (LiCor) for 1 hr, followed by incubation with primary antibodies including anti-myc (1:2000), anti-TDP-43 (1:2000), anti- α -Tubulin (1:10000) and anti- γ -Actin (1:10000) overnight at 4°C, and incubation with secondary antibodies (1:10000, LI-COR) in blocking buffer in 1 \times PBS with 0.1% Tween 20 for 1 hr at RT. Biotinylated proteins were detected with IRDye Streptavidin (1:10000). Blots were scanned on an Odyssey imager (LiCor).

2.18 Sample digestion for mass spectrometry analysis

Neutravidin beads were spun down and residual urea was removed. Digestion buffer (200 μ L of 50 mM NH_4HCO_3) was added and the bead solution was then treated with 1 mM dithiothreitol (DTT) at 25°C for 30 mins, followed by 5 mM iodoacetamide (IAA) treatment at 25°C for 30 mins in the dark. Proteins were digested with 1 μ g of lysyl endopeptidase (Wako) at RT for 2 hrs and further digested overnight with 1:50 (w/w) trypsin (Promega) at RT. Resulting peptides were desalted with a Sep-Pak C18 column (Waters) and dried under vacuum.

2.19 LC-MS/MS analysis

Peptides were resuspended in 10 μ L of loading buffer (0.1% formic acid, 0.03% trifluoroacetic acid, 1% acetonitrile). Peptide mixtures (2 μ L) were separated on a self-packed C18 (1.9 μ m Dr. Maisch, Germany) fused silica column (25 cm x 75 μ m internal diameter (ID); New Objective, Woburn, MA) by a Dionex Ultimate 3000 RSLCNano and monitored on a Fusion mass spectrometer (ThermoFisher Scientific). Elution was performed over a 120-min gradient at a rate of 350 nl/min with buffer B ranging from 3% to 80% (buffer A: 0.1% formic acid in water, buffer B: 0.1% formic in acetonitrile). The mass spectrometer cycle was programmed to collect at the top speed for 3 second cycles. The MS scans (400-1600 m/z range, 200,000 AGC, 50 ms maximum ion time) were collected at a resolution of 120,000 at m/z 200 in profile mode and the HCD MS/MS spectra (0.7 m/z isolation width, 30% collision energy, 10,000 AGC target, 35 ms maximum ion time) were detected in the ion trap. Dynamic exclusion was set to exclude

previous sequenced precursor ions for 20 seconds within a 10 ppm window. Precursor ions with +1, and +8 or higher charge states were excluded from sequencing.

2.20 Database search

Spectra were searched using Proteome Discoverer 2.0 against a mouse uniprot database (downloaded April 15 2015, 53291 target sequences) supplemented with 2 BirA*-fusion sequences. Methionine oxidation (+15.9949 Da), asparagine and glutamine deamidation (+0.9840 Da), lysine ubiquitination (+114.04293), protein N-terminal acetylation (+42.0106 Da) and biotinylation (+226.2994 Da) on N terminus and lysine were variable modifications (up to 3 allowed per peptide); cysteine was assigned a fixed carbamidomethyl modification (+57.0215 Da). Only fully digested tryptic peptides were considered with up to 2 miscleavages in the database search. A precursor mass tolerance of ± 10 ppm and a fragment mass tolerance of 0.6 Da was applied. Spectra matches were filtered by Percolator to a PSM FDR of less than 1 percent.

2.21 Identification of the TDP-43 and TDP-CTF interactome

Urea homogenates were collected from N2a cells transfected with expression vectors for GFP, BirA*-TDP-43 and BirA*-TDP-CTF. The experiment was performed with two biological replicates. Four different comparisons of proteomic data were performed: (1) BirA*-TDP-43 versus GFP control; (2) BirA*-TDP-CTF versus GFP control; (3) BirA*-TDP-43 versus BirA*-TDP-CTF; (4) BirA*-TDP-CTF versus BirA*-TDP-43. To filter the results, in comparisons 1 and 2, a protein was identified as TDP-43 or TDP-CTF associated if there was no missing data, the average number of peptide spectrum matches

(PSM) in the TDP-43 or TDP-CTF associated proteome was ≥ 5 and the fold increase was $\geq 2^{0.4}$ as compared to the PSM in the GFP control. In comparisons 3 and 4, the same criteria were also applied to a protein considering a TDP-43-preferred interactor when the PSM in BirA*-TDP-43 was ≥ 5 and the fold increase was $\geq 2^{0.4}$ as compared to the PSM in BirA*-TDP-CTF, and vice versa. GFP transfected cells provided the background levels of endogenous biotinylation and unspecific pulldown. The identification of BirA*-TDP-43- or BirA*-TDP-CTF-preferred interactors addresses their cellular compartment- and function-specific roles. These proteins were analyzed and categorized on the basis of biological process, cellular component and molecular function using the Database for Annotation, Visualization, and Integrated Discovery (DAVID) (<https://david.ncifcrf.gov/>).

2.22 Bioinformatics analysis

Prion-like amino acid composition of human Nups and TFs was predicted by the PLAAC algorithm (<http://plaac.wi.mit.edu/>). The log-likelihood ratio (LLR) score allows for the exploratory screening of potential PrLDs. Since low content of hydrophobic residues and high net charge are known predictors for low-complexity sequence domains and intrinsically disordered proteins (IDPs), we performed a predictive analysis of mean hydrophobicity using ProtScale (<http://web.expasy.org/protscale/>) with the hydrophobicity scale of Kyte and Doolittle. Hydrophobic amino acids include Ala (1.8), Cys (2.5), Gly (-0.4), Ile (4.5), Leu (3.8), Met (1.9), Phe (2.8) and Val (4.2), and hydrophilic residues include Arg (-4.5), Asn (-3.5), Asp (-3.5), His (-3.2), Lys (-3.9), Pro (-1.6), Gln (-3.5), Glu (-3.5) and Tyr (-1.3). Low-complexity and intrinsic disorder

predictions were performed using DisEMBL (<http://dis.embl.de/>) and GlobPlot (<http://globplot.embl.de/>) to validate the relationship between hydrophobicity and protein intrinsic disorder in human Nups and TFs.

2.23 Protein extract, subcellular fractionation and western blots

For protein extract experiment, N2a cells were co-transfected with mCherry or mCherry-TDP-CTF, and GFP or GFP-tagged PABPN1, PABPN1^{ΔNLS18}, PABPN1^{ΔNLS50} or PABPC1 using Turbofect reagent (Fermentas). Cells were lysed in RIPA buffer (50mM Tris, pH 8.0, 150mM NaCl, 1% NP-40, 0.1% SDS, 0.5% sodium deoxycholate and Roche complete protease inhibitor cocktail). After 20 minutes incubation on ice, cells were sonicated briefly and centrifuged at 20,000g for 15 minutes. The supernatant was collected as the whole-cell lysate. For the protein detergent solubility assay, Neuro2a cells were resuspended in lysis buffer (50mM Tris-HCl pH 8.0, 150mM NaCl, 1mM EDTA, 1% Triton X-100, Roche complete protease inhibitor cocktail). After 20 minutes incubation on ice, cells were sonicated briefly and centrifuged at 20,000g for 15 minutes. The supernatant was collected as the detergent-soluble fraction and the insoluble pellet was recovered in urea buffer (8M urea, 50mM Tri-HCl pH 8.0, Roche complete protease inhibitor cocktail). Following sonication and max-speed centrifugation, the supernatant was collected as the detergent-insoluble fraction. For the nuclear and cytoplasmic fractionation, N2a cells were lysed in hypotonic buffer (10mM HEPES pH 7.9, 20mM KCl, 0.1mM EGTA, 1mM DTT and Roche complete protease inhibitor cocktail), left on ice for 15 minutes, 0.1% NP-40 was added for another 5 minutes, and lysates were centrifuged at 15,600g for 10min at 4°C. The supernatant was collected as cytoplasmic

fraction, and the pellet containing the nuclei was suspended in high salt buffer (20mM HEPES pH 7.9, 0.4M NaCl, 0.1mM EDTA, 0.1mM EGTA, 1mM DTT, 5% glycerol and Roche complete protease inhibitor cocktail). The suspension was incubated on ice for 30 minutes, sonicated once, and centrifuged at 15,600g for 10 minutes at 4°C. The supernatant was saved as the nuclear fraction. For western blot analysis, the samples were boiled in Laemmli sample buffer for 5 minutes and separated by 10% SDS-PAGE. mCherry-TDP-CTF, full-length TDP-43, PABPN1 and α -Tubulin were detected by corresponding primary antibodies. Specific secondary antibodies conjugated with infrared dyes (Li-Cor) were used for detection on an Odyssey scanner (Li-Cor). Primary antibodies were used according to the supplementary table.

2.24 Cycloheximide chase assay

N2a cells were co-transfected with mCherry-TDP-CTF, and GFP or GFP-tagged PABPN1. Twenty-four hours after transfection, cells were treated with 100 μ M cycloheximide (Sigma-Aldrich). At each indicated time point, cells were also treated with either vehicle (DMSO), 100nM Bafilomycin (Cayman Chemical), or 10 μ M MG132 (Sigma-Aldrich), and incubated from 0 to 24 hrs. Cells were lysed in RIPA buffer with Roche complete protease inhibitor cocktail. After 20 minutes incubation on ice, cells were sonicated briefly and centrifuged at 20,000g for 15 minutes. The protein concentration was determined using Bradford protein assay. Western blotting was performed as previously described. Antibodies were used to against mCherry-TDP-CTF, endogenous TDP-43 and α -Tubulin. The protein levels were normalized to the values at 0 hr and represented as the percentage of remaining protein. The temporal changes of

relative protein levels were determined by the ratio change of mCherry-TDP-CTF or endogenous TDP-43 between the PABPN1 and GFP coexpression at each indicated time point.

2.25 Time-lapse live-cell imaging

Two to three thousands of primary cortical neurons were plated in a glass bottom culture dish (MatTek Corporation, 35 mm petri dish, 14 mm microwell) and cultured in conditioned medium for 4 days. To evaluate the dynamics of TDP-CTF, neurons were co-transfected with constitutive CMV promoter-driven mCherry-TDP-CTF and inducible Tet-On promoter-driven GFP or GFP-PABPN1 plasmids using Lipofectamine 2000 reagent for 24 hrs. We monitored neurons by time-lapse microscopy on a Nikon BioStation IM (Nikon Instruments Inc., Melville, NY) using an 80x 0.8 NA objective. Neurons were maintained at 37°C and 5% CO₂ in the chamber throughout the experiment. During the first hr of the experiment, the mean fluorescence intensity of TDP-CTF in the cell body was measured as the basic protein level (100%). Then expression of GFP or GFP-PABPN1 under control of the Tet-On promoter was induced with doxycycline (Dox) (0.5µg/mL) (Clontech) for the next 23 hrs. DMSO was used as vehicle control. Each neuron was captured every 10 min over 24 hrs with phase contrast and fluorescence imaging in the red and green channels. The intensity measurements of mCherry-TDP-CTF were normalized to the basic protein level following treatment and plotted as the change of relative mCherry-TDP-CTF.

2.26 Stress granule formation assay

Primary motor neurons were co-transfected via magnetofection as described¹⁷⁵ with mCherry or mCherry-PABPN1, and GFP or GFP-tagged TDP-43^{WT}, TDP-43^{Q331K} or TDP-CTF for 24 hrs and then exposed to 0.5mM sodium arsenite for 1 hr to induce formation of SGs. Neurons were fixed and SGs were detected by goat anti-eIF3 η (N-20, Santa Cruz Biotechnology; 1:200) antibodies. The number and size of SGs and the percentage of cells with SGs were measured using ImageJ software. To quantify the disassembly of SGs after the removal of sodium arsenite, the number of SGs was measured after 0-hr, 2-hr or 4-hr.

2.27 Statistical analyses

Data from different experiments were analyzed by mean value analysis (Student's *t* test) or analysis of variance (one-way or two-way ANOVA) using GraphPad Prism Software. Bonferroni correction was used in the case where multiple testing occurred. Differences were considered significant when $P < 0.05$. All values are mean and SEM.

Chapter 3

TDP-43 pathology disrupts nuclear pore complexes and nucleocytoplasmic transport in ALS/FTD

Portions of this chapter were adapted from the following manuscript:

Ching-Chieh Chou*, Yi Zhang*, Mfon E. Umoh, Spencer W. Vaughan, Paul G. Donlin-Asp, Yu Han Chen, Duc M. Duong, Nicholas T. Seyfried, Maureen A. Powers, Thomas Kukar, Kevin B. Boylan, Dennis W. Dickson, Rosa Rademakers, Daniela C. Zarnescu, Jonathan D. Glass & Wilfried Rossoll. Proximity-dependent biotin identification of protein interactome links nucleocytoplasmic transport defects to TDP-43 pathology. (*co-first author) (Under review at Nature Neuroscience)

3.1 Abstract

The cytoplasmic mislocalization and aggregation of TAR DNA-binding protein-43 (TDP-43) is a common histopathological hallmark of the amyotrophic lateral sclerosis and frontotemporal dementia disease spectrum (ALS/FTD). However, the composition of aggregates and their contribution to the disease process remained unknown. Here, we used proximity-dependent biotin identification (BioID) to determine the interactome of detergent-insoluble TDP-43 aggregates, and found them enriched for components of the nuclear pore complex (NPC) and nucleocytoplasmic transport machinery. Aggregated and disease-linked mutant forms of TDP-43 triggered the sequestration and mislocalization of nucleoporins and other transport factors, partially mediated by their prion-like features, and interfered with nuclear protein import and RNA export. Moreover, nuclear pore pathology is present in ALS patient brain tissue from sporadic cases and those caused by genetic mutations in *TARDBP* and *C9orf72*. Our data strongly implicate TDP-43-mediated nucleocytoplasmic transport defects as a common disease mechanism in ALS/FTD.

3.2 Introduction

ALS represent the most common form of adult onset motor neuron disease, whereas FTD is the second most common form of dementia under the age of 65 years. ALS and FTD are relentlessly progressive and fatal neurodegenerative disorders that show a considerable overlap in genetics, clinical features, and neuropathology, suggesting that they are part of a disease spectrum with a shared pathomechanism¹⁵. A common histopathological feature in ALS and FTD patient brains is the cytoplasmic

mislocalization of the normally predominately nuclear RNA-binding TDP-43 and the accumulation of its hyper-phosphorylated and ubiquitinated fragments in detergent-insoluble aggregates^{13,14,30}. This pathology is observed in ~97% of ALS and ~50% of FTD cases, but also frequently present in Alzheimer's disease and other neurodegenerative diseases, suggesting a broad role in neurodegeneration¹⁵. TDP-43 is encoded by the *TARDBP* gene and contains two RNA-recognition motifs (RRM1 and RRM2), a nuclear localization sequence (NLS), and a nuclear export signal (NES), allowing it to shuttle between the nucleus and cytosol and participating in biological functions in both compartments. The C-terminal glycine-rich region of TDP-43 consists of a low-complexity domain with a prion-like Q/N-rich sequence, which is involved in alternative splicing and mediates protein-protein interactions with heterogeneous ribonucleoprotein (hnRNP) family members⁹⁸. Remarkably, the C-terminus harbors most of the disease-causing missense mutations identified in ALS/FTD patients, which promote cytoplasmic mislocalization and pathological aggregation of TDP-43^{101,103}. Under conditions of cellular stress, persistent stress granule formation in the cytosol may increase stability of TDP-43 and facilitate toxic aggregation¹¹⁷. Although aberrant aggregation and sequestration of RBPs and other interacting proteins is thought to lead to an impairment of RNA and protein homeostasis¹⁵, the exact molecular mechanism by which TDP-43 pathology causes neurodegeneration remains poorly understood.

To explore the mechanisms through which TDP-43 pathology contributes to neurodegeneration, we adapted the BioID method to interrogate the proteome of detergent-insoluble cytoplasmic TDP-43 aggregates. Our proteomic analysis identified components of nucleocytoplasmic transport pathways as a major group of proteins

present in pathological TDP-43 aggregates. Morphological and functional analyses in neuronal cells and primary neurons confirmed that TDP-43 pathology cause the mislocalization and aggregation of nucleoporins and nuclear export factors, as well as morphological defects in the nuclear envelope and nuclear pore complexes, leading to reduced nuclear protein import and mRNA export. In addition, we found that mutations in Nup genes act as genetic modifiers in *Drosophila* models of TDP-43 proteinopathy. Our finding of NPC pathology in ALS cases with *TARDBP* mutations and in sporadic ALS cases indicate that TDP-43 pathology can cause nucleocytoplasmic transport defects as a common disease mechanism in ALS/FTD.

3.3 Results

3.3.1 Cytoplasmic TDP-43 aggregates are enriched for components of nucleocytoplasmic transport pathway

A 25kDa C-terminal fragment of TDP-43 generated by proteolytic cleavage at Arg208 (TDP-CTF) is found as a major component of insoluble cytoplasmic aggregates in ALS/FTD patient brain tissue³⁰. Its expression as a fusion protein *in vitro* recapitulates histopathological features present in human patients^{113,125,132}. To compare the TDP-43 interactome under normal and pathological conditions, we used the BioID approach, which is based on the fusion of a promiscuous mutant of *E. coli* biotin ligase (BirA*) to proteins of interest. BirA* catalyzes the formation of a local ‘cloud’ of reactive biotinoyl-5 -AMP, resulting in biotinylation of proximate proteins in the natural cellular environment^{171,180,181}.

To determine physiological and aggregate-specific interacting partners of TDP-43, we transfected Neuro-2A (N2a) neuroblastoma cells with expression vectors for myc-BirA*-tagged human TDP-43 (myc-BirA*-TDP-43) or its C-terminal fragment (myc-BirA*-TDP-CTF) (**Fig. 3-1a**). Cells were incubated with excess biotin in the growth media to induce biotinylation of proximate proteins (**Supplementary Fig. 3-1a, b**), followed by denaturing lysis in 8M urea to solubilize protein aggregates, and affinity-purification via neutravidin beads (**Fig. 3-1b**). Biotinylated proteins co-localized with myc-BirA*-TDP-43 in the nucleus, and with myc-BirA*-TDP-CTF in cytoplasmic aggregates that were positive for hyper-phosphorylated TDP-43 (Ser 409/410), ubiquitin, and p62/SQSTM1 (**Fig. 3-1c**, and **Supplementary Fig. 3-1c, d**). Proximity-dependent biotinylation of BirA*-TDP-43 and BirA*-TDP-CTF associated proteins showed distinct patterns in protein lysates and pulldown samples (**Fig. 3-1d**).

Affinity purified TDP-43 and TDP-CTF associated biotinylated proteins were subjected to unbiased proteomic analysis. We found 622 proteins associated with myc-BirA*-TDP-43, and 810 proteins with myc-BirA*-TDP-CTF (**Fig. 3-2a**). The 523 proteins present in both datasets accounted for 84% of the TDP-43 and 65% of the TDP-CTF associated proteome. Gene ontology (GO) analysis of TDP-43 or TDP-CTF associated proteome versus mock transfected control showed several common functional annotations including translation, RNA processing, intracellular transport and cell cycle (**Supplementary Fig. 3-2a-c**), but also distinct categories of strongest interacting proteins (**Supplementary Fig. 3-2d, e**). The comparison of the TDP-CTF and TDP-43 associated proteome revealed their cell compartment and function-specific interaction networks (**Fig. 3-2b, c**). Proteins involved in RNA processing/splicing and transcription

primarily associated with TDP-43 (**Supplementary Fig. 3-3a, c**), whereas the TDP-CTF associated proteome was enriched for proteins involved in intracellular transport, translation, and proteolysis (**Supplementary Fig. 3-3b**). We identified components of nucleocytoplasmic transport pathway as major interactors within TDP-CTF aggregates (**Fig. 3-2d**, and **Supplementary Fig. 3-3d**). These proteomics data implicate the sequestration of the proteins involved in nucleocytoplasmic transport as a novel cellular phenotype caused by TDP-43 proteinopathies.

3.3.2 TDP-43 pathology causes the cytoplasmic aggregation and mislocalization of nucleoporins (Nups) and transport factors (TFs)

NPCs are created by the annular junction of inner and outer NMs and act as multiprotein channels and gatekeepers that regulate the receptor-mediated nucleocytoplasmic transport of macromolecules. NPCs contain ~30 different Nups and are among the largest proteinaceous assemblies in the eukaryotic cell¹⁸². To confirm putative targets of TDP-43 pathology identified in our proteomic analysis, we co-expressed GFP-tagged or epitope-tagged Nups and TFs together with mCherry-tagged TDP-CTF in N2a cells. We identified four different interaction patterns, as summarized in the schematic of the NPC (**Fig. 3-2e**, and **Supplementary Fig. 3-4, 5**): **(1)** Co-aggregation with TDP-CTF was found for the top-ranked hit Nup214 and other phenylalanine-glycine (FG) repeat-containing Nups (e.g. Nup62, Nup98 and Nup358) and scaffold Nups (e.g. Nup107 and Nup205), but also nuclear export factors (e.g. Xpo5 and Gle1); **(2)** Separate aggregation of transmembrane Nups (e.g. Pom121 and Gp210) from TDP-CTF inclusions indicated a major structural disruption of NPCs; **(3)** Dis-aggregation of TDP-CTF was caused by Nup85, Tpr and Kpnb1; **(4)** No effect on protein localization was found for Nups only

weakly associated with TDP-CTF (e.g. Nup50), further validating data from our proteomic analysis.

ALS-causing missense mutations, such as Q331K, increase cytoplasmic TDP-43 mislocalization and neurotoxicity¹⁰². To test whether wild-type and mutant TDP-43 differentially affect the localization of Nups and TFs, we co-expressed GFP or epitope-tagged Nups and TFs together with mCherry-tagged TDP-43^{WT} or TDP-43^{Q331K} in N2a cells. We found that TDP-43^{Q331K} increased the propensity of Nup98, Nup107 and Nup214 to form cytoplasmic aggregates as compared to TDP-43^{WT} (**Supplementary Fig. 3-6**).

In summary, our results show that cytoplasmic TDP-CTF aggregates impact the localization of nucleocytoplasmic transport proteins to varying degrees, causing the sequestration of several FG-Nups and nuclear export factors, and the mislocalization of transmembrane Nups. Although mutant TDP-43 remains mainly nuclear and does not form cytoplasmic aggregates in this cell culture model, it can still compromise the localization of FG-Nups.

3.3.3 FG-Nups contain prion-like domains (PrLDs) that mediate cytoplasmic co-aggregation with TDP-CTF

TDP-43 harbors a low-complexity and prion-like domain (PrLD) at the C-terminus, which contributes to self-assembly and protein-protein interactions¹¹⁷. PrLDs are usually found in transcription factors and RNA-binding proteins¹⁸³, but have been recently identified also in phenylalanine-glycin rich (FG) domains of yeast Nups¹⁸⁴. FG repeats are also present in mammalian Nups and form natively unfolded sites and amyloid-like

interaction within sieve-like hydrogels that act as effective barriers to normal macromolecules, but are permeable to shuttling nuclear transport receptor complexes¹⁸⁵.

We used the PLAAC algorithm¹⁸⁶ and other online tools (see **Methods**) to identify prion-like and low-complexity sequences in human Nups and TFs. Quantitative analysis revealed the presence of a PrLD and low-complexity domain in the hydrogel-forming Nup214¹⁸⁷ and other FG-Nups, including Nup54, Nup58, Nup62, Nup98, Nup153, Nup358 and CG1 (**Supplementary Fig. 3-7**). We next investigated whether the PrLD can mediate co-aggregation by co-expressing the PrLD and non-PrLD fragments of Nup98, Nup153 and Nup214 with TDP-CTF. The PrLDs of FG-Nups were both required and sufficient to mediate cytoplasmic co-aggregation (**Supplementary Fig. 3-8**). These results suggest that prion-like sequences present human FG-Nups may trigger their cytoplasmic aggregation in TDP-43 pathology.

3.3.4 TDP-43 pathology disrupts the morphology of the nuclear membrane (NM) and nuclear pore complexes (NPCs)

To visualize the nuclear morphology of transfected cells at high resolution in electron microscopy (EM), we fused an engineered peroxidase APEX2 to TDP-43 and TDP-CTF (**Fig. 3-3a**). APEX2-TDP-CTF formed pTDP-43-positive aggregates in the cytosol (**Fig. 3-3b**). APEX2 catalyzed the deposition of diaminobenzidine (DAB) near nuclear APEX2-TDP-43 and cytoplasmic APEX2-TDP-CTF aggregates, which can be visualized in EM (**Fig. 3-3c**). APEX2-TDP-CTF as well as GFP-TDP-CTF expressing cells exhibited irregularly shaped nuclei with deep invaginations of the NM (**Fig. 3-3c**).

To further investigate morphological deficits affecting the NM and NPCs via fluorescence microscopy, we undertook a series of experiments in mouse primary cortical neurons expressing either GFP, TDP-CTF, wild-type TDP-43 (TDP-43^{WT}), ALS-causing mutants (TDP-43^{Q331K} and TDP-43^{M337V}), or an NLS mutant (TDP-43^{mtNLS}). TDP-43 pathology caused cytoplasmic mislocalization and aggregation of endogenous FG-Nups concomitant with morphological abnormalities in the NM stained with anti-lamin B antibodies (**Fig. 3-4a**). A total of 49.5% of TDP-CTF expressing cells and 30 to 35% of TDP-43^{Q331K}, TDP-43^{M337V}, and TDP-43^{mtNLS} expressing cells exhibited abnormal NM morphology (**Fig. 3-4b**). 3D-reconstruction of nuclei stained with anti-lamin B antibodies further confirmed pathological invaginations of the NM in the presence of cytoplasmic TDP-CTF aggregates (**Supplementary Fig. 3-9a**). Knock-down of TDP-43 did not cause any obvious NM defects, demonstrating that the observed morphological defects in the NM are a consequence of TDP-43-mediated proteotoxicity instead of loss-of-function (**Fig. 3-4c**).

The nuclear lamina plays major roles in maintaining nuclear morphology, anchoring NPCs, organizing chromatin, and triggering DNA repair¹⁸⁸. We found that the impairment of lamina structure in TDP-CTF expressing neurons led to increased γ H2AX immunoreactivity, indicating elevated levels of DNA damage (**Fig. 3-4d**). Laminopathy-related DNA damage has also been observed in Alzheimer's disease with tau pathology, suggesting that lamin dysfunction may be a common defect in neurodegeneration¹⁸⁹. To anchor the nuclear lamina to the inner NM, lamins are tethered to the cytoskeleton through the LInkers of Nucleoskeleton and Cytoskeleton (LINC) complex¹⁹⁰. We found that expression of TDP-CTF and TDP-43^{Q331K} but not TDP-43^{WT} caused the

mislocalization of the LINC proteins sun2 and nesprin-2 as well as disorganization of F-actin in cortical neurons (**Supplementary Fig. 3-9b, c**). Lamins were not significantly presented in the interactome of myc-BirA*-TDP-CTF. However, as nesprin-2 is required for nuclear integrity and lamin B localization¹⁹¹, these data suggest that TDP-43 pathology causes the disruption of the nuclear lamina by interfering with the structural support from LINC complex proteins and the peripheral cytoskeleton.

To overcome the limits of resolution in fluorescence microscopy and clearly resolve the distribution of NPCs in the NM under normal and pathological conditions, we employed structured-illumination super-resolution microscopy. We found severely disturbed NPC distribution in the NM of N2a cells expressing GFP-TDP-CTF, with signs of NPC aggregation and clustering in some parts of the NM, and complete depletion in other regions (**Fig. 3-4e**). These strong morphological NM defects and the mislocalization of Nups and TFs caused by mutant or aggregated forms of TDP-43 suggested a consequential effect on nucleocytoplasmic transport processes.

3.3.5 TDP-43 pathology disrupts nuclear import of proteins and export of mRNA

To examine nuclear protein import, we co-expressed GFP or GFP-TDP-43 constructs with a fluorescent reporter protein flanked by NES and NLS sequences (NES-tdTomato-NLS)¹⁹² in primary cortical neurons. Quantitative analysis revealed a significant reduction of the nuclear-to-cytoplasmic (N-to-C) ratio of reporter protein in cells expressing TDP-CTF and TDP-43 mutants as compared to TDP-43^{WT} and the GFP control (**Fig. 3-4f, g**). Treatment with the nuclear import inhibitor importazole (IPZ) reduced the N-to-C ratio to a similar degree, whereas staurosporine (STS)-induced

apoptosis did not, thus ruling out that the observed protein import defects were caused by cell death (**Fig. 3-4g**). Compared to TDP-43^{WT}, we found a slight increase in cytoplasmic localization for TDP-43^{M337V} and a strong increase for TDP-43^{mtNLS} (TDP-43^{M337V}/ TDP-43^{WT}: 1.33x, TDP-43^{mtNLS}/ TDP-43^{WT}: 4.26x) (**Supplementary Fig. 3-9d, e**) as well as a reduction of the N-to-C ratio (TDP-43^{WT}: 7.18±0.36, TDP-43^{M337V}: 5.99±0.29, TDP-43^{mtNLS}: 0.86±0.03) (**Fig. 3-4h**). The moderate correlation of the N-to-C ratio of reporter to the N-to-C ratio of TDP-43 (**Fig. 3-4i**) and the cytoplasmic TDP-43 levels (**Supplementary Fig. 3-9f, g**) suggested that subcellular TDP-43 levels need to be tightly regulated, and that increased levels of cytoplasmic TDP-43 may interfere with nuclear protein import. To investigate whether TDP-43 pathology affects RNA export, poly(A) RNA was quantified via fluorescence *in situ* hybridization (FISH) with oligo-(dT) probes in the nucleus and cytoplasm. Expression of TDP-CTF and TDP-43 mutants caused significant nuclear retention of poly(A) RNA, indicating mRNA export defects (**Fig. 3-4j, k** and **Supplementary Fig. 3-9h**). As a likely consequence of this defect, we observed a significant reduction of steady state levels of protein translation in cells expressing TDP-CTF but not TDP-43^{WT}, as measured by metabolic labeling of newly synthesized proteins via azidohomoalanine (AHA) incorporation (**Fig. 3-4l**).

3.3.6 PABPN1, a suppressor of TDP-43 toxicity, rescues nucleocytoplasmic transport defects

Previously, we had identified poly(A)-binding protein nuclear 1 (PABPN1) as a potent suppressor of TDP-43 toxicity that acts via a proteasome-dependent mechanism¹²⁵. To assess its activity on the nucleocytoplasmic transport defect, we co-expressed GFP-

tagged TDP-CTF with mCherry or mCherry-tagged PABPN1. Overexpression of PABPN1 promoted the robust clearance of soluble and insoluble TDP-CTF (**Supplementary Fig. 3-10a**) and restored the proper localization of endogenous Nups and lamin B in cortical neurons (**Supplementary Fig. 3-10b, c**). TDP-CTF-mediated defects in nucleocytoplasmic transport of proteins (**Supplementary Fig. 3-10d**) and nuclear export of poly(A) RNA (**Supplementary Fig. 3-10e**) were also rescued by PABPN1 expression.

3.3.7 Nucleoporin genes act as modifiers of TDP-43 pathology in *Drosophila* models for ALS

To identify genetic interactions between TDP-43 toxicity and nucleoporin function *in vivo*, we tested whether mutations in *Nup* genes could alter TDP-43 toxicity in *Drosophila* disease models for ALS. Interestingly, expression of mutant TDP-43 in *Drosophila* motor neurons causes nuclear morphology defects¹⁹³, similar to nuclear contour irregularities found in spinal cord motor neurons of ALS patients¹⁵⁴.

Overexpression of human WT TDP-43 or the G298S mutant led to retinal degeneration and larval motor dysfunction (**Fig. 3-5a**)¹⁹³. In addition to a *Nup50* mutation previously implicated as a genetic suppressor of TDP-43 toxicity¹⁶⁹, we identified several loss-of-function mutations as genetic suppressors of TDP-43 pathology-dependent eye phenotypes, including *Nup93*, *Nup98-96*, *Nup107* and *Nup214* (**Fig. 3-5a**). In larval turning assays, these mutations also rescued the locomotor dysfunction that is caused by TDP-43^{WT} and TDP-43^{G298S} expression in motor neurons (**Fig. 3-5b**). The results show

that at least some aspects of TDP-43 toxicity *in vivo* depend on the nucleocytoplasmic transport machinery.

3.3.8 Nuclear pore pathology is common in brain tissue of ALS cases with TDP-43 inclusions

We next investigated the presence of nuclear pore pathology in patient's brain tissues with pTDP-43-positive inclusions, including sALS cases, and those caused by genetic mutations in *TARDBP* (TDP-ALS) or *C9orf72* (C9-ALS) (**Supplementary Table 3-1**, and **Supplementary Fig. 3-11**). Indeed, in the motor cortex, TDP-ALS and sALS cases but not age-matched controls presented with widespread loss of Nup205 immunoreactivity and large Nup205-positive cytoplasmic inclusions, whereas neurons in C9-ALS cases exhibited abnormal perinuclear punctate staining (**Fig. 3-6a**). Cytoplasmic Nup205-positive inclusions were also observed in the frontal cortices of ALS cases (**Supplementary Fig. 3-12**). Abnormal NM staining with anti-lamin B1 was occasionally present in the motor cortex of TDP-ALS but rarely found in C9-ALS and sALS cases (**Fig. 3-6b**). We did not observe obvious defects in Rangap1 staining among our cohorts (**Supplementary Fig. 3-13**). These data suggest that nuclear pore defects are a histopathological hallmark of ALS cases with TDP-43 proteinopathy, even in the absence of *C9orf72* repeat expansion.

3.4 Discussion

Here we have established a modified BioID procedure as a novel method to interrogate the proteome of insoluble aggregates associated with neurodegenerative diseases. Our

study provides evidence that (1) proteins involved in nucleocytoplasmic transport are major components of pathological TDP-43 aggregates; (2) TDP-43 pathology causes the aggregation of many Nups and nuclear TFs in the cytoplasm; (3) PrLDs present in human Nups containing FG repeats are required and sufficient for co-aggregation; (4) TDP-43 pathology causes morphological defects in the nuclear lamina and NPCs, as well as functional deficits in nuclear protein import and mRNA export; (5) several nucleoporin genes act as genetic modifiers of TDP-43 toxicity in *Drosophila*; and (6) NPC pathology is present in motor and frontal cortices of sporadic ALS cases and those caused by genetic mutations in the *TARDBP* gene, thus representing a general neuropathological hallmark of ALS that is not limited to ALS cases with *C9orf72* mutations.

The specific composition of TDP-43 aggregates has remained unknown, perhaps due to technical limitations in preserving protein interactions under the harsh lysis conditions required for the extraction of insoluble aggregates. To address this open question, we adapted a method for proximity-based biotinylation of proteins within a labeling range of ca. 10nm in the natural environment of the cell^{171,180,181}. The high affinity of streptavidin/neutravidin to biotin, which is among the strongest noncovalent biological interactions known, allowed us to perform affinity-purification of biotinylated proteins under the strong denaturing condition required for solubilizing protein aggregates. Robust labeling of proteins within detergent-insoluble aggregates suggests that this method has a broad applicability to study a wide range of neuropathological inclusions. Our proteomic analysis of pathological TDP-43 aggregates led to the unexpected discovery that cytoplasmic TDP-43 aggregates are highly enriched for structural components of NPCs as well as TFs. This finding suggested that TDP-43 may

not only be mislocalized as a consequence of defects in nucleocytoplasmic transport, but may directly inhibit the nuclear import and export of macromolecules.

We found that the majority of Nups was affected by TDP-43 pathology, causing their cytoplasmic mislocalization and aggregation. This was also true for several nuclear export factors including Gle1, which plays a role in mRNA export and stress granule formation¹⁵⁸. *GLE1* mutations have also been identified as causative for ALS¹⁹⁴.

Interestingly, we discovered several components of the nucleocytoplasmic transport machinery that were not affected by TDP-43 pathology, but instead prevented the cytoplasmic aggregation of TDP-CTF. The most pronounced effect was found for Kpnb1, which is also involved in the nuclear import of TDP-43 in concert with NLS-binding Kpna proteins. A previous screen of 82 proteins involved in nuclear transport has found that downregulation of Kpnb1 can cause cytoplasmic accumulation of TDP-43¹⁵⁵.

Several recent studies have linked ALS/FTD caused specifically by G4C2 hexanucleotide repeat expansion in the *C9orf72* gene to nucleocytoplasmic transport defects, proposing that the cytoplasmic accumulation of TDP-43 observed in *C9orf72*-linked ALS/FTD may be a consequence of these defects¹¹⁹⁻¹²¹. Dipeptide repeat proteins (DPRs) expressed via repeat-associated non-ATG (RAN) translation may impair the function of NPCs by sequestering nucleocytoplasmic transport proteins^{170,195,196}. Here we show that TDP-43 pathology itself can disrupt nucleocytoplasmic transport and disturb the morphology of the NM and NPCs. This is further supported by the identification of mutations in nucleoporin genes as genetic suppressors of TDP-43 toxicity in *Drosophila* models of ALS. Our discovery of nuclear pore pathology in TDP-ALS and sALS patients suggests that even in the absence of *C9orf72* mutations, nucleocytoplasmic transport

defects represent a common pathological feature in the vast majority of ALS cases that are characterized by TDP-43 pathology, and potentially other TDP-43-associated diseases. Rescue of TDP-43-induced toxicity by eliminating aggregated or mutant forms of TDP-43 may be required for restoring proper RNA and protein localization in the cell. How TDP-43 proteinopathy interferes with nucleocytoplasmic transport remains to be investigated in detail. A possible mechanism has been suggested by the finding that various aggregation-prone proteins have the potential to compromise nucleocytoplasmic transport via the cytoplasmic mislocalization of THOC2 when they are directed to the cytoplasm¹⁹⁷, but the lack of THO complex components in our proteomic data sets suggests a different mechanism at least in our models of TDP-43 proteinopathy.

As a possible mechanistic explanation, we identified PrLDs similar to those frequently found in RBPs such as TDP-43 within FG domains of several human Nups. These PrLDs were both required and sufficient for co-aggregation with TDP-CTF. Recently, it has been shown that polyPR DPRs encoded by the *C9orf72* repeat expansion bind directly to FG repeat domains in the central channel of NPCs, thus causing inhibition of the nucleocytoplasmic transport of macromolecules¹⁹⁸. The sorting capability of NPCs is driven by the phase separation of FG domains into dense and sieve-like hydrogels. A similar phase separation process driven by disordered protein domains has also been recognized as pivotal for the formation of membraneless ribonucleoprotein organelles such as stress granules and their pathological transition into insoluble aggregates, making this process an important emerging principle in neurodegeneration^{141,199}. Our findings suggest that the interaction of PrLDs in TDP-43

and those that we discovered in FG-Nups may trigger the pathological cascade in a similar way.

This study supports a model where TDP-43 protein presents as both a ‘victim’ and a ‘perpetrator’ in the context of nucleocytoplasmic transport defects. Based on our findings, we propose that (1) cytoplasmic mislocalization of TDP-43 due to unrelated nucleocytoplasmic transport defects may exacerbate these defects in a positive feedback loop; and (2) TDP-43 can play a role in directly triggering nucleocytoplasmic transport defects by disrupting the localization of Nups and TFs (**Fig. 3-7**). A better understanding of the role of TDP-43 in intracellular transport pathways may help in developing therapeutic strategies for ALS/FTD and other TDP-43 proteinopathies.

3.5 Figures

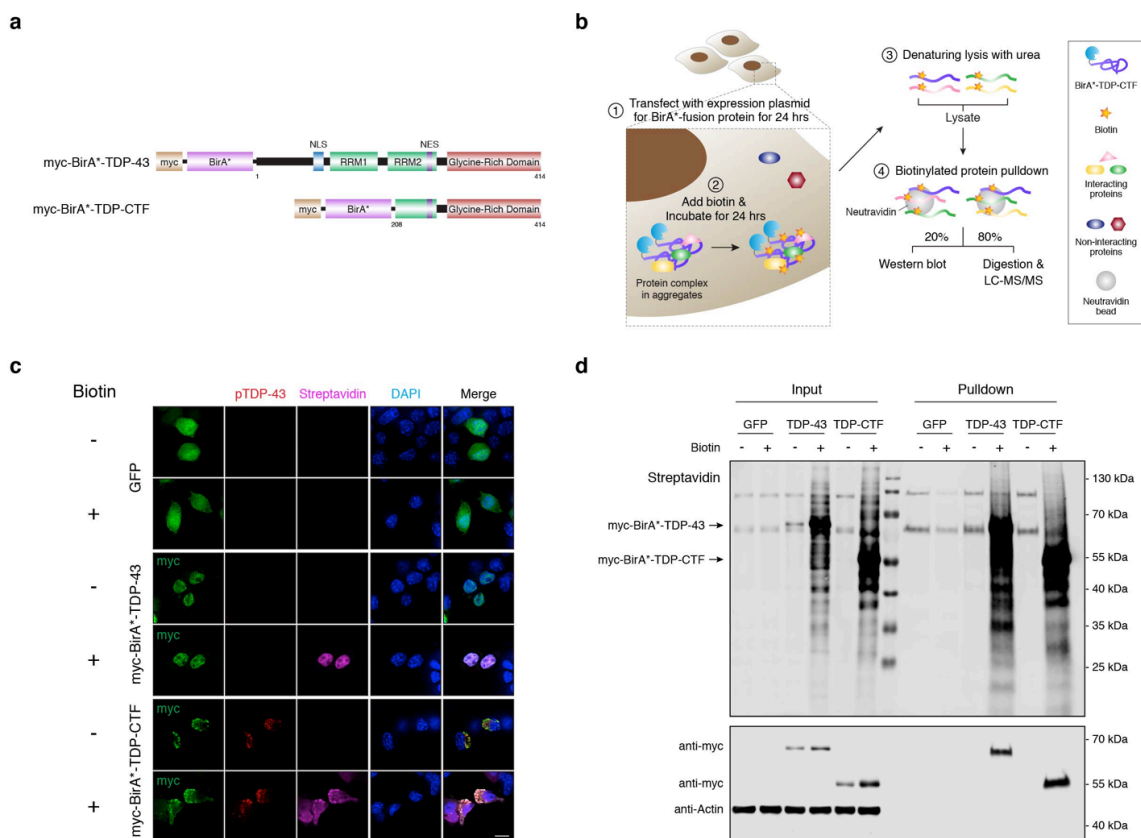


Figure 3-1 | A modified BioID method identifies the composition of pathological detergent-insoluble TDP-43 aggregates.

a, Domain structures of myc-BirA* fusion constructs with human full-length TDP-43 and TDP-CTF protein. **b**, Schematic for the proximity-dependent biotinylation and identification of proteins associated with myc-BirA*-TDP-CTF. **c**, Anti-myc staining shows nuclear myc-BirA*-TDP-43 and cytoplasmic aggregates of myc-BirA*-TDP-CTF (green) that are positive for phospho-TDP-43^{S409/410} (red) and biotin (magenta). **d**, Western blot analysis of biotinylated proteins in lysates and after pulldown with neutravidin beads. Scale bar: 10 μ m.

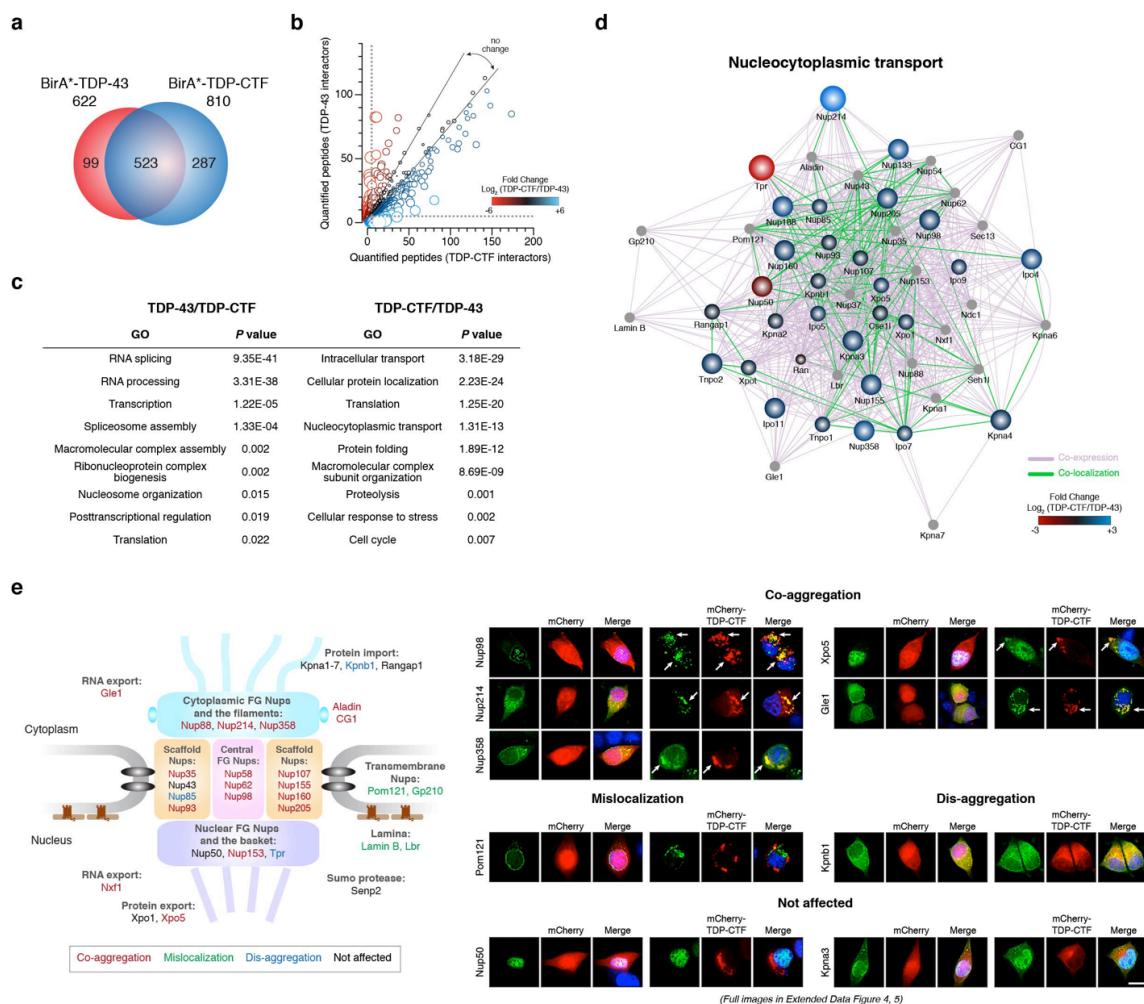


Figure 3-2 | Pathological TDP-43 aggregates contain components of the nucleocytoplasmic transport machinery.

a, Mass spectrometry analysis of proximity-biotinylated proteins associated with BirA*-TDP-43 and BirA*-TDP-CTF. **b**, Mapping the number of identified peptide spectra matches (PSMs) for the interacting protein of TDP-43 and TDP-CTF. The relative abundance ratio (\log_2 -fold change) between TDP-CTF and TDP-43 associated proteome is shown. Positive values indicate predominant association with TDP-CTF (blue), and negative values with TDP-43 (red). **c**, Functional annotation of proteins preferentially associated with TDP-43 or TDP-CTF. **d**, Network analysis of the TDP-CTF (blue) and

TDP-43 (red) interactome in the nucleocytoplasmic transport pathway. **e**, Summary diagram of the TDP-CTF interaction screen with 37 proteins involved in nucleocytoplasmic transport. Representative images of the co-aggregation (arrows) of GFP-tagged proteins with mCherry-TDP-CTF in N2a cells. Images for all tested components of the nucleocytoplasmic transport machinery are shown in **Supplementary Fig. 3-4** and **3-5**. Scale bar: 10 μm .

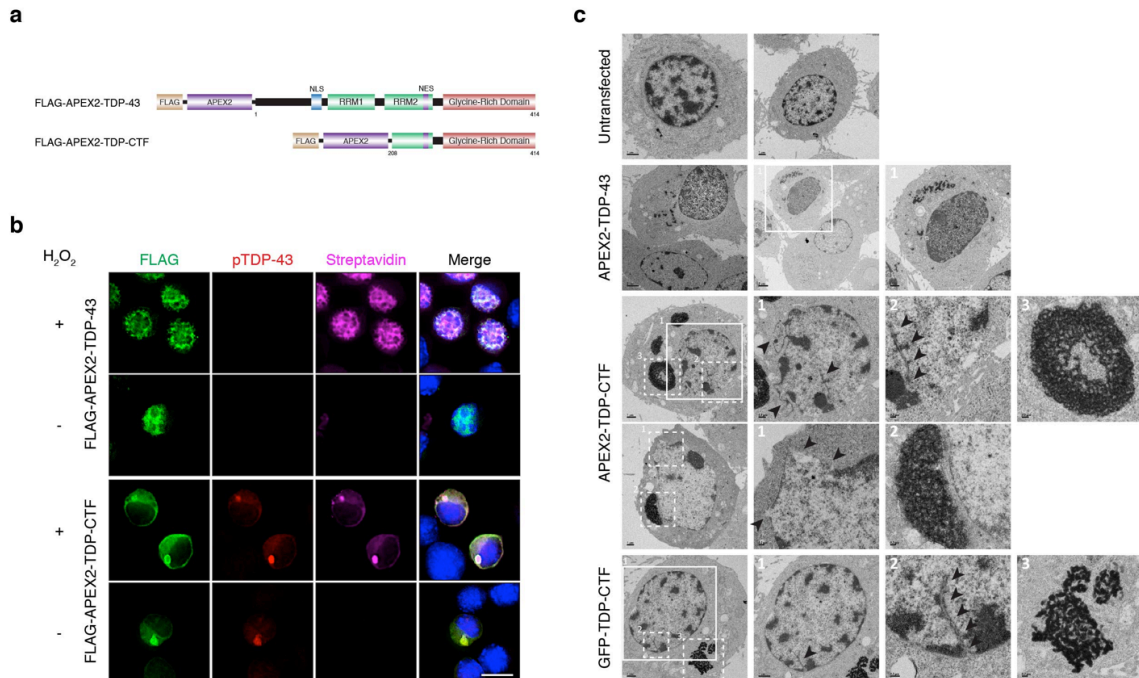


Figure 3-3 | Electron microscopy (EM) analysis reveals abnormal nuclear membrane (NM) morphology in N2a cells.

a, Schematic domain structures of engineered peroxidase, APEX2, fusion TDP-43 and

TDP-CTF. **b**, Nuclear signals of FLAG-APEX2-TDP-43 and cytoplasmic aggregates of

FLAG-APEX2-TDP-CTF were detected by anti-FLAG antibody (green). TDP-CTF

phosphorylation was detected by anti-pTDP-43 (S409/410) antibody (red). Protein

biotinylation catalyzed by APEX2 was detected by cy5-conjugated streptavidin

(magenta). Scale bar: 10 μ m. **c**, EM analysis of untransfected N2a cells and cells

expressing FLAG-APEX2-TDP-43, FLAG-APEX2-TDP-CTF or GFP-TDP-CTF.

Untransfected cells revealed dense chromatin and round-shape nucleus. APEX2 fusion

TDP-43 catalyzed the DAB deposit mostly in the nucleus. APEX2 fusion TDP-CTF

catalyzed the DAB deposit in the cytoplasmic aggregates. The internal invagination of

NM and abnormal nuclear morphology were observed in cells expressing FLAG-APEX2-

TDP-CTF. GFP-TDP-CTF generated electron-dense cytoplasmic aggregates and also caused the internal invagination of NM.

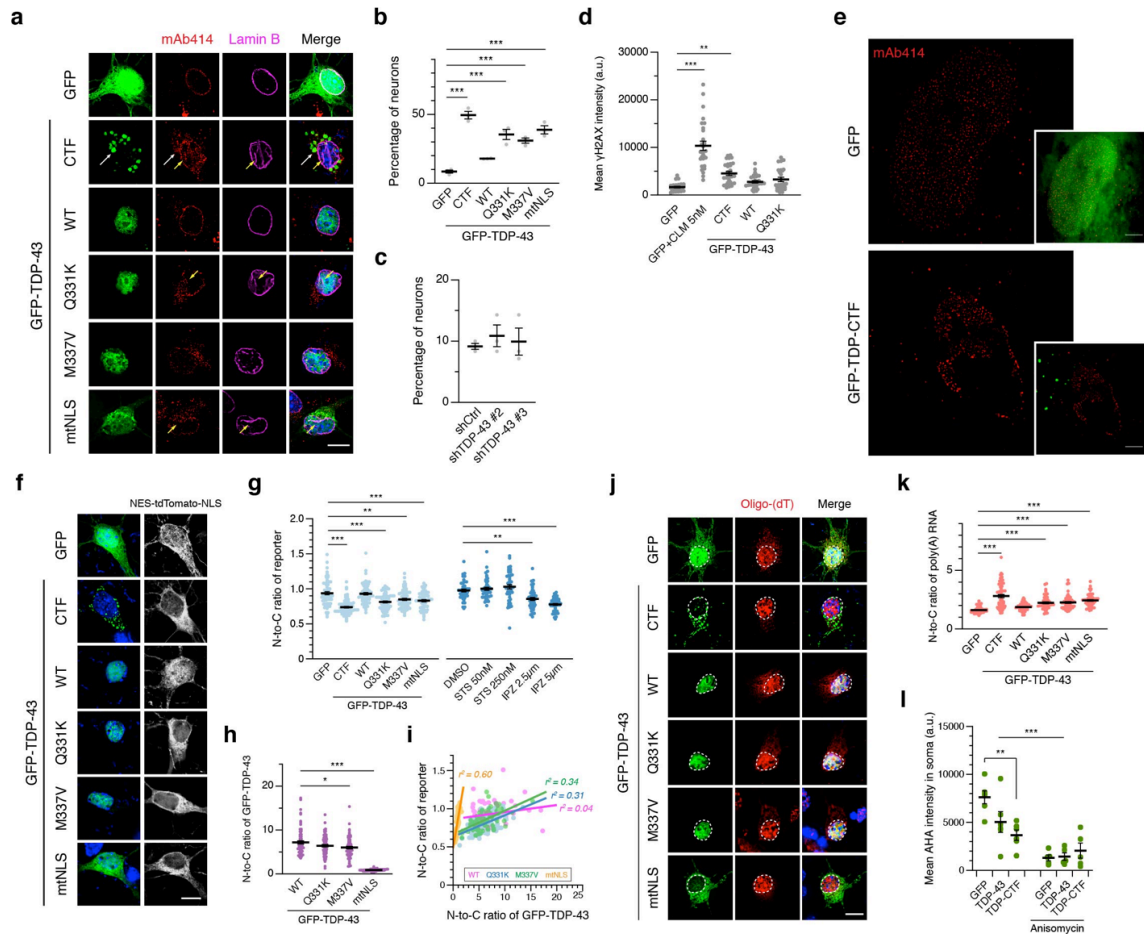


Figure 3-4 | TDP-43 pathology disrupts NPC and nuclear lamina structures and nucleocytoplasmic transport.

a, Immunostaining of endogenous Nups (mAb414, red) and lamin B (magenta) in cortical neurons expressing GFP or GFP-tagged TDP-43 constructs. **b**, **c**, Quantification of transfected cells exhibiting abnormal lamin B staining after transfection with TDP-43 expression vectors (**b**), or TDP-43 knock-down constructs (**c**). **d**, Quantification of mean γ H2AX intensity in cortical neurons expressing GFP or GFP-tagged TDP-CTF, TDP-43^{WT} or TDP-43^{Q331K}. Calicheamicin (CLM) was added at 5 nM to induce DNA damage. **e**, Super-resolution microscopy (SIM) of endogenous FG-Nups (mAb414, red) in N2a cells expressing GFP or GFP-TDP-CTF. Scale bar: 5 μ m. **f**, **g**, Quantification of N-to-C

ratio of a transport reporter encoding NES-tdTomato-NLS. Staurosporin (STS). Importazole (IPZ). **h**, N-to-C ratio of GFP-TDP-43. (**b**, $***P < 0.001$, GFP ($n = 73$) or GFP-tagged TDP-CTF ($n = 79$), TDP-43^{WT} ($n = 73$) or TDP-43^{Q331K} ($n = 84$), TDP-43^{M337V} ($n = 78$) or TDP-43^{mtNLS} ($n = 82$); **c**, shCtrl ($n = 33$), shTDP-43 #2 ($n = 36$) or shTDP-43 #3 ($n = 33$); **d**, $**P < 0.01$, $***P < 0.001$, GFP ($n = 26$), GFP+CLM 5 nM treatment ($n = 28$) or GFP-tagged TDP-CTF ($n = 29$), TDP-43^{WT} ($n = 29$) or TDP-43^{Q331K} ($n = 26$); **g**, $**P < 0.01$, $***P < 0.001$. For quantifying the nucleocytoplasmic transport of protein reporter, cortical neurons expressing GFP ($n = 70$) or GFP-tagged TDP-CTF ($n = 72$), TDP-43^{WT} ($n = 70$), TDP-43^{Q331K} ($n = 70$), TDP-43^{M337V} ($n = 70$) or TDP-43^{mtNLS} ($n = 61$) were collected. For STS induction experiment: 50 nM ($n = 46$), 250 nM ($n = 47$) and for IPZ induction: 2.5 μ M ($n = 45$), 5 μ M ($n = 45$). DMSO was used as the vehicle control ($n = 46$); **h**, $*P < 0.05$, $***P < 0.001$, GFP-tagged TDP-43^{WT} ($n = 70$), TDP-43^{Q331K} ($n = 70$), TDP-43^{M337V} ($n = 70$) or TDP-43^{mtNLS} ($n = 61$); all by one-way ANOVA, Bonferroni's post hoc test). **i**, R-square (r^2) in regression analysis of N-to-C ratio of NES-tdTomato-NLS and GFP-TDP-43. **j**, **k**, Quantification of N-to-C ratio of poly(A) RNA. ($***P < 0.001$, GFP ($n = 46$) or GFP-tagged TDP-CTF ($n = 61$), TDP-43^{WT} ($n = 49$), TDP-43^{Q331K} ($n = 51$), TDP-43^{M337V} ($n = 60$) or TDP-43^{mtNLS} ($n = 58$), one-way ANOVA, Bonferroni's post hoc test). **l**, Quantification of levels of newly synthesized protein via metabolic labeling with azidohomoalanine (AHA). Anisomycin was added as a translation inhibitor. ($**P < 0.01$, $***P < 0.001$, GFP ($n = 57$) or GFP-tagged TDP-43^{WT} ($n = 59$) or TDP-CTF ($n = 60$) were collected. Anisomycin control: GFP ($n = 59$) or GFP-tagged TDP-43^{WT} ($n = 50$) or TDP-CTF ($n = 48$), two-way

ANOVA, Bonferroni's post hoc test). Graphs represent mean and SEM. Scale bar: 10 μm .

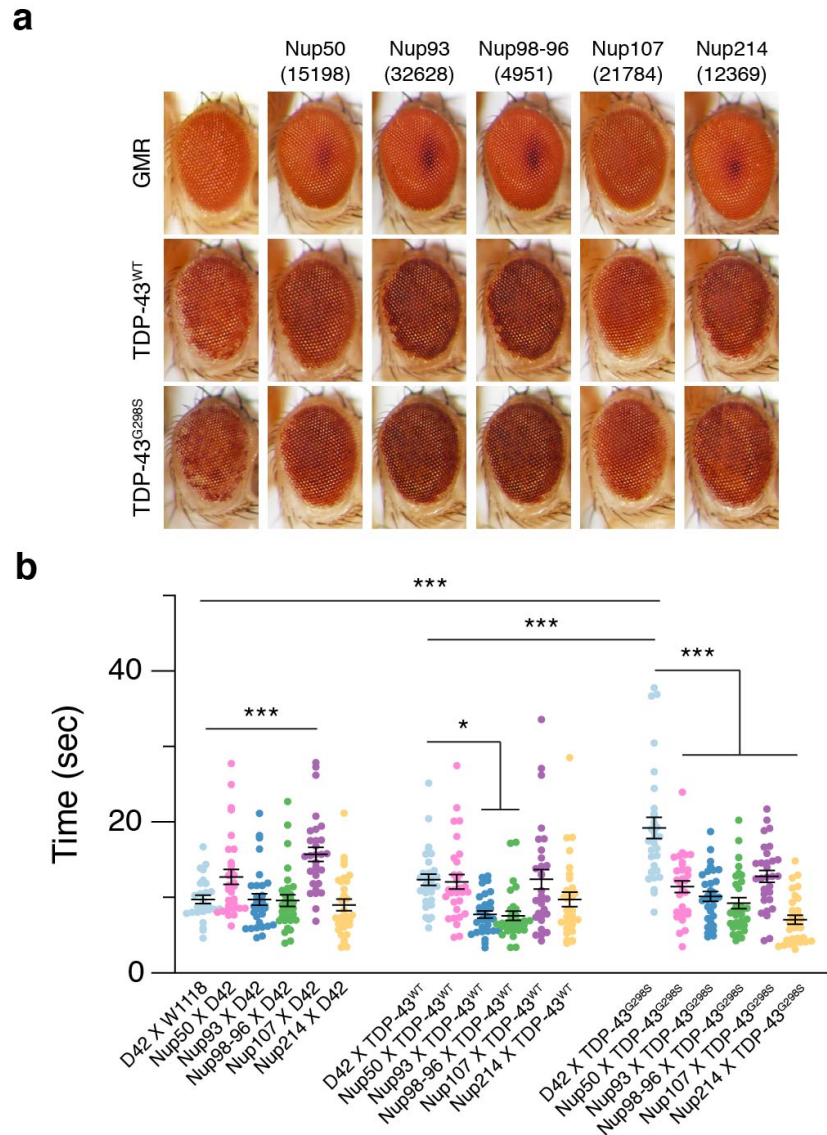


Figure 3-5 | Identification of genetic suppression of TDP-43 toxicity in *Drosophila* disease models of ALS.

a, b, Overexpression of human TDP-43^{WT} and TDP-43^{G298S} in *Drosophila* leads to neurodegeneration in the adult retina (**a**) and impairment in larval locomotor function (**b**). Loss-of-function mutations in several *Drosophila* Nup genes rescue the TDP-43 proteinopathy phenotypes. (** $P < 0.01$, *** $P < 0.001$, 26 to 30 larvae per genotype, two-way ANOVA, Bonferroni's post hoc test). Graphs represent mean and SEM.

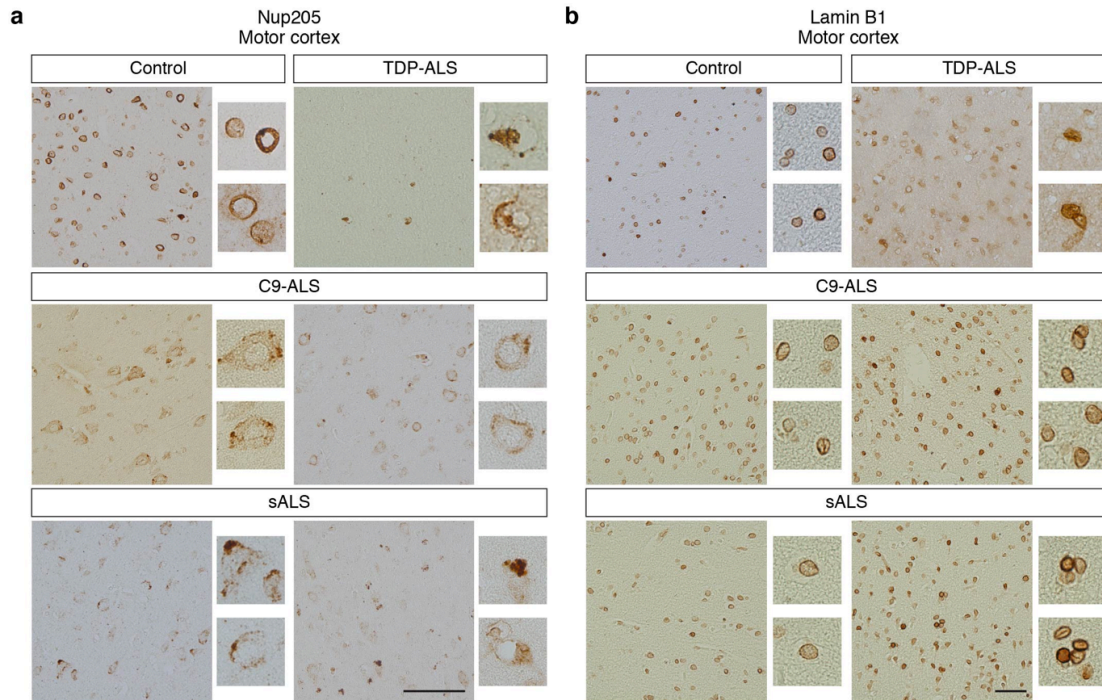


Figure 3-6 | Nuclear pore pathology in ALS patient brain tissue with TDP-43 inclusions.

a, b, Immunohistochemical staining of Nup205 (**a**) Lamin B1 (**b**) in human motor cortices of control, TDP-ALS, C9-ALS and sALS cases. Scale bar: 100 μ m.

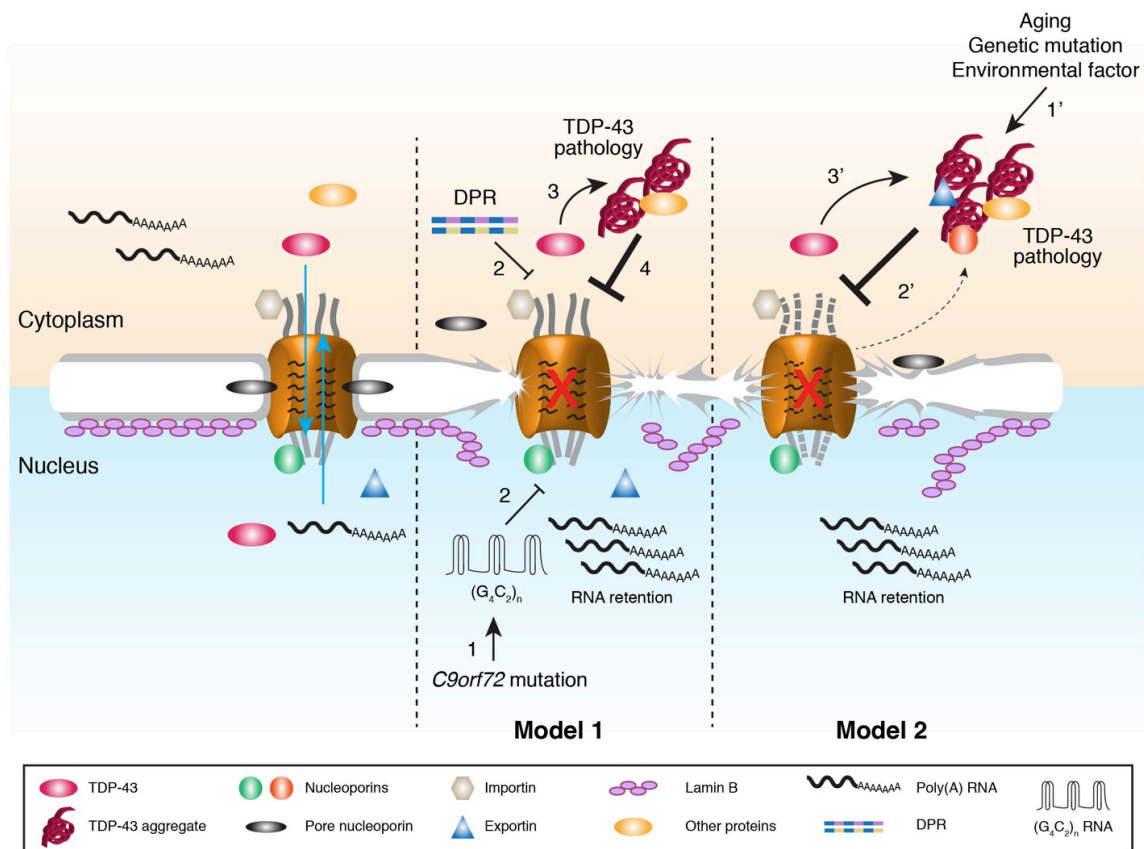
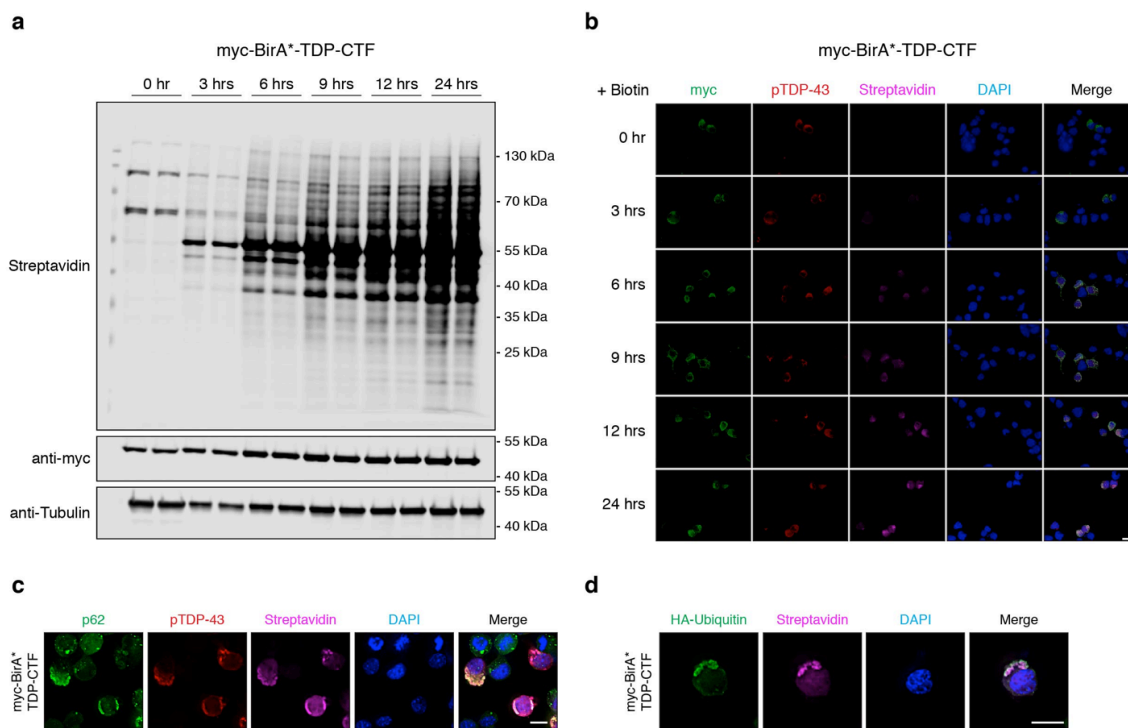


Figure 3-7 | A model for TDP-43 pathology-mediated nucleocytoplasmic transport defects.

Model 1 is based on the published observation¹¹⁹⁻¹²¹ that (1) *C9orf72* mutation induces the generation of G4C2 repeat-expansion RNA transcripts and DPRs, (2) leading to the defects in nuclear protein import and (3) results in the cytoplasmic accumulation of TDP-43. We propose that (4) mislocalized cytoplasmic TDP-43 further exacerbates nucleocytoplasmic transport defects. **Model 2** proposes that (1') TDP-43 aggregation is initiated by normal aging, genetic mutations, and/or environmental stressors^{117,118}. (2') TDP-43 aggregates directly impair the nucleocytoplasmic transport by causing the sequestration or mislocalization of Nups and TFs. (3') Compromised nuclear protein import exacerbates the cytoplasmic accumulation of TDP-43 in a positive feedback loop.

The impairment of protein and RNA homeostasis can subsequently contribute to the neurodegeneration observed in ALS/FTD.

3.6 Supplementary Figures

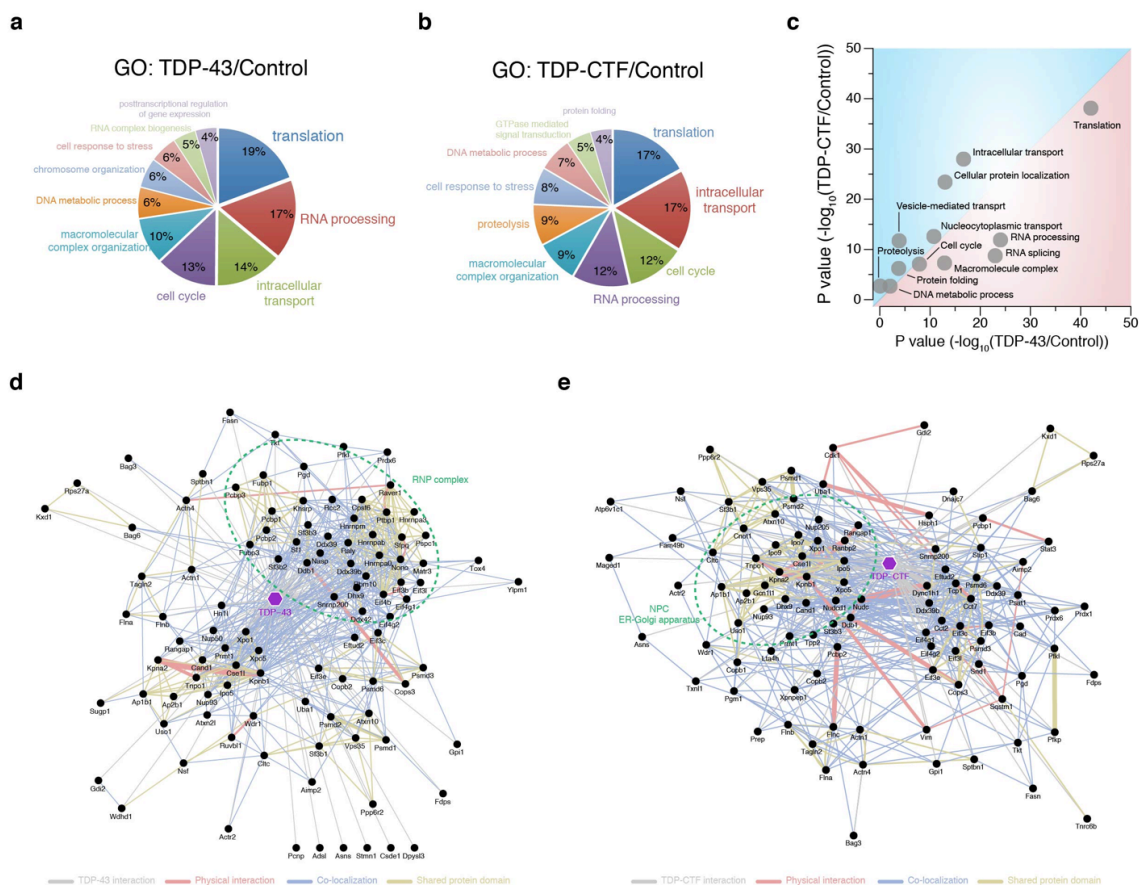


Supplementary Figure 3-1 | BirA*-tagged TDP-CTF catalyzes the biotinylation of proximate proteins in cytoplasmic aggregates.

a, Western blotting analysis of the time courses of protein biotinylation in N2a cells expressing myc-BirA*-TDP-CTF after the incubation of excess biotin. Biotinylation signals were detected by streptavidin. Myc-BirA*-TDP-CTF was detected by anti-myc antibody. Tubulin staining was as the reference. **b**, Immunofluorescence analysis of the time courses of protein biotinylation in N2a cells expressing myc-BirA*-TDP-CTF. Phosphorylated TDP-CTF was detected by anti-pTDP-43 (S409/410) antibody (red) and biotinylated proteins were detected by cy5-conjugated streptavidin (magenta). **c**, Myc-BirA*-TDP-CTF formed cytoplasmic aggregates positive to p62 (green) and pTDP-43 (red) staining. The majority of biotinylated proteins were detected in the aggregates via

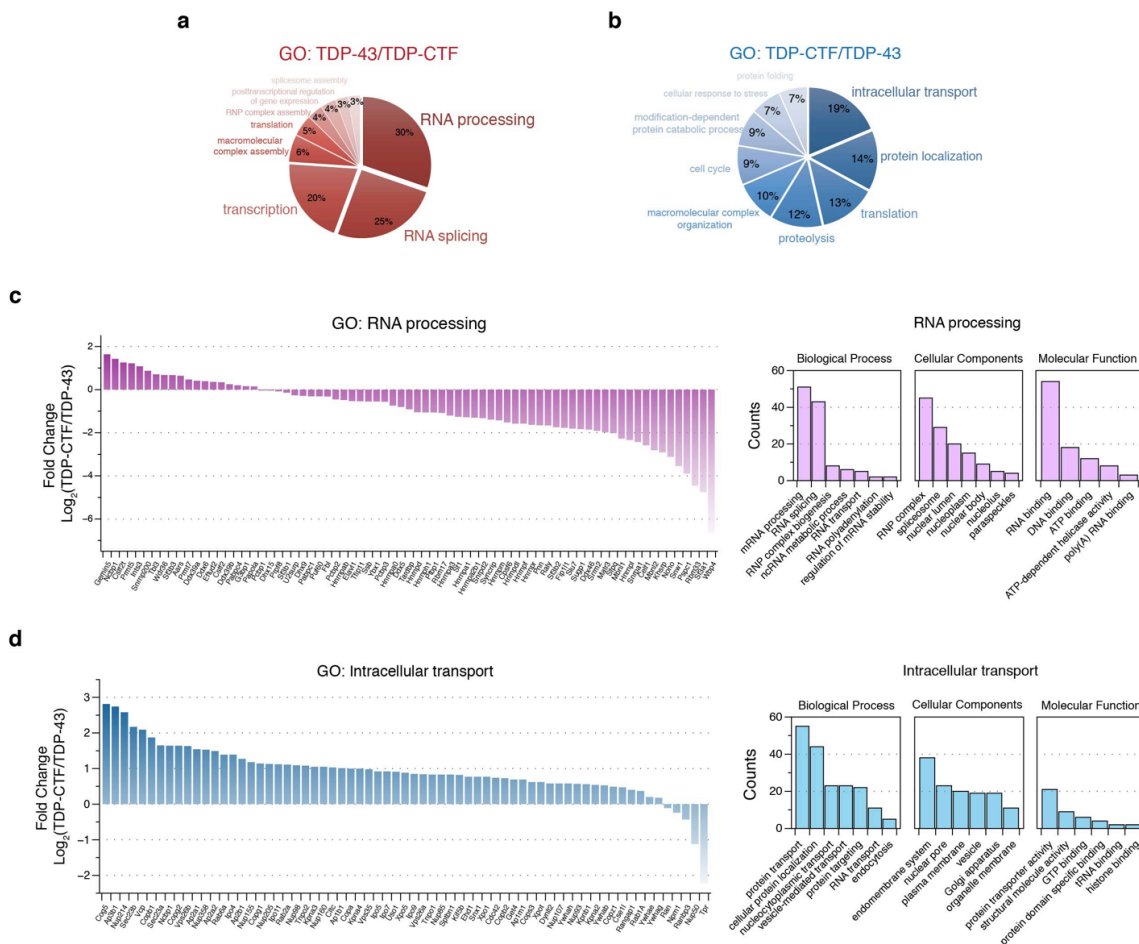
streptavidin staining (magenta). **d**, HA-tagged ubiquitin was co-expressed with myc-BirA*-TDP-CTF. The BirA*-TDP-CTF formed ubiquitin-positive aggregates (green).

Scale bar: 10 μm .



Supplementary Figure 3-2 | Gene ontology (GO) analysis of the TDP-43 and TDP-CTF interactomes.

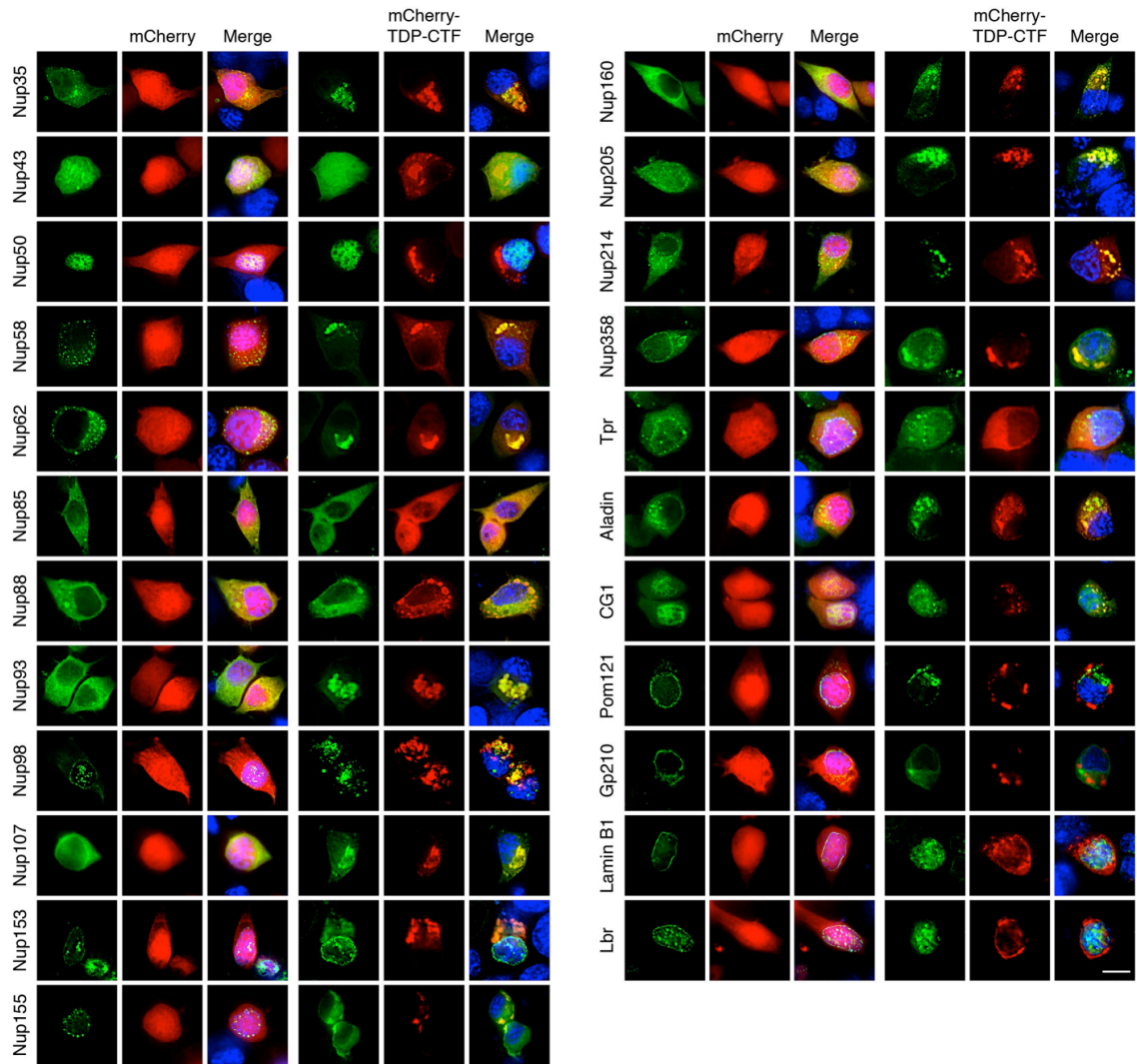
a, b, Mass spectrometry analysis of the biotinylated proteins through neutravidin pull-down from N2a cells expressing mock transfected control, myc-BirA*-TDP-43 or myc-BirA*-TDP-CTF. List of functional annotation by comparing TDP-43 (**a**) or TDP-CTF (**b**) to control proteome. **c**, The y-axis indicates the *P* value of the annotation in TDP-CTF/control, and the x-axis designates the *P* value of the annotation in TDP-43/control. **d, e**, Network analysis of the top 100 protein interactors of TDP-43 (**d**) or TDP-CTF (**e**) by GeneMANIA.



Supplementary Figure 3-3 | GO analysis of differential protein interactions with TDP-43 and TDP-CTF.

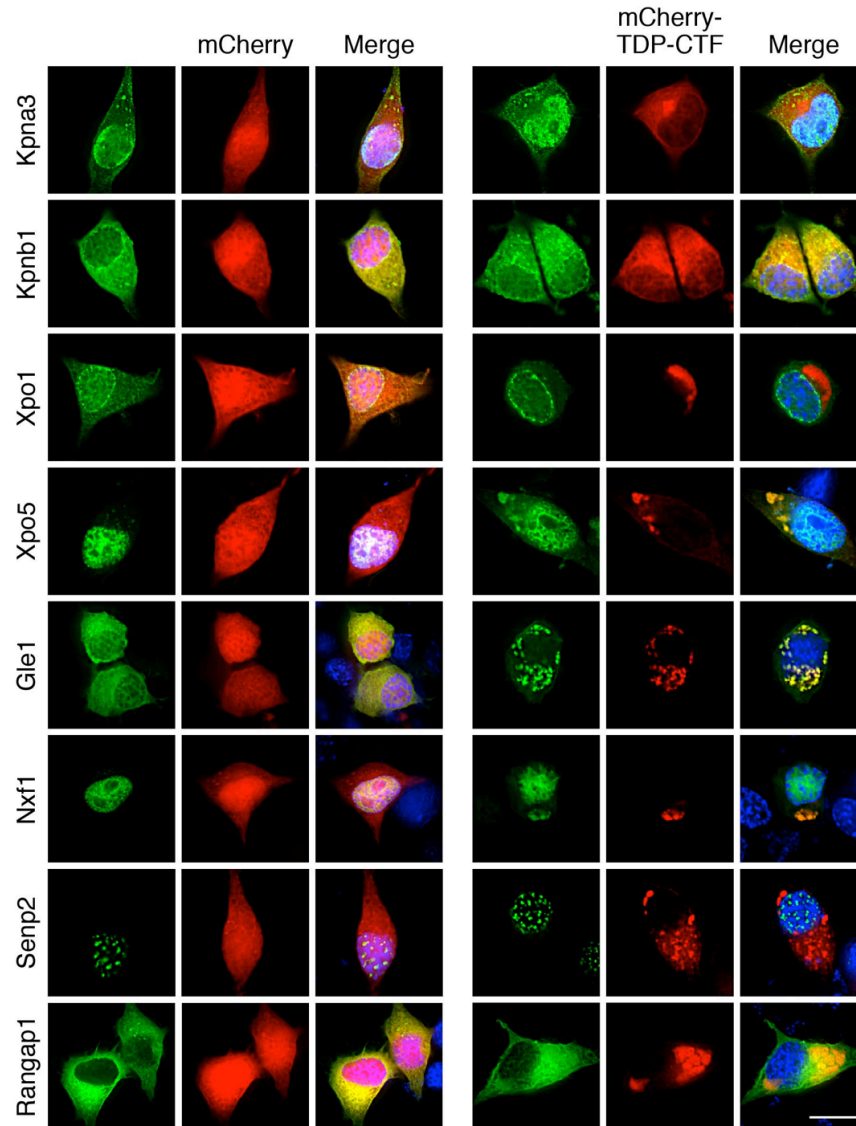
a, GO analysis of the functional annotation groups via the comparison of TDP-43 and TDP-CTF. The annotation reveals that RNA processing as the top ranked functional group in TDP-43/TDP-CTF proteome. **b**, GO analysis reveals that intracellular transport as the top ranked functional group in TDP-CTF/TDP-43 proteome. **c**, Differential expression of proteins related to RNA processing. The y-axis indicates the relative abundance ratio (\log_2 -fold change). GO analysis of RNA processing in terms of biological processing, cellular components and molecular function. **d**, Differential

expression the biological function and localization of proteins involved in intracellular transport.



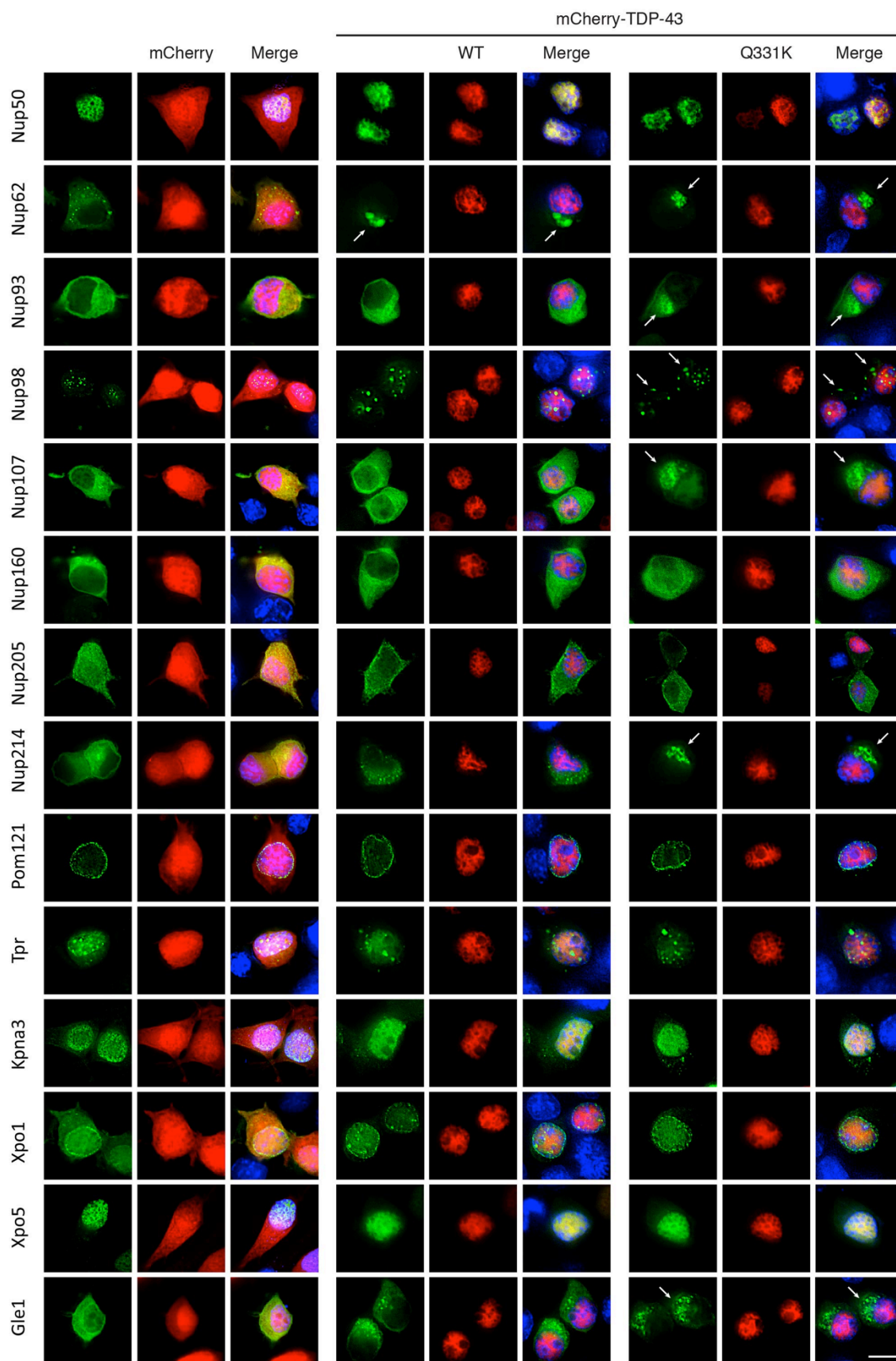
Supplementary Figure 3-4 | TDP-CTF expression alters the cellular localization of nucleoporins (Nups) and lamins in N2a cells.

N2a cells were co-expressed with mCherry or mCherry-tagged TDP-CTF, and GFP or epitope-tagged Nup35, Nup43, Nup50, Nup58, Nup62, Nup85, Nup88, Nup93, Nup98, Nup107, Nup153, Nup155, Nup160, Nup205, Nup214, Nup358, Tpr, Aladin, CG1, Pom121, Gp210, Lamin B and Lamin B receptor (Lbr) proteins. GFP or epitope-tagged expression plasmids were listed on the left. Scale bar: 10 μm .



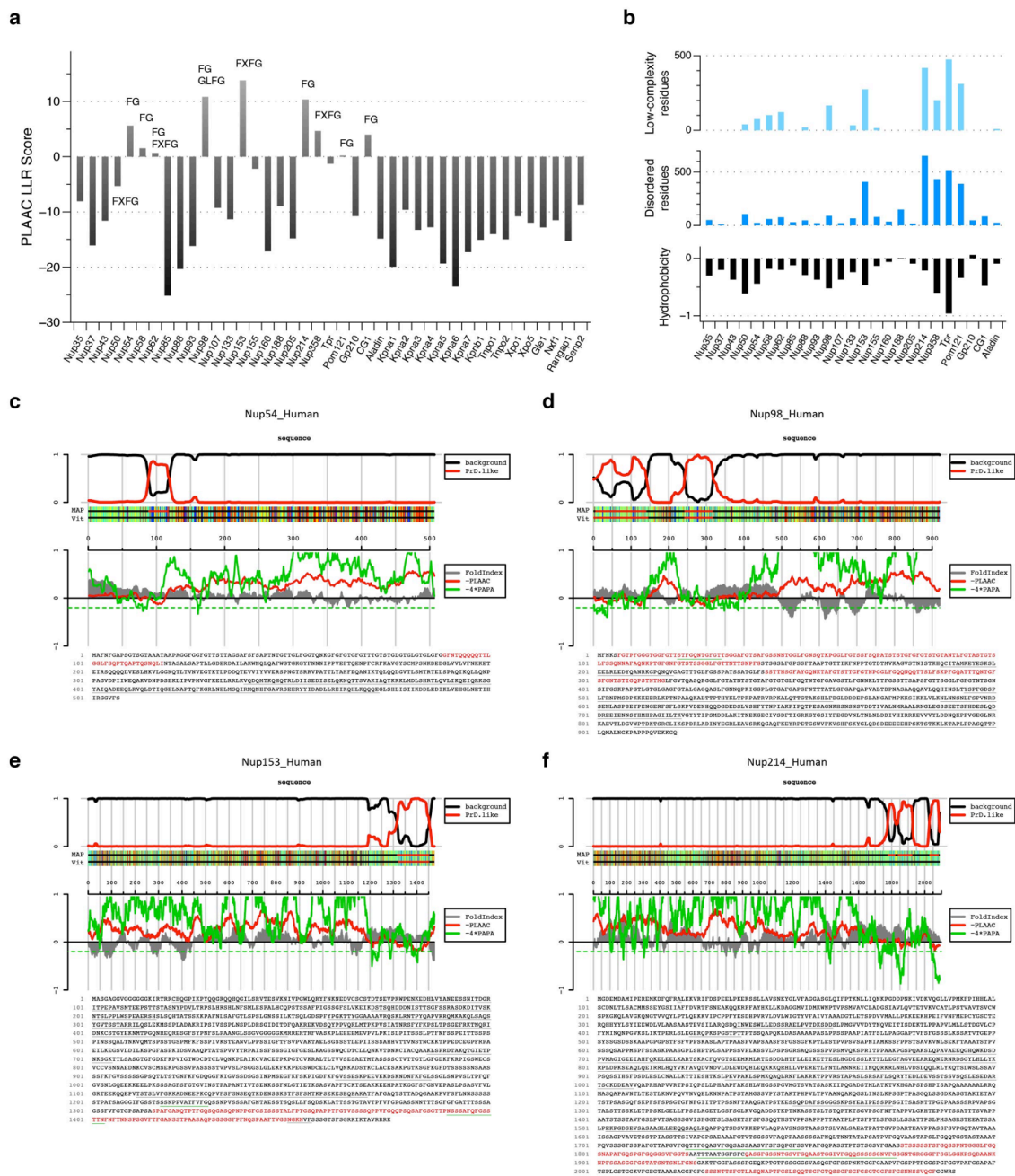
Supplementary Figure 3-5 | TDP-CTF expression alters the cellular localization of nucleocytoplasmic transport factors (TFs) in N2a cells.

N2a cells were co-expressed with mCherry or mCherry-tagged TDP-CTF, and GFP or epitope-tagged Kpna3, Kpnb1, Xpo1, Xpo5, Gle1, Nxf1, Senp2 and Rangap1. GFP or epitope-tagged expression plasmids were listed on the left. Scale bar: 10 μ m.



Supplementary Figure 3-6 | ALS-causing TDP-43 mutation enhances mislocalization and cytoplasmic aggregation of Nups and TFs as compared to wild-type TDP-43 in N2a cells.

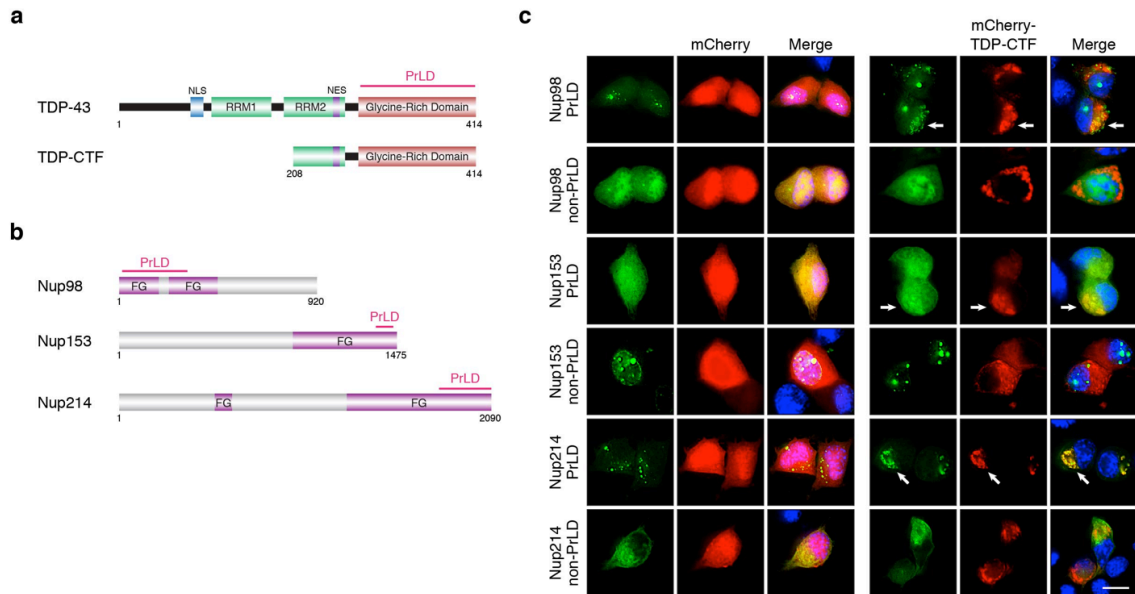
N2a cells were co-expressed with mCherry or mCherry-tagged TDP-43^{WT} or TDP-43^{Q331K}, and GFP or epitope-tagged Nup50, Nup62, Nup93, Nup98, Nup107, Nup160, Nup205, Nup214, Pom121, Tpr, Kpna3, Xpo1, Xpo5 and Gle1. GFP or epitope-tagged expression plasmids were listed on the left. Arrow indicates the aggregation. Scale bar: 10 μ m.



Supplementary Figure 3-7 | Prediction of prion-like domains (PrLDs) and intrinsically disordered regions in human Nups and TFs.

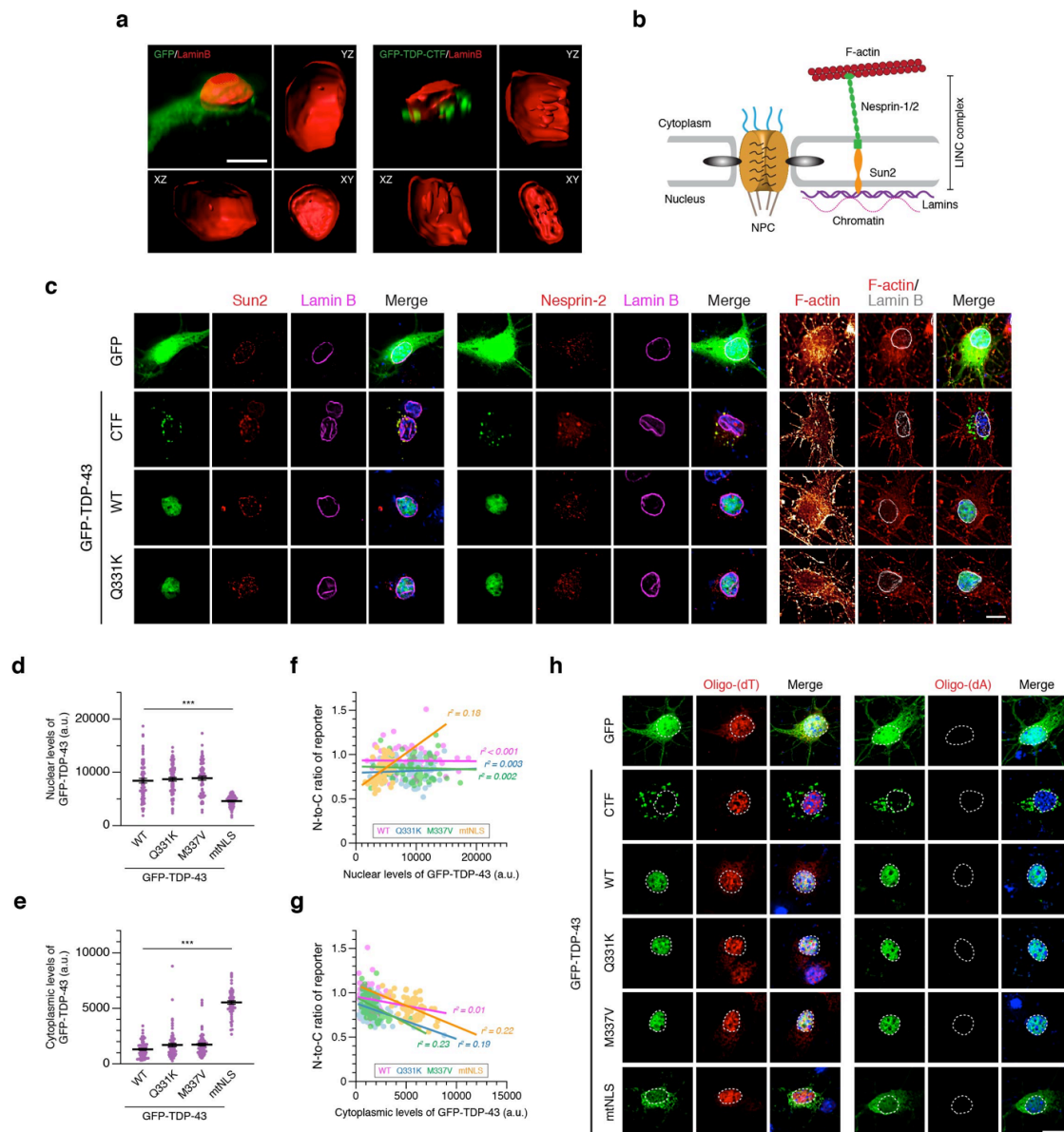
a, PrLD scores of human Nups and TFs were predicted by PLAAC. Positive score depicts the prion-like tendency. **b**, Prediction of the low-complexity residues, intrinsically disordered regions, and hydrophobicity of human Nups and TFs. **c-f**, Color-coded

visualization of amino acid sequences and predicted PrLDs in human Nup54 (c), Nup98 (d), Nup153 (e) and Nup214 (f) from PLACC.



Supplementary Figure 3-8 | PrLDs of FG-Nups mediate the co-aggregation with TDP-CTF.

a, Schematic PrLD in the C-terminus of TDP-43. **b**, Schematic PrLD in human Nup98, Nup153 and Nup214. **c**, Co-expression of GFP-tagged PrLD and non-PrLD of Nup98, Nup153 and Nup214 with mCherry or mCherry-tagged TDP-CTF in N2a cells. Arrow indicates the co-aggregation. Scale bar: 10 μ m.

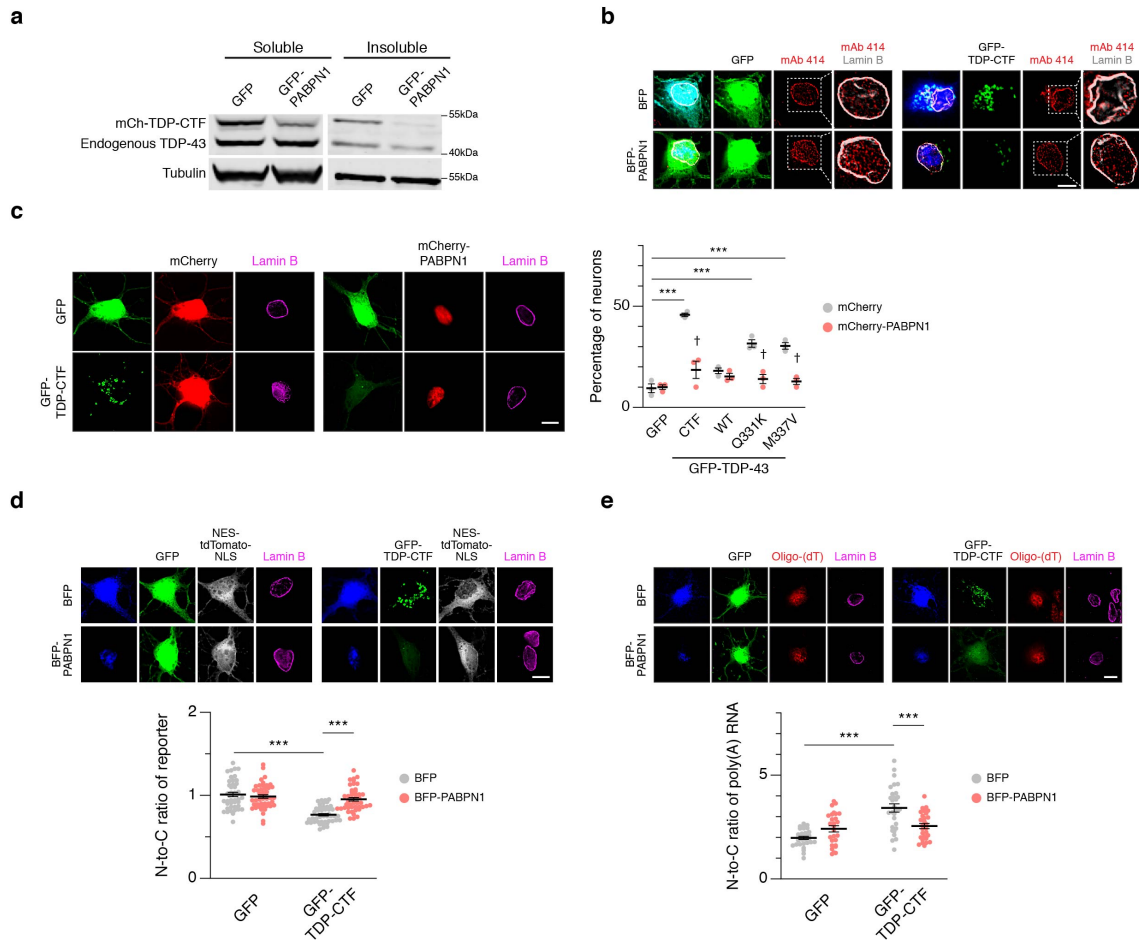


Supplementary Figure 3-9 | Mutant and aggregated forms of TDP-43 cause disruption of the nuclear lamina and nucleocytoplasmic transport defects.

a, Primary cortical neurons expressing GFP or GFP-tagged TDP-CTF were stained with anti-lamin B antibody. Three-dimensional reconstruction of nuclei from lamin B signal provided the spatial information of nuclear morphology at XY, XZ and YZ plane.

Nuclear invagination was observed in cells expressing TDP-CTF. Scale bar: 10 μ m. **b**,

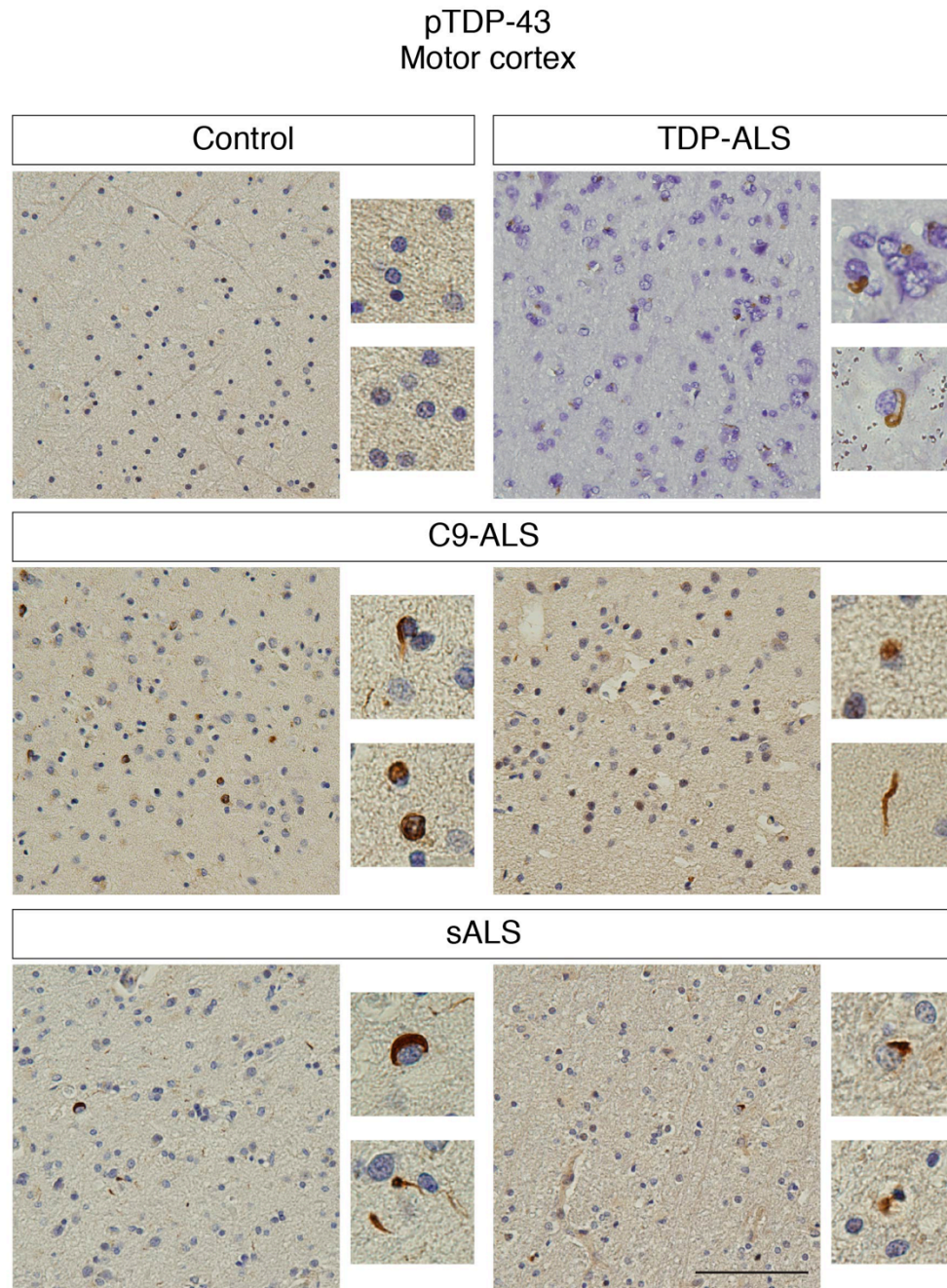
Diagram of NPC, Linkers of Nucleoskeleton and Cytoskeleton (LINC) complex and nuclear lamina. **c**, Immunostaining of LINC complex proteins, sun2 and nesprin-2 (red), F-actin (red) and lamin B (magenta/grey) in cortical neurons expressing GFP or GFP-tagged TDP-CTF, TDP-43^{WT} or TDP-43^{Q331K}. **d, e**, Quantitative analysis of nuclear GFP-TDP-43 levels (**d**) and cytoplasmic GFP-TDP-43 levels (**e**) in cortical neurons expressing GFP-tagged TDP-43^{WT}, TDP-43^{Q331K}, TDP-43^{M337V} or TDP-43^{mtNLS}. **f, g**, R-square (r^2) in regression analysis of N-to-C ratio of reporter and nuclear levels (**f**) or cytoplasmic levels (**g**) of GFP-TDP-43. **h**, Detection of poly(A) RNA with oligo-(dT) or (dA) probes. (**d**, $***P < 0.001$; **e**, $***P < 0.001$; GFP-tagged TDP-43^{WT} ($n = 70$), TDP-43^{Q331K} ($n = 70$), TDP-43^{M337V} ($n = 70$) or TDP-43^{mtNLS} ($n = 61$), all by one-way ANOVA, Bonferroni's post hoc test). Graphs represent mean and SEM. Scale bar: 10 μm .



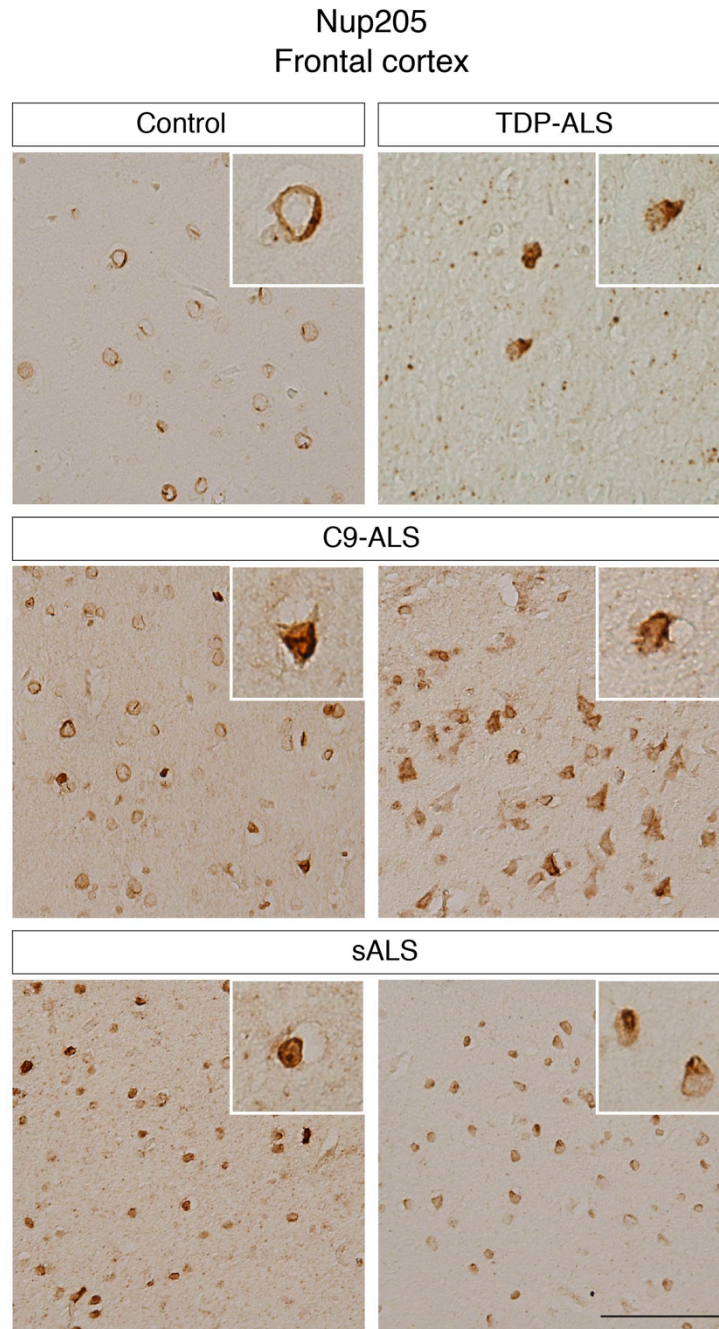
Supplementary Figure 3-10 | PABPN1 promotes the clearance of TDP-CTF and ameliorates nucleocytoplasmic transport defects.

a, Western-blotting analysis shows that co-expression of PABPN1 leads to reduction of TDP-CTF levels in the soluble and insoluble fraction. **b**, Nups (red) and lamin B (grey) staining in neurons expressing BFP or BFP-tagged PABPN1 and GFP or GFP-tagged TDP-CTF. **c**, Representative images and percentage of cortical neurons exhibited abnormal nuclear structure by anti-lamin B staining (magenta). Cells were transfected with expression constructs for GFP or GFP-tagged TDP-CTF, TDP-43^{WT}, TDP-43^{Q331K} or TDP-43^{M337V} and mCherry or mCherry-tagged PABPN1. (***) $P < 0.001$; mCherry versus mCherry-PABPN1: † $P < 0.001$; GFP (with mCherry: $n = 43$ or PABPN1: $n = 49$)

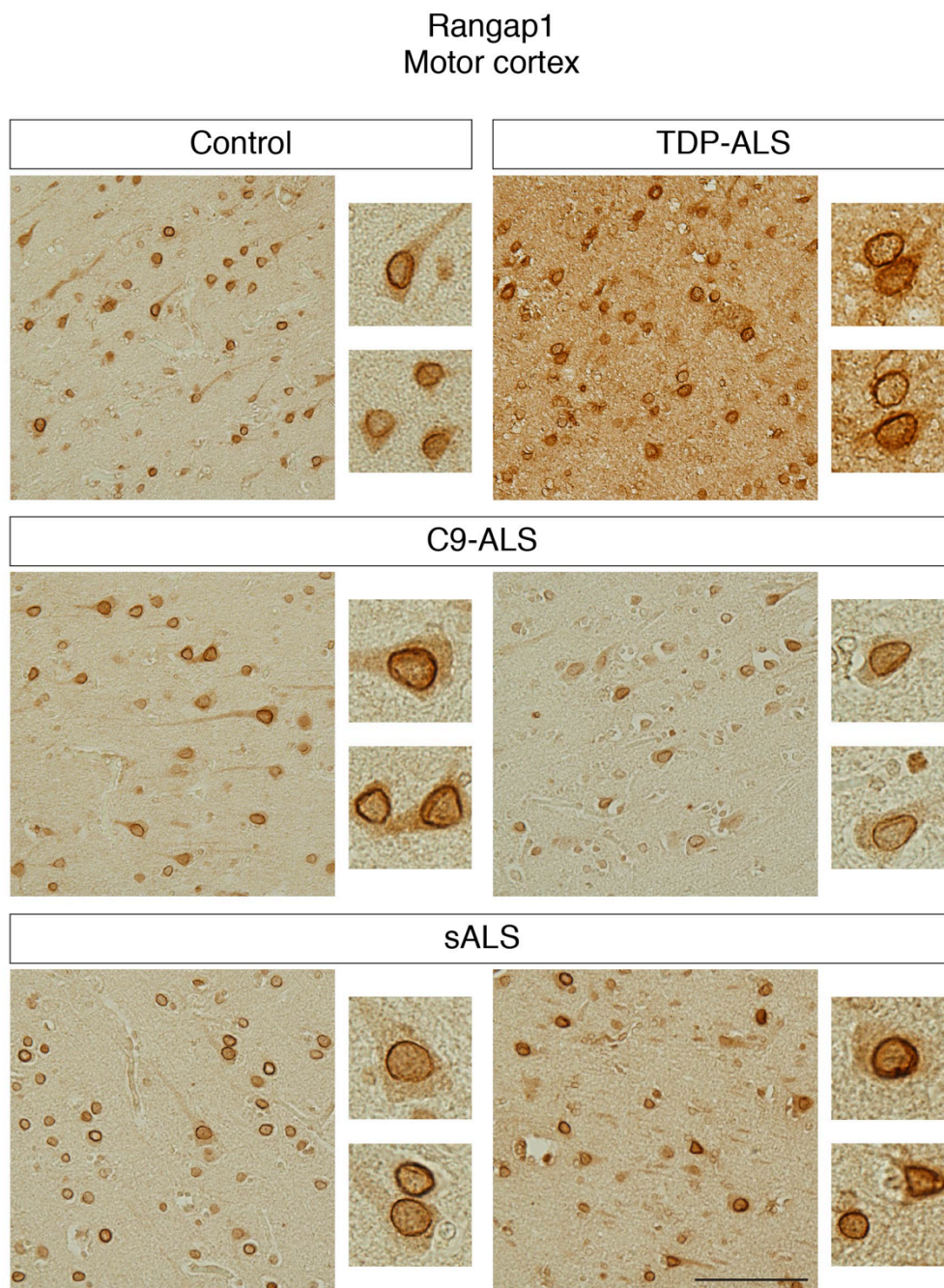
or GFP-tagged TDP-CTF (with mCherry: $n = 48$ or PABPN1: $n = 58$), TDP-43^{WT} (with mCherry: $n = 44$ or PABPN1: $n = 40$) or TDP-43^{Q331K} (with mCherry: $n = 44$ or PABPN1: $n = 41$) or TDP-43^{M337V} (with mCherry: $n = 46$ or PABPN1: $n = 45$); two-way ANOVA, Bonferroni's post hoc test). **d**, Quantitative analysis of the N-to-C ratio of the NES-tdTomato-NLS reporter in neurons expressing BFP or BFP-tagged PABPN1 and GFP or GFP-tagged TDP-CTF. **e**, Quantitative analysis of the N-to-C ratio of poly(A) RNA in neurons expressing BFP or BFP-tagged PABPN1 and GFP or GFP- TDP-CTF. (**d**, $***P < 0.001$, GFP (with BFP: $n = 44$ or PABPN1: $n = 46$) or GFP-tagged TDP-CTF (with BFP: $n = 47$ or PABPN1: $n = 45$); **e**, $***P < 0.001$, GFP (with BFP: $n = 30$ or PABPN1: $n = 27$) or GFP-tagged TDP-CTF (with BFP: $n = 29$ or PABPN1: $n = 28$); all by two-way ANOVA, Bonferroni's post hoc test). Graphs represent mean and SEM. Scale bar: 10 μm .



Supplementary Figure 3-11 | Immunohistochemical staining of pTDP-43 in the motor cortices of *TARDBP*, *C9orf72*, and sporadic ALS cases. Scale bar: 100 μ m.



Supplementary Figure 3-12 | Immunohistochemical staining of Nup205 in the frontal cortices of *TARDBP*, *C9orf72*, and sporadic ALS cases. Scale bar: 100 μ m.



Supplementary Figure 3-13 | Immunohistochemical staining of Rangap1 in the motor cortices of *TARDBP*, *C9orf72*, and sporadic ALS cases. Scale bar: 100 μ m.

3.7 Supplementary Tables

Supplementary Table 3-1. Summary of human cases

Case ID	Disease diagnosis	Genetic status	Gender	Age at death (years)	Disease duration (years)	TDP-43 inclusions
1	Control	---	Female	61	N/A	N/A
2	Control	---	Male	56	N/A	N/A
3	Control	---	Female	91	N/A	N/A
4	Control	---	Female	43	N/A	N/A
5	ALS	TARDBP	Male	67	1	Yes
6	ALS	C9orf72	Male	67	1.5	Yes
7	ALS	C9orf72	Female	64	5	Yes
8	ALS	C9orf72	Female	57	2.5	Yes
9	ALS	C9orf72	Female	57	7	Yes
10	ALS	C9orf72	Male	65	2	Yes
11	ALS	C9orf72	Male	69	3.5	Yes
12	ALS	C9orf72	Female	55	4	Yes
13	ALS	Sporadic	Male	64	8	Yes
14	ALS	Sporadic	Female	73	3	Yes
15	ALS	Sporadic	Female	62	2.5	Yes
16	ALS	Sporadic	Male	48	3	Yes
17	ALS	Sporadic	Female	49	1.5	Yes
18	ALS	Sporadic	Male	61	7	Yes
19	ALS	Sporadic	Female	68.5	5.5	Yes
20	ALS	Sporadic	Male	70	2.5	Yes
21	ALS	Sporadic	Male	59	1	Yes

TDP-ALS = ALS patient with *TARDBP* mutation (c.892G>A; p.Gly298Ser)

C9-ALS = ALS patients with *C9orf72* mutation

sALS = sporadic ALS

Supplementary Table 3-2. Summary of reagents and sources

Reagents	Source
Antibodies	
Mouse monoclonal anti-myc (9E10)	DSHB
Mouse monoclonal anti-FLAG (M2)	Sigma-Aldrich
Mouse monoclonal anti-HA (HA.11)	Covance
Rabbit polyclonal anti-T7	Millipore
Rabbit polyclonal anti-TDP-43	Proteintech Group
Rabbit polyclonal anti-phospho-TDP-43 (S409/410)	Cosmo Bio
Mouse monoclonal anti- α -Tubulin	Sigma-Aldrich
Mouse monoclonal anti- γ -Actin	Santa Cruz
Mouse monoclonal anti-SQSTM1/p62	Abcam
Mouse monoclonal anti-nuclear pore complex proteins (mAb414)	BioLegend
Rabbit polyclonal anti-Nup205	Novus Biologicals
Goat polyclonal anti-Lamin B (M-20)	Santa Cruz
Rabbit monoclonal anti-Lamin B1 (EPR8985(B))	Abcam
Rabbit monoclonal anti-Sun2 (EPR6557)	Abcam
Mouse monoclonal anti-Nesprin-2 (K20-478)	Millipore
Rabbit polyclonal anti-Rangap1 (H-180)	Santa Cruz
Mouse monoclonal anti-phospho-Histone H2AX (Ser139)/ γ H2AX	Millipore
Fluorescent Dye	
Anti-Mouse IgG, Alexa Fluor® 488 conjugated	Jackson ImmunoResearch
Anti-Mouse IgG, Cy3 conjugated	Jackson ImmunoResearch
Anti-Rabbit IgG, Alexa Fluor® 488 conjugated	Jackson ImmunoResearch
Anti-Rabbit IgG, Cy3 conjugated	Jackson ImmunoResearch
Anti-Goat IgG, Cy5 conjugated	Jackson ImmunoResearch
Streptavidin Rhodamine conjugated	Jackson ImmunoResearch
Streptavidin Cy5 conjugated	Jackson ImmunoResearch
Phalloidin Rhodamine conjugated	ThermoFisher Scientific
Anti-Mouse IgG, IRDye® 800CW	LI-COR
Streptavidin, IRDye® 680LT	LI-COR
Chemicals and Reagents	
Staurosporine	Sigma-Aldrich
Importazole	Sigma-Aldrich
Calicheamicin γ 1	Pfizer; Gift from Thomas Kukar ²⁰⁰
Anisomycin	Sigma-Aldrich
NeuroMag	OZ Biosciences
PolyMag Neo	OZ Biosciences
Lipofectamine 3000	ThermoFisher Scientific
Protease inhibitor	Roche
PhosSTOP - Phosphatase inhibitor	Roche
NeutrAvidin UltraLink Resin	ThermoFisher Scientific
ProLong® Diamond Antifade Mountant with DAPI	ThermoFisher Scientific
ProLong® Diamond Antifade Mountant	ThermoFisher Scientific
Biotinylated oligo-(dT) and (dA) probes	Biosearch Technologies

Commercial assay	
QuikChange II	Agilent Technologies
Click-iT Assay Kits	ThermoFisher Scientific
Click-iT AHA (L-Azidohomoalanine)	ThermoFisher Scientific
Click-iT Alexa Fluor 647 alkyne	ThermoFisher Scientific
Plasmids	
GFP	This paper
GFP-TDP-CTF	This paper
GFP-TDP-43 ^{WT}	This paper
GFP-TDP-43 ^{Q331K}	This paper
GFP-TDP-43 ^{M337V}	This paper
GFP-TDP-43 ^{mtNLS} (KRK...KVKR > AAA...AVAA)	This paper
GFP-PABPN1	This paper
mCherry	This paper
mCherry-TDP-CTF	This paper
mCherry-TDP-43 ^{WT}	This paper
mCherry-TDP-43 ^{Q331K}	This paper
mCherry-PABPN1	This paper
BFP	This paper
BFP-PABPN1	This paper
pcDNA3.1 mycBioID	Addgene # 35700; gift from Kyle Roux ¹⁷¹
Myc-BirA*-TDP-43	This paper
Myc-BirA*-TDP-CTF	This paper
FLAG-APEX2-TDP-43	This paper
FLAG-APEX2-TDP-CTF	This paper
HA-Ubiquitin	This paper
NES-tdTomato-NLS	Gift from Martin Hetzer ¹⁹²
pEGFP-Nup35	Euroscarf # P30479; gift from Jan Ellenberg ²⁰¹
pEGFP-Nup43	Euroscarf # P30481; gift from Jan Ellenberg ²⁰¹
pEGFP2-Nup50	Euroscarf # P30482; gift from Jan Ellenberg ²⁰¹
pEGFP2-Nup58	Euroscarf # P30483; gift from Jan Ellenberg ²⁰¹
pNup62-EGFP3	Euroscarf # P30484; gift from Jan Ellenberg ²⁰¹
pEGFP3-Nup85	Euroscarf # P30485; gift from Jan Ellenberg ²⁰¹
GFP-Nup88	Gift from Maureen Powers
pNup93-EGFP3	Euroscarf # P30486; gift from Jan Ellenberg ²⁰¹
pEGFP-Nup98	Euroscarf # P30487; gift from Jan Ellenberg ²⁰¹
pEGFP-Nup98 PrLD	This paper
pEGFP-Nup98 non-PrLD	This paper
GFP-Nup107	Gift from Valérie Doye ²⁰²
pNup153-EGFP	Euroscarf # P30650; gift from Jan

	Ellenberg ²⁰³
pNup153-EGFP PrLD	This paper
pNup153-EGFP non-PrLD	This paper
Nup155-GFP	Gift from Maureen Powers
GFP-Nup160	Gift from Valérie Doye ²⁰²
FLAG-Nup205	Gift from Jose Teodoro ²⁰⁴
pEGFP-Nup214	Euroscarf # P30488; gift from Jan Ellenberg ²⁰¹
pEGFP-Nup214 PrLD	This paper
pEGFP-Nup214 non-PrLD	This paper
GFP-Nup358/Ranbp2	Gift from Jomon Joseph ²⁰⁵
EGFP-Tpr	Addgene # 35024; gift from Larry Gerace ²⁰⁶
pEGFP-hAladin	Euroscarf # P30475; gift from Jan Ellenberg ²⁰¹
pCG1-EGFP3	Euroscarf # P30476; gift from Jan Ellenberg ²⁰¹
pPom121-EGFP3	Euroscarf # P30459; gift from Jan Ellenberg ²⁰³
pGp210-EGFP3	Euroscarf # P30477; gift from Jan Ellenberg ²⁰¹
pEGFP-Lamin B1	Euroscarf # P30455; gift from Jan Ellenberg ²⁰³
pLbr1TM-GFP	Euroscarf # P30453; gift from Jan Ellenberg ²⁰⁷
T7-Kpna1	Addgene # 26677; gift from Bryce Paschal ²⁰⁸
T7-Kpna2	Addgene # 26678; gift from Bryce Paschal ²⁰⁸
T7-Kpna3	Addgene # 26679; gift from Bryce Paschal ²⁰⁸
T7-Kpna4	Addgene # 26680; gift from Bryce Paschal ²⁰⁸
T7-Kpna5	Addgene # 26681; gift from Bryce Paschal ²⁰⁸
T7-Kpna6	Addgene # 26682; gift from Bryce Paschal ²⁰⁸
T7-Kpna7	Addgene # 26683; gift from Bryce Paschal ²⁰⁸
pEGFP-Importin B1/Kpnb1	Euroscarf # P30478; gift from Jan Ellenberg ²⁰¹
FLAG-hCrm1/Xpo1	Addgene # 17647; gift from Xin Wang ²⁰⁹
pEGFP-Xpo5	Addgene # 58331; gift from Matthew Wood ²¹⁰
GFP-Gle1	Gift from Maureen Powers
GFP-Tap/Nxf1	Gift from Maureen Powers
pEGFP-Senp2	Addgene # 13382; gift from Mary Dasso ²¹¹

pEGFP-Rangap1	Addgene # 13378; gift from Mary Dasso ²¹²
shCtrl	GE Dharmacon; ¹¹³
shTDP-43 #2	GE Dharmacon; ¹¹³
shTDP-43 #3	GE Dharmacon; ¹¹³
<i>Drosophila</i> lines	
Nup 50 (15198): y[1]; P{y[+mDint2] w[BR.E.BR]=SUPor-P}Nup50[KG09557]; ry[506]	
Nup 93 (32628): w[*] P{w[+mC]=EP}Nup93-1[G9996]	
Nup98/96 (4951): Nup98-96[339]/TM3, Sb[1]	
Nup107 (21784): y[1] w[67c23]; P{y[+t7.7] w[+mC]=wHy}Nup107[DG40512]/SM6a	
Nup214 (12369): P{ry[+t7.2]=PZ}Nup214[10444] cn[1]/CyO; ry[506]	
Open source platform and algorithm	
DAVID Bioinformatics Resources	https://david.ncifcrf.gov/ ; ²¹³
ProtScale	http://web.expasy.org/protscale/ ; ²¹⁴
DisEMBL	http://dis.embl.de/ ; ²¹⁵
GlobPlot	http://globplot.embl.de/ ; ²¹⁶
ImageJ	https://imagej.nih.gov/ij/
Cytoscape	http://www.cytoscape.org/ ; ²¹⁷
Cytoscape plugin - GeneMANIA	http://apps.cytoscape.org/apps/genemania
Image Studio Lite	https://www.licor.com/bio/products/software/image_studio_lite/

Chapter 4

PABPN1 suppresses TDP-43 toxicity in ALS disease models

Portions of this chapter were adapted from the following manuscript:

Ching-Chieh Chou, Olga M. Alexeeva, Shizuka Yamada, Amy Pribadi, Yi Zhang, Bi Mo, Kathryn R. Williams, Daniela C. Zarnescu, and Wilfried Rossoll. PABPN1 suppresses TDP-43 toxicity in ALS disease models. *Hum Mol Genet.* 2015.

4.1 Abstract

TAR DNA-binding protein 43 (TDP-43) is a major disease protein in amyotrophic lateral sclerosis (ALS) and related neurodegenerative diseases. Both the cytoplasmic accumulation of toxic ubiquitinated and hyperphosphorylated TDP-43 fragments and the loss of normal TDP-43 from the nucleus may contribute to the disease progression by impairing normal RNA and protein homeostasis. Therefore, both the removal of pathological protein and the rescue of TDP-43 mislocalization may be critical for halting or reversing TDP-43 proteinopathies. Here, we report poly(A)-binding protein nuclear 1 (PABPN1) as a novel TDP-43 interaction partner that acts as a potent suppressor of TDP-43 toxicity. Overexpression of full-length PABPN1 but not a truncated version lacking the nuclear localization signal (NLS) protects from pathogenic TDP-43-mediated toxicity, promotes the degradation of pathological TDP-43, and restores normal solubility and nuclear localization of endogenous TDP-43. Reduced levels of PABPN1 enhances the phenotypes in several cell culture and *Drosophila* models of ALS and results in the cytoplasmic mislocalization of TDP-43. Moreover, PABPN1 rescues the dysregulated stress granule (SG) dynamics and facilitates the removal of persistent SGs in TDP-43-mediated disease conditions. These findings demonstrate a role for PABPN1 in rescuing several cytopathological features of TDP-43 proteinopathy by increasing the turnover of pathologic proteins.

4.2 Introduction

TAR-DNA binding protein 43 (TDP-43) has emerged as a key player in the pathogenesis of neurodegenerative diseases, based on genetic and pathological studies²¹⁸. TDP-43 has

first been identified as a major component of abnormal cytoplasmic aggregates in amyotrophic lateral sclerosis (ALS) and frontotemporal lobar degeneration (FTLD)^{13,14}. The vast majority of both familial and sporadic ALS cases (ca. 97%) and the most common type of FTLD (ca. 45%), now classified as FTLD-TDP, are characterized by TDP-43 pathology, and are now recognized as belonging to the same disease spectrum²¹⁹. A direct causal link was established by the discovery of more than 30 different missense mutations in exon 6 of the *TARDBP* gene encoding TDP-43, accounting for ca. 4% of inherited and 1.5% of sporadic ALS cases and rare patients with FTLD-TDP²²⁰. Pathologic accumulation of TDP-43 in ubiquitin-positive aggregates was subsequently found in different neurodegenerative diseases including Alzheimer's disease, Parkinson's disease and Huntington's disease^{104,221}, indicating that TDP-43 proteinopathy may contribute broadly to neurodegeneration.

TDP-43 is an RNA-binding protein that shares a similar structure with heterogeneous nuclear ribonucleoproteins (hnRNPs)⁸³. TDP-43 contains two RNA recognition motifs (RRM1 and 2) and a Q/N-rich prion-like C-terminal region, which makes it intrinsically aggregation-prone and plays a key role in pathogenesis²²². TDP-43 is predominantly expressed in the nucleus but can shuttle between nuclear and cytoplasmic compartments, and plays multiple roles in RNA processing in both compartments⁹⁰. The disease-associated changes found in ALS and FTLD-TDP cases include aberrant aggregation of ubiquitinated and hyperphosphorylated TDP-43, the accumulation of truncated 20-25-kDa TDP43 C-terminal fragments (TDP-CTF), cytoplasmic mislocalization and loss of TDP-43 from the nucleus. Various cellular stress factors cause TDP-43 to localize in cytoplasmic stress granules (SGs) as a normal

physiological response^{35,111,137}. It has been speculated that chronic and prolonged SG formation may be an initiating event triggering irreversible TDP-43 inclusion pathology^{117,223,224}. TDP-43 inclusion pathology may reflect an exaggeration of normal accumulation of TDP-43 into cytoplasmic RNA granules under disease-associated mutations^{101,225} or stressful conditions¹¹⁷. While the effect of hyperphosphorylation on the properties of TDP-43 is still controversial, it may modulate the oligomerization^{226,227} and increase protease resistance²²⁸. Not only are proteins that target proteins for degradation present in TDP-43 aggregates, but mutations in several genes affecting protein degradation cause ALS/FTLD-TDP characterized by TDP-43 aggregation. Taken together, these studies implicate a failure of TDP-43 clearance via autophagy and/or the ubiquitin proteasome system (UPS) in human ALS/FTLD-TDP²²⁹. The biological role of TDP-43 in RNA processing and the fact that TDP-43 accumulation can be triggered by a dysfunction of protein degradation pathways support the hypothesis that disruption of both RNA and protein homeostasis are central to ALS pathogenesis¹⁵.

ALS and other TDP-43 proteinopathies are characterized by both the formation of TDP-43 containing aggregates in the cytoplasm and the loss of normal TDP-43 from the nucleus¹³. Numerous studies have provided evidence for a toxic gain-of-function of pathologic TDP-43 that accumulates in the cytoplasm²³⁰. Overexpression of wild-type or mutant TDP-43 in neurons has been shown to mimic key features of TDP-43 proteinopathy *in vitro*, including the sequestration of RNA-binding proteins into detergent insoluble aggregates^{124,231}. Especially expression of TDP-CTF, a C-terminal fragment of TDP-43 from aa 208-414 found in ALS/FTLD-TDP patients, recapitulates key features of TDP-43 proteinopathy in transfected neurons^{30,132}. Other studies show

that similarly, partial loss of TDP-43 can cause progressive neurodegeneration phenotypes similar to ALS^{232,233}. Taken together, this suggests that the toxic gain-of-function and the loss-of-function hypotheses are not mutually exclusive and could both contribute to neurodegeneration^{127,234-236}. This also suggests that targeting the deleterious effects of TDP-43 proteinopathy requires both the removal of pathological cytoplasmic TDP-43 and the restoration of nuclear TDP-43 levels.

Here, we report poly(A)-binding protein nuclear 1 (PABPN1, also known as PABP2) as a novel modifier of TDP-43 proteinopathy in several *in vitro* and *in vivo* models of ALS and FTLD-TDP. PABPN1 is thought to function during post-transcriptional processing of RNA in the nucleus, regulating polyadenylation and nuclear export of mRNAs, and the turnover of lncRNA²³⁷. Expansion of an N-terminal poly-alanine repeat region causes the muscle disease oculopharyngeal muscular dystrophy (OPMD), which is also characterized by the presence of TDP-43-positive aggregates²³⁸, suggesting a potential functional link between TDP-43 and PABPN1. In this study, we identified PABPN1 as a novel direct interaction partner of TDP-43 that also acts as a potent suppressor for TDP-43-induced toxicity, whereas the loss of PABPN1 conversely enhances the phenotype in various models of TDP-43 proteinopathy ranging from yeast to *Drosophila* and mammalian primary neurons. PABPN1 overexpression strongly reduces protein levels of exogenously expressed ALS patient-specific mutant and truncated TDP-43 but only weakly affects wild-type TDP-43. PABPN1 does not change levels of endogenous full-length TDP-43, and restores its solubility and proper nuclear localization under disease conditions. Our data show that increased protein turnover of pathological TDP-43 by PABPN1 is mainly mediated via the UPS. In addition, PABPN1

rescues the dysregulation of SG dynamics in TDP-43-mediated disease conditions. In summary, PABPN1 acts as a protective modifier across various cell culture and animal models of TDP-43 proteinopathy by rescuing important disease phenotypes.

4.3 Results

4.3.1 TDP-43 is a novel interaction partner of PABPN1

In a yeast-two-hybrid screen for proteins that directly interact with human TDP-43, aside from known TDP-43-associated proteins such as hnRNPA3, we also identified PABPN1 as a putative novel interaction partner. PABPN1 is a ubiquitously expressed protein that is involved in processive polyadenylation of pre-mRNA transcripts²³⁷. PABPN1 shares similarity with RNA regulatory proteins and interacts with hnRNPA1 and hnRNPA2/B1²³⁹, as well as its nuclear import receptor transportin²⁴⁰ and poly(A) polymerase (PAP)²⁴¹. To verify the yeast-two-hybrid interaction, we cloned full-length human TDP-43 and PABPN1 into bait and prey vectors. Both proteins were able to homodimerize as reported previously^{88,242}, but also showed specific interactions with each other (**Table 4-1**).

To confirm the protein-protein interaction in mammalian cells, we co-transfected Neuro-2a (N2a) neuroblastoma cells with expression constructs for FLAG-tagged TDP-43, and GFP-tagged full-length or truncated PABPN1 (full-length: FL; deletion of C-terminal nuclear localization signal 18aa: Δ NLS18; deletion of C-terminal 50aa: Δ NLS50) (**Fig. 4-1A**). The C-terminus of PABPN1 is highly enriched in methylated arginine residues and contains a nuclear localization signal (NLS)²⁴³. Deletion of the last 18aa partially inactivated the NLS function and caused uniform nucleocytoplasmic

distribution, whereas deletion of the last 50aa led to cytoplasmic localization (**Fig. 4-1B**). FLAG-tagged TDP-43 associates with full-length PABPN1 and to a lesser degree with PABPN1^{ΔNLS50} and PABPN1^{ΔNLS18}, demonstrating that the C-terminal region of PABPN1 is not essential for their interaction (**Fig. 4-1C**). Treatment with RNaseA did not abolish the association between TDP-43 and PABPN1, showing that this interaction is not mediated via RNA. The C-terminal fragment TDP-CTF was also found to specifically associate with full-length PABPN1 in pull-down assays (**Supplementary Fig. 4-1**). To verify association of the endogenous proteins, we used anti-PABPN1 antibodies to co-immunoprecipitate endogenous TDP-43 from embryonic mouse brain lysates (**Fig. 4-1D**). Taken together, our results identify PABPN1 as a novel direct interaction partner of TDP-43.

4.3.2 PABPN1 modulates TDP-43 toxicity in yeast and primary neuron models

The budding yeast *Saccharomyces cerevisiae* has emerged as an important tool for investigating protein misfolding as a cause of several human neurodegenerative disorders, including a yeast model for TDP-43 proteinopathy^{97,131,244}. Remarkably, overexpression of human TDP-43 in yeast triggers spontaneous formation of aggregates similar to those observed in degenerating neurons of ALS patients¹³¹. To determine whether PABPN1 can modulate TDP-43 toxicity in the yeast model, we performed spotting assays with a yeast strain transformed with expression plasmids for yellow and cyan fluorescent protein-tagged human TDP-43 (hTDP-43) and PABPN1 (hPABPN1) under control of the galactose-inducible GAL1 promoter. Inducing strong overexpression of hTDP-43-YFP from a multicopy plasmid resulted in dramatic inhibition of yeast

growth as compared with a control plasmid expressing YFP alone¹³¹. Importantly, we found that whereas mCerulean-hPABPN1 alone only weakly inhibited proliferation, it strongly mitigated the toxic effect of hTDP-43 on cell growth (**Fig. 4-2A**). The result demonstrates that PABPN1 acts as a potent suppressor of TDP-43 toxicity in a yeast model of TDP-43 proteinopathy.

Previously, we have shown that expression of GFP-TDP-CTF in primary motor neurons leads to the formation of cytoplasmic inclusions with the hallmarks of TDP-43 pathology¹¹³. These aggregates stain positive for ubiquitin, hyperphosphorylated TDP-43 (Ser409/410), and the autophagy adapter SQSTM1/p62 (**Supplementary Fig. 4-2**). To test further how PABPN1 expression affects neuronal TDP-43 proteinopathy models, primary cortical neurons were transfected with GFP-fusion constructs for wild-type TDP-43 (TDP-43^{WT}), disease-associated mutants (TDP-43^{Q331K}, TDP-43^{M337V} and TDP-43^{A382T}) or TDP-CTF and measured how rates of cell death were altered by co-overexpression of BFP-PABPN1. Cell death among the transfected neurons was determined by scoring the nuclear uptake of the fluorescent dye ethidium homodimer I (EthD-I) (**Fig. 4-2B**). Consistent with previous reports that mutant or truncated TDP-43 enhanced cellular toxicity in cultured cell lines^{34,35}, primary neurons^{113,124,245} and animal models¹²⁷, expression of ALS-specific mutant TDP-43 and TDP-CTF was more toxic than TDP-43^{WT} and increased the percentage of cell death in transfected neurons (Control: 2.7±0.8%; TDP-43^{WT}: 9.8±1.2%; TDP-43^{Q331K}: 15.6±1.8%; TDP-43^{M337V}: 15.3±0.6%; TDP-43^{A382T}: 11.9±1.3%; TDP-CTF: 20.4±0.5%) (**Fig. 4-2C**). The co-overexpression of PABPN1 greatly reduced cell death induced by TDP-CTF and mutant

TDP-43 by 55% ($9.2 \pm 0.7\%$) and ca. 45-49% (TDP-43^{Q331K}: 7.9 ± 0.6 ; TDP-43^{M337V}: 8.3 ± 1.3). The overexpression of PABPN1 itself was not toxic (3.4 ± 1.0) (**Fig. 4-2C**).

Based on this finding, we tested whether reducing PABPN1 level had an impact on TDP-43 toxicity. We employed two different PABPN1-specific shRNA constructs (shPABPN1), which efficiently decreased endogenous PABPN1 protein levels in Western-blot analysis (**Fig. 4-3C**). Reduction of PABPN1 alone did not significantly affect rates of cell death (shCtrl: 4.2 ± 1.1 ; shPABPN1: 7.2 ± 0.8 , $P > 0.99$), but enhanced TDP-CTF-induced cell death by 35% (shCtrl: 19.2 ± 1.6 ; shPABPN1: 26.0 ± 1.8 , $P = 0.004$) (**Fig. 4-2D**).

To rule out an unspecific effect caused by overexpressing mRNA-binding proteins, we used as a control hnRNPA3, a known TDP-43 associated protein that we have also identified as a direct interaction partner of TDP-43 in our yeast two-hybrid screen. Co-overexpression of hnRNPA3 was neither toxic, nor did it reduce TDP-CTF-induced cell death (**Fig. 4-2E-F**), suggesting a specific effect of PABPN1 overexpression on TDP-43 toxicity.

To find out whether nuclear localization of PABPN1 was required for suppression of TDP-43 toxicity, we co-expressed PABPN1 NLS mutants with TDP-CTF in primary neurons. Whereas nucleocytoplasmic PABPN1 ^{Δ NLS18} itself slightly increased cell death but acted as a weak suppressor of TDP-CTF-induced cell death, cytoplasmic PABPN1 ^{Δ NLS50} strongly enhanced cell death and had no positive effect on survival of TDP-CTF expressing cells (**Fig. 4-2E-F**). Our data suggest that ameliorating TDP-43 toxicity by PABPN1 requires its normal nuclear localization.

4.3.3 PABPN1 loss of function enhances TDP-43 toxicity in *Drosophila* models

Several groups have developed *Drosophila* models of ALS based on overexpression of human TDP-43 that recapitulate several aspects of pathology, including neurotoxicity, loss of motor neurons, locomotor dysfunction, and reduced survival^{126,173,246-249}. To test the effect of PABPN1 in an *in vivo* model of TDP-43 proteinopathy, we employed several transgenic fly lines expressing human wild-type (hwt) or ALS-specific mutant TDP-43 (hA315T, hD169G) in the developing retina using the Gal4-UAS system²⁵⁰. Overexpression of hwt and hA315T using the GMR Gal4 driver induced neurodegeneration in the adult retina that is visible as loss of pigmentation in the eye¹⁷³. When combined with a loss-of-function mutant of PABPN1 (PABP2[55])²⁵¹, we observed that the loss of PABPN1 itself was not toxic, whereas it enhanced the TDP-43-induced neurodegeneration (**Fig. 4-2G**). As an additional assay, we used the motor neuron-specific D42 Gal4 driver to investigate locomotor dysfunction in larvae. Expression of the hwt and mutant alleles significantly increased the time the larva needed to turn back from the dorsal side and resume crawling on the ventral side^{173,252}. The PABPN1 loss-of-function genetic background exacerbated TDP-43-dependent locomotor defects (**Fig. 4-2H**). In summary, our results show that PABPN1 modulates TDP-43-mediated toxicity across several *in vitro* and *in vivo* genetic models of TDP-43 proteinopathy, acting as a protective modifier when overexpressed and enhancing TDP-43 toxicity when reduced.

4.3.4 PABPN1 specifically reduces protein levels of pathological TDP-43

The accumulation of pathological cytoplasmic inclusions containing TDP-43 is a key feature of ALS and FTLD-TDP^{13,14}. Normally, TDP-43 protein levels appear tightly regulated and even modest levels of overexpression can trigger neurodegeneration¹⁵.

Cytoplasmic mislocalization in combination with post-translational modification, and the intrinsic aggregation propensity of TDP-43 may promote its accumulation in disease²³⁴.

To investigate whether PABPN1 overexpression can reduce pathological TDP-43, N2a cells and primary motor neurons were transfected with TDP-CTF to induce formation of ubiquitinated and hyperphosphorylated aggregates (**Supplementary Fig. 4-2**). Co-overexpression of PABPN1^{FL} significantly promoted the clearance of TDP-CTF by ~70%, whereas the truncated nucleocytoplasmic PABPN1^{ΔNLS18} lost the ability to reduce the pathological protein (**Fig. 4-3A-B**). PABPN1^{ΔNLS50} co-localized with TDP-CTF in the cytoplasm and enhanced the accumulation of TDP-CTF by 1.5 fold. Importantly, endogenous TDP-43 protein levels were not changed by PABPN1 (**Fig. 4-3B**). Furthermore, we assessed the effect of shRNA-mediated knockdown of PABPN1 on the protein level of TDP-CTF. Reducing PABPN1 levels exacerbated the accumulation of TDP-CTF but had no significant effect on endogenous TDP-43 (**Fig. 4-3C**).

To examine the specificity of PABPN1 for TDP-CTF, we co-overexpressed the TDP-43 associated mRNA-binding protein hnRNP-A3 as a negative control. HnRNP-A3 expression had no significant effect on TDP-CTF levels (**Supplementary Fig. 4-3A**). Since a recent study has shown that the upregulation of the *Drosophila* poly(A)-binding protein cytoplasmic 1 (PABPC1) ortholog (dPABP) enhanced TDP-43 toxicity in a fly model of ALS and dPABP downregulation led to a slight reduction of cytoplasmic TDP-

43 protein levels¹⁴⁵, we compared the effect of co-overexpressing either PABPN1 or PABPC1 on TDP-CTF protein accumulation in N2a cells. Indeed, PABPC1 exhibited an opposite role to PABPN1 by increasing TDP-CTF levels (PABPC1: 117.9±6.1%; PABPN1: 35.1±1.8%, $P < 0.001$) (**Fig. 4-3D**). Our results demonstrate an opposite role of nuclear and cytoplasmic poly(A)-binding proteins in modulating TDP-43 toxicity and protein accumulation.

To investigate whether PABPN1 may exhibit a general effect on pathologic protein inclusions, we used a model for pathogenic huntingtin (Htt) protein containing an expansion of poly-glutamine that causes Huntington's disease²⁵³. To induce Htt aggregate formation, we co-transfected expression constructs for an N-terminal mutant huntingtin construct harboring 150 CAG repeats (mHtt) and PABPN1 into primary cortical neurons. PABPN1 did not alter the levels of aggregated mHtt suggesting a specific effect of PABPN1 on the removal of pathological TDP-43 instead of a more general effect on other pathological proteins (**Supplementary Fig. 4-3B**).

To find out whether PABPN1 overexpression specifically targets both diffusely distributed TDP-CTF monomers and oligomers, as well as the larger insoluble aggregates, we partitioned TDP-CTF into detergent-soluble and insoluble fractions. PABPN1^{FL} overexpression significantly reduced TDP-CTF protein levels in both fractions, whereas the cytoplasmic PABPN1^{ANLS50} truncation mutant did not show significant changes but a trend towards increasing levels of both soluble and insoluble TDP-CTF (**Fig. 4-3E**). Importantly, in cells expressing TDP-CTF, PABPN1 co-expression caused a shift of endogenous full-length TDP-43 from the insoluble to the

soluble fraction, demonstrating that the clearance of pathologic TDP-CTF protein by PABPN1 restores the solubility of endogenous TDP-43 (**Fig. 4-3E**).

4.3.5 PABPN1 facilitates the clearance of pre-formed pathological TDP-43 aggregates

To find out whether PABPN1 overexpression acts by preventing the accumulation of pathologic TDP-CTF or whether it can also target existing aggregates in the cytoplasm, we performed time-lapse live-cell imaging experiments. Primary cortical neurons were co-transfected with constructs for expression of fluorescent protein-tagged TDP-CTF from the constitutive CMV promoter and PABPN1 from the doxycycline (Dox)-inducible Tet-ON promoter. Twenty-four hours after transfection, mCherry-TDP-CTF was strongly expressed in the cytoplasm and formed bright fluorescent foci indicating cytoplasmic aggregates. Then expression of GFP-PABPN1 was induced and the changes of mCherry-TDP-CTF levels were dynamically monitored by quantification of fluorescence intensity in time-lapse live-cell imaging (**Fig. 4-4A-B**). Whereas mCherry-TDP-CTF levels slightly increased over time in the vehicle group ($120.2 \pm 4.1\%$, $n = 20$) or GFP control groups (vehicle: $111.5 \pm 5.2\%$; Dox: $120.6 \pm 4.2\%$, $n = 20$), we observed a gradual reduction of mCherry-TDP-CTF levels (including the distinct cytoplasmic foci) by ca. 65% within 24 hrs ($35.6 \pm 3.4\%$, $n = 20$) after co-expression GFP-PABPN1 was induced (**Fig. 4-4B-D**).

4.3.6 PABPN1 facilitates the clearance of pathological TDP-43 via the ubiquitin-proteasome mechanism

To determine the underlying mechanism by which PABPN1 reduced pathological TDP-43 protein, we first examined whether PABPN1 could alter the phosphorylation level of TDP-CTF. We transfected N2a cells with mCherry-TDP-CTF and GFP or GFP-PABPN1, and found that PABPN1 did not significantly change the relative phosphorylation level of TDP-CTF (**Fig. 4-5A**).

Western-blot analysis showed that PABPN1 expression strongly reduced protein levels of TDP-CTF (32.8 ± 8.6), and also ALS related mutant TDP-43 (TDP-43^{Q331K}: $47.0 \pm 13.2\%$; TDP-43^{M337V}: $62.3 \pm 5.1\%$; TDP-43^{A382T}: $49.9 \pm 17.3\%$), but only weakly reduced TDP-43^{WT} levels ($81.4 \pm 1.9\%$) (**Fig. 4-5B**). Therefore, we decided to test whether PABPN1 increases the turnover of these proteins. We performed cycloheximide chase experiments to determine the half-life ($t_{1/2}$) of TDP-CTF and the temporal changes of relative TDP-CTF levels. PABPN1 co-expression reduced the half-life of TDP-CTF from 11.9 to 6.8 hrs (**Fig. 4-5C1-2**). We also observed that PABPN1 expression caused a steady decline in the relative TDP-CTF protein levels from 55% to 9.3% as compared to the GFP control over the 24-hr time period (**Fig. 4-5C4**). The half-life and the relative level of endogenous TDP-43 were not affected (**Fig. 4-5C3, C5**). The results show that PABPN1 expression enhances the turnover of truncated TDP-43 protein.

We used specific inhibitors to identify whether PABPN1 promoted the turnover of TDP-CTF via one of the two major protein degradation pathways: the UPS for soluble monomeric proteins and autophagy for soluble oligomeric proteins and insoluble large aggregates²²⁹. Inhibiting autophagy by preventing the fusion between autophagosomes

and lysosomes with bafilomycin A1 slightly prolonged the half-life of TDP-CTF but did not impair the PABPN1-dependent increase in turnover (GFP: $t_{1/2} = 12.4$ hrs; PABPN1: $t_{1/2} = 7.4$ hrs) (**Fig. 4-5D1-2**). The changes of the relative level of TDP-CTF resembled the results from the DMSO vehicle treatment (**Fig. 4-5D4**). However, inhibiting the proteolytic activity of 26S proteasome with MG-132 greatly decreased the degradation of TDP-CTF (GFP control: $t_{1/2} = 29.6$ hrs; GFP-PABPN1: $t_{1/2} = 30.5$ hrs) and completely abolished PABPN1's effect on TDP-CTF protein levels (**Fig. 4-5E1-2**). The relative level of TDP-CTF remained unchanged for the extended time period (**Fig. 4-5E4**). These results demonstrate that PABPN1 facilitates the removal of soluble monomeric TDP-CTF via the UPS.

We also observed a similar effect of PABPN1 expression on the protein turnover of mutant TDP-43^{M337V} and TDP-43^{WT}. Their half-life ($t_{1/2}$) changed from 28.6 to 16.7 hrs and 37.8 to 29.4 hrs, respectively (**Fig. 4-6A1-3**), and there was a steady decline in the relative mutant TDP-43^{M337V} protein levels from 92.5% to 56.1% as compared to the GFP control over the 24-hr time period (**Fig. 4-6A4**). Inhibiting autophagy by bafilomycin A1 prolonged the protein half-life ($t_{1/2}$) but did not abolish PABPN1's effects (**Fig. 4-6B**). However, inhibiting UPS activity compromised the PABPN1-specific rescue effect (**Fig. 4-6C**). These results confirm the suppression effect of PABPN1 on TDP-43 pathology, via a proteasome-dependent mechanism.

4.3.7 PABPN1 levels regulates nuclear localization of endogenous TDP-43

Cytoplasmic mislocalization of TDP-43 and its depletion from the nucleus is a prominent pathological feature in ALS. To investigate whether the expression of mutant TDP-43 or

TDP-CTF leads to the mislocalization of endogenous full-length TDP-43, we transfected N2a cells with GFP-tagged TDP-43^{WT}, mutant TDP-43^{Q331K} and TDP-CTF. An antibody specific for the N-terminus of TDP-43 was used to determine the percentage of transfected cells that were positive for full-length TDP-43 in the cytoplasm and in the inclusions. The expression of TDP-CTF led to abundant cytoplasmic inclusions (61.0±1.6%) and cytoplasmic mislocalization of endogenous TDP-43 (50.7±2.9%). TDP-43^{WT} and TDP-43^{Q331K} predominantly localized to the nucleus with only ~10% of cells exhibiting cytoplasmic TDP-43 inclusions. Mutant TDP-43^{Q331K} slightly increased the percentage of diffuse cytoplasmic mislocalization (32.8±1.4%) as compared to TDP-43^{WT} (21.1±1.2%) (**Fig. 4-7A-C**). These results suggested that the presence of cytoplasmic inclusions of pathologic TDP-43 fragments and ALS-specific mutations was detrimental to TDP-43 localization and caused the redistribution of full-length TDP-43 from the nucleus to the cytoplasm. This raised the question whether PABPN1 overexpression can reduce cytoplasmic mislocalization of TDP-43. The co-expressed PABPN1 significantly reduced the cytoplasmic inclusions (TDP-43^{WT}: 4.9±1.2%; TDP-43^{Q331K}: 4.14±0.6%; TDP-CTF: 14.0±0.6%) and rescued TDP-43 nuclear localization in the cells expressing TDP-43^{WT}, TDP-43^{Q331K} and TDP-CTF (TDP-43^{WT}: 8.4±0.6%; TDP-43^{Q331K}: 13.7±1.7%; TDP-CTF: 18.2±2.1%) (**Fig. 4-7A-C**). Similar results were also found in primary motor neurons, where PABPN1 expression reduced the number of cells with TDP-CTF aggregates by 54.8% and the number of cells with diffuse cytoplasmic TDP-43 mislocalization by 72.4% (**Supplementary Fig. 4-4**). These results led us to investigate whether PABPN1 overexpression can rescue loss of normal TDP-43 from the nucleus. We performed nuclear-cytoplasmic fractionation experiments and western blot analyses

with antibody specific for the N-terminus of TDP-43. Our results demonstrated a shift of endogenous TDP-43 towards the cytoplasmic fraction upon TDP-CTF expression (**Fig. 4-7D**). Overexpression of PABPN1 partially reversed the pathologic changes to the ratio of nuclear-to-cytoplasmic endogenous TDP-43, demonstrating that PABPN1 overexpression can restore the proper nuclear localization of endogenous TDP-43. The knockdown of PABPN1, on the other hand, resulted in increased cytoplasmic localization of endogenous TDP-43 by 60.5% (**Fig. 4-7E**) and decreased the ratio of nuclear-to-cytoplasmic endogenous TDP-43 by 41.5% (**Fig. 4-7F**) in N2a cells and primary motor neurons.

4.3.8 PABPN1 overexpression rescues defects in SGs caused by TDP-43 pathology

TDP-43 inclusions have been shown to colocalize with SG markers (e.g., TIA1, TIAR) in cultured cells and postmortem tissues from ALS patients²⁵⁴. These studies suggest that genetic or environmental factors leading to persistent SGs in the early stage of disease may not only interfere with RNA processing, but also serve as precursors of pathological protein inclusions and trigger the irreversible formation of TDP-43 protein aggregates¹³⁶.

To investigate how TDP-43 pathology affects SG dynamics in primary motor neurons, we induced SGs by oxidative stress and quantified the SG assembly and disassembly in terms of SG formation and the $t_{1/2}$ of SG dissipation after removal of oxidative stress. Upon exposure to sodium arsenite (0.5mM, 1 hr), SG numbers differed greatly among the GFP control and the three TDP-43 constructs. TDP-43^{WT} and TDP-43^{Q331K} significantly increased SG numbers (GFP: 5.7±0.1; TDP-43^{WT}: 8.2±0.4; TDP-43^{Q331K}: 7.5±0.2) (**Fig. 4-8A-B**), whereas TDP-CTF dramatically decreased the SG

numbers (1.7 ± 0.2) and the percentage of SG-positive cells (GFP: $71.8 \pm 3.3\%$; TDP-CTF: $39.3 \pm 4.8\%$) (**Fig. 4-8D**). The SG size showed a similar trend (GFP: 0.35 ± 0.04 ; TDP-43^{WT}: 0.45 ± 0.06 ; TDP-43^{Q331K}: 0.40 ± 0.03 ; TDP-CTF: 0.21 ± 0.03) (Fig. 4-8C). Under normal conditions, SGs rapidly disassemble when the stressor is removed. However, TDP-43^{Q331K} expression caused SG persistence after stress resolution ($t_{1/2} = 187.2$ minutes) as compared with GFP control and TDP-43^{WT} (GFP: $t_{1/2} = 97.4$ minutes; TDP-43^{WT}: $t_{1/2} = 106.3$ minutes) (**Fig. 4-8E**). These results show that the ALS-specific mutation in TDP-43^{Q331K} causes overactive SG assembly and slow SG disassembly. Previous studies reported that the mutant TDP-43 was more stable and resistant to degradation than wild-type TDP-43¹⁰¹. The failure in the dissipation of SGs could further increase the propensity of TDP-43 to form pathologic aggregates. To test whether PABPN1 can rescue TDP-43-specific impairment of SG dynamics, we co-expressed either mCherry or mCherry-PABPN1. Most strikingly, PABPN1 specifically restored SG formation in cells expressing TDP-CTF (**Fig. 4-8A**). Quantification of SG dynamics showed that PABPN1 expression alone did not perturb SG formation but rescued abnormal SG numbers (5.7 ± 0.3) and the percentage of SG-positive cells caused by pathological TDP-43 (**Fig. 4-8A-D**). Moreover, PABPN1 partially rescued the slower rate of SG disassembly caused by TDP-43^{Q331K} ($t_{1/2} = 129.0$ minutes) (**Fig. 4-8E**). These results show that PABPN1 expression restores SG dynamics, a process that involves protein aggregation as part of its normal function, and may be closely linked to the disease process^{117,136,223,224}.

4.4 Discussion

Identifying regulators of TDP-43-induced pathogenesis could potentially provide therapeutic opportunities for a range of neurologic diseases. Evidence from genetic and neuropathological studies strongly implicates TDP-43 as a key player in the pathogenesis of primary TDP-43 proteinopathies in the ALS/FTLD-TDP clinicopathological spectrum^{15,234}. For other major neurodegenerative diseases where TDP-43 pathology is found at high rates, such as AD, Huntington's disease, dementia with Lewy bodies, and chronic traumatic encephalopathy, the extent of the contribution of TDP-43 proteotoxicity to the disease phenotype is currently not well-understood³⁶.

Rescue of toxic gain of function of overexpressed TDP-43 variants in primary neurons, yeast, and Drosophila models

TDP-43 pathology is characterized by two hallmarks: the accumulation of ubiquitinated, hyper-phosphorylated and cleaved TDP-43 in mostly cytoplasmic aggregates, and the depletion of TDP-43 from the nucleus¹³. Whether the pathogenesis of ALS is caused by a toxic gain-of-function of cytoplasmic mislocalized TDP-43 or by loss of its normal nuclear function is still under debate, but it appears likely that a combination of both contributes to the disease process^{15,234}. TDP-43 protein levels are tightly regulated⁸⁶, and increased or decreased levels may reduce cellular tolerance to intracellular or extracellular stress²⁵⁵.

The gain-of-function hypothesis suggests that cytoplasmic TDP-43 mislocalization and its pathologic posttranslational modifications may directly acquire toxic properties, or trap mRNAs and proteins in insoluble aggregates²³⁴. Therefore, most

TDP-43 proteinopathy disease models are based on the overexpression of TDP-43 constructs. While modeling ALS pathology by transgenic overexpression of TDP-43 has not been entirely successful, these efforts have established that increasing wild-type or mutant TDP-43 levels by less than two-fold over endogenous levels is harmful²⁵⁶.

To model this pathogenic mislocalization and aggregation in mammalian cells *in vitro*, several cellular models based on overexpression of C-terminal fragments of TDP-43 have been described¹³². Most of these studies were performed in cell lines, but we and others have found that TDP-CTF forms hyperphosphorylated and ubiquitin-positive cytoplasmic aggregates in primary neurons and that disease-specific mutations increase the cytoplasmic localization of full-length TDP-43^{113,124}. Increasing toxicity is correlated with elevated TDP-43 levels and cytoplasmic TDP-43 mislocalization in cortical neurons²⁵⁷. In this study we used wild-type human TDP-43 and several disease-specific mutations, as well as a C-terminal fragment of TDP-43 beginning at Arg208 that was found as a major component of pathologic inclusions in the brain of ALS and FTLTDP patients and recapitulates pathological features of TDP-43 proteinopathy when overexpressed^{30,132}. We found that overexpression of TDP-43 with disease-specific mutations enhanced the moderate toxicity of full-length TDP-43, and TDP-CTF caused the highest levels of cell death in primary cortical neurons (**Fig. 4-2C,D**). PABPN1 protein levels modulate TDP-43 toxicity, acting as a strong suppressor when overexpressed. Overexpression of PABPN1 alone did not show toxicity in primary neurons, well in agreement with data from transgenic mice overexpressing normal PABPN1 from a strong ubiquitous promoter with no obvious pathology²⁵⁸.

TDP-43 proteinopathies and other neurodegenerative disorders characterized by the aggregation of proteins can be modeled in the budding yeast *Saccharomyces cerevisiae*¹³¹. Not only TDP-43 but also FUS, α -synuclein, and polyglutamate repeats, are toxic and form cytoplasmic aggregates in yeast²⁵⁹. Using suppressor screens, several functionally diverse yeast genes that can modulate TDP-43 toxicity have been identified^{143,260,261}. Pbp1 (poly(A)-binding protein (Pab1p)-Binding Protein), and its ortholog ataxin-2, were identified as a modulator of TDP-43 toxicity across multiple models, leading to the discovery of a significant association of ataxin-2 intermediate-length polyQ tract expansions with ALS¹⁴³. Loss of the RNA lariat debranching enzyme Dbr1 was able to antagonize the toxic effect of cytoplasmic TDP-43 aggregates in yeast and primary neurons²⁶⁰. Accumulated intronic lariat RNAs may act as decoys that sequester TDP-43 away from binding to and disrupting functions of other RNAs. Another modifier of FUS- and TDP-43-mediated toxicity in yeast is ECM32, a component of the nonsense-mediated mRNA decay (NMD) surveillance mechanism that degrades mRNAs containing a premature termination codon²⁶¹. Overexpression of its human ortholog UPF1 protects primary neuronal cultures from TDP-43 cytotoxicity and preserves forelimb function in a rat model of TDP-43-induced motor paralysis, possibly by upregulating NMD²⁶². Expression of mutant variants of yeast Hsp104 was found to enhance the solubility of TDP-43 aggregates and suppress TDP-43 toxicity²⁶³. In this study we employed a yeast model to find out whether PABPN1 expression can mitigate TDP-43 toxicity. While induced overexpression weakly inhibits growth in yeast, it acted as a strong suppressor of TDP-43 toxicity (**Fig. 4-2A**). Taken together with the direct

interaction in the yeast-two-hybrid tests, our results suggest a direct effect of PABPN1 on TDP-43 in yeast.

Several *Drosophila* models for TDP-43-associated ALS have provided evidence for both loss and gain of function hypotheses²⁶⁴. Larvae expressing human TDP-43 in motor neurons are impaired in larval turning behavior, with disease-specific mutations having a more severe effect than wild-type TDP-43^{173,252}. We evaluated the role of PABPN1 in regulating TDP-43 toxicity in vivo in a *Drosophila* model of ALS. Loss of PABPN1 function exacerbated TDP-43-specific neurodegeneration in both the adult retina and in larval motor neurons (**Fig. 4-2G,H**).

The C-terminus of PABPN1 contains a non-classical proline-tyrosine nuclear localization signal (PY-NLS), which is also present in FUS and other RNA-binding proteins and recognized by the nuclear import protein Transportin 1²⁶⁵. Although this signal is not essential for the nuclear import of human PABPN1²⁶⁶, larger deletions are required to confer nucleocytoplasmic (PABPN1^{ΔNLS18}) or cytoplasmic (PABPN1^{ΔNLS50}) localization²⁴³. The PABPN1^{ΔNLS50} deletion mutant is still able to associate with TDP-43 in co-IPs (**Fig. 4-1C**) and even shows co-aggregation with TDP-CTF (**Fig. 4-3A**), although has weaker neuroprotective effects, which suggests that nuclear localization of PABPN1 is required for suppression of TDP-43 proteotoxicity. One possible model is that PABPN1 interacts with monomeric and/or soluble forms of TDP-43, which are localized to the nucleus, thus preventing the formation of cytoplasmic aggregates of TDP-43.

TDP-43 toxicity may be caused by mislocalization of soluble cytoplasmic TDP-43 or by misfolding and/or aggregation into insoluble inclusions. The aberrant clusters of

TDP-43, members of hnRNP family (e.g. hnRNP-A1, A2/B1), HuD, SG proteins (e.g. TIA-1, eIF3), SQSTM1/p62 and proteasome subunits suggested that cytoplasmic TDP-43 aggregation may disturb RNA and protein homeostasis¹⁵. Alternatively, inclusion formation could protect cells from mislocalized cytoplasmic soluble TDP-43 protein (monomers or oligomers) by sequestering them into aggregates²⁶⁷. To investigate how PABPN1 affects different populations of pathologic and normal TDP-43, we performed extensive analyses by fluorescence microscopy and western blot analysis of cell extracts. PABPN1 exhibits a remarkable specificity for pathologic forms of TDP-43. PABPN1 overexpression specifically reduced protein levels of both detergent soluble and insoluble forms of TDP-CTF (**Fig. 4-3E**), but it did not affect protein levels of endogenous full-length TDP-43. However, it caused a shift of endogenous TDP-43 from the insoluble to the soluble fraction, which suggested that PABPN1 may prevent the formation and/or facilitate the removal of existing TDP-CTF aggregates and also limit the co-aggregation of normal full-length TDP-43 (**Fig. 4-3E**). This finding was further supported by time-lapse live-cell imaging experiments to measure protein levels of TDP-CTF when PABPN1 expression was induced with a delay of 24 hrs. At this time point cells exhibited high levels of TDP-CTF in the cytoplasm. PABPN1 but not GFP overexpression led to a rapid reduction of TDP-CTF protein levels throughout the cytoplasm. While live cell imaging does not allow for discriminating soluble and insoluble TDP-CTF protein, we observed a reduction of both focal and more diffuse staining in the cytoplasm. This suggests that PABPN1 can cause the removal of existing aggregates either by facilitating their degradation or by preventing the formation of new aggregates. It remains to be

investigated whether PABPN1 causes the release of TDP-43 associated proteins or RNAs that may be trapped by pathologic cytoplasmic TDP-43 aggregates.

Rescue of normal localization and solubility of endogenous TDP-43

The gain-of-function hypothesis suggests that cytoplasmic mislocalization and co-aggregation of TDP-43 may lead to its depletion from the nucleus, thus impairing its normal nuclear functions in regulating transcription and mRNA processing^{232,234,268}.

While early-onset motor dysfunction in motor neuron-specific TDP-43 knockout mice may reflect an essential function of TDP-43 in development²⁶⁹, knock-out of TDP-43 in postnatal motor neurons led to an age-dependent progressive motor dysfunction accompanied by neuropathological alterations typical for ALS, including axonal degenerations preceding atrophy of motor neurons^{270,271}. A specific vulnerability of motor neurons to low TDP-43 levels is supported by transgenic CNS-specific TDP-43 knockdown mice that exhibit age-dependent neurological symptoms, including muscle weakness and paralysis, concomitant with degeneration of spinal motor neurons²³³.

In cell lines, the overexpression of different TDP-CTF variants leads to the recruitment of endogenous TDP-43 into the cytoplasm^{225,272,273}. Consistent with a loss-of-nuclear function phenotype, the expression of TDP-CTF constructs can affect the TDP-43-dependent regulation of CFTR alternative splicing^{106,225,273}. When we overexpressed TDP-CTF in N2a cells, we also observed reduced nuclear levels of endogenous TDP-43 (**Fig. 7D**). These results suggest that the presence of TDP-CTF, exhibiting abundant cytoplasmic aggregates, drives endogenous TDP-43 from the nucleus into the cytoplasm, which may disturb neuronal function via a loss-of-function mechanism. Therefore,

removal of pathogenic TDP-43 concurrent with restoring normal levels of nuclear TDP-43 may be required for a complete rescue of TDP-43 proteinopathy models. Importantly, we found that PABPN1 overexpression not only failed to disturb protein levels of endogenous TDP-43, but also rescued its nuclear localization and solubility (**Fig. 3E and 7D**). This effect is likely due to the reduction of TDP-CTF protein levels and cytoplasmic aggregates, which allows the release of trapped TDP-43 and the recovery of its nuclear localization and function.

Interestingly, the neuromuscular disease OPMD, caused by polyalanine expanded mutant PABPN1, is characterized by TDP-43 positive aggregates in affected muscle cells²³⁸. While initially toxic gain-of-function models have been proposed²⁷⁴, low levels of PABPN1 observed in skeletal muscle and a loss of normal PABPN1 function may contribute to the muscle-specific pathology in OPMD^{237,275,276}. Since we observed an increase in TDP-CTF protein levels (**Fig. 4-3C**) and cytoplasmic redistribution of endogenous TDP-43 (**Fig. 4-7E-F**) after knockdown of PABPN1, it is tempting to speculate that low levels of functional PABPN1 could contribute to the accumulation and mislocalization of TDP-43 in OPMD.

Rescue of stress granule formation by PABPN1

SG formation involves protein accumulation as a normal mechanism and might play an important role in the pathogenesis of TDP-43 proteinopathies, by acting as a seed for pathological inclusions and by sequestering RNAs and associated proteins^{136,224}. TDP-43 has been found colocalized with several SG proteins (e.g. TIA-1, TIAR, eIF3) in cultured cells and brain tissues from ALS and FTLTDP patients, which hypothetically links the

prolonged misregulation of SG dynamics to the cytoplasmic aggregation formation¹¹⁷. However, whether the genetic mutation or protein aggregation could conversely interfere with the SG formation is poorly understood. TDP-43 modulates SG dynamics through the regulation of the essential SG nucleators TIA-1 and G3BP¹¹⁶. Q331K and Q343R mutation were found to enhance SG formation in BE-M17 cells³⁵, suggesting that the aggregation-prone and degradation-resistant properties of mutant TDP-43 may contribute to the dysregulation of SG dynamics.

In the present study, we demonstrated that mutant or aggregated TDP-43 impeded normal SG dynamics in primary motor neurons under conditions of oxidative stress (**Fig. 4-8**). We observed the overactive SG formation in cells overexpressing wild-type TDP-43 or mutant Q331K but loss of SGs in TDP-CTF expressing neurons. Moreover, we also found the prolonged SG disassembly in TDP-43^{Q331K} instead of TDP-43^{WT} (**Fig. 4-8**). While TDP-CTF lacks the RNA-binding domains necessary for SG association²⁵⁴, its aggregation in the cytoplasm may potentially interfere with normal SG formation by trapping essential SG components into its aggregates, which may render neurons more vulnerable to sublethal stress condition. The rescue effect of PABPN1 on SG dynamics in TDP-43 pathology is likely due to enhancing the turnover of pathogenic TDP-43 and restoring solubility and localization of normal TDP-43 protein.

How does PABPN1 regulate levels of pathologic TDP-43?

Two principal pathways of protein degradation have been described as complementary neuroprotective mechanisms, the UPS characterized by the degradation of polyubiquitinated substrates via the proteasome, and the autophagy pathway, typically

targeting larger aggregates for degradation in lysosomes²⁷⁷. Previous studies have shown that induction of autophagy and proteasome activity both facilitate TDP-43 clearance and ameliorated toxicity^{257,278,279}. Several studies have reported distinct roles for protein degradation pathways in the clearance of pathological TDP-43 proteins^{229,280}. As pathological TDP-43 exists in various forms, the UPS appears to preferentially degrade soluble monomeric TDP-43, whereas autophagy removes oligomeric and aggregated TDP-43.

Our data show that inhibition of proteasomes but not autophagy completely blocked PABPN1-dependent degradation of TDP-CTF and mutant TDP-43 (**Fig. 4-5 & 6**). Although we cannot exclude the contribution of autophagy system to the protein degradation of detergent-insoluble large aggregates, the UPS appears to be more important to degrade pathological TDP-43 isoforms in the presence of PABPN1. Our results demonstrate that PABPN1 enhanced the protein turnover of exogenously expressed wild-type and mutant TDP-43 and TDP-CTF preferentially through the UPS degradation pathway by driving the equilibrium towards small soluble species and preventing the formation of macroaggregates (**Fig. 4-9**).

Further studies are needed to establish the exact mechanism how PABPN1 specifically targets pathologic TDP-43. The observation that the C-terminal NLS of PABPN1 is required for this activity suggests that it may directly affect the localization of TDP-43, perhaps by facilitating its nuclear import. Alternatively, PABPN1 may have a direct effect on the degradation of TDP-43 via regulating UPS pathways. In addition, there are several functional links between poly(A)-binding proteins and TDP-43 toxicity. In yeast, Pbp1 enhances TDP-43 toxicity. Pbp1 interacts with Pab1 to regulate mRNA

polyadenylation and is involved in stress granule assembly, and the same has been found for their mammalian homologs ataxin-2 and PABPC1¹⁴³. In a *Drosophila* model of ALS, *dPABP* expression exacerbates TDP-43 toxicity and PABPC1 was found to be mislocalized in cytoplasmic accumulations in ALS patient motor neurons¹⁴⁵. This is further supported by our finding that PABPC1 overexpression had an opposite effect of PABPN1 and increased TDP-CTF protein levels (**Fig. 4-3D**).

In conclusion, whether TDP-43 proteinopathy is due to gain or loss of function mechanisms or a combination of both, our results suggest that the specific removal of pathologic TDP-43 protein by modulating PABPN1 protein levels can rescue various phenotypes caused by TDP-43 toxicity, and restore normal localization of TDP-43 across several *in vitro* and *in vivo* disease models (**Fig. 4-9**). A better understanding of pathways that regulate TDP-43 proteinopathy may form the basis of novel strategies for therapeutic intervention in ALS, FTL-D-TDP, and other neurodegenerative diseases.

4.5 Figures

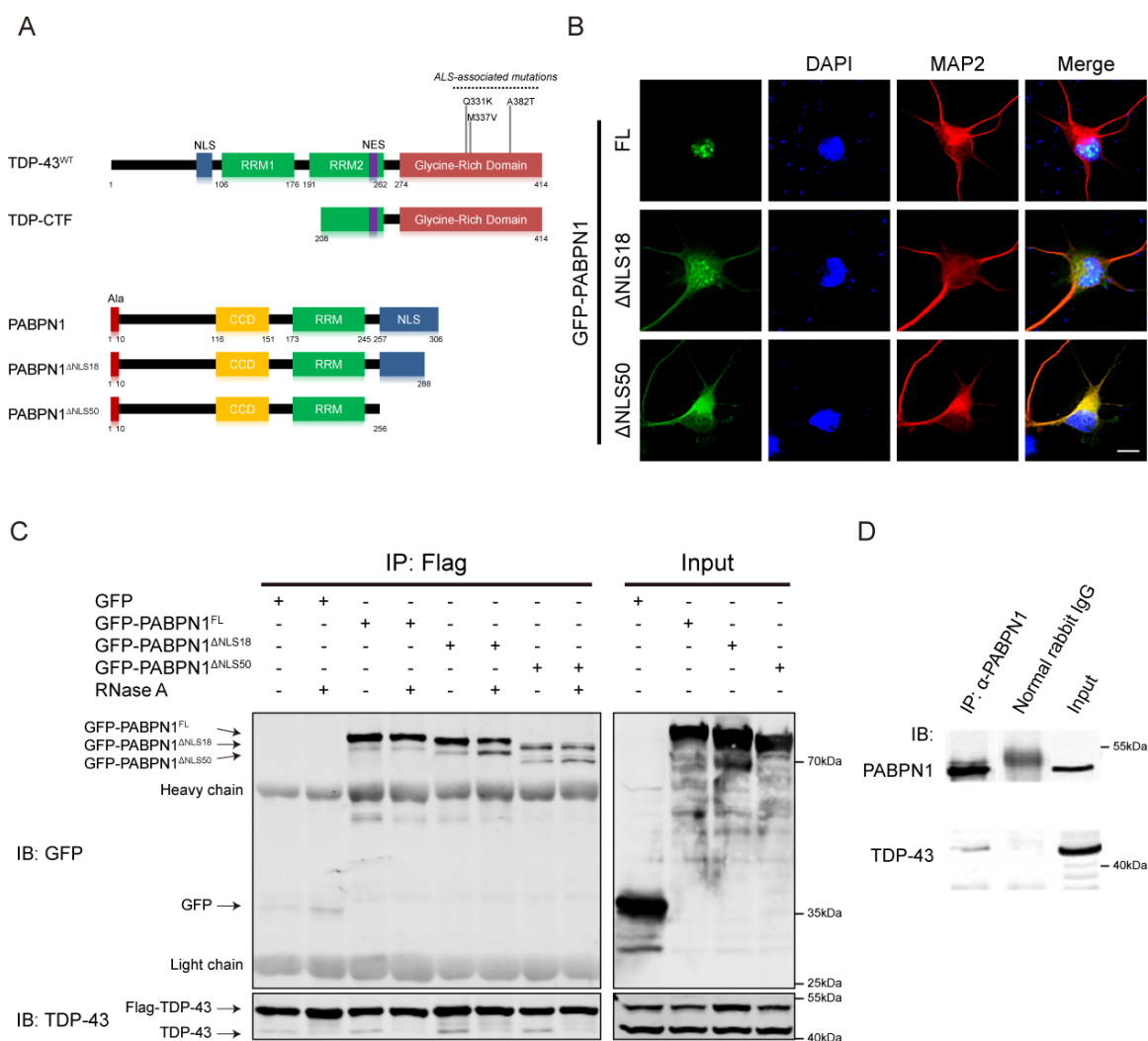


Figure 4-1 | TDP-43 and PABPN1 associate by protein-protein interaction in mammalian cells and tissue.

(A) Schematic domain structures of human TDP-43 and PABPN1 constructs used in this study. (Top) Human TDP-43 protein contains NLS, two RRM, (NES), and a glycine-rich C-terminal domain. We cloned fusion constructs of wild-type TDP-43, the ALS-specific missense mutations Q331K, M337V and A382T, and a C-terminal fragment from aa 208-414 (TDP-CTF) that accumulates as a cleavage product in ALS and FTLD-

TDP patient tissue. (Bottom) Human poly(A)-binding protein nuclear 1 (PABPN1) contains an N-terminal stretch of 10 alanines (Ala), a coiled-coil domain (CCD), one RRM domain and an NLS in the arginine-rich C-terminus. We use two C-terminal truncation mutations of PABPN1 with a partial (aa 289-306, PABPN1^{ΔNLS18}) or full deletion of the NLS region (aa 257-306, PABPN1^{ΔNLS50}). **(B)** Localization of PABPN1 constructs in primary motor neurons. Fluorescence microscopy images show that GFP-PABPN1 is predominantly localized in the nucleus. GFP-PABPN1^{ΔNLS18} shows nucleocytoplasmic localization, whereas GFP-PABPN1^{ΔNLS50} is confined to the cytoplasm. Scale bar: 10μm. **(C)** Association of PABPN1 with TDP-43 in transfected N2a cells. Left panel: Western blot analysis of anti-FLAG immunoprecipitates from N2a cells co-expressing FLAG-tagged TDP-43 and GFP or GFP-tagged PABPN1 shows association of TDP-43 with PABPN1 that is independent of RNA-binding or the presence of the PABPN1 C-terminal region (full-length: FL; ΔNLS18 and ΔNLS50). RNase A treatment is indicated. Right panel: Western blot analysis of cell lysates (Input). **(D)** Association of TDP-43 with PABPN1 in mouse brain tissue. Western blot analysis of anti-PABPN1 immunoprecipitates from mouse brain lysates with anti-TDP-43 confirms the specific association of both proteins.

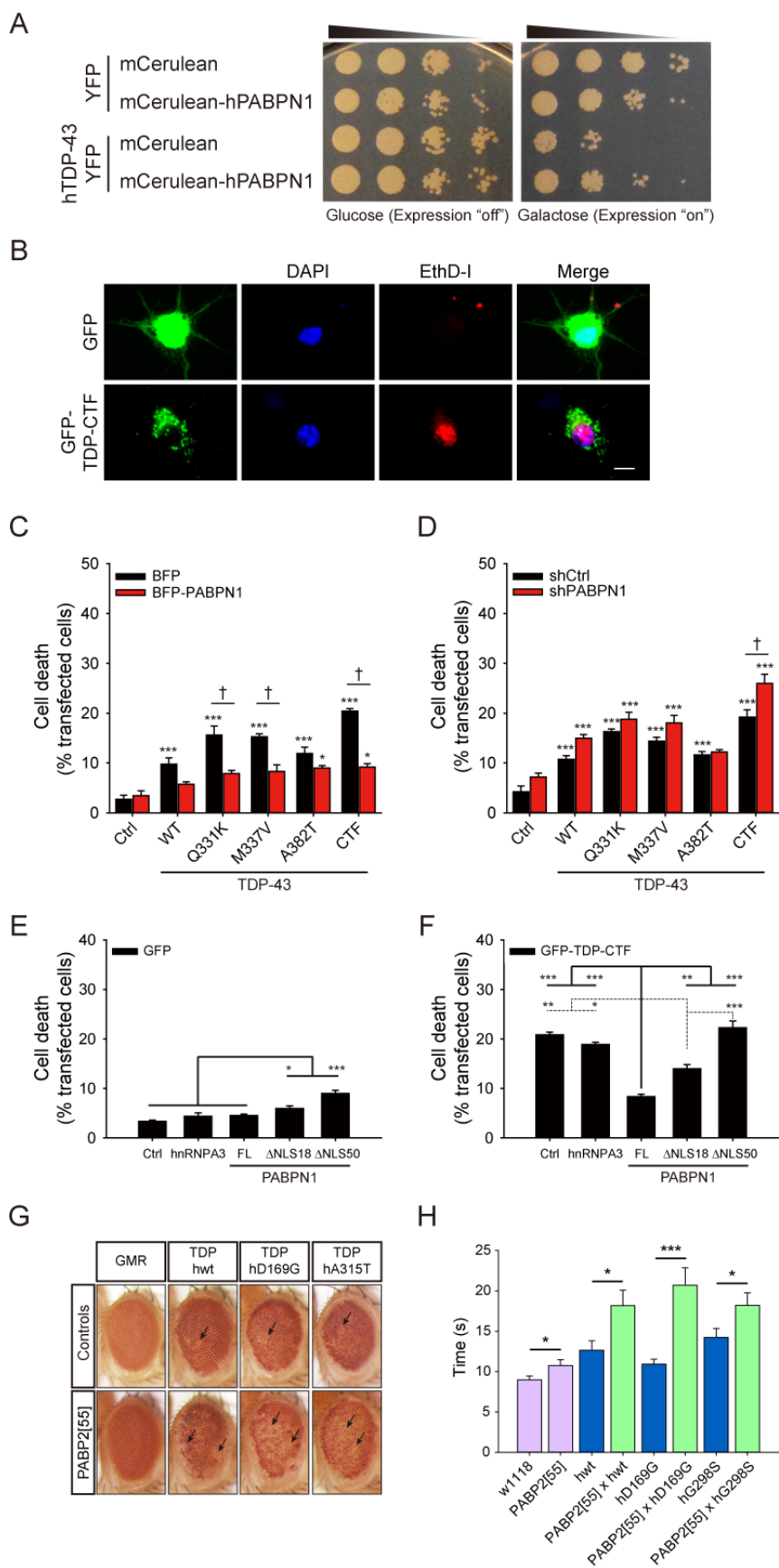


Figure 4-2 | PABPN1 modulates TDP-43 toxicity in several *in vitro* and *in vivo* models of TDP-43 proteinopathy.

(A) TDP-43 and PABPN1 toxicity in yeast. Spotting assays were used to measure cellular growth in yeast co-expressing human TDP-43 (hTDP-43) fused with yellow fluorescent protein (YFP) or the YFP control, together with monomeric Cerulean fluorescent protein tagged human PABPN1 (mCerulean-hPABPN1) or the mCerulean control. Co-expression of PABPN1 strongly suppressed TDP-43 toxicity. **(B)** Cell death assay with the membrane-impermeable DNA-binding fluorescent dye Ethidium homodimer I (EthD-I). Fluorescence microscopy of primary cortical neurons shows red fluorescent staining of nuclei in dead or dying cells when membranes are compromised. Cells were transfected with expression plasmids for GFP (Top) or GFP-TDP-CTF (Bottom). Scale bar: 10 μ m. **(C)** Quantification of TDP-43-mediated cell death upon overexpression of PABPN1. Neurons were transfected with GFP control (Ctrl), and GFP-tagged human wild-type TDP-43 (TDP-43^{WT}), ALS-specific mutant TDP-43 (TDP-43^{Q331K}, TDP-43^{M337V} and TDP-43^{A382T}) or TDP-CTF expression plasmids. Co-expression of blue fluorescent protein-tagged PABPN1 (BFP-PABPN1) but not the BFP control reduced TDP-43 toxicity. Statistical analysis was performed with two-way ANOVA and Bonferroni's post hoc test (*five independent experiments, *P < 0.05, ***P < 0.001, TDP-43 constructs versus Ctrl; †P < 0.05, BFP-PABPN1 versus BFP. BFP: Ctrl (n=564), WT (n=517), Q331K (n=341), M337V (n=393), A382T (n=350), CTF (n=333); BFP-PABPN1: Ctrl (n=509), WT (n=529), Q331K (n=378), M337V (n=335), A382T (n=352), CTF (n=317)*). **(D)** Quantification of TDP-43-mediated cell death upon knockdown of PABPN1. Neurons were transfected with BFP control (Ctrl) and BFP-tagged TDP-43

expression constructs. Co-expression of the PABPN1-specific shRNA construct (shPABPN1) but not the nonsilencing control (shCtrl) exacerbated TDP-43 toxicity. Statistical analysis was performed with two-way ANOVA and Bonferroni's post hoc test (*five independent experiments, *P < 0.05, ***P < 0.001, TDP-43 constructs versus Ctrl; †P < 0.05, shPABPN1 versus shCtrl. BFP: Ctrl (n=447), WT (n=370), Q331K (n=253), M337V (n=265), A382T (n=256), CTF (n=379); BFP-PABPN1: Ctrl (n=507), WT (n=412), Q331K (n=286), M337V (n=288), A382T (n=273), CTF (n=446)*). **(E)**

Quantification of cell death in neurons expressing hnRNPA3 or PABPN1 variants (full-length: FL; lacking 18aa of NLS: Δ NLS18; lacking 50aa of NLS: Δ NLS50). Only expression of PABPN1 ^{Δ NLS50} led to increased cell death. Statistical analysis was performed with one-way ANOVA and Bonferroni's post hoc test (*three independent experiments, *P < 0.05, **P < 0.01, ***P < 0.001. Ctrl (n=302), hnRNPA3 (n=300), FL (n=309), Δ NLS18 (n=304), Δ NLS50 (n=301)*). **(F)**

Quantification of cell death in neurons co-expressing TDP-CTF and hnRNPA3 or PABPN1 variants. PABPN1 ^{Δ NLS18} suppressed TDP-43 toxicity only weakly, whereas PABPN1 ^{Δ NLS50} and hnRNPA3 had no obvious effect. Statistical analysis was performed with one-way ANOVA and Bonferroni's post hoc test (*three independent experiments, *P < 0.05, **P < 0.01, ***P < 0.001. Ctrl (n=275), hnRNPA3 (n=302), FL (n=233), Δ NLS18 (n=295), Δ NLS50 (n=280)*). **(G)**

Neurodegeneration phenotype in the adult *Drosophila* retina. Overexpression of human wild-type or mutant TDP-43 (hwt, hD169G, and hA315T) in photoreceptor neurons using the GMR Gal4 driver causes a depigmentation (arrows) phenotype in the retina (*n = 10*). The loss of function mutant of the *Drosophila* PABPN1 ortholog PABP2[55] enhanced TDP-43-dependent depigmentation phenotype (arrows). **(H)**

Locomotor phenotype in

Drosophila larvae. Overexpression of human transgene variants (hwt, hD169G and hG298S) in motor neurons driven by the D42 Gal4 driver causes a significant time delay to turn over following a ventral-up inversion in larval turning assays. The PABP2[55] mutation enhanced TDP-43-dependent locomotor defects. ($n = 30-47$). $*P < 0.05$, $***P < 0.001$. Graphs represent mean and SEM.

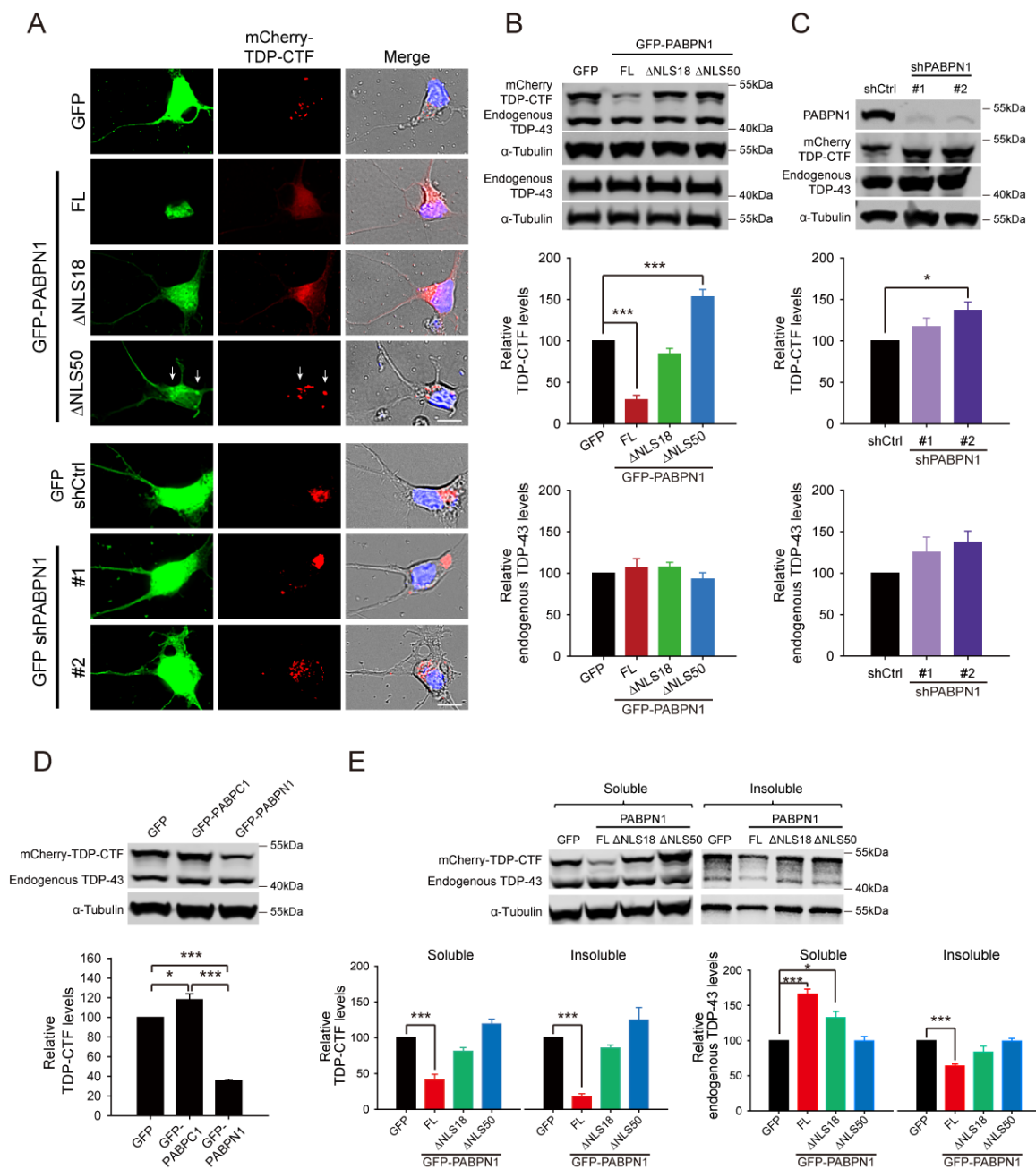


Figure 4-3 | PABPN1 overexpression reduces pathological TDP-43 protein levels.

(A) Fluorescence microscopy analysis of TDP-CTF aggregation. Top: Representative images of primary motor neurons expressing mCherry-TDP-CTF (red), and GFP-PABPN1 (FL, ΔNLS18 and ΔNLS50) (green). White arrows indicate co-aggregation of PABPN1^{ΔNLS50} with TDP-CTF in the cytoplasm. Bottom: Co-expression of mCherry-

TDP-CTF with shRNA constructs encoding GFP. One control shRNA (shCtrl) and two shRNAs specific for PABPN1 knockdown (shPABPN1#1, shPABPN1#2) were used (green). Merged images show mCherry-TDP-CTF (red), nuclei (blue), and differential interference contrast. Scale bar: 10 μ m. **(B-C)** Western blot analyses and quantification of TDP-CTF and endogenous TDP-43 protein levels in N2a cells after PABPN1 overexpression ($n = 7,7$) (B) or PABPN1 knockdown ($n = 7,6$) (C). Full-length PABPN1 and PABPN1 ^{Δ NLS50} expression had opposite effects on TDP-CTF levels. Statistical analysis was performed with one-way ANOVA and Bonferroni's post hoc test ($*P < 0.05$, $***P < 0.001$). **(D)** Quantification of TDP-CTF protein levels upon overexpression of PABPC1 and PABPN1. Co-expression of mCherry-TDP-CTF with either GFP, GFP-PABPC1, or GFP-PABPN1 in N2a cells showed opposite effects on TDP-CTF levels. Statistical analysis was performed with one-way ANOVA and Bonferroni's post hoc test ($*P < 0.05$, $***P < 0.001$, $n = 5$). **(E)** Western blot analyses of detergent-soluble and insoluble protein fractions from N2a cells expressing TDP-CTF. PABPN1 overexpression reduced both soluble and insoluble TDP-CTF, statistical analysis with one-way ANOVA and Bonferroni's post hoc test ($***P < 0.001$, $n = 7$), and causes a shift of endogenous TDP-43 from insoluble to soluble form, statistical analysis with one-way ANOVA and Bonferroni's post hoc test ($*P < 0.05$, $***P < 0.001$, $n = 7$).

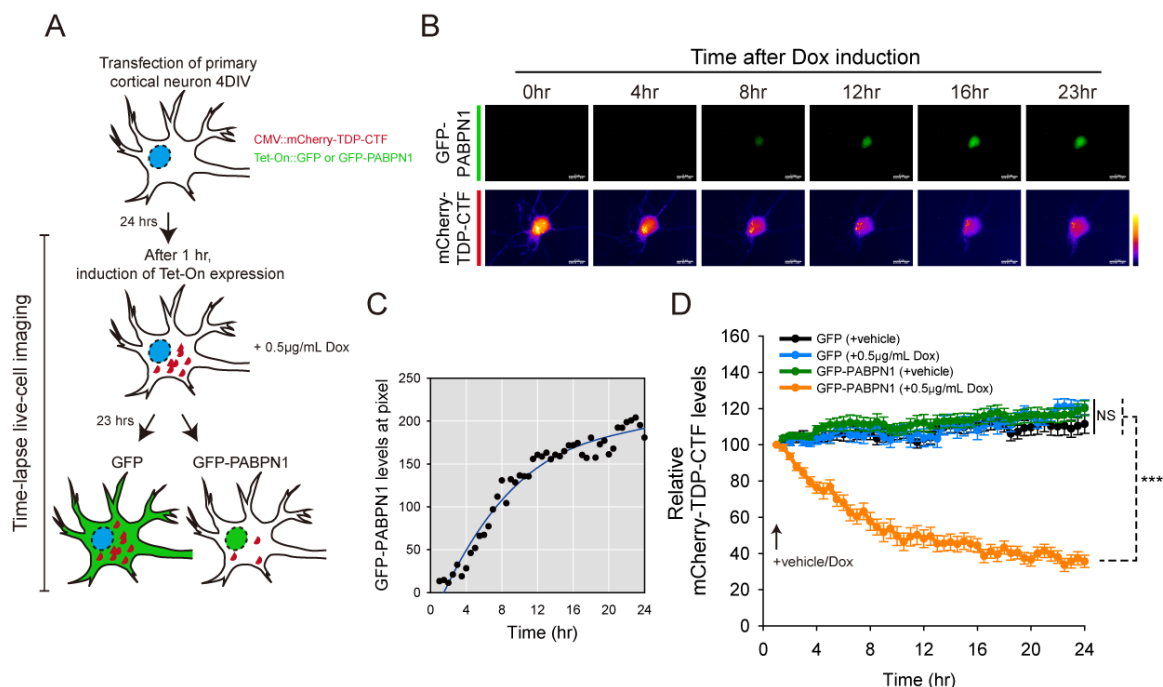


Figure 4-4 | Induction of PABPN1 expression promotes the clearance of pre-formed pathological TDP-43 aggregates.

(A) Schematic of time-lapse live-cell imaging to monitor TDP-CTF protein levels over time in the Dox-inducible system. Primary cortical neurons were co-transfected with plasmids for constitutive CMV promoter-driven mCherry-TDP-CTF expression and inducible Tet-On promoter-driven GFP or GFP-PABPN1 expression. After 24 hrs, cells were imaged for 1 hr to establish basal cellular TDP-CTF levels, and then GFP or GFP-PABPN1 expression were induced by adding Dox. Imaging continued for another 23 hrs to monitor changes in TDP-CTF levels. (B) Representative images of the induction of PABPN1 expression (green) and the subsequent reduction of TDP-CTF shown by heat map. (C) Quantification of PABPN1 protein levels after Dox induction. (D) Quantification of TDP-CTF protein levels over time. In the vehicle and GFP control groups, TDP-CTF steadily increased during the recording period, whereas the inducible PABPN1 expression caused a quick and sustained reduction of TDP-CTF levels. TDP-

CTF protein levels from three independent experiments were normalized to the basal levels. Statistical analysis was performed with two-way repeat-measures ANOVA and Bonferroni's post hoc test (*values at different time points versus value at 0 hr, NS: not significant, *** $P < 0.001$, $n = 20$ per group*). Graphs represent mean and SEM.

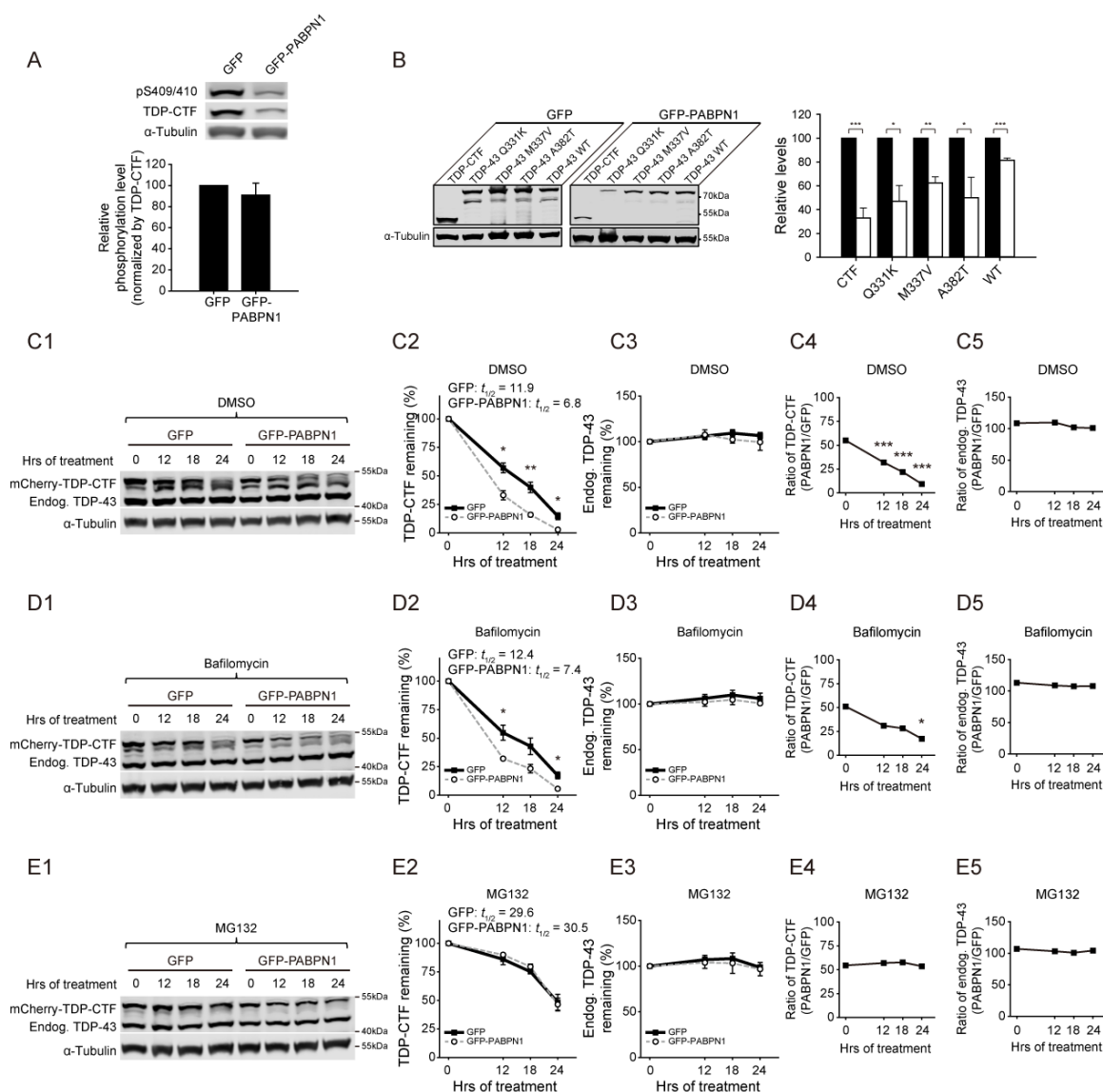


Figure 4-5 | PABPN1 promotes TDP-CTF turnover through proteasomal degradation.

(A) Quantification of phosphorylated TDP-CTF (normalized to total TDP-CTF protein levels). An antibody specific for phosphorylated Ser409/410 of TDP-43 was used. Statistical analysis was performed with Student's *t*-test. (B) PABPN1 expression reduces TDP-CTF, ALS-specific mutant TDP-43 (Q331K, M337V and A382T) and wild-type TDP-43 (WT). Statistical analysis with Student's *t*-test ($*P < 0.05$, $**P < 0.01$, $***P < 0.001$, $n = 3$). (C1-E1) Cycloheximide chase assays to determine the half-life ($t_{1/2}$) and

the relative protein levels of TDP-CTF. Representative western blots of lysates from N2a cells co-expressing mCherry-TDP-CTF with either GFP or GFP-PABPN1 are shown. Cells were treated with CHX (100 μ M) together with DMSO vehicle control (C1), autophagy inhibitor Bafilomycin (100nM) (D1), or proteasome inhibitor MG132 (10 μ M) (E1) at the indicated time points. PABPN1 promoted TDP-CTF degradation only in the absence of proteasome inhibitors. **(C2-E2)** Quantification of TDP-CTF protein levels and half-life ($t_{1/2}$) after treatment with DMSO (C2), Bafilomycin (D2), or MG132 (E2). Protein levels were normalized to the values at 0 hr and represented as the percentage of remaining protein. Statistical analysis is performed with Student's *t*-test (*GFP-PABPN1 versus GFP*, **P* < 0.05, ***P* < 0.01, *n*=3). **(C3-E3)** Quantification of endogenous TDP-43 protein levels and half-life ($t_{1/2}$). **(C4-E4)** Ratio of the relative TDP-CTF levels with PABPN1 vs. GFP co-expression after treatment with DMSO (C4), Bafilomycin (D4), or MG132 (E4). TDP-CTF levels remained constant under conditions of proteasome inhibition. Statistical analysis was performed with one-way ANOVA and Bonferroni's post hoc test (*values at different time points versus value at 0 hr*, **P* < 0.05, ****P* < 0.001, *n*=3). **(C5-E5)** Ratio of the relative endogenous TDP-43 levels with PABPN1 vs. GFP co-expression. Graphs represent mean and SEM.

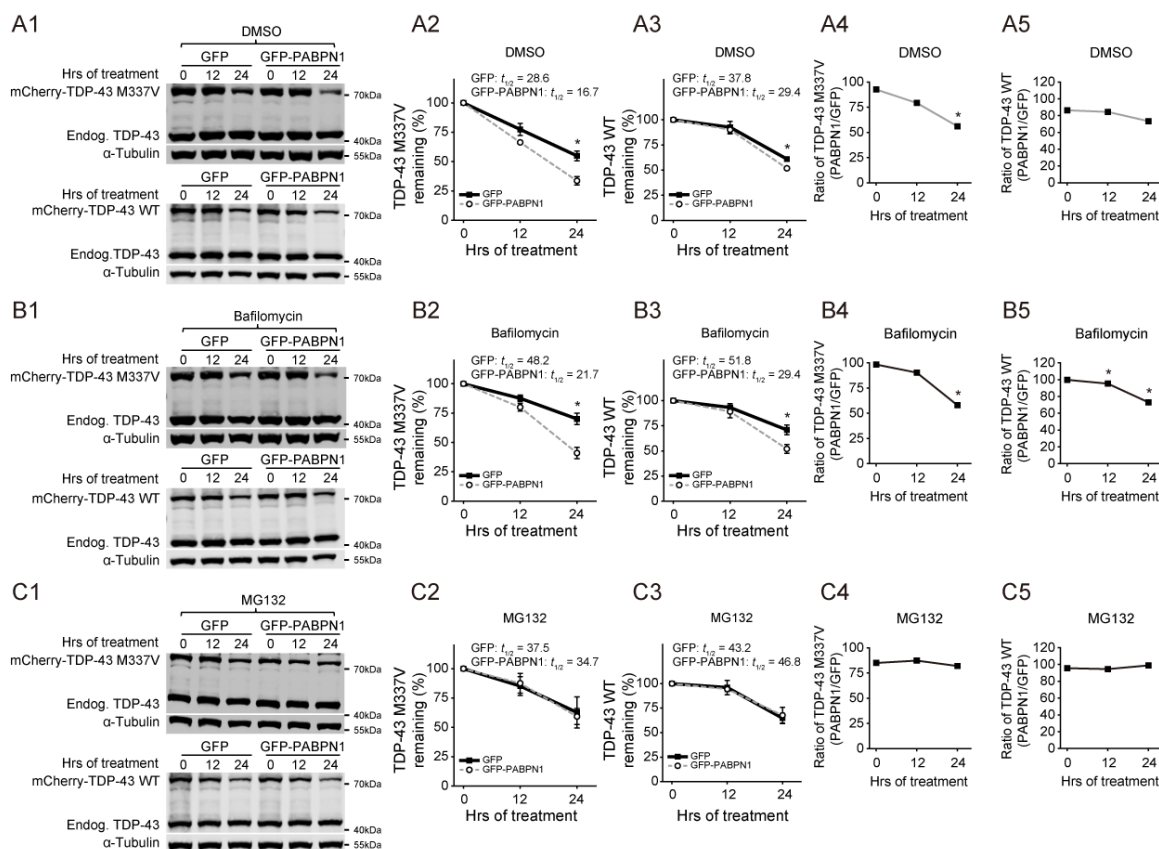


Figure 4-6 | PABPN1 promotes mutant and wild-type TDP-43 turnover through proteasomal degradation.

(A1-C1) Cycloheximide chase assays to determine the half-life ($t_{1/2}$) and the relative protein levels of mutant TDP-43 M337V and wild-type TDP-43 (WT). Representative western blots of lysates from N2a cells co-expressing mCherry-TDP-43 M337V or TDP-43 WT with either GFP or GFP-PABPN1 are shown. Cells were treated with CHX (100 μ M) together with DMSO vehicle control (A1), autophagy inhibitor Bafilomycin (100nM) (B1), or proteasome inhibitor MG132 (10 μ M) (C1) at the indicated time points. PABPN1 promoted mutant and WT TDP-43 degradation only in the absence of proteasome inhibitors. (A2-C2) Quantification of TDP-43 M337V protein levels and half-life ($t_{1/2}$) after treatment with DMSO (A2), Bafilomycin (B2), or MG132 (C2).

Protein levels were normalized to the values at 0 hr and represented as the percentage of remaining protein. Statistical analysis is performed with Student's t-test (*GFP-PABPN1* versus *GFP*, $*P < 0.05$, $n=3$). **(A3-C3)** Quantification of TDP-43 WT protein levels and half-life ($t_{1/2}$). **(A4-C4)** Ratio of the relative TDP-43 M337V levels with PABPN1 vs. GFP co-expression after treatment with DMSO (A3), Bafilomycin (B3), or MG132 (C3). TDP-43 M337V levels remained constant under conditions of proteasome inhibition. Statistical analysis was performed with one-way ANOVA and Bonferroni's post hoc test (*values at different time points versus value at 0 hr*, $*P < 0.05$, $***P < 0.001$, $n=3$). **(A5-C5)** Ratio of the relative TDP-43 WT levels with PABPN1 vs. GFP co-expression. Graphs represent mean and SEM.

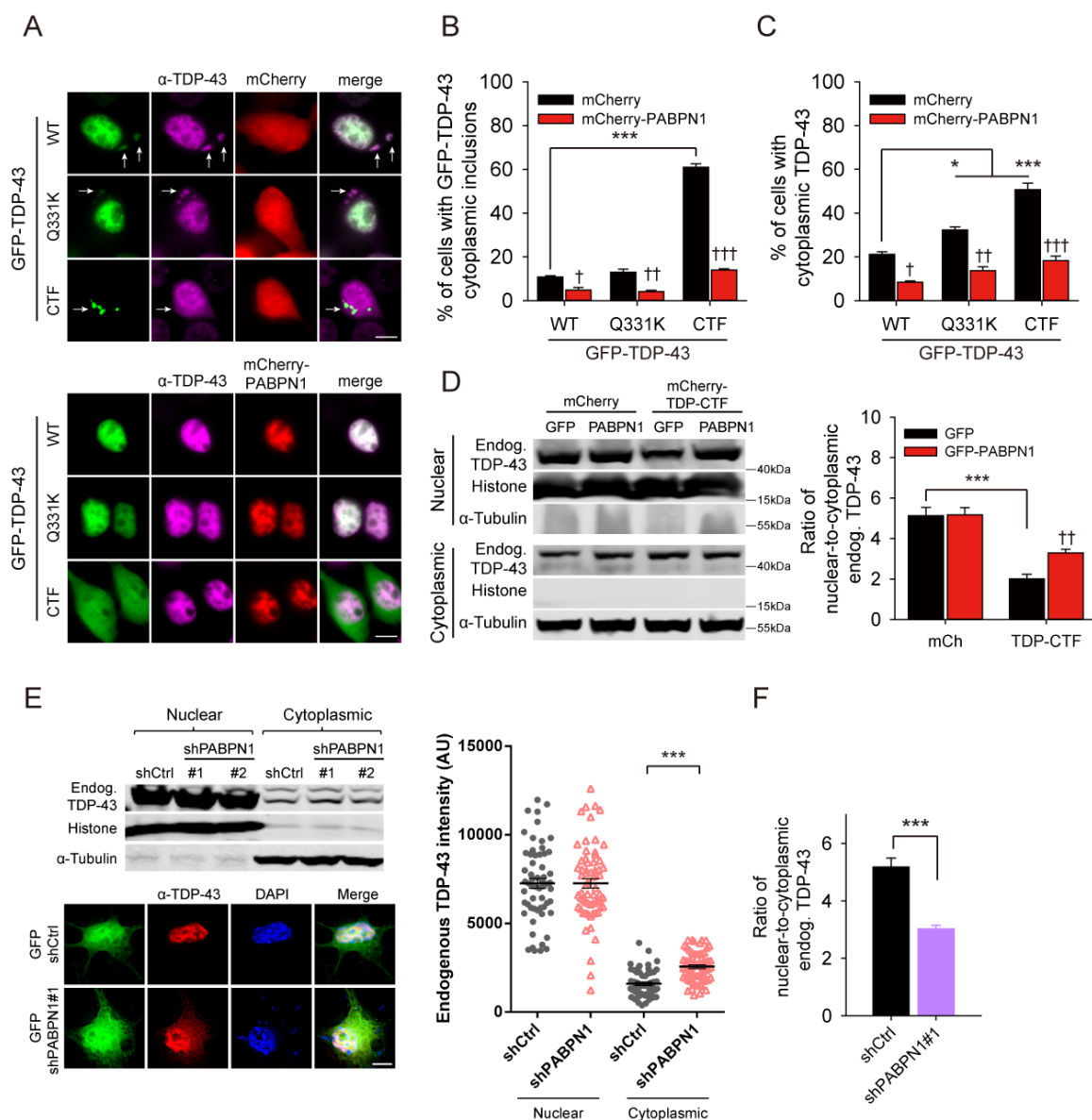


Figure 4-7 | PABPN1 expression restores the nuclear localization of endogenous TDP-43.

(A) Representative fluorescence microscopy images of N2a cells co-expressing GFP-tagged TDP-43^{WT}, TDP-43^{Q331K} or TDP-CTF, with either mCherry (top panels) or mCherry-PABPN1 (bottom panels). Full-length TDP-43 was stained with an antibody against an N-terminal region of TDP-43 (magenta). Mislocalized cytoplasmic TDP-43 is marked (white arrows). Scale bar: 10 μ m. (B-C) Quantification of cells with GFP-TDP-43

cytoplasmic inclusions (B) and diffuse cytoplasmic TDP-43 staining (C). PABPN1 co-expression reduced the percentage of cells exhibiting cytoplasmic mislocalization and inclusions of full-length TDP-43. **(D)** Quantification of the nuclear-to-cytoplasmic ratio of endogenous TDP-43 in response to TDP-CTF co-expression with mCherry or mCherry-PABPN1. PABPN1 expression partially restored nuclear localization of endogenous TDP-43. Statistical analysis is performed with two-way ANOVA and Bonferroni's post hoc test ($*P < 0.05$, $***P < 0.001$; $†P < 0.05$, $††P < 0.01$, $†††P < 0.001$, *PABPN1 versus GFP or mCherry*, $n=3$). **(E-F)** Representative western blots and fluorescence microscopy images of endogenous TDP-43 in N2a cells (top panels) and primary motor neurons (bottom panels) after PABPN1 knockdown. Quantification of fluorescent intensity (AU) of nuclear and cytoplasmic TDP-43 (E) and nuclear-to-cytoplasmic ratio of endogenous TDP-43 in response to PABPN1 knockdown (F). Statistical analysis is performed with Student's *t*-test (*three independent experiments, shCtrl versus shPABPN1#1*, $***P < 0.001$. *shCtrl* ($n=59$), *shPABPN1* ($n=65$)). Graphs represent mean and SEM.

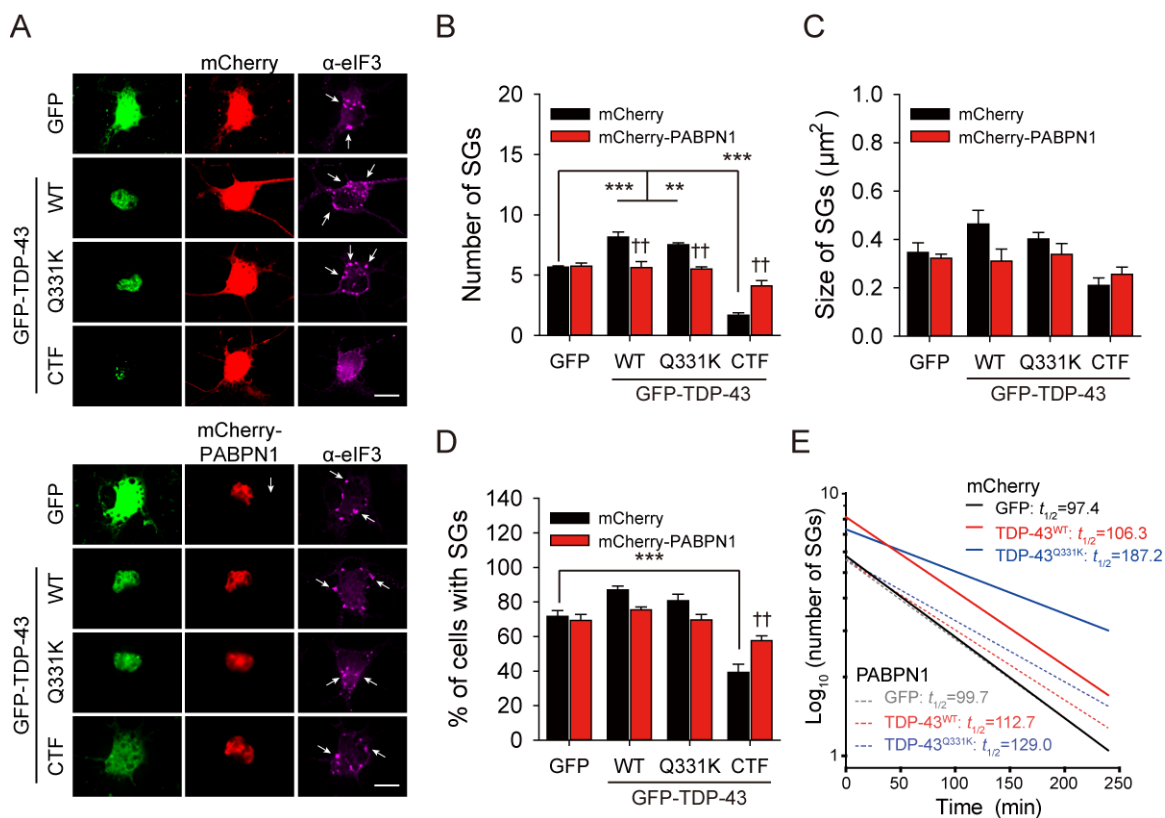


Figure 4-8 | PABPN1 expression rescues SG formation defects caused by TDP-43 pathology.

(A) Representative fluorescence microscopy images of eIF3-positive stress granules (SGs) of primary motor neurons after exposure to 0.5mM sodium arsenite for 24 hrs. Cells were co-transfected with GFP or GFP-tagged TDP-43^{WT}, TDP-43^{Q331K} or TDP-CTF with mCherry (top panels) or mCherry-PABPN1 (bottom panels). SGs were stained with an antibody against eIF3 η (magenta). PABPN1 rescued TDP-CTF expression-mediated reduction of SG formation (white arrows). Scale bar: 10 μm . (B-D) Quantification of SG numbers (B) and sizes (C) and the percentage of cells with SGs (D). PABPN1 expression restored normal SG formation. Statistical analysis was performed with two-way ANOVA and Bonferroni's post hoc test (*five independent experiments*, * $P < 0.05$, ** $P < 0.01$, *** $P < 0.001$; † $P < 0.05$, †† $P < 0.01$, ††† $P < 0.001$, mCherry-

PABPN1 versus *mCherry*, *mCherry*: *GFP* ($n=65$), *WT* ($n=86$), *Q331K* ($n=76$), *CTF* ($n=74$); *mCherry-PABPN1*: *GFP* ($n=60$), *WT* ($n=69$), *Q331K* ($n=62$), *CTF* ($n=73$)).

Graphs represent mean and SEM. **(E)** Quantification of averaged half-time ($t_{1/2}$) of SG-disassembly in terms of SG numbers after the removal of oxidative stress (*R0*: *GFP* ($n=47$), *WT* ($n=49$), *Q331K* ($n=57$); *R2*: *GFP* ($n=38$), *WT* ($n=51$), *Q331K* ($n=51$); *R4*: *GFP* ($n=48$), *WT* ($n=51$), *Q331K* ($n=46$)). *PABPN1* expression rescued TDP-43-specific SG disassembly defects.

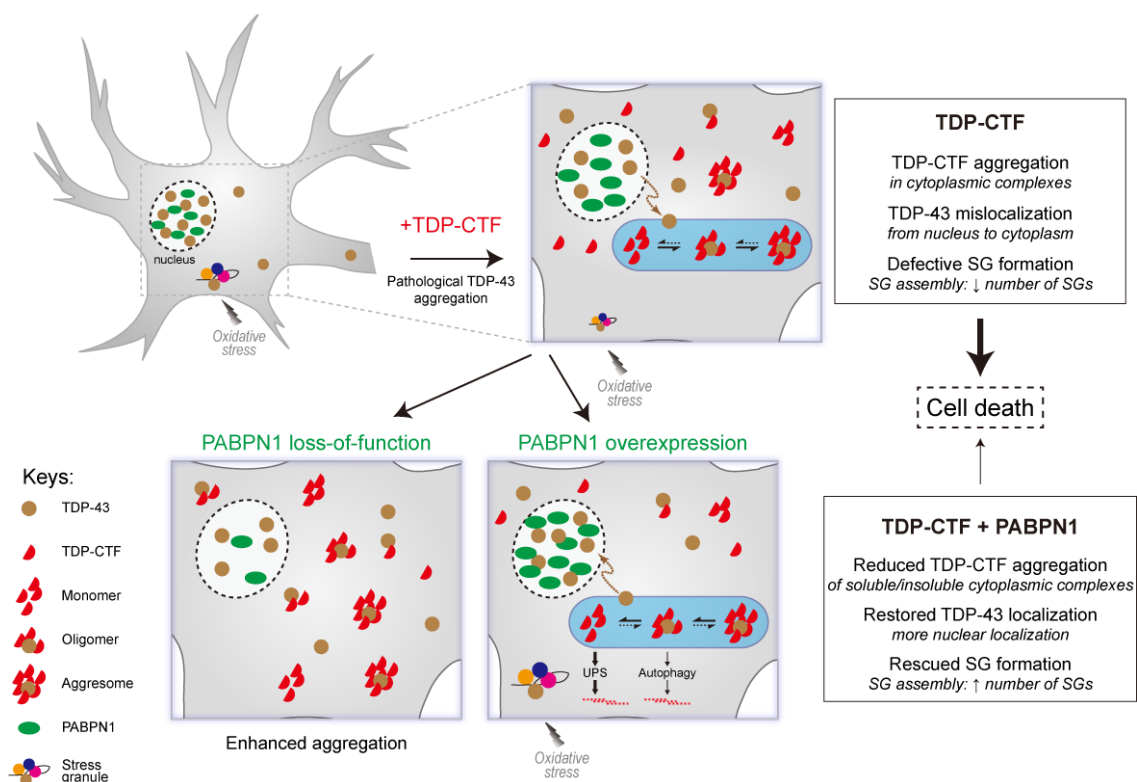
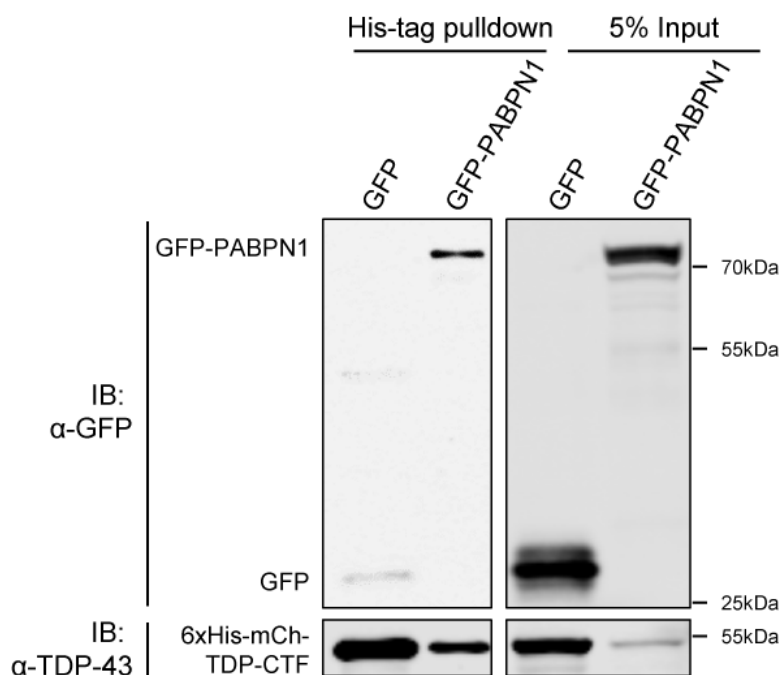


Figure 4-9 | Model of PABPN1's effects on TDP-43 proteinopathy phenotypes.

(Top): In healthy neurons, TDP-43 (brown) and PABPN1 (green) are primarily localized to the nucleus and TDP-43 is incorporated into SG under conditions of oxidative stress. Expression of pathological TDP-CTF (red) forms cytoplasmic aggregates, leads to mislocalization of full-length TDP-43 into the cytoplasm and compromises SG formation in response to oxidative stress. **(Bottom left):** PABPN1 loss-of-function exacerbates the accumulation of TDP-CTF and endogenous TDP-43 in the cytoplasm. **(Bottom right):** PABPN1 overexpression selectively promotes the degradation of TDP-CTF protein mainly via the UPS by driving the equilibrium towards soluble species and preventing the aggregation. The interaction of PABPN1 with TDP-43 directly or indirectly restores normal solubility and localization of TDP-43, and rescues SG assembly and disassembly

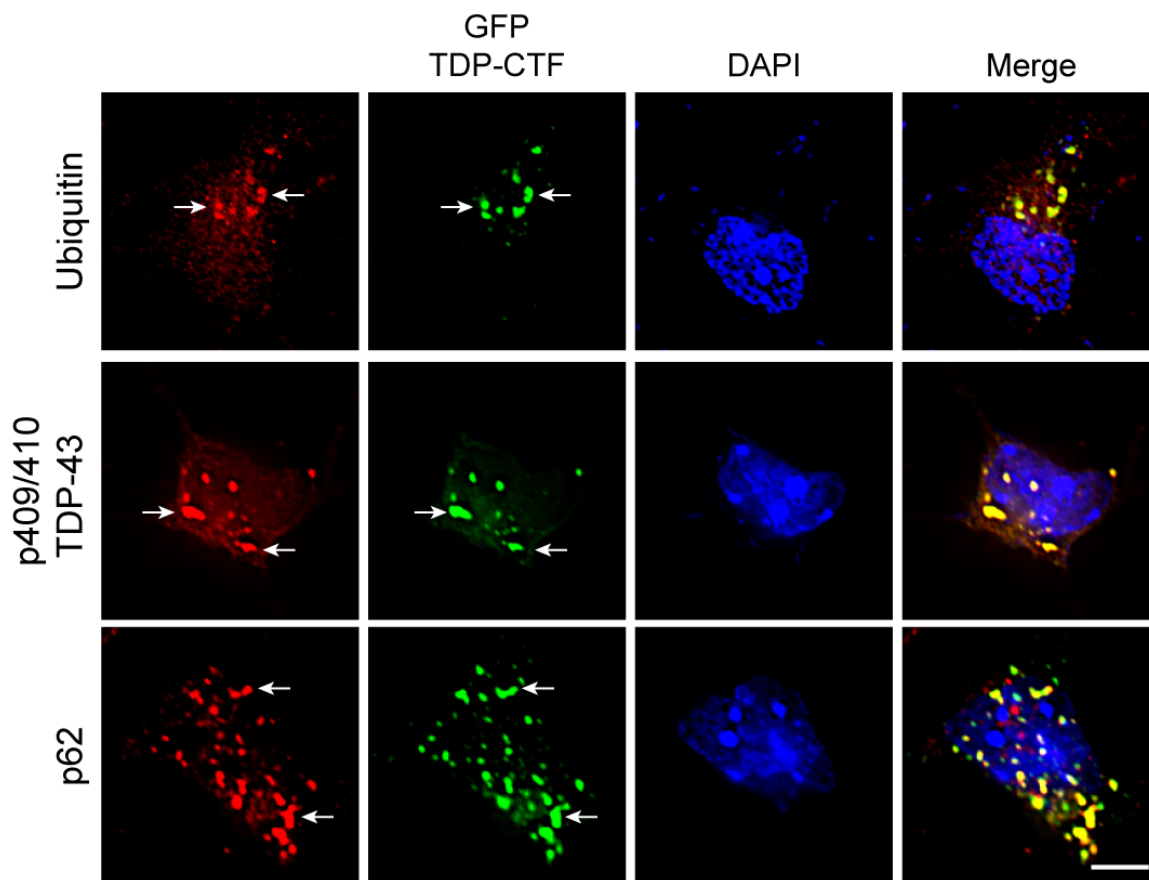
defects under stress conditions. Taken together, these actions lead to the suppression of TDP-43-induced cell death.

4.6 Supplementary Figures



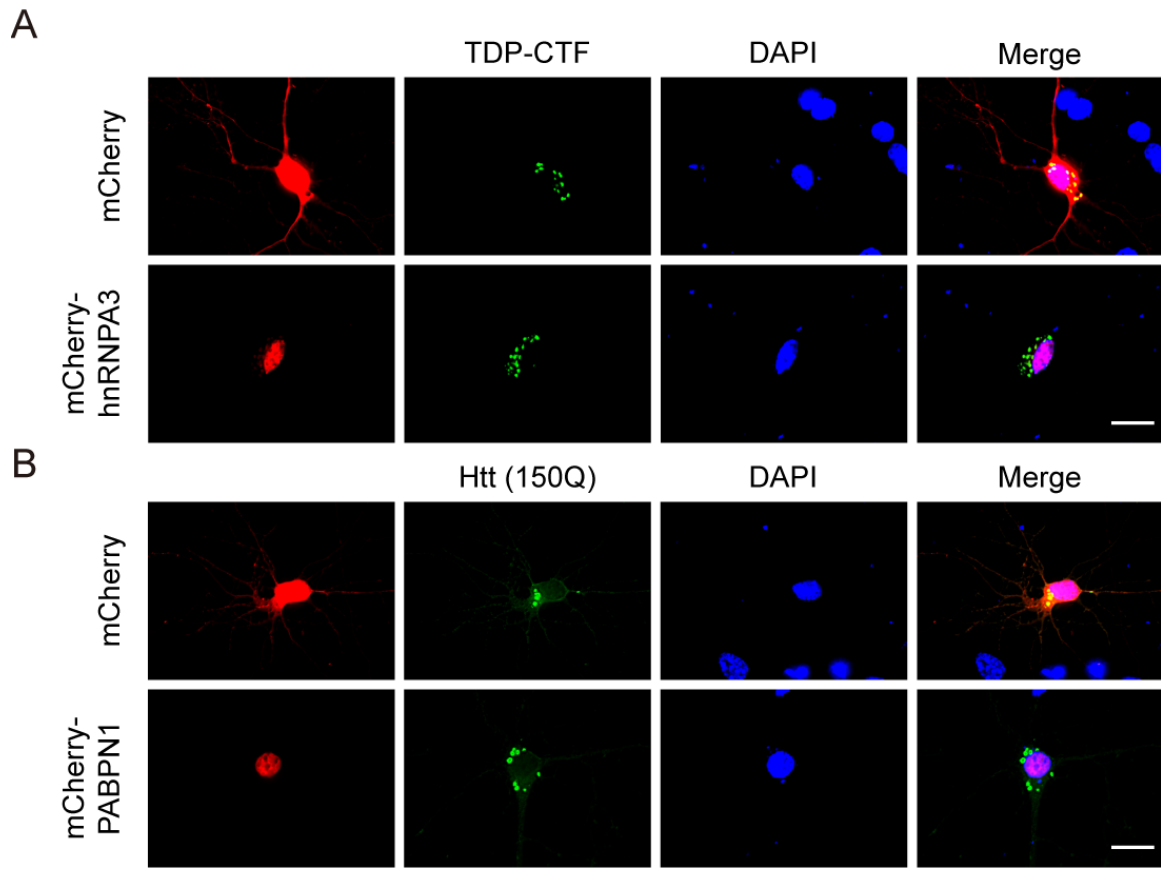
Supplementary Figure 4-1 | TDP-CTF interacts with PABPN1.

Left panel: Western blot analysis of 6xHis-tag pulldown assay from N2a cells co-expressing 6xHis-tagged mCherry-TDP-CTF and GFP or GFP-tagged PABPN1 shows specific association of TDP-CTF with PABPN1 (top) despite reduced TDP-CTF levels (bottom). Right panel: Western blot analysis of cell lysates (Input).



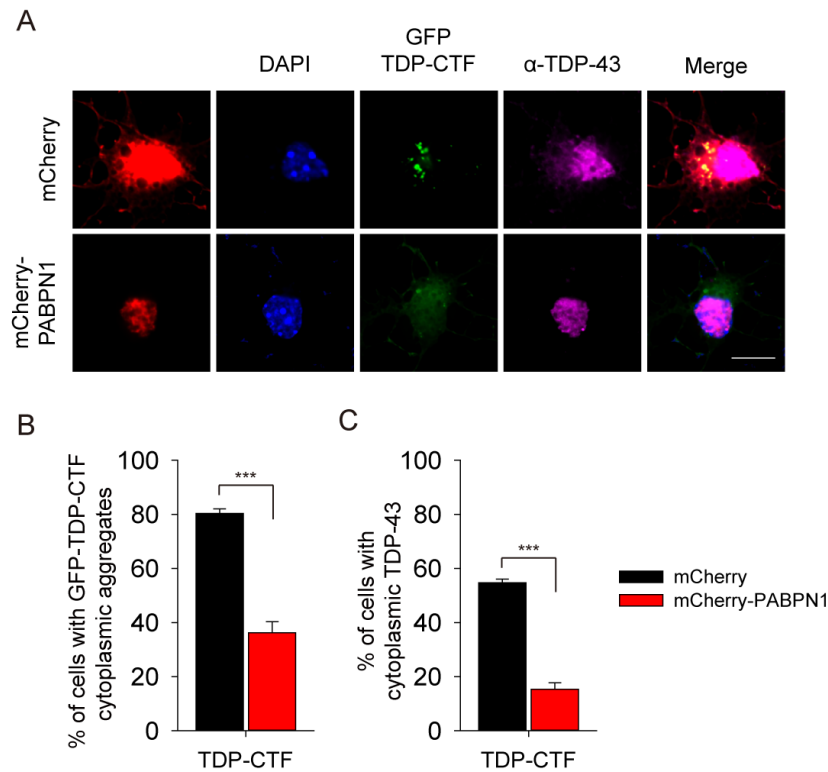
Supplementary Figure 4-2 | Expression of GFP-TDP-CTF induces the formation of cytoplasmic aggregates with the hallmarks of pathogenic TDP-43 inclusions in motor neurons.

Representative images of primary motor neurons transfected with GFP-tagged TDP-CTF show cytoplasmic aggregates that stained positive for ubiquitin, phosphorylated TDP-43 (Ser409/410), and SQSTM1/p62.



Supplementary Figure 4-3 | PABPN1 but not hnRNPA3 specifically reduces pathological TDP-CTF and does not affect aggregation of poly-glutamine repeat containing huntingtin.

Fluorescence imaging of primary cortical neurons expressing GFP-TDP-CTF. **(A)** Co-expression of the mCherry-tagged TDP-43-interacting protein hnRNPA3 had no effect on TDP-CTF aggregation. **(B)** PABPN1 overexpression did not reduce aggregation of the HA-tagged N-terminal fragment of the human huntingtin protein with a 150aa poly-glutamine repeat expansion (Htt-150Q). Scale bar: 20 μ m.



Supplementary Figure 4-4 | PABPN1 restores localization of endogenous TDP-43 in primary motor neurons.

(A) Representative fluorescence microscopy images of primary motor neurons co-expressing GFP-TDP-CTF together with mCherry (top panels) or mCherry-PABPN1 (bottom panels). Full-length endogenous TDP-43 is stained with an antibody against an N-terminal region of TDP-43 (magenta). Scale bar: 10 μ m. **(B-C)** Quantification of cells with GFP-TDP-CTF cytoplasmic aggregates (B) and cytoplasmic accumulation of endogenous TDP-43 (C). PABPN1 co-expression strongly reduces the percentage of motor neurons with TDP-CTF aggregates and mislocalized endogenous TDP-43. Statistical analysis was performed with Student's *t*-test ($***P < 0.001$, *mCherry-PABPN1* versus *mCherry*, $n=3$). Graphs represent mean and SEM.

4.7 Table

Table 4-1. TDP-43 and PABPN1 interact in yeast two-hybrid assays.

Full-length human TDP-43 (hTDP-43) and PABPN1 (hPABPN1) were cloned into yeast-two-hybrid vectors and co-transformed into a reporter strain. Columns represent empty pGADT7 prey vector and hPABPN1 and hTDP-43 cloned into pGADT7, respectively; rows represent empty pGBKT7 bait vector and hPABPN1 and hTDP-43 cloned into pGBKT7, respectively. Strength of interaction was measured by scoring growth on selective media (SD/–Ade/–His/–Leu/–Trp) from weak (+) to strong (+++). Both TDP-43 and PABPN1 interact with themselves (indicating dimerization) but also with each other.

		Activation domain		
		pGADT7 <i>vector</i>	hPABPN1	hTDP-43
Binding domain	pGBKT7 <i>vector</i>	–	–	–
	hPABPN1	–	++	+
	hTDP-43	–	+	+++

4.8 Supplementary Table

Supplementary Table 4-1. List of primary antibodies used in the present study.

Antigen	Host / Type (clone)	Source	Dilution
TDP-43 (recognizes N-terminus)	Rabbit / polyclonal	Proteintech Group # 10782-2-AP	IF: 1:500 WB: 1:4000
TDP-43 (recognizes C-terminus)	Rabbit / polyclonal	Proteintech Group # 12892-1-AP	IF: 1:500 WB: 1:4000
phospho(409/410)- TDP43	Rabbit / polyclonal	Proteintech Group # 22309-1-AP	WB: 1:2000
PABPN1	Rabbit / monoclonal (EP3000Y)	Epitomics # 2428-1	IF: 1:500 WB: 1:2000
PABP	Rabbit / polyclonal	Abcam # ab21060	WB: 1:2000
Ubiquitin	Mouse / monoclonal	Invitrogen # 13-1600	IF: 1:300 WB: 1:2000
SQSTM1/p62	Mouse / monoclonal	Abcam # ab56416	IF: 1:1000
eIF3 η	Goat / polyclonal (N-20)	Santa Cruz Biotechnology # sc-16377	IF: 1:200
GFP	Mouse / monoclonal (JL-8)	Clontech # 8371-2	WB: 1:2000
HA	Mouse / monoclonal (HA.11)	Covance # MMS-101P	IF: 1:500
Histone	Rabbit / polyclonal (H3.3)	Abcam # ab97968	WB: 1:2000
α -Tubulin	Mouse / monoclonal	Sigma-Aldrich # T6074	WB: 1:10000
MAP2	Mouse / monoclonal	Sigma-Aldrich # M1406	IF: 1:500

Chapter 5

Conclusions and Future Directions

5.1 Summary

ALS is a rapidly progressive and fatal degenerative disease with an average survival time of 3–5 years¹⁷. ALS was traditionally seen as a pure motor neuron disease, while compelling clinical, genetic and pathological evidence supports that ALS is not a single entity of motor neuron disease, but rather a heterogeneous disorder with large phenotypic variability including an involvement of a wide range of cognitive impairments^{2,16,49,54,55,58,74}. About half of individuals with ALS exhibit different degrees of cognitive impairments and ~20% of the group are clinically diagnosed as FTD, the second most common cause of dementia^{55,58}. The aggregation of ubiquitinated and hyperphosphorylated TDP-43 in the CNS tissue has been identified as a hallmark of histopathology in the vast majority of ALS and about half of all FTD cases^{13,14}. The identification of several causative mutations in *TARDBP* gene in both diseases^{7,8,10-12}, established a causative role for TDP-43 pathology in the disease process and suggested that ALS and FTD could be parts of a disease continuum. Moreover, TDP-43 pathology was further discovered in AD, PD, HD and chronic traumatic encephalopathy (CTE)³⁶. For these conditions, the extent of the contribution of TDP-43 proteinopathy to the disease phenotype is currently not known. TDP-43 inclusion pathology may reflect an exaggeration of normal accumulation of predominantly nuclear TDP-43 into cytoplasmic RNA granules under stress conditions through its intrinsically disordered prion-like domain^{15,117}. Taken together, these data suggest that understanding how TDP-43 protein aggregation contributes to the disease phenotype may benefit the majority of individuals with ALS and FTD, and perhaps a large number of other patients with TDP-43 proteinopathies.

A G₄C₂ HRE in the *C9orf72* gene locus has been identified as the most common genetic cause of ALS^{5,6}. Albeit aberrant accumulation of RNA foci and DPRs have been considered as potential causes of *C9orf72* ALS⁴⁶, ubiquitinated TDP-43 aggregates are also frequently observed in those affected motor neurons^{44,45}. Notably, three papers published at the same time showed that a consequence of the G₄C₂ repeat expansion was the appearance of deficits in nucleocytoplasmic transport, and that several Nups and TFs acted as disease modifiers in yeast and *Drosophila* models of *C9orf72* ALS¹¹⁹⁻¹²¹. These data suggested that compromised nucleocytoplasmic transport could interfere with nuclear import of protein and cause cytoplasmic accumulation of TDP-43. The discovery of ALS-linked mutations in genes involved in nuclear transport, *Gle1* and *VAPB*, further strengthen the hypothesis and reveal a novel mechanism of neurodegeneration^{159,194}. These findings suggested that cytoplasmic mislocalization of TDP-43 may be a consequence of nucleocytoplasmic transport defects. However, these data do not fully explain why TDP-43 proteinopathy is present in the vast majority of ALS/FTD cases without obvious genetic cause.

Deciphering the components of TDP-43 aggregates can provide better insights into disease pathogenesis. In an effort to characterize molecular pathways and cellular mechanisms that regulate TDP-43 pathology, we have used expression of a patient-derived TDP-CTF to mimic the formation of ubiquitinated and hyper-phosphorylated TDP-43 aggregates that show the hallmark of aggregates found in patient tissue^{30,125,132}. The composition of TDP-43 inclusions was largely unknown until now, as they are by definition detergent-insoluble and not accessible to commonly used isolation methods such as co-immunoprecipitation. Therefore, the purpose of this project was to establish a

new method for characterizing the interactome of aggregated TDP-43 and investigating the molecular pathways underlying TDP-43 pathology, and to identify novel candidates for the suppression of TDP-43 toxicity and aggregates.

In Chapter 3, I have demonstrated that BioID can be used to reliably label the protein components of insoluble TDP-43 aggregates, which are highly associated with the pathogenesis of ALS/FTD. Proteomic analysis revealed an enrichment of proteins involved in RNA metabolism, transcription and intracellular transport. Notably, many known proteins in the nucleocytoplasmic transport pathway, Nups and TFs, were among the major interactors of aggregated TDP-CTF. We validated that TDP-CTF triggered the cytoplasmic aggregation of most FG-Nups, scaffold Nups and nuclear export factors, and a discontinuous distribution of transmembrane Nups (**Fig. 3-2e**, and **Supplementary Fig. 3-4, 3-5**). Intriguingly, mutant TDP-43^{Q331K} also induced the formation of cytoplasmic aggregates in a small subset of Nups. Super-resolution imaging showed that NPCs had an uneven and clustered distribution in the NM of cells expressing TDP-CTF. The cytoplasmic aggregation of human Nups containing PrLDs was mediated by this domain. Cells expressing aggregated and mutant form of TDP-43 exhibited abnormalities in the nuclear lamina with internal invagination, which was correlated with the elevated levels of DNA damage but independent of the change in TDP-43 levels. Furthermore, aggregated and mutant form of TDP-43 resulted in functional deficits in nuclear protein import, which was not associated with apoptosis, as well as nuclear RNA export defects, and a reduction of protein synthesis. These defects were correlated with the increased levels of cytoplasmic TDP-43. The elimination of TDP-43 pathology by overexpression of PABPN1 restored normal morphological patterns of lamin and Nups staining, and

normal functions of nuclear transport of protein and RNA. We also identified novel genetic interaction between TDP-43 and *Nup* genes. Mutations in five of these genes, serving as genetic modifiers, rescued the deficits in eye morphology and motor behavior in *Drosophila* expressing wild-type and mutant TDP-43. Immunohistochemical staining of postmortem motor and frontal cortices from sALS cases, and those caused by genetic mutations in *TARDBP* (TDP-ALS) or *C9orf72* (C9-ALS) revealed Nup205-positive cytoplasmic inclusions and widespread loss of Nup205 immunoreactivity, and occasional abnormalities in lamin B.

In Chapter 4, I have described our discovery of PABPN1 as a novel interaction partner of TDP-43, which also acted as a protective modifier of TDP-43 toxicity with unique properties. We first performed a yeast-two-hybrid screen to identify proteins that interacted with TDP-43, and further tested their effect on modulating pathological TDP-43 aggregates. PABPN1 was the only protein discovered in this screen that showed promise as a suppressor of TDP-43 toxicity. In the co-immunoprecipitation experiment, we confirmed the interaction of TDP-43 and TDP-CTF with PABPN1 *in vivo* and *in vitro*. Overexpression of PABPN1 significantly reduced neurotoxicity mediated by aggregated or mutant form of TDP-43, whereas knockdown of PABPN1 enhanced the toxicity in mouse primary neurons and *Drosophila* models of TDP-43 proteinopathy. PABPN1 promoted selective clearance of aggregated and mutant forms of TDP-43 but did not affect the levels of endogenous TDP-43, whereas the loss of PABPN1 caused an accumulation of TDP-CTF. Quantification of time-lapse live-cell imaging of TDP-CTF levels revealed a gradual reduction following the doxycycline-induced expression of PABPN1. The enhanced protein degradation by PABPN1 results from faster protein

turnover of pathological TDP-43 through the ubiquitin proteasome system but not autophagy (**Fig. 4-3, 4-5 & 4-6**). The presence of TDP-CTF enhanced the redistribution and cytoplasmic accumulation of endogenous TDP-43, whereas PABPN1 co-expression restored the nuclear levels of TDP-43. Moreover, mutant TDP-43 led to an increased number of SGs. TDP-CTF expression reduced the number of normal SGs, which may be caused by the sequestration of essential SG-associated proteins to TDP-CTF aggregates. Mutant TDP-43^{Q331K} with increased aggregation propensity also delayed the disassembly of SG after stress was removed. PABPN1 overexpression could rescue the TDP-43-induced dysregulation of SG dynamics.

5.2 Remaining Questions and Future Directions

5.2.1 Mapping PABPN1 protein functional domains

We have previously reported the interaction of TDP-43 and TDP-CTF with full-length PABPN1 in N2a cells. The full deletion of the C-terminal PY-NLS domain of PABPN1 dramatically reduced their protein-protein interaction.

For the purpose of mapping the minimum domain of PABPN1 that is both necessary and sufficient for protein interaction with TDP-43, we have generated a series of truncation mutants of PABPN1, including Δ NLS18, Δ NLS50, aa 1-245, aa 1-172, aa 172-306 and aa 245-306 (**Fig. 5-1A, B**). Immunoprecipitation experiments showed that the last C-terminal region (aa 245-306) of PABPN1 was the critical domain for protein interaction with TDP-43 (**Fig. 5-1C**). Treatment with RNase did not abolish the interaction between TDP-43 and PABPN1^{FL}, PABPN1 ^{Δ NLS18} or PABPN1²⁴⁵⁻³⁰⁶, suggesting that the protein-protein interaction is independent of RNA-binding. A future

experiment is to conduct co-immunoprecipitation of TDP-43 with PABPN1^{ΔNLS50} fused with a canonical SV40 NLS (PABPN1^{ΔNLS50+SV40}) to confirm the aa 245-306 sequence of PABPN1 as the primary interaction domain with TDP-43.

5.2.2 PABPN1 rescues TDP-43 toxicity mediated by gain-of-function but not loss-of-function

We have shown that the overexpression of PABPN1 efficiently suppressed TDP-43 toxicity caused by TDP-CTF or TDP-43 mutants, but the knockdown of PABPN1 enhanced the toxicity.

We further investigate whether the suppression of TDP-43 toxicity by PABPN1 is mediated by its general anti-apoptotic function²⁸¹. As TDP-43 is an essential protein for transcription regulation and RNA metabolism, the reduction of TDP-43 levels is early embryonic lethal in mouse development and cytotoxic, and also triggers motor neuron phenotypes in transgenic animal models of ALS^{127,234}. We showed that knockdown of TDP-43 levels indeed increased the rate of cell death in primary cortical neurons. The co-expression of PABPN1 did not rescue the survival, suggesting the PABPN1's suppression effect may only target the toxic gain-of-function in TDP-43 pathology rather than the loss-of-function (**Fig. 5-2A**). However, PABPN1 expression is likely to prevent nuclear depletion of TDP-43 caused by trapping of the protein in cytoplasmic aggregates. To further characterize the toxicity of TDP-CTF and PABPN1 after long-term expression, cortical neurons were transfected with GFP or GFP-PABPN1 and mCherry or mCherry-TDP-CTF. The survival of neurons was monitored by automated microscopy for a total of 100 hrs. Kaplan-Meier survival analysis revealed that TDP-CTF expression

significantly increased cumulative risk of death, whereas PABPN1 expression did not. The co-expression of PABPN1 could suppress the increased cumulative risk of death caused by TDP-CTF (**Fig. 5-2B**).

5.2.3 Effects of PABPN1 truncation mutants on TDP-CTF levels

We have shown that overexpression of PABPN1 was a potent suppressor of TDP-43 aggregation, whereas knockdown of PABPN1 enhanced the accumulation.

We further investigate whether short peptides derived from PABPN1 can be developed for reducing the burden of pathological TDP-43. Identifying peptides or peptidomimetic based upon PABPN1 could help us to better understand the mechanism behind this activity and may be more suitable for a potential future use in targeting pathologic TDP-43. We co-transfected the cortical neurons with GFP or GFP-tagged PABPN1 and mCherry-tagged TDP-CTF. Our data showed that the C-terminal 60aa fragment, a crucial domain for the biological interaction of PABPN1 with TDP-43, converted TDP-CTF from an aggregated state to a diffuse distribution (**Fig. 5-3A**). However, the expression of the 60aa peptide did not reduce TDP-CTF protein levels (**Fig. 5-3B**). Thus, given PABPN1's effect on TDP-CTF protein localization and degradation, the fusion of specific degradation signals to PABPN1-derived peptides may direct the pathological TDP-43 to the protein degradation machinery.

5.2.4 Effects of PABPN1 on the degradation of aggregate-prone proteins

We confirmed that overexpression of PABPN1 promotes the clearance of TDP-CTF aggregates and TDP-43 mutants (**Fig. 4-3**)¹²⁵, whereas PABPN1-derived peptides failed to reduce TDP-CTF protein levels.

Next, we tested whether PABPN1 where the C-terminal NLS has been replaced with the SV4-derived NLS (PABPN1^{ΔNLS50+SV40}) and an OPMD-associated N-terminal poly-alanine expansion mutant of PABPN1 (PABPN1^{Ala17}) affect the protein level of TDP-CTF in N2a cells. We found that the expression of PABPN1^{ΔNLS50+SV40} or PABPN1^{Ala17} increased the soluble and insoluble protein levels of TDP-CTF, suggesting that only fully functional PABPN1 possesses the ability to promote TDP-CTF degradation (**Fig. 5-3A**). We further showed that TDP-CTF degradation was dependent on the expression levels of full-length PABPN1. When the plasmid expression vector for PABPN1 was increased to 2-fold, it greatly promoted the clearance of TDP-CTF as compared to the regular expression level, whereas when the expression level was reduced, it increased the levels of TDP-CTF in the soluble and insoluble fraction (**Fig. 5-4A**). The data may explain the detection of TDP-43 inclusions in the muscle tissue of OPMD patients. Potentially, the polyalanine expansion mutation of PABPN1 may cause a dominant-negative effect and lead to a reduction of normal PABPN1 function^{237,238}.

To test whether PABPN1 has a global effect on promoting the degradation of disease-associated aggregation-prone proteins, we co-expressed PABPN1 with wild-type and ALS-associated mutant FUS lacking its C-terminal NLS (Δexon15), α-synuclein, tau as well as C9orf72-associated DPRs, GA and GR with 80 repeats. Western blotting analysis showed that PABPN1 overexpression led to significant reduction of wild-type

and mutant FUS and tau in the soluble and insoluble fraction (**Fig. 5-4B**), whereas PABPN1 had a mild effect or no effect on α -synuclein, (GA)₈₀ and (GR)₈₀ (**Fig. 5-4C**). This may be because the absence of lysine residues in the poly-GA and GR prevents the linking of ubiquitination signals for degradation, although poly-GA has been shown to co-localize with ubiquitin and p62²⁸².

5.2.5 Effects of PABPN1 on ubiquitin-proteasomal degradation

Evidence that aggregated TDP-43 is labeled with K48- and K63-linked poly-ubiquitin chains and co-localized with p62 suggests the involvement of (1) the UPS for the removal of soluble monomeric TDP-43 and (2) autophagy for clearance of soluble oligomeric proteins and insoluble large aggregates²²⁹. While PABPN1 is known to regulate poly(A) tail length, mRNA export, poly(A) cleavage site selection, and long non-coding RNAs (lncRNA)²⁸³, little is known about its effect on the UPS. We have used cycloheximide chase assays coupling with the autophagy inhibitor bafilomycin A1 and proteasome inhibitor MG132, to determine the half-life ($t_{1/2}$) of TDP-CTF and found that PABPN1 co-expression reduced the $t_{1/2}$ from 11.9 hrs to 6.8 hrs, whereas treatment of the cells with MG132 abolished this effect.

First, to confirm the ubiquitination of TDP-CTF, a triple-transfection of poly-histidine-tagged TDP-CTF, HA-tagged ubiquitin and various GFP-tagged PABPN1 constructs was performed in N2a cells. 6His-TDP-CTF was purified from the cell lysates via Ni-NTA resin. The input and pulldown samples were subjected to western blot analysis to monitor the levels of monoubiquitin and ubiquitinated substrate. The input showed a change in TDP-CTF protein levels in parallel with ubiquitin levels. Histidine

pulldown samples demonstrated the ubiquitination of TDP-CTF. PABPN1 overexpression led to the reduction of TDP-CTF and ubiquitinated substrate levels, while PABPN1^{ΔNLS50} increased both levels, suggesting that PABPN1 indeed promotes the degradation of ubiquitinated TDP-CTF in the cultured cells (**Fig. 5-5A**).

Ubiquitin can be conjugated to a protein as a monomer or a poly-ubiquitin chain. Poly-ubiquitin chains vary on the basis of linkages through these seven lysine residues of ubiquitin (i.e. K6, K11, K27, K29, K33, K48 and K63) or Met²⁸⁴. Linkage types determine the fate for the protein. K48 linkage is a canonical signal for proteasomal degradation. K11 can also serve as a signal for proteasomal degradation, particularly on cell cycle regulatory proteins²⁸⁵. The K63 linkage has proteasome-independent functions and can target substrates for autophagic degradation²⁸⁶. In the follow-up experiment, N2a cells were co-transfected with histidine-tagged TDP-CTF and different HA-tagged ubiquitin mutants that contain only a single lysine, limiting poly-ubiquitin linkage to one type. Histidine-pulldown data demonstrated that TDP-CTF contained various poly-ubiquitination chains. Except for the canonical K48 linkage, K11, K27, K29 and K63 linkages were also detected in the TDP-CTF aggregates (**Fig. 5-5B**).

Ubiquitin levels need to be tightly regulated. Both the excess or inadequate ubiquitin levels can contribute to neurological diseases²⁸⁷. The involvement of K11 and K48 linkages are the most common regulatory signals for protein homeostasis including ubiquitin itself. To maintain ubiquitin homeostasis, K11 and K48 linked ubiquitin is added onto excess or damaged ubiquitin to target it for proteasomal degradation, whereas a balance between deubiquitinating enzymes and the inhibitors is another pathway to regulate ubiquitin homeostasis. Ubiquitin C-terminal hydrolase-L1 (Uch-L1) belongs to

the family of deubiquitinating enzymes responsible for hydrolyzing C-terminal esters and amides of ubiquitin to generate monomeric ubiquitin for conjugation. The protein also functions as a mono-ubiquitin stabilizer via direct protein-protein interaction. Mutations in *Uch11* gene were found in neurodegenerative diseases and may result in the accumulation of ubiquitinated proteins²⁸⁸. Additionally, ubiquitin-specific protease 14 (USP14) is one of the proteasome-associated deubiquitinating enzymes responsible for negative regulation of proteasome activity by progressively trimming a single ubiquitin from the distal end of the poly-ubiquitin chain that binds to the substrate. The depletion of USP14 enhances proteasomal activity and accelerates the turnover of ubiquitin and ubiquitinated proteins²⁸⁹.

We have shown a role for PABPN1 in protein degradation. To investigate whether PABPN1 directly regulates ubiquitin homeostasis, N2a cells were co-transfected with GFP or GFP-tagged PABPN1 and HA-tagged ubiquitin. Western blot analysis showed the significant reduction of mono- and poly-ubiquitin levels when PABPN1 was overexpressed, while MG132 inhibited the effect and caused the accumulation of ubiquitin, suggesting a role for PABPN1 in ubiquitin turnover (**Fig. 5-5C**). In addition, PABPN1 knockdown via shPABPN1 vector increased the protein levels of endogenous ubiquitin as well as exogenously expressed HA-ubiquitin (**Fig. 5-5D**). To investigate how PABPN1 affects the specific types of ubiquitin linkage, N2a cells were co-transfected with shPABPN1 vector and different HA-tagged ubiquitin mutants. We found a widespread increase in protein levels of wild-type ubiquitin and different ubiquitin linkages when PABPN1 level was reduced (**Fig. 5-5D**).

To examine whether ubiquitin modulates the solubility of TDP-CTF aggregates, we co-transfected N2a cells with mCherry-tagged TDP-CTF and different HA-tagged ubiquitin mutants and employed subcellular fractionation for soluble and insoluble fractionation. Interestingly, although different types of ubiquitin linkages did not affect levels of soluble TDP-CTF, K29 and K63 linkages significantly increased the accumulation of TDP-CTF in the insoluble fraction (**Fig. 5-5E**). Ubiquitin K63 linkage has been reported to play an important role in inclusion formation, such as SOD1 and tau²⁸⁶. A recent study also indicated that ubiquitin K27 and K29 linkages participated in the aggregate formation of PD-associated mutant LRRK2²⁹⁰. Moreover, following PABPN1 overexpression, we found a significant reduction of wide-type, and K11 and K48-linked poly-ubiquitin chains in the soluble fraction, while it increased the accumulation of K29-linked poly-ubiquitin chain in the insoluble fraction (**Fig. 5-5F**). These data suggest that TDP-CTF contains various ubiquitin linkages that act as molecular signals for protein degradation or aggregation. PABPN1 may have a non-canonical role in the regulation of ubiquitin proteasome degradation, and a change in PABPN1 protein levels affects ubiquitin homeostasis.

5.2.6 Effects of PABPN1 on proteasome activity

To investigate whether PABPN1 mediates the degradation of excess ubiquitin and ubiquitinated TDP-CTF by regulating the activity of proteasomes, we used GFP fused to a constitutively active degradation signal (Ub-G76V-GFP) as a proteasome activity reporter and co-transfected cortical neurons with mCherry or mCherry-tagged PABPN1. Ub-M-GFP as a control is not subject to proteasomal degradation. The treatment of

MG132 as a positive control led to the accumulation of Ub-G76V-GFP. Interestingly, TDP-CTF overexpression caused a similar effect as MG132, suggesting that cytoplasmic TDP-43 aggregates may inhibit proteasome function for a vicious cycle of aggregation (**Fig. 5-6A, B**). PABPN1 overexpression, on the other hand, increased the clearance of Ub-G76V-GFP, indicating that PABPN1 mediates the accelerated turnover of ubiquitinated proteins by enhancing proteasome activity (**Fig. 5-6B**). We further found a U-shaped correlation between PABPN1 and Ub-G76V-GFP levels. A medium PABPN1 expression level had a stronger effect on enhancing proteasome activity than higher expression levels, which instead interfered with proteasome function (**Fig. 5-6C**). This may be due to the aggregation property of PABPN1. The N-terminal alanine expansion in PABPN1 associates with the pathogenesis of OPMD and can induce intranuclear aggregation^{291,292}. Live-cell imaging analysis showed a decreased half-life of Ub-G76V-GFP when PABPN1 was overexpressed, confirming that PABPN1 stimulates the degradation of poly-ubiquitinated substrates by enhancing proteasome activity (**Fig. 5-6D**).

5.2.7 Future directions

PABPN1 is ubiquitously expressed in metazoan and known for the direct roles in the stimulation of polyadenylation, the regulation of RNA export and selection of alternative cleavage and polyadenylation site²⁸³. The identification of PABPN1 as a potent suppressor of TDP-43 proteinopathy provides a new target for therapeutic intervention. We have also identified that the last C-terminal 60aa as the main interaction domain of PABPN1 with TDP-43 that can promote the solubility of TDP-CTF, although it does not

reduce its overall protein levels. We will investigate whether the fusion of a classic NES with a degron, a signal for ubiquitin proteasomal degradation, to the C-terminal PABPN1-derived peptides can recognize and redirect the cytoplasmic TDP-43 aggregates to the UPS (**Fig. 5-7**). Identification of sufficiently short and biologically active peptide sequences will allow us to design peptidomimetic drugs.

Parkin is the only E3 ligase that has been reported to target TDP-43. Parkin can mediate the formation of poly-ubiquitin K48 and K63 linkages on TDP-43 and facilitate the cytoplasmic translocation and accumulation²⁹³. As a E2 conjugase and E3 ligase are both responsible for determining the ubiquitin linkages of substrates, we test and further characterize the E2 conjugases and E3 ligases that we found to be associated with TDP-CTF in our BioID experiments. Moreover, to understand how PABPN1 enhances proteasome activity, we will overexpress or knockdown PABPN1 and collect the cell lysates for quantitative mass spectrometric analysis to examine the change in the proteins involved in proteasome degradation, such as E2 conjugases, E3 ligases, deubiquitinating enzymes or proteasome subunits. The comparison of the TDP-CTF interactome and PABPN1-dependent proteome may provide the information of the overlapping proteins, which can be further used to test their effects on the protein level and solubility of TDP-CTF and ubiquitin-proteasome degradation.

5.3 Conclusions

Our results demonstrate that TDP-43 pathology itself can disrupt the nucleocytoplasmic transport of protein and RNA, and the structure of NMs and NPCs even in the absence of the *C9orf72* mutation, which has been reported to cause the nucleocytoplasmic transport

defects in a subset of ALS/FTD patients. The discovery of massive nuclear pore pathology in the brain of sporadic ALS and TDP-ALS cases suggested the nucleocytoplasmic transport defect as a common theme in the vast majority of ALS cases and potentially other TDP-43-associated diseases. In addition, we identified PABPN1 as a potent suppressor of TDP-43 toxicity and aggregate formation. Our study link the neuroprotective properties of PABPN1 to the accelerated protein turnover of pathogenic TDP-43 in an ubiquitin proteasome-dependent manner, and to the restoration of nuclear localization of TDP-43 and proper stress responses that were compromised by cytoplasmic TDP-43 aggregates. Taken together, these findings advance our understanding of the role of TDP-43 in the intracellular transport and suggest novel therapeutic strategies that are designed to halt or even reverse the progression of TDP-43 pathology.

5.4 Figures

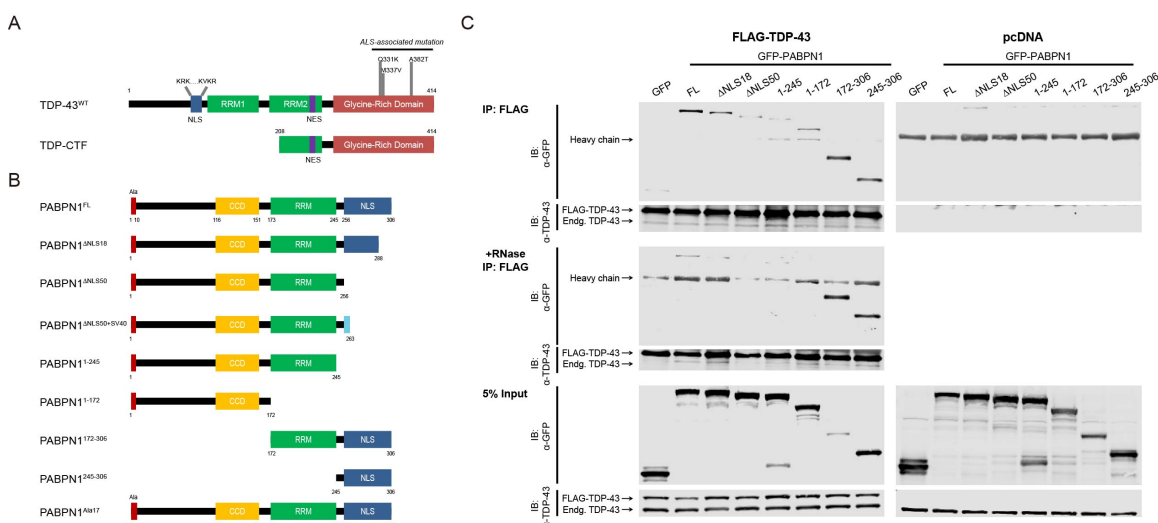


Figure 5-1 | PABPN1 associates with TDP-43 via last C-terminal 50 aa.

Schematic domain structures of human TDP-43 and PABPN1 constructs. **(A)** Human TDP-43 protein contains an NLS, two RRMs, an NES, and a glycine-rich C-terminal domain where the majority of ALS-associated mutations are located. **(B)** Human PABPN1 contains an N-terminal stretch of 10 alanines (Ala), a coiled-coil domain (CCD), one RRM domain and an NLS in the arginine-rich C-terminus. We generated different truncation mutations of PABPN1. PABPN1^{ΔNLS50} was used with an SV40 sequence, a canonical NLS (PABPN1^{ΔNLS50+SV40}). PABPN1^{Ala17} is an OPMD-associated mutant PABPN1 with an expanded 17-alanine stretch. **(C)** Upper panel: Western blot analysis of anti-FLAG immunoprecipitates from N2a cells co-expressing FLAG-tagged TDP-43 or pcDNA and GFP or GFP-tagged PABPN1 shows association of TDP-43 with PABPN1 that is independent of RNA-binding. RNase A treatment is indicated. The

presence of the PABPN1 C-terminal region (aa 245-306) is sufficient for the protein interaction with TDP-43. Bottom panel: Western blot analysis of cell lysates (Input).

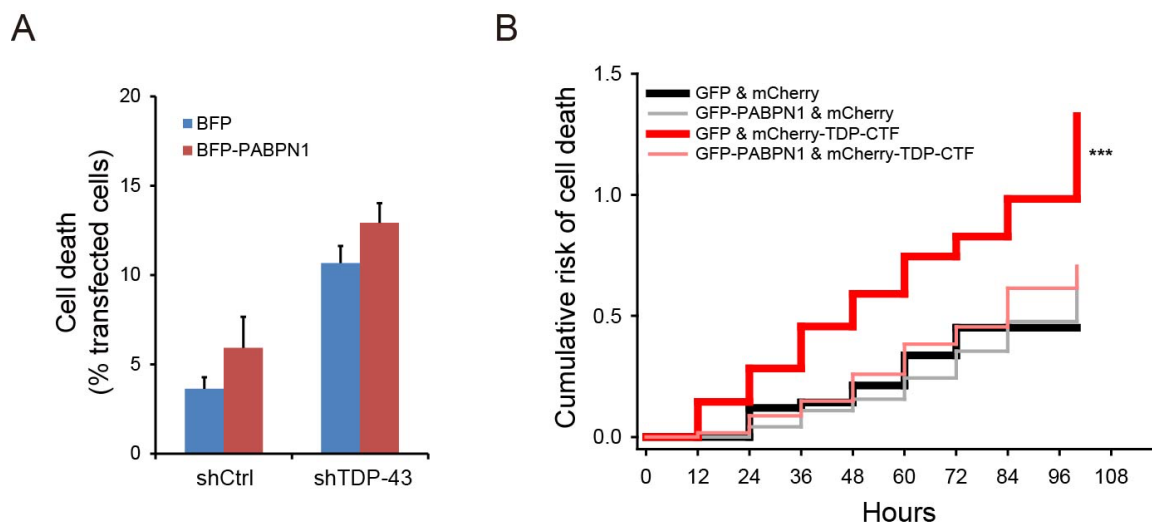


Figure 5-2 | PABPN1 modulates TDP-43 toxic gain-of-function.

(A) Quantification of TDP-43 knockdown-mediated cell death upon overexpression of PABPN1. (B) Cortical neurons were transfected with GFP or GFP-PABPN1 and mCherry or mCherry-TDP-CTF and followed by automated microscopy at 1-hr interval for total 100 hrs. Kaplan-Meier survival analysis was used to create cumulative risk of death functions for each population of transfected neurons. $***P < 0.001$. Graphs represent mean and SEM.

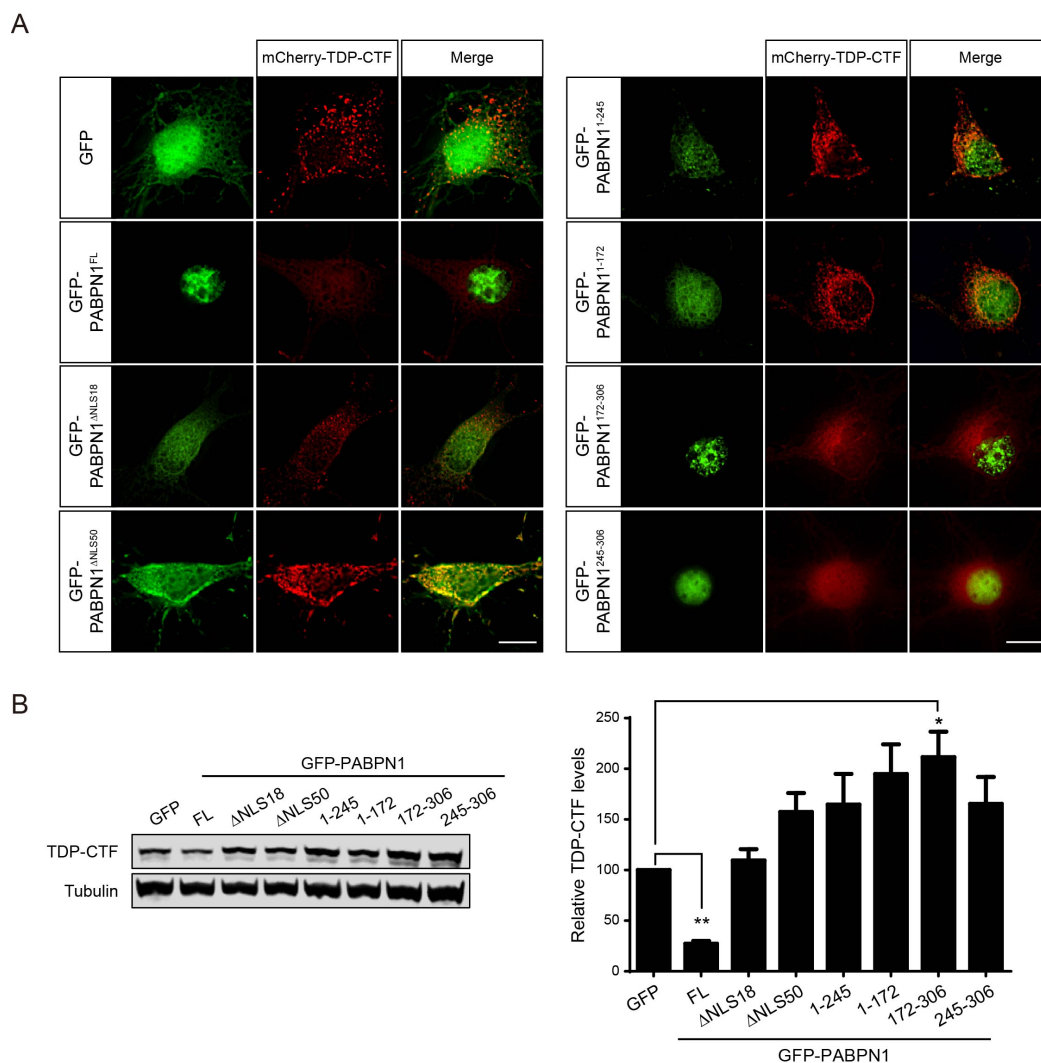


Figure 5-3 | PABPN1 truncation mutants affect TDP-CTF levels.

(A) Fluorescence microscopy analysis of TDP-CTF aggregation. Representative images of primary cortical neurons expressing mCherry-TDP-CTF (red), and truncation mutants of GFP-PABPN1 (FL, Δ NLS18, Δ NLS50, aa 1-245, aa 1-172, aa172-306 and aa 245-306) (green). **(B)** Western blot analysis and quantification of TDP-CTF protein levels in N2a cells expressing mCherry-TDP-CTF and truncation mutants of GFP-PABPN1. Statistical analysis was performed with one-way ANOVA and Bonferroni's post hoc test ($*P < 0.05$, $**P < 0.01$). Graphs represent mean and SEM.

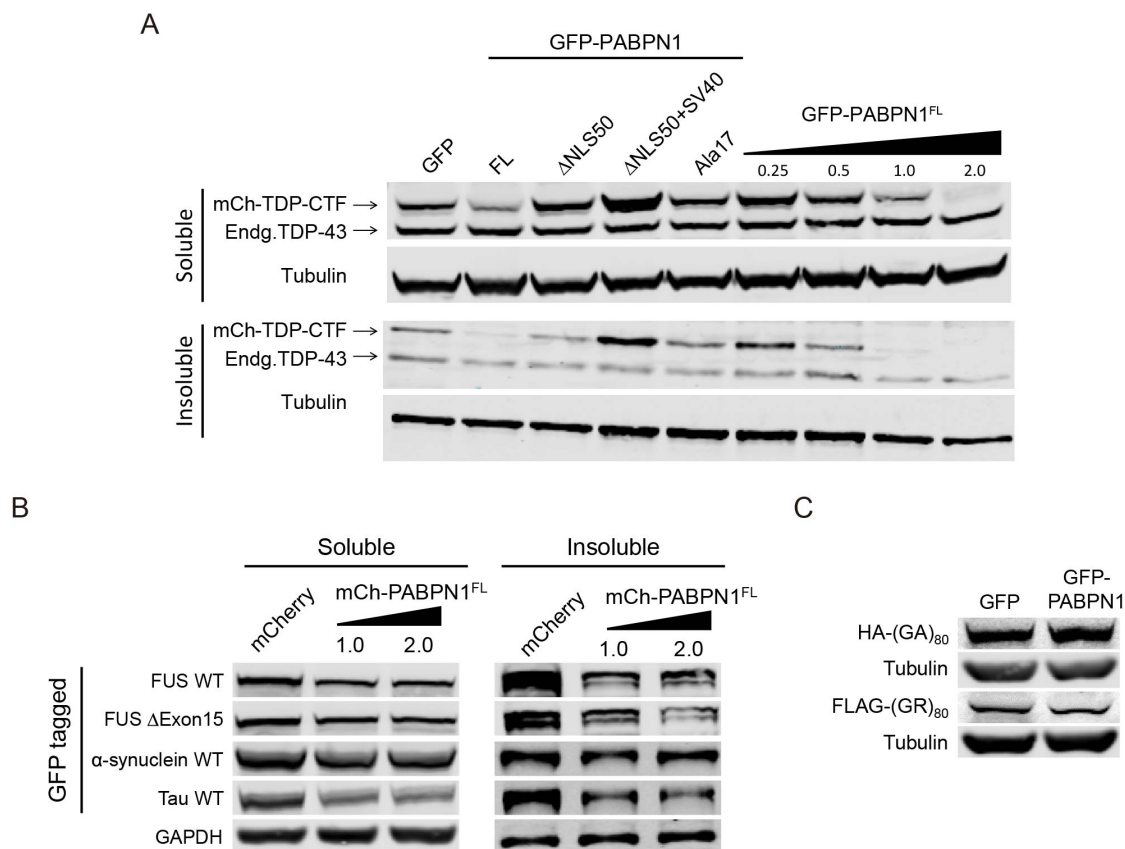


Figure 5-4 | PABPN1 changes the levels of TDP-CTF and other aggregation-prone proteins.

(A) Western blot analysis and quantification of TDP-CTF protein levels in N2a cells in the soluble and insoluble fraction. N2a cells were co-transfected with mCherry-tagged TDP-CTF and GFP, GFP-PABPN1 (FL, Δ NLS50 and Δ NLS50+SV40) or GFP-PABPN1^{Ala17}. Quantification reveals how PABPN1 expression levels in titration series change TDP-CTF protein levels. **(B)** Western blot analysis of the levels of FUS, α -synuclein and tau in N2a cells with the co-expression of mCherry or mCherry-PABPN1^{FL} in the soluble and insoluble fraction. **(C)** Levels of C9orf72-associated DPRs, (GA)₈₀ and (GR)₈₀, in N2a cells with the co-expression of GFP or GFP-PABPN1^{FL}.

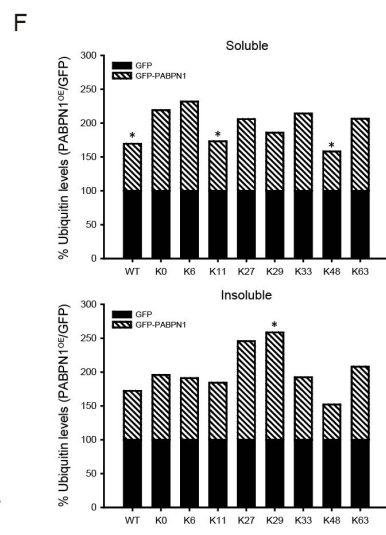
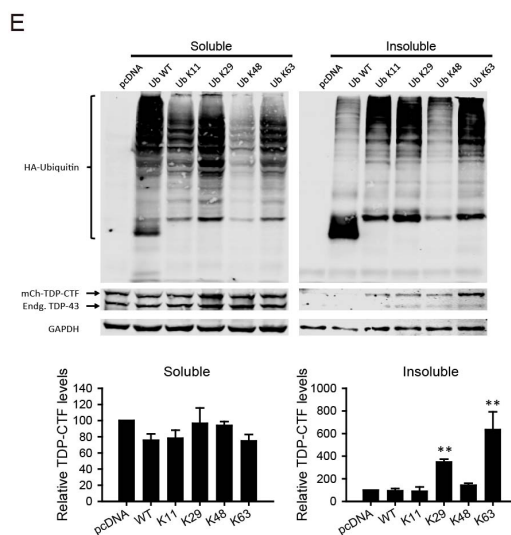
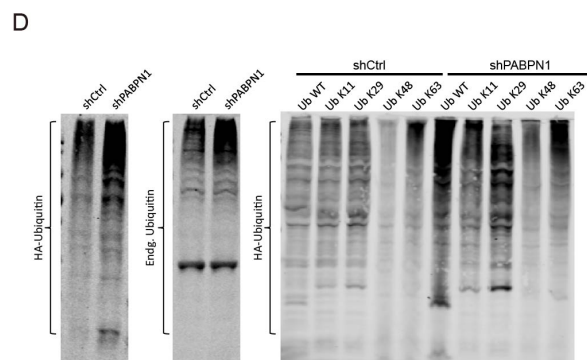
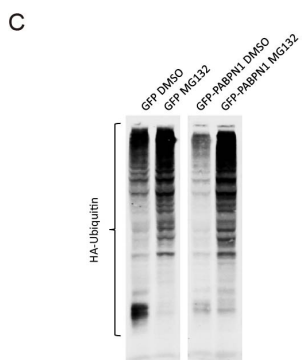
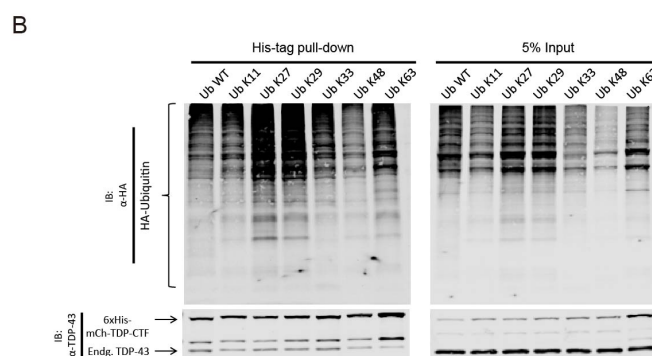
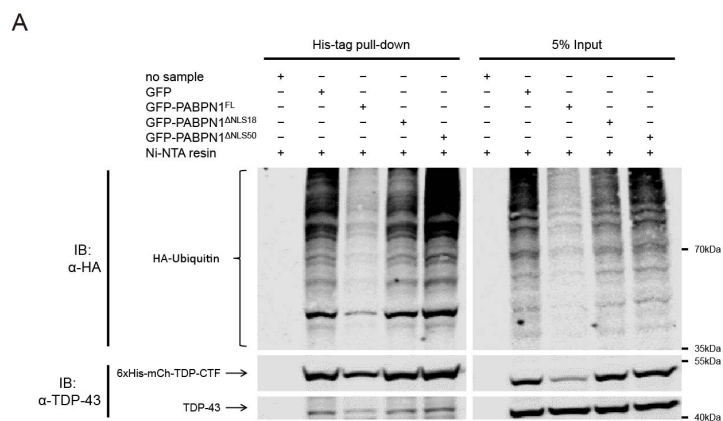


Figure 5-5 | PABPN1 modulates ubiquitin homeostasis.

(A) Left panel: Western blot analysis of histidine-pulldown assay from N2a cells tri-expressing HA-tagged ubiquitin, 6xHis-tagged mCherry-TDP-CTF and GFP or GFP-tagged PABPN1 (FL, Δ NLS18 and Δ NLS50). Right panel: Western blot analysis of cell lysates (Input). **(B)** Left panel: Western blot analysis of histidine-pulldown assay from N2a cells co-expressing 6xHis-tagged mCherry-TDP-CTF and HA-tagged ubiquitin with different single-lysine mutations (K11, K27, K29, K33, K48, K63). Right panel: Western blot analysis of cell lysates (Input). **(C)** Western blot analysis of the levels of HA-tagged ubiquitin with PABPN1 co-expression. Treatment of MG132 inhibits ubiquitin proteasomal degradation. **(D)** Western blot analysis of the effect of PABPN1 knockdown on the levels of endogenous ubiquitin and different HA-tagged ubiquitin constructs. **(E)** Western blot analysis and quantification of TDP-CTF protein levels in N2a cells with the co-expression of different HA-tagged ubiquitin constructs in the soluble and insoluble fraction. **(F)** Western blot quantification of the levels of different HA-tagged ubiquitin constructs when PABPN1 was overexpressed in the soluble and insoluble fraction.

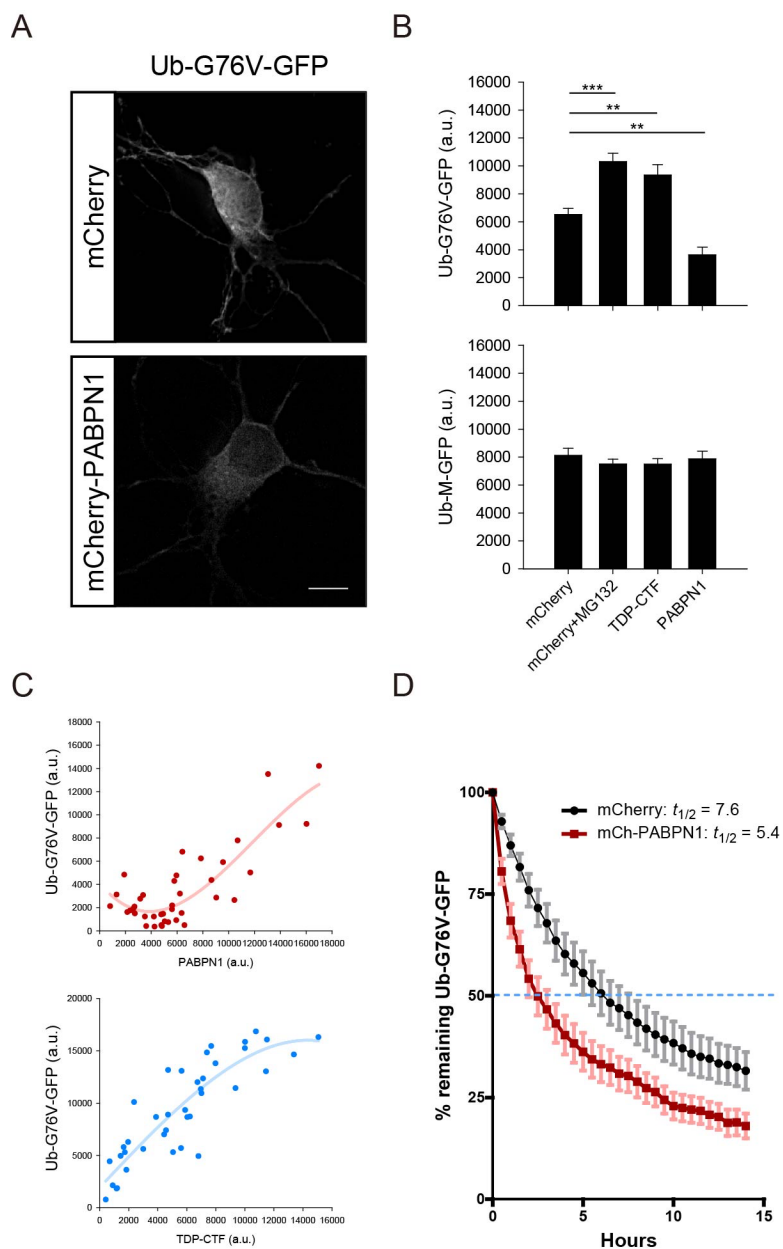


Figure 5-6 | PABPN1 promotes protein degradation via enhancing proteasome activity.

(A) Representative images for the expression of mCherry or mCherry-PABPN1 and GFP-based reporter for proteasomal degradation in cortical neurons. Ub-G76V-GFP is a short-lived protein and an N-terminal ubiquitin mutant in frame with GFP. The glycine residue of Ub-G76V-GFP is substituted by valine. **(B)** Ub-X-GFP chimeras (Ub-G76V-

GFP: ubiquitin fusion degradation; Ub-M-GFP: stable) were co-expressed in neurons with mCherry, TDP-CTF or PABPN1. Treatment of MG132 inhibits proteasomal degradation. **(C)** Correlation between the levels of Ub-G76V-GFP and PABPN1 (Top) or TDP-CTF (Bottom). **(D)** The fluorescence half-life of Ub-G76V-GFP in the presence of mCherry or mCherry-PABPN1.

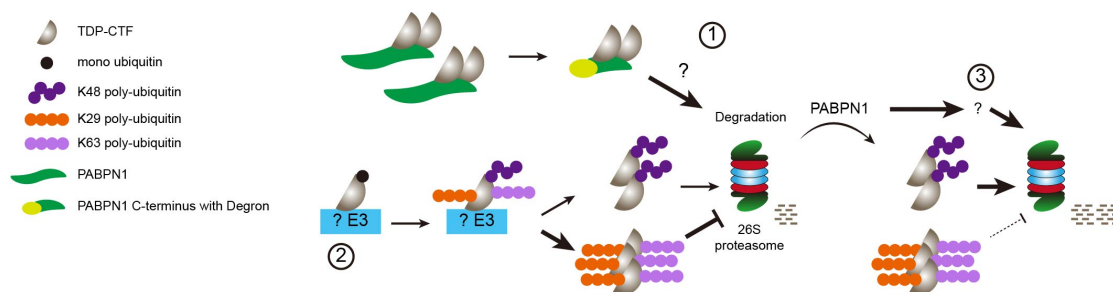


Figure 5-7 | Future directions.

A proposed model for PABPN1-mediated and ubiquitin-dependent TDP-CTF aggregation and degradation. **(1)** PABPN1 directly interacts with TDP-CTF through the C-terminus. We would like to determine whether PABPN1-derived peptides and mimics could suppress TDP-43 toxicity. The small peptide fused with degron (an targeting sequence for ubiquitin-dependent degradation by the proteasome) can bind to TDP-CTF and promote the degradation. **(2)** We would like to identify the E3 ligases mediating the ubiquitination of TDP-CTF. **(3)** Using the data from quantitative mass spectrometry, we could investigate how PABPN1 facilitates the protein degradation via the ubiquitin-proteasome pathway by examining the changes in E2 conjugases, E3 ligases, deubiquitinating enzymes (DUBs) or proteasome subunits. Development of small molecules for enhancing proteasomal degradation of TDP-CTF might be feasible.

References

- 1 Rosen, D. R. *et al.* Mutations in Cu/Zn superoxide dismutase gene are associated with familial amyotrophic lateral sclerosis. *Nature* **362**, 59-62, doi:10.1038/362059a0 (1993).
- 2 Cirulli, E. T. *et al.* Exome sequencing in amyotrophic lateral sclerosis identifies risk genes and pathways. *Science* **347**, 1436-1441, doi:10.1126/science.aaa3650 (2015).
- 3 Al-Chalabi, A., van den Berg, L. H. & Veldink, J. Gene discovery in amyotrophic lateral sclerosis: implications for clinical management. *Nat Rev Neurol* **13**, 96-104, doi:10.1038/nrneurol.2016.182 (2017).
- 4 Keller, M. F. *et al.* Genome-wide analysis of the heritability of amyotrophic lateral sclerosis. *JAMA Neurol* **71**, 1123-1134, doi:10.1001/jamaneurol.2014.1184 (2014).
- 5 DeJesus-Hernandez, M. *et al.* Expanded GGGGCC hexanucleotide repeat in noncoding region of C9ORF72 causes chromosome 9p-linked FTD and ALS. *Neuron* **72**, 245-256, doi:10.1016/j.neuron.2011.09.011 (2011).
- 6 Renton, A. E. *et al.* A hexanucleotide repeat expansion in C9ORF72 is the cause of chromosome 9p21-linked ALS-FTD. *Neuron* **72**, 257-268, doi:10.1016/j.neuron.2011.09.010 (2011).
- 7 Sreedharan, J. *et al.* TDP-43 mutations in familial and sporadic amyotrophic lateral sclerosis. *Science* **319**, 1668-1672, doi:10.1126/science.1154584 (2008).
- 8 Kabashi, E. *et al.* TARDBP mutations in individuals with sporadic and familial amyotrophic lateral sclerosis. *Nat Genet* **40**, 572-574, doi:10.1038/ng.132 (2008).

- 9 Chio, A. *et al.* Amyotrophic lateral sclerosis-frontotemporal lobar dementia in 3 families with p.Ala382Thr TARDBP mutations. *Arch Neurol* **67**, 1002-1009, doi:10.1001/archneurol.2010.173 (2010).
- 10 Borroni, B. *et al.* Mutation within TARDBP leads to frontotemporal dementia without motor neuron disease. *Hum Mutat* **30**, E974-983, doi:10.1002/humu.21100 (2009).
- 11 Rutherford, N. J. *et al.* Novel mutations in TARDBP (TDP-43) in patients with familial amyotrophic lateral sclerosis. *PLoS Genet* **4**, e1000193, doi:10.1371/journal.pgen.1000193 (2008).
- 12 Benajiba, L. *et al.* TARDBP mutations in motoneuron disease with frontotemporal lobar degeneration. *Ann Neurol* **65**, 470-473, doi:10.1002/ana.21612 (2009).
- 13 Neumann, M. *et al.* Ubiquitinated TDP-43 in frontotemporal lobar degeneration and amyotrophic lateral sclerosis. *Science* **314**, 130-133, doi:10.1126/science.1134108 (2006).
- 14 Arai, T. *et al.* TDP-43 is a component of ubiquitin-positive tau-negative inclusions in frontotemporal lobar degeneration and amyotrophic lateral sclerosis. *Biochem Biophys Res Commun* **351**, 602-611, doi:10.1016/j.bbrc.2006.10.093 (2006).
- 15 Ling, S. C., Polymenidou, M. & Cleveland, D. W. Converging mechanisms in ALS and FTD: disrupted RNA and protein homeostasis. *Neuron* **79**, 416-438, doi:10.1016/j.neuron.2013.07.033 (2013).

- 16 Burrell, J. R. *et al.* The frontotemporal dementia-motor neuron disease continuum. *Lancet* **388**, 919-931, doi:10.1016/s0140-6736(16)00737-6 (2016).
- 17 Rowland, L. P. & Shneider, N. A. Amyotrophic lateral sclerosis. *N Engl J Med* **344**, 1688-1700, doi:10.1056/nejm200105313442207 (2001).
- 18 Bensimon, G., Lacomblez, L. & Meininger, V. A controlled trial of riluzole in amyotrophic lateral sclerosis. ALS/Riluzole Study Group. *N Engl J Med* **330**, 585-591, doi:10.1056/nejm199403033300901 (1994).
- 19 Kiernan, M. C. *et al.* Amyotrophic lateral sclerosis. *Lancet* **377**, 942-955, doi:10.1016/s0140-6736(10)61156-7 (2011).
- 20 Al-Chalabi, A. & Hardiman, O. The epidemiology of ALS: a conspiracy of genes, environment and time. *Nat Rev Neurol* **9**, 617-628, doi:10.1038/nrneurol.2013.203 (2013).
- 21 Chio, A. *et al.* Global epidemiology of amyotrophic lateral sclerosis: a systematic review of the published literature. *Neuroepidemiology* **41**, 118-130, doi:10.1159/000351153 (2013).
- 22 Mehta, P. *et al.* Prevalence of Amyotrophic Lateral Sclerosis - United States, 2012-2013. *MMWR Surveill Summ* **65**, 1-12, doi:10.15585/mmwr.ss6508a1 (2016).
- 23 White, M. A. & Sreedharan, J. Amyotrophic lateral sclerosis: recent genetic highlights. *Curr Opin Neurol* **29**, 557-564, doi:10.1097/wco.0000000000000367 (2016).
- 24 Taylor, J. P., Brown, R. H., Jr. & Cleveland, D. W. Decoding ALS: from genes to mechanism. *Nature* **539**, 197-206, doi:10.1038/nature20413 (2016).

- 25 Renton, A. E., Chio, A. & Traynor, B. J. State of play in amyotrophic lateral sclerosis genetics. *Nat Neurosci* **17**, 17-23, doi:10.1038/nn.3584 (2014).
- 26 Sau, D. *et al.* Mutation of SOD1 in ALS: a gain of a loss of function. *Hum Mol Genet* **16**, 1604-1618, doi:10.1093/hmg/ddm110 (2007).
- 27 Shibata, N. *et al.* Intense superoxide dismutase-1 immunoreactivity in intracytoplasmic hyaline inclusions of familial amyotrophic lateral sclerosis with posterior column involvement. *J Neuropathol Exp Neurol* **55**, 481-490 (1996).
- 28 Sheng, Y., Chattopadhyay, M., Whitelegge, J. & Valentine, J. S. SOD1 aggregation and ALS: role of metallation states and disulfide status. *Curr Top Med Chem* **12**, 2560-2572 (2012).
- 29 Pesiridis, G. S., Lee, V. M. & Trojanowski, J. Q. Mutations in TDP-43 link glycine-rich domain functions to amyotrophic lateral sclerosis. *Hum Mol Genet* **18**, R156-162, doi:10.1093/hmg/ddp303 (2009).
- 30 Igaz, L. M. *et al.* Enrichment of C-terminal fragments in TAR DNA-binding protein-43 cytoplasmic inclusions in brain but not in spinal cord of frontotemporal lobar degeneration and amyotrophic lateral sclerosis. *Am J Pathol* **173**, 182-194, doi:10.2353/ajpath.2008.080003 (2008).
- 31 Neumann, M. *et al.* Phosphorylation of S409/410 of TDP-43 is a consistent feature in all sporadic and familial forms of TDP-43 proteinopathies. *Acta Neuropathol* **117**, 137-149, doi:10.1007/s00401-008-0477-9 (2009).
- 32 Brandmeir, N. J. *et al.* Severe subcortical TDP-43 pathology in sporadic frontotemporal lobar degeneration with motor neuron disease. *Acta Neuropathol* **115**, 123-131, doi:10.1007/s00401-007-0315-5 (2008).

- 33 Hasegawa, M. *et al.* Phosphorylated TDP-43 in frontotemporal lobar degeneration and amyotrophic lateral sclerosis. *Ann Neurol* **64**, 60-70, doi:10.1002/ana.21425 (2008).
- 34 Zhang, Y. J. *et al.* Aberrant cleavage of TDP-43 enhances aggregation and cellular toxicity. *Proc. Natl. Acad. Sci. USA* **106**, 7607-7612, doi:10.1073/pnas.0900688106 (2009).
- 35 Liu-Yesucevitz, L. *et al.* Tar DNA binding protein-43 (TDP-43) associates with stress granules: analysis of cultured cells and pathological brain tissue. *PLoS One* **5**, e13250, doi:10.1371/journal.pone.0013250 (2010).
- 36 Geser, F., Martinez-Lage, M., Kwong, L. K., Lee, V. M. & Trojanowski, J. Q. Amyotrophic lateral sclerosis, frontotemporal dementia and beyond: the TDP-43 diseases. *J Neurol* **256**, 1205-1214, doi:10.1007/s00415-009-5069-7 (2009).
- 37 Tassone, F. *et al.* CGG repeat length correlates with age of onset of motor signs of the fragile X-associated tremor/ataxia syndrome (FXTAS). *Am J Med Genet B Neuropsychiatr Genet* **144b**, 566-569, doi:10.1002/ajmg.b.30482 (2007).
- 38 Harley, H. G. *et al.* Size of the unstable CTG repeat sequence in relation to phenotype and parental transmission in myotonic dystrophy. *Am J Hum Genet* **52**, 1164-1174 (1993).
- 39 Levine, T. P., Daniels, R. D., Gatta, A. T., Wong, L. H. & Hayes, M. J. The product of C9orf72, a gene strongly implicated in neurodegeneration, is structurally related to DENN Rab-GEFs. *Bioinformatics* **29**, 499-503, doi:10.1093/bioinformatics/bts725 (2013).

- 40 O'Rourke, J. G. *et al.* C9orf72 is required for proper macrophage and microglial function in mice. *Science* **351**, 1324-1329, doi:10.1126/science.aaf1064 (2016).
- 41 Atanasio, A. *et al.* C9orf72 ablation causes immune dysregulation characterized by leukocyte expansion, autoantibody production, and glomerulonephropathy in mice. *Sci Rep* **6**, 23204, doi:10.1038/srep23204 (2016).
- 42 Zu, T. *et al.* RAN proteins and RNA foci from antisense transcripts in C9ORF72 ALS and frontotemporal dementia. *Proc Natl Acad Sci U S A* **110**, E4968-4977, doi:10.1073/pnas.1315438110 (2013).
- 43 Mori, K. *et al.* Bidirectional transcripts of the expanded C9orf72 hexanucleotide repeat are translated into aggregating dipeptide repeat proteins. *Acta Neuropathol* **126**, 881-893, doi:10.1007/s00401-013-1189-3 (2013).
- 44 Mori, K. *et al.* The C9orf72 GGGGCC repeat is translated into aggregating dipeptide-repeat proteins in FTL/ALS. *Science* **339**, 1335-1338, doi:10.1126/science.1232927 (2013).
- 45 Gomez-Deza, J. *et al.* Dipeptide repeat protein inclusions are rare in the spinal cord and almost absent from motor neurons in C9ORF72 mutant amyotrophic lateral sclerosis and are unlikely to cause their degeneration. *Acta Neuropathol Commun* **3**, 38, doi:10.1186/s40478-015-0218-y (2015).
- 46 Haeusler, A. R., Donnelly, C. J. & Rothstein, J. D. The expanding biology of the C9orf72 nucleotide repeat expansion in neurodegenerative disease. *Nat Rev Neurosci* **17**, 383-395, doi:10.1038/nrn.2016.38 (2016).
- 47 Onyike, C. U. & Diehl-Schmid, J. The epidemiology of frontotemporal dementia. *Int Rev Psychiatry* **25**, 130-137, doi:10.3109/09540261.2013.776523 (2013).

- 48 Bang, J., Spina, S. & Miller, B. L. Frontotemporal dementia. *Lancet* **386**, 1672-1682, doi:10.1016/s0140-6736(15)00461-4 (2015).
- 49 Sieben, A. *et al.* The genetics and neuropathology of frontotemporal lobar degeneration. *Acta Neuropathol* **124**, 353-372, doi:10.1007/s00401-012-1029-x (2012).
- 50 Kipps, C. M., Hodges, J. R. & Hornberger, M. Nonprogressive behavioural frontotemporal dementia: recent developments and clinical implications of the 'bvFTD phenocopy syndrome'. *Curr Opin Neurol* **23**, 628-632, doi:10.1097/WCO.0b013e3283404309 (2010).
- 51 Neary, D. *et al.* Frontotemporal lobar degeneration: a consensus on clinical diagnostic criteria. *Neurology* **51**, 1546-1554 (1998).
- 52 Seeley, W. W. *et al.* The natural history of temporal variant frontotemporal dementia. *Neurology* **64**, 1384-1390, doi:10.1212/01.wnl.0000158425.46019.5c (2005).
- 53 Gorno-Tempini, M. L. *et al.* Classification of primary progressive aphasia and its variants. *Neurology* **76**, 1006-1014, doi:10.1212/WNL.0b013e31821103e6 (2011).
- 54 Phukan, J., Pender, N. P. & Hardiman, O. Cognitive impairment in amyotrophic lateral sclerosis. *Lancet Neurol* **6**, 994-1003, doi:10.1016/s1474-4422(07)70265-x (2007).
- 55 Ringholz, G. M. *et al.* Prevalence and patterns of cognitive impairment in sporadic ALS. *Neurology* **65**, 586-590, doi:10.1212/01.wnl.0000172911.39167.b6 (2005).

- 56 Burrell, J. R., Kiernan, M. C., Vucic, S. & Hodges, J. R. Motor neuron dysfunction in frontotemporal dementia. *Brain* **134**, 2582-2594, doi:10.1093/brain/awr195 (2011).
- 57 Lomen-Hoerth, C., Anderson, T. & Miller, B. The overlap of amyotrophic lateral sclerosis and frontotemporal dementia. *Neurology* **59**, 1077-1079 (2002).
- 58 Wheaton, M. W. *et al.* Cognitive impairment in familial ALS. *Neurology* **69**, 1411-1417, doi:10.1212/01.wnl.0000277422.11236.2c (2007).
- 59 Murphy, J. M. *et al.* Continuum of frontal lobe impairment in amyotrophic lateral sclerosis. *Arch Neurol* **64**, 530-534, doi:10.1001/archneur.64.4.530 (2007).
- 60 Hutton, M. *et al.* Association of missense and 5'-splice-site mutations in tau with the inherited dementia FTDP-17. *Nature* **393**, 702-705, doi:10.1038/31508 (1998).
- 61 Baker, M. *et al.* Mutations in progranulin cause tau-negative frontotemporal dementia linked to chromosome 17. *Nature* **442**, 916-919, doi:10.1038/nature05016 (2006).
- 62 Cruts, M. *et al.* Null mutations in progranulin cause ubiquitin-positive frontotemporal dementia linked to chromosome 17q21. *Nature* **442**, 920-924, doi:10.1038/nature05017 (2006).
- 63 Le Ber, I. Genetics of frontotemporal lobar degeneration: an up-date and diagnosis algorithm. *Rev Neurol (Paris)* **169**, 811-819, doi:10.1016/j.neurol.2013.07.014 (2013).

- 64 Foster, N. L. *et al.* Frontotemporal dementia and parkinsonism linked to chromosome 17: a consensus conference. Conference Participants. *Ann Neurol* **41**, 706-715, doi:10.1002/ana.410410606 (1997).
- 65 Roks, G. *et al.* Mutation screening of the tau gene in patients with early-onset Alzheimer's disease. *Neurosci Lett* **277**, 137-139 (1999).
- 66 Rademakers, R., Cruts, M. & van Broeckhoven, C. The role of tau (MAPT) in frontotemporal dementia and related tauopathies. *Hum Mutat* **24**, 277-295, doi:10.1002/humu.20086 (2004).
- 67 Pittman, A. M., Fung, H. C. & de Silva, R. Untangling the tau gene association with neurodegenerative disorders. *Hum Mol Genet* **15 Spec No 2**, R188-195, doi:10.1093/hmg/ddl190 (2006).
- 68 Gass, J. *et al.* Mutations in progranulin are a major cause of ubiquitin-positive frontotemporal lobar degeneration. *Hum Mol Genet* **15**, 2988-3001, doi:10.1093/hmg/ddl241 (2006).
- 69 Ryan, C. L. *et al.* Progranulin is expressed within motor neurons and promotes neuronal cell survival. *BMC Neurosci* **10**, 130, doi:10.1186/1471-2202-10-130 (2009).
- 70 Van Damme, P. *et al.* Progranulin functions as a neurotrophic factor to regulate neurite outgrowth and enhance neuronal survival. *J Cell Biol* **181**, 37-41, doi:10.1083/jcb.200712039 (2008).
- 71 Rademakers, R., Neumann, M. & Mackenzie, I. R. Advances in understanding the molecular basis of frontotemporal dementia. *Nat Rev Neurol* **8**, 423-434, doi:10.1038/nrneurol.2012.117 (2012).

- 72 Yin, F. *et al.* Exaggerated inflammation, impaired host defense, and neuropathology in progranulin-deficient mice. *J Exp Med* **207**, 117-128, doi:10.1084/jem.20091568 (2010).
- 73 Devenney, E. *et al.* Frontotemporal dementia associated with the C9ORF72 mutation: a unique clinical profile. *JAMA Neurol* **71**, 331-339, doi:10.1001/jamaneurol.2013.6002 (2014).
- 74 Baborie, A. *et al.* Pathological correlates of frontotemporal lobar degeneration in the elderly. *Acta Neuropathol* **121**, 365-371, doi:10.1007/s00401-010-0765-z (2011).
- 75 Kukull, W. A. *et al.* Dementia and Alzheimer disease incidence: a prospective cohort study. *Arch Neurol* **59**, 1737-1746 (2002).
- 76 Hebert, L. E., Weuve, J., Scherr, P. A. & Evans, D. A. Alzheimer disease in the United States (2010-2050) estimated using the 2010 census. *Neurology* **80**, 1778-1783, doi:10.1212/WNL.0b013e31828726f5 (2013).
- 77 Zanetti, O., Solerte, S. B. & Cantoni, F. Life expectancy in Alzheimer's disease (AD). *Arch Gerontol Geriatr* **49 Suppl 1**, 237-243, doi:10.1016/j.archger.2009.09.035 (2009).
- 78 Jack, C. R., Jr. *et al.* Hypothetical model of dynamic biomarkers of the Alzheimer's pathological cascade. *Lancet Neurol* **9**, 119-128, doi:10.1016/s1474-4422(09)70299-6 (2010).
- 79 Huang, Y. & Mucke, L. Alzheimer mechanisms and therapeutic strategies. *Cell* **148**, 1204-1222, doi:10.1016/j.cell.2012.02.040 (2012).

- 80 Amador-Ortiz, C. *et al.* TDP-43 immunoreactivity in hippocampal sclerosis and Alzheimer's disease. *Ann Neurol* **61**, 435-445, doi:10.1002/ana.21154 (2007).
- 81 Josephs, K. A. *et al.* Staging TDP-43 pathology in Alzheimer's disease. *Acta Neuropathol* **127**, 441-450, doi:10.1007/s00401-013-1211-9 (2014).
- 82 Chang, X. L., Tan, M. S., Tan, L. & Yu, J. T. The Role of TDP-43 in Alzheimer's Disease. *Mol Neurobiol* **53**, 3349-3359, doi:10.1007/s12035-015-9264-5 (2016).
- 83 Krecic, A. M. & Swanson, M. S. hnRNP complexes: composition, structure, and function. *Curr Opin Cell Biol* **11**, 363-371, doi:10.1016/s0955-0674(99)80051-9 (1999).
- 84 Wang, H. Y., Wang, I. F., Bose, J. & Shen, C. K. Structural diversity and functional implications of the eukaryotic TDP gene family. *Genomics* **83**, 130-139 (2004).
- 85 Ayala, Y. M. *et al.* Human, Drosophila, and C.elegans TDP43: nucleic acid binding properties and splicing regulatory function. *J Mol Biol* **348**, 575-588, doi:10.1016/j.jmb.2005.02.038 (2005).
- 86 Polymenidou, M. *et al.* Long pre-mRNA depletion and RNA missplicing contribute to neuronal vulnerability from loss of TDP-43. *Nat Neurosci* **14**, 459-468, doi:10.1038/nn.2779 (2011).
- 87 Tollervey, J. R. *et al.* Characterizing the RNA targets and position-dependent splicing regulation by TDP-43. *Nat Neurosci* **14**, 452-458, doi:10.1038/nn.2778 (2011).

- 88 Kuo, P. H., Doudeva, L. G., Wang, Y. T., Shen, C. K. & Yuan, H. S. Structural insights into TDP-43 in nucleic-acid binding and domain interactions. *Nucleic Acids Res* **37**, 1799-1808, doi:10.1093/nar/gkp013 (2009).
- 89 Janssens, J. & Van Broeckhoven, C. Pathological mechanisms underlying TDP-43 driven neurodegeneration in FTL-D-ALS spectrum disorders. *Hum Mol Genet* **22**, R77-87, doi:10.1093/hmg/ddt349 (2013).
- 90 Ayala, Y. M. *et al.* Structural determinants of the cellular localization and shuttling of TDP-43. *J Cell Sci* **121**, 3778-3785, doi:10.1242/jcs (2008).
- 91 Winton, M. J. *et al.* Disturbance of nuclear and cytoplasmic TAR DNA-binding protein (TDP-43) induces disease-like redistribution, sequestration, and aggregate formation. *J. Biol. Chem.* **283**, 13302-13309, doi:10.1074/jbc.M800342200 (2008).
- 92 Fuentealba, R. A. *et al.* Interaction with polyglutamine aggregates reveals a Q/N-rich domain in TDP-43. *J Biol Chem* **285**, 26304-26314, doi:10.1074/jbc.M110.125039 (2010).
- 93 Udan, M. & Baloh, R. H. Implications of the prion-related Q/N domains in TDP-43 and FUS. *Prion* **5**, 1-5 (2011).
- 94 Guo, J. L. & Lee, V. M. Seeding of normal Tau by pathological Tau conformers drives pathogenesis of Alzheimer-like tangles. *J Biol Chem* **286**, 15317-15331, doi:10.1074/jbc.M110.209296 (2011).
- 95 Hansen, C. *et al.* alpha-Synuclein propagates from mouse brain to grafted dopaminergic neurons and seeds aggregation in cultured human cells. *J Clin Invest* **121**, 715-725, doi:10.1172/jci43366 (2011).

- 96 Chen, A. K. *et al.* Induction of amyloid fibrils by the C-terminal fragments of TDP-43 in amyotrophic lateral sclerosis. *J Am Chem Soc* **132**, 1186-1187, doi:10.1021/ja9066207 (2010).
- 97 Johnson, B. S. *et al.* TDP-43 is intrinsically aggregation-prone, and amyotrophic lateral sclerosis-linked mutations accelerate aggregation and increase toxicity. *J Biol Chem* **284**, 20329-20339, doi:10.1074/jbc.M109.010264 (2009).
- 98 Buratti, E. *et al.* TDP-43 binds heterogeneous nuclear ribonucleoprotein A/B through its C-terminal tail: an important region for the inhibition of cystic fibrosis transmembrane conductance regulator exon 9 splicing. *J Biol Chem* **280**, 37572-37584, doi:10.1074/jbc.M505557200 (2005).
- 99 Ayala, Y. M., Misteli, T. & Baralle, F. E. TDP-43 regulates retinoblastoma protein phosphorylation through the repression of cyclin-dependent kinase 6 expression. *Proc Natl Acad Sci U S A* **105**, 3785-3789, doi:10.1073/pnas.0800546105 (2008).
- 100 Abhyankar, M. M., Urekar, C. & Reddi, P. P. A novel CpG-free vertebrate insulator silences the testis-specific SP-10 gene in somatic tissues: role for TDP-43 in insulator function. *J Biol Chem* **282**, 36143-36154, doi:10.1074/jbc.M705811200 (2007).
- 101 Guo, W. *et al.* An ALS-associated mutation affecting TDP-43 enhances protein aggregation, fibril formation and neurotoxicity. *Nat Struct Mol Biol* **18**, 822-830, doi:10.1038/nsmb.2053 (2011).
- 102 Lim, L., Wei, Y., Lu, Y. & Song, J. ALS-Causing Mutations Significantly Perturb the Self-Assembly and Interaction with Nucleic Acid of the Intrinsically

- Disordered Prion-Like Domain of TDP-43. *PLoS Biol* **14**, e1002338, doi:10.1371/journal.pbio.1002338 (2016).
- 103 Nonaka, T., Kametani, F., Arai, T., Akiyama, H. & Hasegawa, M. Truncation and pathogenic mutations facilitate the formation of intracellular aggregates of TDP-43. *Hum. Mol. Genet.* **18**, 3353-3364, doi:10.1093/hmg/ddp275 (2009).
- 104 Lagier-Tourenne, C., Polymenidou, M. & Cleveland, D. W. TDP-43 and FUS/TLS: emerging roles in RNA processing and neurodegeneration. *Hum Mol Genet* **19**, R46-64, doi:10.1093/hmg/ddq137 (2010).
- 105 Ou, S. H., Wu, F., Harrich, D., Garcia-Martinez, L. F. & Gaynor, R. B. Cloning and characterization of a novel cellular protein, TDP-43, that binds to human immunodeficiency virus type 1 TAR DNA sequence motifs. *J Virol* **69**, 3584-3596 (1995).
- 106 Buratti, E. *et al.* Nuclear factor TDP-43 and SR proteins promote in vitro and in vivo CFTR exon 9 skipping. *Embo J* **20**, 1774-1784, doi:10.1093/emboj/20.7.1774 (2001).
- 107 Mercado, P. A., Ayala, Y. M., Romano, M., Buratti, E. & Baralle, F. E. Depletion of TDP 43 overrides the need for exonic and intronic splicing enhancers in the human apoA-II gene. *Nucleic Acids Res* **33**, 6000-6010, doi:10.1093/nar/gki897 (2005).
- 108 Bose, J. K., Wang, I. F., Hung, L., Tarn, W. Y. & Shen, C. K. TDP-43 overexpression enhances exon 7 inclusion during the survival of motor neuron pre-mRNA splicing. *J Biol Chem* **283**, 28852-28859, doi:10.1074/jbc.M805376200 (2008).

- 109 Ayala, Y. M. *et al.* TDP-43 regulates its mRNA levels through a negative feedback loop. *Embo j* **30**, 277-288, doi:10.1038/emboj.2010.310 (2011).
- 110 Avendano-Vazquez, S. E. *et al.* Autoregulation of TDP-43 mRNA levels involves interplay between transcription, splicing, and alternative polyA site selection. *Genes Dev* **26**, 1679-1684, doi:10.1101/gad.194829.112 (2012).
- 111 Freibaum, B. D., Chitta, R. K., High, A. A. & Taylor, J. P. Global analysis of TDP-43 interacting proteins reveals strong association with RNA splicing and translation machinery. *J Proteome Res* **9**, 1104-1120, doi:10.1021/pr901076y (2010).
- 112 Kawahara, Y. & Mieda-Sato, A. TDP-43 promotes microRNA biogenesis as a component of the Drosha and Dicer complexes. *Proc Natl Acad Sci U S A* **109**, 3347-3352, doi:10.1073/pnas.1112427109 (2012).
- 113 Fallini, C., Bassell, G. J. & Rossoll, W. The ALS disease protein TDP-43 is actively transported in motor neuron axons and regulates axon outgrowth. *Hum Mol Genet* **21**, 3703-3718, doi:10.1093/hmg/dds205 (2012).
- 114 Alami, N. H. *et al.* Axonal Transport of TDP-43 mRNA Granules Is Impaired by ALS-Causing Mutations. *Neuron* **81**, 536-543, doi:10.1016/j.neuron.2013.12.018 (2014).
- 115 Moisse, K. *et al.* Cytosolic TDP-43 expression following axotomy is associated with caspase 3 activation in NFL^{-/-} mice: support for a role for TDP-43 in the physiological response to neuronal injury. *Brain Res* **1296**, 176-186, doi:10.1016/j.brainres.2009.07.023 (2009).

- 116 McDonald, K. K. *et al.* TAR DNA-binding protein 43 (TDP-43) regulates stress granule dynamics via differential regulation of G3BP and TIA-1. *Hum. Mol. Genet.* **20**, 1400-1410, doi:10.1093/hmg/ddr021 (2011).
- 117 Li, Y. R., King, O. D., Shorter, J. & Gitler, A. D. Stress granules as crucibles of ALS pathogenesis. *J Cell Biol* **201**, 361-372, doi:10.1083/jcb.201302044 (2013).
- 118 Wilson, R. S. *et al.* TDP-43 pathology, cognitive decline, and dementia in old age. *JAMA Neurol* **70**, 1418-1424, doi:10.1001/jamaneurol.2013.3961 (2013).
- 119 Zhang, K. *et al.* The C9orf72 repeat expansion disrupts nucleocytoplasmic transport. *Nature* **525**, 56-61, doi:10.1038/nature14973 (2015).
- 120 Freibaum, B. D. *et al.* GGGGCC repeat expansion in C9orf72 compromises nucleocytoplasmic transport. *Nature* **525**, 129-133, doi:10.1038/nature14974 (2015).
- 121 Jovicic, A. *et al.* Modifiers of C9orf72 dipeptide repeat toxicity connect nucleocytoplasmic transport defects to FTD/ALS. *Nat Neurosci* **18**, 1226-1229, doi:10.1038/nn.4085 (2015).
- 122 Xu, Y. F. *et al.* Wild-type human TDP-43 expression causes TDP-43 phosphorylation, mitochondrial aggregation, motor deficits, and early mortality in transgenic mice. *J Neurosci* **30**, 10851-10859, doi:10.1523/JNEUROSCI.1630-10.2010 (2010).
- 123 Xu, Y. F. *et al.* Expression of mutant TDP-43 induces neuronal dysfunction in transgenic mice. *Mol Neurodegener* **6**, 73, doi:10.1186/1750-1326-6-73 (2011).

- 124 Barmada, S. J. *et al.* Cytoplasmic mislocalization of TDP-43 is toxic to neurons and enhanced by a mutation associated with familial amyotrophic lateral sclerosis. *J. Neurosci.* **30**, 639-649, doi:10.1523/JNEUROSCI.4988-09.2010 (2010).
- 125 Chou, C. C. *et al.* PABPN1 suppresses TDP-43 toxicity in ALS disease models. *Hum Mol Genet* **24**, 5154-5173, doi:10.1093/hmg/ddv238 (2015).
- 126 Li, Y. *et al.* A Drosophila model for TDP-43 proteinopathy. *Proc Natl Acad Sci U S A* **107**, 3169-3174, doi:10.1073/pnas.0913602107 (2010).
- 127 Kabashi, E. *et al.* Gain and loss of function of ALS-related mutations of TARDBP (TDP-43) cause motor deficits in vivo. *Hum Mol Genet* **19**, 671-683, doi:10.1093/hmg/ddp534 (2010).
- 128 Smethurst, P. *et al.* In vitro prion-like behaviour of TDP-43 in ALS. *Neurobiol Dis* **96**, 236-247, doi:10.1016/j.nbd.2016.08.007 (2016).
- 129 Tanji, K. *et al.* p62/sequestosome 1 binds to TDP-43 in brains with frontotemporal lobar degeneration with TDP-43 inclusions. *J Neurosci Res* **90**, 2034-2042, doi:10.1002/jnr.23081 (2012).
- 130 Fang, Y. S. *et al.* Full-length TDP-43 forms toxic amyloid oligomers that are present in frontotemporal lobar dementia-TDP patients. *Nat Commun* **5**, 4824, doi:10.1038/ncomms5824 (2014).
- 131 Johnson, B. S., McCaffery, J. M., Lindquist, S. & Gitler, A. D. A yeast TDP-43 proteinopathy model: Exploring the molecular determinants of TDP-43 aggregation and cellular toxicity. *Proc Natl Acad Sci U S A* **105**, 6439-6444, doi:10.1073/pnas.0802082105 (2008).

- 132 Igaz, L. M. *et al.* Expression of TDP-43 C-terminal Fragments in Vitro Recapitulates Pathological Features of TDP-43 Proteinopathies. *J Biol Chem* **284**, 8516-8524, doi:10.1074/jbc.M809462200 (2009).
- 133 Wils, H. *et al.* TDP-43 transgenic mice develop spastic paralysis and neuronal inclusions characteristic of ALS and frontotemporal lobar degeneration. *Proc Natl Acad Sci U S A* **107**, 3858-3863, doi:10.1073/pnas.0912417107 (2010).
- 134 Kedersha, N. & Anderson, P. Mammalian stress granules and processing bodies. *Methods Enzymol* **431**, 61-81, doi:10.1016/s0076-6879(07)31005-7 (2007).
- 135 Anderson, P. & Kedersha, N. Stress granules: the Tao of RNA triage. *Trends Biochem Sci* **33**, 141-150, doi:10.1016/j.tibs.2007.12.003 (2008).
- 136 Bentmann, E., Haass, C. & Dormann, D. Stress granules in neurodegeneration-- lessons learnt from TAR DNA binding protein of 43 kDa and fused in sarcoma. *FEBS J* **280**, 4348-4370, doi:10.1111/febs.12287 (2013).
- 137 Colombrita, C. *et al.* TDP-43 is recruited to stress granules in conditions of oxidative insult. *J Neurochem* **111**, 1051-1061, doi:10.1111/j.1471-4159.2009.06383.x (2009).
- 138 Dormann, D. *et al.* ALS-associated fused in sarcoma (FUS) mutations disrupt Transportin-mediated nuclear import. *Embo j* **29**, 2841-2857, doi:10.1038/emboj.2010.143 (2010).
- 139 Guil, S., Long, J. C. & Caceres, J. F. hnRNP A1 relocalization to the stress granules reflects a role in the stress response. *Mol Cell Biol* **26**, 5744-5758, doi:10.1128/mcb.00224-06 (2006).

- 140 Patel, A. *et al.* A Liquid-to-Solid Phase Transition of the ALS Protein FUS Accelerated by Disease Mutation. *Cell* **162**, 1066-1077, doi:10.1016/j.cell.2015.07.047 (2015).
- 141 Molliex, A. *et al.* Phase separation by low complexity domains promotes stress granule assembly and drives pathological fibrillization. *Cell* **163**, 123-133, doi:10.1016/j.cell.2015.09.015 (2015).
- 142 Cohen, T. J., Hwang, A. W., Unger, T., Trojanowski, J. Q. & Lee, V. M. Redox signalling directly regulates TDP-43 via cysteine oxidation and disulphide cross-linking. *EMBO J* **31**, 1241-1252, doi:10.1038/emboj.2011.471 (2012).
- 143 Elden, A. C. *et al.* Ataxin-2 intermediate-length polyglutamine expansions are associated with increased risk for ALS. *Nature* **466**, 1069-1075, doi:10.1038/nature09320 (2010).
- 144 Sproviero, W. *et al.* ATXN2 trinucleotide repeat length correlates with risk of ALS. *Neurobiol Aging* **51**, 178.e171-178.e179, doi:10.1016/j.neurobiolaging.2016.11.010 (2017).
- 145 Kim, H. J. *et al.* Therapeutic modulation of eIF2alpha phosphorylation rescues TDP-43 toxicity in amyotrophic lateral sclerosis disease models. *Nat. Genet.* **46**, 152-160, doi:10.1038/ng.2853 (2014).
- 146 Hart, M. P. & Gitler, A. D. ALS-associated ataxin 2 polyQ expansions enhance stress-induced caspase 3 activation and increase TDP-43 pathological modifications. *J Neurosci* **32**, 9133-9142, doi:10.1523/JNEUROSCI.0996-12.2012 (2012).

- 147 Swisher, K. D. & Parker, R. Localization to, and effects of Pbp1, Pbp4, Lsm12, Dhh1, and Pab1 on stress granules in *Saccharomyces cerevisiae*. *PLoS One* **5**, e10006, doi:10.1371/journal.pone.0010006 (2010).
- 148 Terry, L. J. & Wentz, S. R. Flexible gates: dynamic topologies and functions for FG nucleoporins in nucleocytoplasmic transport. *Eukaryot Cell* **8**, 1814-1827, doi:10.1128/ec.00225-09 (2009).
- 149 D'Angelo, M. A. & Hetzer, M. W. Structure, dynamics and function of nuclear pore complexes. *Trends Cell Biol* **18**, 456-466, doi:10.1016/j.tcb.2008.07.009 (2008).
- 150 D'Angelo, M. A., Raices, M., Panowski, S. H. & Hetzer, M. W. Age-dependent deterioration of nuclear pore complexes causes a loss of nuclear integrity in postmitotic cells. *Cell* **136**, 284-295, doi:10.1016/j.cell.2008.11.037 (2009).
- 151 Chu, C. T., Plowey, E. D., Wang, Y., Patel, V. & Jordan-Sciutto, K. L. Location, location, location: altered transcription factor trafficking in neurodegeneration. *J Neuropathol Exp Neurol* **66**, 873-883, doi:10.1097/nen.0b013e318156a3d7 (2007).
- 152 Nofrini, V., Di Giacomo, D. & Mecucci, C. Nucleoporin genes in human diseases. *Eur J Hum Genet*, doi:10.1038/ejhg.2016.25 (2016).
- 153 Sheffield, L. G., Miskiewicz, H. B., Tannenbaum, L. B. & Mirra, S. S. Nuclear pore complex proteins in Alzheimer disease. *J Neuropathol Exp Neurol* **65**, 45-54 (2006).

- 154 Kinoshita, Y. *et al.* Nuclear contour irregularity and abnormal transporter protein distribution in anterior horn cells in amyotrophic lateral sclerosis. *J Neuropathol Exp Neurol* **68**, 1184-1192, doi:10.1097/NEN.0b013e3181bc3bec (2009).
- 155 Nishimura, A. L. *et al.* Nuclear import impairment causes cytoplasmic trans-activation response DNA-binding protein accumulation and is associated with frontotemporal lobar degeneration. *Brain* **133**, 1763-1771, doi:10.1093/brain/awq111 (2010).
- 156 Bolger, T. A. & Wentz, S. R. Gle1 is a multifunctional DEAD-box protein regulator that modulates Ded1 in translation initiation. *J Biol Chem* **286**, 39750-39759, doi:10.1074/jbc.M111.299321 (2011).
- 157 Aditi, Folkmann, A. W. & Wentz, S. R. Cytoplasmic hGle1A regulates stress granules by modulation of translation. *Mol Biol Cell* **26**, 1476-1490, doi:10.1091/mbc.E14-11-1523 (2015).
- 158 Aditi, Glass, L., Dawson, T. R. & Wentz, S. R. An amyotrophic lateral sclerosis-linked mutation in GLE1 alters the cellular pool of human Gle1 functional isoforms. *Adv Biol Regul* **62**, 25-36, doi:10.1016/j.jbior.2015.11.001 (2016).
- 159 Tran, D., Chalhoub, A., Schooley, A., Zhang, W. & Ngsee, J. K. A mutation in VAPB that causes amyotrophic lateral sclerosis also causes a nuclear envelope defect. *J Cell Sci* **125**, 2831-2836, doi:10.1242/jcs.102111 (2012).
- 160 Suzuki, H. & Matsuoka, M. Amyotrophic lateral sclerosis-linked mutant VAPB enhances TDP-43-induced motor neuronal toxicity. *J Neurochem* **119**, 1099-1107, doi:10.1111/j.1471-4159.2011.07491.x (2011).

- 161 Müller, S. *Studies of VAPB and TDP-43 in neurodegeneration* Doctor of Philosophy thesis, King's College London, (2015).
- 162 McGathey, T. J. *Nucleocytoplasmic Transport Defects in Mouse Model of Amyotrophic Lateral Sclerosis* Master of Science thesis, University of Maine, (2016).
- 163 Yamashita, T., Akamatsu, M. & Kwak, S. Altered Intracellular Milieu of ADAR2-Deficient Motor Neurons in Amyotrophic Lateral Sclerosis. *Genes (Basel)* **8**, doi:10.3390/genes8020060 (2017).
- 164 Yamashita, T. *et al.* A role for calpain-dependent cleavage of TDP-43 in amyotrophic lateral sclerosis pathology. *Nat Commun* **3**, 1307, doi:10.1038/ncomms2303 (2012).
- 165 Bano, D., Hengartner, M. O. & Nicotera, P. Nuclear pore complex during neuronal degeneration: cracking the last barrier! *Nucleus* **1**, 136-138, doi:10.4161/nucl.1.2.10798 (2010).
- 166 Yamashita, T., Aizawa, H., Teramoto, S., Akamatsu, M. & Kwak, S. Calpain-dependent disruption of nucleo-cytoplasmic transport in ALS motor neurons. *Sci Rep* **7**, 39994, doi:10.1038/srep39994 (2017).
- 167 Ward, M. E. *et al.* Early retinal neurodegeneration and impaired Ran-mediated nuclear import of TDP-43 in progranulin-deficient FTLD. *J Exp Med* **211**, 1937-1945, doi:10.1084/jem.20140214 (2014).
- 168 Prpar Mihevc, S., Baralle, M., Buratti, E. & Rogelj, B. TDP-43 aggregation mirrors TDP-43 knockdown, affecting the expression levels of a common set of proteins. *Sci Rep* **6**, 33996, doi:10.1038/srep33996 (2016).

- 169 Zhan, L., Hanson, K. A., Kim, S. H., Tare, A. & Tibbetts, R. S. Identification of genetic modifiers of TDP-43 neurotoxicity in *Drosophila*. *PLoS One* **8**, e57214, doi:10.1371/journal.pone.0057214.g001 (2013).
- 170 Zhang, Y. J. *et al.* C9ORF72 poly(GA) aggregates sequester and impair HR23 and nucleocytoplasmic transport proteins. *Nat Neurosci* **19**, 668-677, doi:10.1038/nn.4272 (2016).
- 171 Roux, K. J., Kim, D. I., Raida, M. & Burke, B. A promiscuous biotin ligase fusion protein identifies proximal and interacting proteins in mammalian cells. *J Cell Biol* **196**, 801-810, doi:10.1083/jcb.201112098 (2012).
- 172 Lam, S. S. *et al.* Directed evolution of APEX2 for electron microscopy and proximity labeling. *Nat Methods* **12**, 51-54, doi:10.1038/nmeth.3179 (2015).
- 173 Estes, P. S. *et al.* Wild-type and A315T mutant TDP-43 exert differential neurotoxicity in a *Drosophila* model of ALS. *Hum Mol Genet* **20**, 2308-2321, doi:10.1093/hmg/ddr124 (2011).
- 174 Williams, K. R. *et al.* hnRNP-Q1 represses nascent axon growth in cortical neurons by inhibiting Gap-43 mRNA translation. *Mol Biol Cell* **27**, 518-534, doi:10.1091/mbc.E15-07-0504 (2016).
- 175 Fallini, C., Bassell, G. J. & Rossoll, W. High-efficiency transfection of cultured primary motor neurons to study protein localization, trafficking, and function. *Mol Neurodegener* **5**, 17, doi:10.1186/1750-1326-5-17 (2010).
- 176 Kuo, L. J. & Yang, L. X. Gamma-H2AX - a novel biomarker for DNA double-strand breaks. *In Vivo* **22**, 305-309 (2008).

- 177 Caballero-Benitez, A. & Moran, J. Caspase activation pathways induced by staurosporine and low potassium: role of caspase-2. *J Neurosci Res* **71**, 383-396, doi:10.1002/jnr.10493 (2003).
- 178 Soderholm, J. F. *et al.* Importazole, a small molecule inhibitor of the transport receptor importin-beta. *ACS Chem Biol* **6**, 700-708, doi:10.1021/cb2000296 (2011).
- 179 Fallini, C. *et al.* The survival of motor neuron (SMN) protein interacts with the mRNA-binding protein HuD and regulates localization of poly(A) mRNA in primary motor neuron axons. *J Neurosci* **31**, 3914-3925, doi:10.1523/jneurosci.3631-10.2011 (2011).
- 180 Kim, D. I. *et al.* Probing nuclear pore complex architecture with proximity-dependent biotinylation. *Proc. Natl. Acad. Sci. U.S.A.* **111**, E2453-2461, doi:10.1073/pnas.1406459111 (2014).
- 181 Gupta, G. D. *et al.* A Dynamic Protein Interaction Landscape of the Human Centrosome-Cilium Interface. *Cell* **163**, 1484-1499, doi:10.1016/j.cell.2015.10.065 (2015).
- 182 Rout, M. P. *et al.* The yeast nuclear pore complex: composition, architecture, and transport mechanism. *J Cell Biol* **148**, 635-651 (2000).
- 183 Wright, P. E. & Dyson, H. J. Intrinsically disordered proteins in cellular signalling and regulation. *Nat Rev Mol Cell Biol* **16**, 18-29, doi:10.1038/nrm3920 (2015).
- 184 Halfmann, R., Wright, J. R., Alberti, S., Lindquist, S. & Rexach, M. Prion formation by a yeast GLFG nucleoporin. *Prion* **6**, 391-399, doi:10.4161/pri.20199 (2012).

- 185 Frey, S. & Gorlich, D. A saturated FG-repeat hydrogel can reproduce the permeability properties of nuclear pore complexes. *Cell* **130**, 512-523, doi:10.1016/j.cell.2007.06.024 (2007).
- 186 Lancaster, A. K., Nutter-Upham, A., Lindquist, S. & King, O. D. PLAAC: a web and command-line application to identify proteins with prion-like amino acid composition. *Bioinformatics* **30**, 2501-2502, doi:10.1093/bioinformatics/btu310 (2014).
- 187 Kato, M. *et al.* Cell-free formation of RNA granules: low complexity sequence domains form dynamic fibers within hydrogels. *Cell* **149**, 753-767, doi:10.1016/j.cell.2012.04.017 (2012).
- 188 Broers, J. L., Ramaekers, F. C., Bonne, G., Yaou, R. B. & Hutchison, C. J. Nuclear lamins: laminopathies and their role in premature ageing. *Physiol Rev* **86**, 967-1008, doi:10.1152/physrev.00047.2005 (2006).
- 189 Frost, B., Bardai, F. H. & Feany, M. B. Lamin Dysfunction Mediates Neurodegeneration in Tauopathies. *Curr Biol* **26**, 129-136, doi:10.1016/j.cub.2015.11.039 (2016).
- 190 Crisp, M. *et al.* Coupling of the nucleus and cytoplasm: role of the LINC complex. *J Cell Biol* **172**, 41-53, doi:10.1083/jcb.200509124 (2006).
- 191 Zhang, Q. *et al.* Nesprin-1 and -2 are involved in the pathogenesis of Emery Dreifuss muscular dystrophy and are critical for nuclear envelope integrity. *Hum Mol Genet* **16**, 2816-2833, doi:10.1093/hmg/ddm238 (2007).

- 192 Hatch, E. M., Fischer, A. H., Deerinck, T. J. & Hetzer, M. W. Catastrophic nuclear envelope collapse in cancer cell micronuclei. *Cell* **154**, 47-60, doi:10.1016/j.cell.2013.06.007 (2013).
- 193 Estes, P. S. *et al.* Motor neurons and glia exhibit specific individualized responses to TDP-43 expression in a Drosophila model of amyotrophic lateral sclerosis. *Disease Models & Mechanisms* **6**, 721-733, doi:10.1242/dmm.010710 (2013).
- 194 Kaneb, H. M. *et al.* Deleterious mutations in the essential mRNA metabolism factor, hGle1, in amyotrophic lateral sclerosis. *Hum Mol Genet* **24**, 1363-1373, doi:10.1093/hmg/ddu545 (2015).
- 195 Lee, K. H. *et al.* C9orf72 Dipeptide Repeats Impair the Assembly, Dynamics, and Function of Membrane-Less Organelles. *Cell* **167**, 774-788.e717, doi:10.1016/j.cell.2016.10.002 (2016).
- 196 Khosravi, B. *et al.* Cytoplasmic poly-GA aggregates impair nuclear import of TDP-43 in C9orf72 ALS/FTLD. *Hum Mol Genet*, doi:10.1093/hmg/ddw432 (2016).
- 197 Woerner, A. C. *et al.* Cytoplasmic protein aggregates interfere with nucleocytoplasmic transport of protein and RNA. *Science* **351**, 173-176, doi:10.1126/science.aad2033 (2016).
- 198 Shi, K. Y. *et al.* Toxic PRn poly-dipeptides encoded by the C9orf72 repeat expansion block nuclear import and export. *Proc Natl Acad Sci U S A*, doi:10.1073/pnas.1620293114 (2017).

- 199 Schmidt, H. B. & Gorlich, D. Transport Selectivity of Nuclear Pores, Phase Separation, and Membraneless Organelles. *Trends Biochem Sci* **41**, 46-61, doi:10.1016/j.tibs.2015.11.001 (2016).
- 200 Deng, Q. *et al.* FUS is phosphorylated by DNA-PK and accumulates in the cytoplasm after DNA damage. *J Neurosci* **34**, 7802-7813, doi:10.1523/jneurosci.0172-14.2014 (2014).
- 201 Rabut, G., Doye, V. & Ellenberg, J. Mapping the dynamic organization of the nuclear pore complex inside single living cells. *Nat Cell Biol* **6**, 1114-1121, doi:10.1038/ncb1184 (2004).
- 202 Loiodice, I. *et al.* The entire Nup107-160 complex, including three new members, is targeted as one entity to kinetochores in mitosis. *Mol Biol Cell* **15**, 3333-3344, doi:10.1091/mbc.E03-12-0878 (2004).
- 203 Daigle, N. *et al.* Nuclear pore complexes form immobile networks and have a very low turnover in live mammalian cells. *J Cell Biol* **154**, 71-84 (2001).
- 204 Lu, Y. *et al.* Interaction of adenovirus type 5 E4orf4 with the nuclear pore subunit Nup205 is required for proper viral gene expression. *J Virol* **88**, 13249-13259, doi:10.1128/jvi.00933-14 (2014).
- 205 Vyas, P., Singh, A., Murawala, P. & Joseph, J. Nup358 interacts with Dishevelled and aPKC to regulate neuronal polarity. *Biol Open* **2**, 1270-1278, doi:10.1242/bio.20135363 (2013).
- 206 Frosst, P., Guan, T., Subauste, C., Hahn, K. & Gerace, L. Tpr is localized within the nuclear basket of the pore complex and has a role in nuclear protein export. *J Cell Biol* **156**, 617-630, doi:10.1083/jcb.200106046 (2002).

- 207 Ellenberg, J. *et al.* Nuclear membrane dynamics and reassembly in living cells: targeting of an inner nuclear membrane protein in interphase and mitosis. *J Cell Biol* **138**, 1193-1206 (1997).
- 208 Kelley, J. B., Talley, A. M., Spencer, A., Gioeli, D. & Paschal, B. M. Karyopherin alpha7 (KPNA7), a divergent member of the importin alpha family of nuclear import receptors. *BMC Cell Biol* **11**, 63, doi:10.1186/1471-2121-11-63 (2010).
- 209 Wang, W., Budhu, A., Forgues, M. & Wang, X. W. Temporal and spatial control of nucleophosmin by the Ran-Crm1 complex in centrosome duplication. *Nat Cell Biol* **7**, 823-830, doi:10.1038/ncb1282 (2005).
- 210 Seow, Y., Sibley, C. R. & Wood, M. J. Artificial mirtron-mediated gene knockdown: functional DMPK silencing in mammalian cells. *RNA* **18**, 1328-1337, doi:10.1261/rna.030601.111 (2012).
- 211 Hang, J. & Dasso, M. Association of the human SUMO-1 protease SENP2 with the nuclear pore. *J Biol Chem* **277**, 19961-19966, doi:10.1074/jbc.M201799200 (2002).
- 212 Joseph, J., Tan, S. H., Karpova, T. S., McNally, J. G. & Dasso, M. SUMO-1 targets RanGAP1 to kinetochores and mitotic spindles. *J Cell Biol* **156**, 595-602, doi:10.1083/jcb.200110109 (2002).
- 213 Huang, D. W., Sherman, B. T. & Lempicki, R. A. Systematic and integrative analysis of large gene lists using DAVID bioinformatics resources. *Nat Protoc* **4**, 44-57, doi:10.1038/nprot.2008.211 (2009).
- 214 Gasteiger, E. *et al.* in *The Proteomics Protocols Handbook* (ed J. W. Walker) 571-607 (Humana Press, 2005).

- 215 Linding, R. *et al.* Protein disorder prediction: implications for structural proteomics. *Structure* **11**, 1453-1459 (2003).
- 216 Linding, R., Russell, R. B., Neduva, V. & Gibson, T. J. GlobPlot: Exploring protein sequences for globularity and disorder. *Nucleic Acids Res* **31**, 3701-3708 (2003).
- 217 Shannon, P. *et al.* Cytoscape: a software environment for integrated models of biomolecular interaction networks. *Genome Res* **13**, 2498-2504, doi:10.1101/gr.1239303 (2003).
- 218 Lagier-Tourenne, C. & Cleveland, D. W. Rethinking ALS: the FUS about TDP-43. *Cell* **136**, 1001-1004, doi:10.1016/j.cell.2009.03.006 (2009).
- 219 Mackenzie, I. R. The neuropathology of FTD associated With ALS. *Alzheimer Dis Assoc Disord* **21**, S44-49, doi:10.1097/WAD.0b013e31815c3486 (2007).
- 220 Mackenzie, I. R., Rademakers, R. & Neumann, M. TDP-43 and FUS in amyotrophic lateral sclerosis and frontotemporal dementia. *Lancet Neurol* **9**, 995-1007, doi:10.1016/s1474-4422(10)70195-2 (2010).
- 221 Chen-Plotkin, A. S., Lee, V. M. & Trojanowski, J. Q. TAR DNA-binding protein 43 in neurodegenerative disease. *Nat Rev Neurol* **6**, 211-220, doi:10.1038/nrneurol.2010.18 (2010).
- 222 Cushman, M., Johnson, B. S., King, O. D., Gitler, A. D. & Shorter, J. Prion-like disorders: blurring the divide between transmissibility and infectivity. *J Cell Sci* **123**, 1191-1201, doi:10.1242/jcs.051672 (2010).
- 223 Dewey, C. M. *et al.* TDP-43 aggregation in neurodegeneration: are stress granules the key? *Brain Res* **1462**, 16-25, doi:10.1016/j.brainres.2012.02.032 (2012).

- 224 Wolozin, B. Regulated protein aggregation: stress granules and neurodegeneration. *Mol Neurodegener* **7**, 56, doi:10.1186/1750-1326-7-56 (2012).
- 225 Nonaka, T. *et al.* Phosphorylated and ubiquitinated TDP-43 pathological inclusions in ALS and FTL-D-U are recapitulated in SH-SY5Y cells. *FEBS Lett* **583**, 394-400, doi:10.1016/j.febslet.2008.12.031 (2009).
- 226 Choksi DK *et al.* TDP-43 Phosphorylation by casein kinase I ϵ promotes oligomerization and enhances toxicity in vivo. *Hum Mol Genet* **23**, 1025-1035 (2013).
- 227 Li, H. Y., Yeh, P. A., Chiu, H. C., Tang, C. Y. & Tu, B. P. Hyperphosphorylation as a defense mechanism to reduce TDP-43 aggregation. *PLoS One* **6**, e23075, doi:10.1371/journal.pone.0023075 (2011).
- 228 Zhang, Y. J. *et al.* Phosphorylation regulates proteasomal-mediated degradation and solubility of TAR DNA binding protein-43 C-terminal fragments. *Mol Neurodegener* **5**, 33, doi:10.1186/1750-1326-5-33 (2010).
- 229 Scotter, E. L. *et al.* Differential roles of the ubiquitin proteasome system and autophagy in the clearance of soluble and aggregated TDP-43 species. *J Cell Sci* **127**, 1263-1278, doi:10.1242/jcs.140087 (2014).
- 230 Gendron, T. F., Rademakers, R. & Petrucelli, L. TARDBP mutation analysis in TDP-43 proteinopathies and deciphering the toxicity of mutant TDP-43. *J Alzheimers Dis* **33 Suppl 1**, S35-45, doi:10.3233/JAD-2012-129036 (2013).

- 231 Dammer, E. B. *et al.* Coaggregation of RNA-binding proteins in a model of TDP-43 proteinopathy with selective RGG motif methylation and a role for RRM1 ubiquitination. *PLoS One* **7**, e38658, doi:10.1371/journal.pone.0038658 (2012).
- 232 Xu, Z. S. Does a loss of TDP-43 function cause neurodegeneration? *Mol Neurodegener* **7**, 27, doi:10.1186/1750-1326-7-27 (2012).
- 233 Yang, C. *et al.* Partial loss of TDP-43 function causes phenotypes of amyotrophic lateral sclerosis. *Proc Natl Acad Sci U S A* **111**, E1121-1129, doi:10.1073/pnas.1322641111 (2014).
- 234 Lee, E. B., Lee, V. M. & Trojanowski, J. Q. Gains or losses: molecular mechanisms of TDP43-mediated neurodegeneration. *Nat Rev Neurosci* **13**, 38-50, doi:10.1038/nrn3121 (2012).
- 235 Diaper, D. C. *et al.* Loss and gain of Drosophila TDP-43 impair synaptic efficacy and motor control leading to age-related neurodegeneration by loss-of-function phenotypes. *Hum Mol Genet* **22**, 1539-1557, doi:10.1093/hmg/ddt005 (2013).
- 236 Halliday, G. *et al.* Mechanisms of disease in frontotemporal lobar degeneration: gain of function versus loss of function effects. *Acta Neuropathol* **124**, 373-382, doi:10.1007/s00401-012-1030-4 (2012).
- 237 Banerjee, A., Apponi, L. H., Pavlath, G. K. & Corbett, A. H. PABPN1: molecular function and muscle disease. *FEBS J* **280**, 4230-4250, doi:10.1111/febs.12294 (2013).
- 238 Kusters, B. *et al.* TDP-43 accumulation is common in myopathies with rimmed vacuoles. *Acta Neuropathol.* **117**, 209-211, doi:10.1007/s00401-008-0471-2 (2009).

- 239 Fan, X. *et al.* HnRNP A1 and A/B interaction with PABPN1 in oculopharyngeal muscular dystrophy. *Can J Neurol Sci* **30**, 244-251 (2003).
- 240 Fronz, K. *et al.* Arginine methylation of the nuclear poly(a) binding protein weakens the interaction with its nuclear import receptor, transportin. *J Biol Chem* **286**, 32986-32994, doi:10.1074/jbc.M111.273912 (2011).
- 241 Kerwitz, Y. *et al.* Stimulation of poly(A) polymerase through a direct interaction with the nuclear poly(A) binding protein allosterically regulated by RNA. *EMBO J* **22**, 3705-3714, doi:10.1093/emboj/cdg347 (2003).
- 242 Song, J., McGivern, J. V., Nichols, K. W., Markley, J. L. & Sheets, M. D. Structural basis for RNA recognition by a type II poly(A)-binding protein. *Proc Natl Acad Sci U S A* **105**, 15317-15322, doi:10.1073/pnas.0801274105 (2008).
- 243 Abu-Baker, A. *et al.* Cytoplasmic targeting of mutant poly(A)-binding protein nuclear 1 suppresses protein aggregation and toxicity in oculopharyngeal muscular dystrophy. *Traffic* **6**, 766-779, doi:10.1111/j.1600-0854.2005.00315.x (2005).
- 244 Armakola, M., Hart, M. P. & Gitler, A. D. TDP-43 toxicity in yeast. *Methods* **53**, 238-245, doi:10.1016/j.ymeth.2010.11.006 (2011).
- 245 Liu-Yesucevitz, L. *et al.* ALS-linked mutations enlarge TDP-43-enriched neuronal RNA granules in the dendritic arbor. *J Neurosci* **34**, 4167-4174, doi:10.1523/JNEUROSCI.2350-13.2014 (2014).
- 246 Hanson, K. A., Kim, S. H., Wassarman, D. A. & Tibbetts, R. S. Ubiquilin modifies TDP-43 toxicity in a Drosophila model of amyotrophic lateral sclerosis (ALS). *J Biol Chem* **285**, 11068-11072, doi:10.1074/jbc.C109.078527 (2010).

- 247 Ihara, R. *et al.* RNA binding mediates neurotoxicity in the transgenic *Drosophila* model of TDP-43 proteinopathy. *Hum Mol Genet* **22**, 4474-4484, doi:10.1093/hmg/ddt296 (2013).
- 248 Ritson, G. P. *et al.* TDP-43 mediates degeneration in a novel *Drosophila* model of disease caused by mutations in VCP/p97. *J Neurosci* **30**, 7729-7739, doi:10.1523/jneurosci.5894-09.2010 (2010).
- 249 Fiesel, F. C. *et al.* Knockdown of transactive response DNA-binding protein (TDP-43) downregulates histone deacetylase 6. *Embo J* **29**, 209-221, doi:10.1038/emboj.2009.324 (2010).
- 250 Brand, A. H. & Perrimon, N. Targeted gene expression as a means of altering cell fates and generating dominant phenotypes. *Development* **118**, 401-415 (1993).
- 251 Benoit, B. *et al.* An essential cytoplasmic function for the nuclear poly(A) binding protein, PABP2, in poly(A) tail length control and early development in *Drosophila*. *Dev Cell* **9**, 511-522, doi:10.1016/j.devcel.2005.09.002 (2005).
- 252 Estes, P. S. *et al.* Motor neurons and glia exhibit specific individualized responses to TDP-43 expression in a *Drosophila* model of amyotrophic lateral sclerosis. *Dis Model Mech* **6**, 721-733, doi:10.1242/dmm.010710 (2013).
- 253 Li, S. H. & Li, X. J. Aggregation of N-Terminal Huntingtin is Dependent on the Length of Its Glutamine Repeats. *Hum Mol Genet.* **7**, 777-782 (1998).
- 254 Bentmann, E. *et al.* Requirements for stress granule recruitment of fused in sarcoma (FUS) and TAR DNA-binding protein of 43 kDa (TDP-43). *J Biol Chem* **287**, 23079-23094, doi:10.1074/jbc.M111.328757 (2012).

- 255 Baralle, M., Buratti, E. & Baralle, F. E. The role of TDP-43 in the pathogenesis of ALS and FTL D. *Biochem Soc Trans* **41**, 1536-1540, doi:10.1042/BST20130186 (2013).
- 256 Igaz, L. M. *et al.* Dysregulation of the ALS-associated gene TDP-43 leads to neuronal death and degeneration in mice. *J Clin Invest* **121**, 726-738, doi:10.1172/jci44867 (2011).
- 257 Barmada, S. J. *et al.* Autophagy induction enhances TDP43 turnover and survival in neuronal ALS models. *Nat Chem Biol*, doi:10.1038/nchembio.1563 (2014).
- 258 Hino, H. *et al.* Myopathy phenotype in transgenic mice expressing mutated PABPN1 as a model of oculopharyngeal muscular dystrophy. *Hum Mol Genet* **13**, 181-190, doi:10.1093/hmg/ddh017 (2004).
- 259 Braun, R. J., Buttner, S., Ring, J., Kroemer, G. & Madeo, F. Nervous yeast: modeling neurotoxic cell death. *Trends Biochem Sci* **35**, 135-144, doi:10.1016/j.tibs.2009.10.005 (2010).
- 260 Armakola, M. *et al.* Inhibition of RNA lariat debranching enzyme suppresses TDP-43 toxicity in ALS disease models. *Nat Genet* **44**, 1302-1309, doi:10.1038/ng.2434 (2012).
- 261 Ju, S. *et al.* A yeast model of FUS/TLS-dependent cytotoxicity. *PLoS Biol* **9**, e1001052, doi:10.1371/journal.pbio.1001052 (2011).
- 262 Jackson, K. L. *et al.* Preservation of forelimb function by UPF1 gene therapy in a rat model of TDP-43-induced motor paralysis. *Gene Ther*, doi:10.1038/gt.2014.101 (2014).

- 263 Jackrel, M. E. *et al.* Potentiated Hsp104 variants antagonize diverse proteotoxic misfolding events. *Cell* **156**, 170-182, doi:10.1016/j.cell.2013.11.047 (2014).
- 264 Casci, I. & Pandey, U. B. A fruitful endeavor: Modeling ALS in the fruit fly. *Brain Res*, doi:10.1016/j.brainres.2014.09.064 (2014).
- 265 Twyffels, L., Gueydan, C. & Kruys, V. Transportin-1 and Transportin-2: protein nuclear import and beyond. *FEBS Lett* **588**, 1857-1868, doi:10.1016/j.febslet.2014.04.023 (2014).
- 266 Mallet, P. L. & Bachand, F. A proline-tyrosine nuclear localization signal (PY-NLS) is required for the nuclear import of fission yeast PAB2, but not of human PABPN1. *Traffic* **14**, 282-294, doi:10.1111/tra.12036 (2013).
- 267 Arrasate, M., Mitra, S., Schweitzer, E. S., Segal, M. R. & Finkbeiner, S. Inclusion body formation reduces levels of mutant huntingtin and the risk of neuronal death. *Nature* **431**, 805-810, doi:10.1038/nature02998 (2004).
- 268 Vanden Broeck, L., Callaerts, P. & Dermaut, B. TDP-43-mediated neurodegeneration: towards a loss-of-function hypothesis? *Trends Mol Med* **20**, 66-71, doi:10.1016/j.molmed.2013.11.003 (2014).
- 269 Wu, L. S., Cheng, W. C. & Shen, C. K. Targeted depletion of TDP-43 expression in the spinal cord motor neurons leads to the development of amyotrophic lateral sclerosis-like phenotypes in mice. *J Biol Chem* **287**, 27335-27344, doi:10.1074/jbc.M112.359000 (2012).
- 270 Iguchi, Y. *et al.* Loss of TDP-43 causes age-dependent progressive motor neuron degeneration. *Brain* **136**, 1371-1382, doi:10.1093/brain/awt029 (2013).

- 271 Fischer, L. R. *et al.* Amyotrophic lateral sclerosis is a distal axonopathy: evidence
in mice and man. *Exp Neurol* **185**, 232-240 (2004).
- 272 Yang, C. *et al.* The C-terminal TDP-43 fragments have a high aggregation
propensity and harm neurons by a dominant-negative mechanism. *PLoS One* **5**,
e15878, doi:10.1371/journal.pone.0015878.g001 (2010).
- 273 Budini, M., Romano, V., Quadri, Z., Buratti, E. & Baralle, F. E. TDP-43 loss of
cellular function through aggregation requires additional structural determinants
beyond its C-terminal Q/N prion-like domain. *Hum Mol Genet*,
doi:10.1093/hmg/ddu415 (2014).
- 274 Fan, X., Dion, P., Laganier, J., Brais, B. & Rouleau, G. A. Oligomerization of
polyalanine expanded PABPN1 facilitates nuclear protein aggregation that is
associated with cell death. *Hum Mol Genet* **10**, 2341-2351 (2001).
- 275 Apponi, L. H., Corbett, A. H. & Pavlath, G. K. Control of mRNA stability
contributes to low levels of nuclear poly(A) binding protein 1 (PABPN1) in
skeletal muscle. *Skelet Muscle* **3**, 23, doi:10.1186/2044-5040-3-23 (2013).
- 276 Apponi, L. H. *et al.* Loss of nuclear poly(A)-binding protein 1 causes defects in
myogenesis and mRNA biogenesis. *Hum Mol Genet* **19**, 1058-1065,
doi:10.1093/hmg/ddp569 (2010).
- 277 Nedelsky, N. B., Todd, P. K. & Taylor, J. P. Autophagy and the ubiquitin-
proteasome system: collaborators in neuroprotection. *Biochim Biophys Acta* **1782**,
691-699, doi:10.1016/j.bbadis.2008.10.002 (2008).

- 278 Wang, I. F. *et al.* Autophagy activators rescue and alleviate pathogenesis of a mouse model with proteinopathies of the TAR DNA-binding protein 43. *Proc Natl Acad Sci U S A* **109**, 15024-15029, doi:10.1073/pnas.1206362109 (2012).
- 279 Lee, B. H. *et al.* Enhancement of proteasome activity by a small-molecule inhibitor of USP14. *Nature* **467**, 179-184, doi:10.1038/nature09299 (2010).
- 280 Wang, X. *et al.* Degradation of TDP-43 and its pathogenic form by autophagy and the ubiquitin-proteasome system. *Neurosci Lett* **469**, 112-116, doi:10.1016/j.neulet.2009.11.055 (2010).
- 281 Davies, J. E., Sarkar, S. & Rubinsztein, D. C. Wild-type PABPN1 is anti-apoptotic and reduces toxicity of the oculopharyngeal muscular dystrophy mutation. *Hum Mol Genet* **17**, 1097-1108, doi:10.1093/hmg/ddm382 (2008).
- 282 Zhang, Y. J. *et al.* Aggregation-prone c9FTD/ALS poly(GA) RAN-translated proteins cause neurotoxicity by inducing ER stress. *Acta Neuropathol* **128**, 505-524, doi:10.1007/s00401-014-1336-5 (2014).
- 283 Wigington, C. P., Williams, K. R., Meers, M. P., Bassell, G. J. & Corbett, A. H. Poly(A) RNA-binding proteins and polyadenosine RNA: new members and novel functions. *Wiley Interdiscip Rev RNA*, doi:10.1002/wrna.1233 (2014).
- 284 Yau, R. & Rape, M. The increasing complexity of the ubiquitin code. *Nat Cell Biol* **18**, 579-586, doi:10.1038/ncb3358 (2016).
- 285 Jin, L., Williamson, A., Banerjee, S., Philipp, I. & Rape, M. Mechanism of ubiquitin-chain formation by the human anaphase-promoting complex. *Cell* **133**, 653-665, doi:10.1016/j.cell.2008.04.012 (2008).

- 286 Tan, J. M. *et al.* Lysine 63-linked ubiquitination promotes the formation and autophagic clearance of protein inclusions associated with neurodegenerative diseases. *Hum Mol Genet* **17**, 431-439, doi:10.1093/hmg/ddm320 (2008).
- 287 Hallengren, J., Chen, P. C. & Wilson, S. M. Neuronal ubiquitin homeostasis. *Cell Biochem Biophys* **67**, 67-73, doi:10.1007/s12013-013-9634-4 (2013).
- 288 Bheda, A., Shackelford, J. & Pagano, J. S. Expression and functional studies of ubiquitin C-terminal hydrolase L1 regulated genes. *PLoS One* **4**, e6764, doi:10.1371/journal.pone.0006764 (2009).
- 289 Koulich, E., Li, X. & DeMartino, G. N. Relative structural and functional roles of multiple deubiquitylating proteins associated with mammalian 26S proteasome. *Mol Biol Cell* **19**, 1072-1082, doi:10.1091/mbc.E07-10-1040 (2008).
- 290 Nucifora, F. C., Jr. *et al.* Ubiquitination via K27 and K29 chains signals aggregation and neuronal protection of LRRK2 by WSB1. *Nat Commun* **7**, 11792, doi:10.1038/ncomms11792 (2016).
- 291 Brais, B. *et al.* Short GCG expansions in the PABP2 gene cause oculopharyngeal muscular dystrophy. *Nat Genet* **18**, 164-167, doi:10.1038/ng0298-164 (1998).
- 292 Corbeil-Girard, L. P. *et al.* PABPN1 overexpression leads to upregulation of genes encoding nuclear proteins that are sequestered in oculopharyngeal muscular dystrophy nuclear inclusions. *Neurobiol Dis* **18**, 551-567, doi:10.1016/j.nbd.2004.10.019 (2005).
- 293 Hebron, M. L. *et al.* Parkin ubiquitinates Tar-DNA binding protein-43 (TDP-43) and promotes its cytosolic accumulation via interaction with histone deacetylase 6 (HDAC6). *J Biol Chem* **288**, 4103-4115, doi:10.1074/jbc.M112.419945 (2013).

